ANL-6156
Chemistry - General
(TID-4500, 15th Ed.)
AEC Research and
Development Report

ARGONNE NATIONAL LABORATORY
9700 South Cass Avenue
Argonne, Illinois

THE MOLECULAR AND VISCOUS EFFUSION OF SATURATED VAPORS

by

K. Douglas Carlson

Based on a Thesis
Submitted to the Faculty
of
the University of Kansas
in Partial Fulfillment of the
Requirements for the Degree
of
Doctor of Philosophy

April 1960

Operated by The University of Chicago
under
Contract W-31-109-eng-38

DISCLAIMER

TABLE OF CONTENTS

TABLE OF CONTENTS

TABLE OF CONTENTS

TABLE OF CONTENTS

TABLE OF CONTENTS

TABLE OF CONTENTS

FIGURES

FIGURES

TABLES

ABSTRACT

This study comprises an investigation of the effusive behavior of saturated vapors over a range of source pressures from 10^{-6} atm in the molecular flow region to 1 atm. Measurements such as these reported have never before been carried out to any comparable extent for saturated vapors. The experiments, which are unusually precise for the methods involved, have yielded new information on the effusive behavior of vapors at source pressures near one atmosphere for the flow of vapor through long channels They have unequivocally delineated the transition from the molecular to the hydrodynamical effusive behavior for the flow of vapor through a thin-edged orifice. Some theoretical aspects of the question of vapor saturation in a Knudsen cell are considered The impetus to this investigation is the importance of the effusion method as a thermodynamic tool

Molecular flow is used extensively in the study of thermodynamic properties of vapor-condensed phase equilibria Viscous flow under the conditions of small density gradients is used for the measurement of viscosities. Both of these flow phenomena involve irreversible processes, but the former represents one limiting aspect from which one can derive heats and entropies of vaporization and the latter represents a steady-state process from which one can extract information on intermolecular potentials.

Some limited aspects of these phenomena are investigated. In particular, some aspects of the question of the extent of saturation within a Knudsen cell at low pressures and aspects of the transition from molecular to hydrodynamical effusion under conditions similar to those commonly employed in vapor pressure studies. Specifically, the purposes of this investigation were to clarify the situation regarding the upper pressure limit to effusive flow, to examine the transition of effusive flow from molecular to viscous behavior, and to clarify some limited aspects concerning the question of vapor saturation within an effusion cell.

The question of vapor saturation is considered theoretically. It is shown that a simple but entirely consistent and rigorous analysis from a thermodynamic viewpoint is possible from two assumptions for a limited system under admittedly restrictive conditions. Simple conclusions derivable from this analysis have general applicability within the bounds of the initial specifications. The problem considers a very dilute vapor supplied from the condensed phase and contained within an isothermal enclosure.

The analysis shows the effect of the location of the evaporating surface on the measurable rate of effusion and the dependence of this rate on the geometrical arrangement of the enclosure. It is demonstrated that, aside from thermal restrictions, measurements of the mass transport by beam condensation methods is a more reliable measurement of the vapor pressure than is a measurement of the total rate of effusion. Certain of the irreversible aspects are briefly considered.

The experimental study consists of the measurement of mass flow rates of mercury vapor effusing through a thin-edged orifice or long channels into a vacuum from a region of nearly saturated vapor. Liquid mercury was contained in steel ovens supported on an especially designed vacuum balance. A controller maintained a temperature constancy of 0.25 degree.

The effusion rates of mercury flowing through a thin-edged orifice of 0.02-cm radius are predictable by the molecular effusion formula to a pressure of 0.1 mm. Above this pressure the flow behavior progresses into the hydrodynamical effusion region The flow behavior for vapor effusing through a circular channel of 0.03-cm radius and 3-cm length is similar to the usual viscous flow behavior but systematically differs from an equation deduced by Knudsen for bilateral effusive conditions. At source pressures near one atmosphere, the flow rate approaches a limiting value corresponding to the effusion of vapor from a nearly saturated channel.

ACKNOWLEDGEMENTS

The author acknowledges his indebtedness to Professor Paul W. Gilles of the University of Kansas and Dr. Robert J. Thorn of the Argonne National Laboratory. Their advice, encouragement and friendship are sincerely appreciated.

The author expresses his gratitude to the Argonne National Laboratory for his appointment as Resident Student Associate under the Participating Institutions program and for the privileges and excellent services accorded him. In this regard, he wishes to thank the management and personnel of the Chemistry Division Shops. Especial thanks is given to Mr. Peter Ziegelmeier and Mr. Theodore Kavis, who contributed many ideas to the construction of a vacuum balance; to Mr. Philip O'Hara, who painstakingly constructed the vacuum balance; and to Mr. Robert Flegel, who constructed the effusion cells.

The author appreciates the advice and help of all his associates in the Laboratory and, in particular, the aid given him by Mr. Bert Ercoli and Mr. Robert Sadler. He wishes to thank Dr. George Winslow for his helpful discussions on computer techniques, and Professor T. E. Phipps and his students at the University of Illinois for helpful discussions. He thanks Mrs. Betty Edmunds for assistance in the preparation of the manuscript. These and others have made his residence especially enjoyable.

CHAPTER 1
INTRODUCTION

This thesis is concerned with an investigation of the effusion behavior of saturated vapors under conditions leading to the Knudsen molecular flow phenomena, the hydrodynamical effusion and viscous flow phenomena, and as well the transition between these extremes. These phenomena must be recognized as irreversible processes with those attendant consequences which are the result of the chemical structures and molecular interactions of the species involved and the external conditions prevailing.

Molecular flow, however, represents one limiting aspect of the irreversible flow from which one may extract equilibrium data, the information thereby derivable are heats and entropies and dissociation energies. On the other hand viscous flow under certain conditions may represent a well-defined steady-state process from which one may extract intermolecular potential information. The former encompasses the behavior of matter governed by energy differences and thereby yields information related to gross molecular structure and to the depth of an intermolecular potential well. The latter involves processes which are related to intermolecular forces acting at various interatomic distances and thus may yield information related to the form of the potential energy curve.

Admittedly, these aspects are rather broad, and it is not the intention here to intimate that a combined molecular and viscous flow study would generally lead to such all-encompassing information inevitably, one can explore only those phenomena which for a particular system actually occur under specified conditions. It is rather the present intention to illustrate within a general thermodynamic formalism both the equilibrium and nonequilibrium aspects of effusive flow.

In this study only limited aspects of the flow of saturated vapors are examined. The impetus to this study is the importance of molecular

effusion methods as a thermodynamic tool. In particular, it is the purpose here to examine those aspects for which some clarification of behavior and theory seemed important and of interest in relation to molecular effusion techniques because, for example, they have been used extensively for the study of saturated vapors at low pressures.

The molecular effusion methods generally are understood in principle, but there appeared to be two aspects which required further study. The first concerns the so-called upper limit, which is the upper pressure region for which the molecular flow formulas fail to predict the correct pressure or, conversely, the correct flow rate. The earliest studies of this limit suggested an answer to this problem. Yet the literature contains contradictory information. In addition, some of the early studies were concerned with common gases under bilateral flow conditions (strictly speaking, under small pressure gradients). Since these are not the conditions met in the studies of saturated vapors, and since it seems particularly advantageous to be able to employ the Knudsen method at higher pressures within the region where measurements by other methods are not feasible, this aspect of the method is of interest.

A second problem of interest concerns the extent of vapor saturation within the Knudsen cell at small pressures. Previous attempts to analyze this problem are misleading and not adequately handled, whereas it is possible to clarify this problem by a simple but consistent analysis. Consequently, a portion of this thesis is devoted to a theoretical discussion of this matter.

This study, therefore, is concerned in part with some aspects of the question of saturation within an effusion cell and in part with the investigation of some of the effusion problems initially investigated in the early part of this century by Martin Knudsen. It differs principally from the latter in that the gas studied is a nearly saturated vapor flowing under unilateral conditions into high vacuum. The immediate aims are to clarify the situation regarding the upper limit to molecular flow

and to examine the extent of vapor saturation in a Knudsen cell under the conditions of molecular effusive flow.

A brief review of some of the consequences of hydrodynamical theory of flow and a more extensive survey of the important aspects of the effusion method with some of its applications and history are presented in the first chapters. This survey and review delineate the problems to be studied and present some of the theory pertinent to an examination of the experiments. This certainly is not an exhaustive review, but it is hoped that important contributions which might be buried in the copious literature and not described in more readily available sources have not been overlooked.

The analysis of the extent of vapor saturation in a Knudsen cell is presented after a summary of the literature survey and a progressive development of the character of the cosine law. It is most convenient to do this at that time since the analysis draws upon the theory previously discussed and furthermore outlines the equations necessary for a presentation of some recent calculations of the Clausing factors or transmission coefficients for molecular flow.

Except for some brief concluding discussions, the problem of the transition from molecular to fluid flow is not theoretically examined in detail. Although others have made some initial inquiries into this problem, it is naturally difficult to treat and would comprise a separate study in itself.

The equipment used in the experimental work is described in detail. Not only is this necessary but the description should be of value to others interested in carrying out precision effusion experiments. The principal component of the equipment which has contributed to the precision of the data is the temperature controller, for with this unit it has been possible to maintain temperatures within a constancy of 0.25 degree, which, relative to the experimental methods and heating equipment used, is exceptionally good. The problems of uniformity

and constancy of temperature generally give the greatest trouble in vapor pressure measurements by effusion methods.

The experimental data are presented and analyzed both in regard to the observed general features of the effusive behavior of mercury under the conditions of these experiments and in regard to the previous concepts and observations by others.

Mercury was chosen as a particularly appropriate substance for study. The flow of saturated mercury vapor contained in a Knudsen oven having a thin-edged orifice or a long channel of small cross-sectional area was studied over the pressure range from 10^{-6} atmosphere in the molecular flow pressure region to one atmosphere. The results of this study clearly demonstrate the transition in the effusive behavior of a vapor flowing through a thin-edged orifice. The experiments on the flow of vapor through narrow channels show an agreement except in one region with the predictions deduced by Knudsen from less refined experiments under flow conditions ostensibly different from those of this research. The experimental conditions in the present study appear to lead to a new limiting flow rate at source pressures near one atmosphere.

CHAPTER 2
REVIEW OF SELECTED EXPERIMENTAL AND THEORETICAL ASPECTS OF GASEOUS FLOW

A fluid description and a molecular description of gaseous flow are only limiting descriptions which are maintained because of the mathematical difficulties in manipulating quantitatively the kinetic theories which in principle describe a gas existing under an arbitrary set of conditions.

The flow of a gas through a system whose macroscopic dimensions are small compared with the mean free path may be described with principles which are a consequence of equilibrium theory; the correspondence of the resulting deductions with experimental observations depends, however, on the validity of such applications of equilibrium theory to an irreversible process.

The flow of a gas whose molecular aggregates have a negligible mean free path is described by the application of dynamical principles to a continuous body. A gas flowing under a pressure gradient, however, expands irreversibly by processes which depend both on the physical boundaries and properties of the gas. A priori theories are difficult to deduce for this situation, and thus equilibrium considerations become a part of the description. The extent to which these deductions represent the flow behavior of normally dense gases is consequently limited.

In this chapter are reviewed some aspects of the hydrodynamical flow of gases and, in slightly more detail, some of the experimental and theoretical results of studies on molecular flow and the transition from molecular to viscous flow.

2.1 Historical Summary

The earliest experiments on the behavior of gases may be traced back many years before the organization of a quantitative kinetic theory of matter. Indeed, these and other experiments furnished a part of the

evidence portending and later confirming a theory of molecular constituency of matter which theretofore remained principally an intuitive and speculative concept. The notion of a gas being a continuous, homogeneous substance, as embodied in fluid mechanics, served adequately in many circumstances to provide the quantitative description of gaseous flow. Yet a number of experiments could not be reconciled with a description embracing a concept of strict material continuity. Kinetic theory, on the other hand, yielded the exact description which was demanded in the explanation of some experimental observations. The gaseous flow researches of Martin Knudsen, studies which were based on the simplest consequences of kinetic theory, probably first offered "the most direct and convincing proof of the correctness of the fundamental assumptions of the kinetic theory."(1)

Knudsen's studies represent the beginning of a quantitative understanding of the behavior of gases at low pressures, partly because of his critical experiments and partly because of the experimental and theoretical activities of the scientists then prominent in kinetic theory. Prior to the work of Knudsen, the understanding of gaseous flow principally was centered about three kinds of experiments: the viscous flow or "transpiration" of gases through narrow tubes, the "diffusive" or "atmolytic" flow of gases through porous substances, and the "effusive" flow of gases through thin orifices. For the most part, the descriptive names appear to have no rigorous, unambiguous definition, but merely describe the kind of experiment. The word "effusion" commonly is applied as a general name for the process of a gas flowing through an orifice from one region to another at a different pressure.

The law discovered by Poiseuille(2) in 1840 to describe the flow of liquid fluids through narrow tubes was found to be applicable to the flow of gases under similar circumstances except when the radius of the tube was so small that its dimensions were less than or equivalent to the mean free path. Under such conditions the flow rate exceeded that predicted by Poiseuille's law. Since one of the assumptions necessary

in the hydrodynamical deduction of this law is that the gas near the wall has zero velocity, as if the layer adjacent to the wall sticks to it, the increased flow rate can be explained by considering the gas layer as slipping along the wall boundary.[3] This phenomenon, however, was not thoroughly examined prior to Knudsen's studies.

The experiments of Graham[4] and others[5] on the flow or "diffusion" gases through porous substances showed quite interesting results. Some porous substances behaved toward gas flow as if they had narrow tubes and thus led to viscous flow or "transpiration" effects. Other substances behaved as if they had narrow slits or collections of thin orifices of molecular dimensions and led to a different kind of flow with a rate inversely proportional to the square root of the gas density or molecular weight. This kind of flow relationship became known as "Graham's law of diffusion," and this diffusion process was later explained in part by the "effusion" formula deduced in 1882 by Hertz[6] from Maxwell's velocity distribution law. This formula prescribes the rate at which molecules pass through a small, thin orifice from a region of uniform pressure p and temperature T into a vacuum. Thus,

$$\frac{dn}{dt} = \frac{p}{\sqrt{2\pi mkT}} S \quad , \tag{2.1-1}$$

where m is the mass of one molecule, k is Boltzmann's constant, and S is the cross-sectional area of the orifice.

Apparently, there were no absolute measurements by which this effusion formula could be exactly tested. In fact, some of the experimental observations did not show any agreement with this; the results were transitional between Graham's diffusion law and hydrodynamical effusion laws.[7] The experiments pertaining to Graham's law applied to the flow of gases at normal pressures through substances having pores of microscopic dimensions. The flow of moderately dense gases through an orifice having visible width but small thickness was known also to have an inverse relationship to the square root of the density.

In these situations the flow rate was governed by laws of fluid dynamics, and methods for measuring relative vapor densities by methods based on these laws were used as far back as 1804.[8]

A critical examination of the various types of flow and deviations and transitions from one to another kind of behavior required the development of vacuum technology to permit the necessary experiments to be carried out at densities for which mean free paths were larger than the dimensions of macroscopic orifices. In the latter part of the nineteenth century, vacuum methods were reasonably well enough perfected to enable Knudsen to carry out a critical and important study of gaseous flow, the incentives for which study were the "curious" observations and ideas outlined above.

2.2 The Flow of Continuous Fluids

Fluid dynamics is both physically and mathematically an intricate science, which in its description of real fluids applies the laws of physics to the macroscopic manifestations of the total resultant molecular and external forces of the bulk fluid. It generally relies on thermodynamic idealizations to handle the rather complicated irreversible expansions, which for a gas become important enough that this property cannot be ignored. Such idealizations are probably satisfactory for small velocity gradients. Turbulence in fluids, however, occurs under severe pressure gradients and large flow velocities, and is mathematically difficult to describe. Apparently there is no entirely satisfactory theory for this phenomenon; it depends on a large number of conditions which are difficult to account for separately.

Problems of fluid flow may be solved by the application of formal equations of motion, continuity, and energy balance. A number of simple situations, however, may be treated by simple energy-balance equations, such as Bernoulli's theorem. The flow of a fluid through a thin orifice from one large reservoir to another may be handled in this simple manner. If there are no frictional losses, the net force on the imaginary faces of a small volume element of fluid, which forces are

those arising from the pressure difference and the work of expansion, is related to the acceleration experienced by the fluid in the direction of flow over a small distance.

Since the fluid motion through a cross section of a large reservoir is negligible compared with the flow rate through an orifice which is many times smaller in cross section, the fluid may be considered to be accelerated from zero velocity inside the reservoir to the final efflux velocity outside the orifice. Thus, one may find[9] that the mass rate of flow is given by the expression

$$\frac{dw}{dt} = \rho_2 S_2 \quad 2\sqrt{\int_{p_2}^{p_1} \frac{dp}{\rho}} \quad , \tag{2.2-1}$$

where ρ_2 is the density of the efflux stream, S_2 is the cross-sectional area of the vena contracta, and p_1 and p_2 are the source and exit pressures, respectively. The integration requires a knowledge of the density ρ as a function of the pressure. For a gas, there may be either isothermal or adiabatic expansions, or a combination of processes. Generally, if a priori information is lacking, the expansion is taken to be a reversible expansion by either of these two processes.

If the gas effuses into a vacuum, a curious paradox arises because the assumption of a zero exit pressure leads to an indeterminate flow rate.[10] This problem was resolved by Reynolds[11] by a consideration which physically has the following significance. The efflux velocity has a maximum value independent of the external pressure if it is sufficiently low compared with the reservoir pressure, since the external vacuum conditions cannot be transferred to the gas within the reservoir at a rate exceeding the speed of sound in the gas jet. Accordingly, the efflux rate of a gas into a vacuum or a space of pressure less than about one-half of the reservoir pressure may be expressed as

$$\frac{dw}{dt} = \left\{\frac{2}{\gamma + 1}\right\}^{\frac{\gamma + 1}{2(\gamma - 1)}} \sqrt{\frac{\gamma m}{kT}}\, S_2 p \tag{2.2-2}$$

for an adiabatic expansion, with $\gamma = C_p/C_V$ and p as the reservoir pressure, or

$$\frac{dw}{dt} = \sqrt{\frac{m}{ekT}}\, S_2 p \qquad (2.2\text{-}3)$$

for an isothermal expansion, where e is the base number of the natural logarithms. The symbols m, k and T represent the mass of a molecule, Boltzmann's constant, and the absolute temperature, respectively, and S_2 is the cross-sectional area of the vena contracta. Gaseous flow through an orifice and in accordance with either of these formulas is called adiabatic or isothermal effusion, respectively.

If the orifice is a long, narrow circular tube rather than a thin opening in the reservoir, then viscous effects become important and must be included in the energy-balance equations. Under these conditions, the fluid moves in layers and each layer exerts a force on its neighbors. If the fluid velocity v is uniform along the tube but has a gradient $\partial v/\partial r$ along the normal to the axis of the tube, with r representing the radial position of a layer, then the force is proportional to the gradient. This proportionality constant is called the "coefficient of viscosity" or simply the "viscosity" of the fluid.

Assuming that the fluid has zero velocity at the walls of the tube, one derives Poiseuille's formula for the mass flow rate of a viscous fluid:

$$\frac{dw}{dt} = \frac{\pi m R^4}{8\mu kT}\, p\, \frac{dp}{d\ell} \qquad (2.2\text{-}4)$$

in which R is the radius, ℓ is a length variable, and μ is the coefficient of viscosity. The remaining symbols represent previously defined quantities.

This viscous flow formula is valid for an incompressible fluid but must be modified for applications to the viscous flow of gases. An important correction is that to account for the expansion of the gas.[12] Again one must idealize the situation by attributing to the gas an

a priori expansion process. If sufficiently long tubes and small pressure differences are used, this correction, however, becomes negligible. A second necessary correction is one deduced by Kundt and Warburg[3] prior to Knudsen's work and having a direct bearing on Knudsen's first investigation. This correction is one to account for the slipping of the gas along the wall at low pressures or for extremely narrow tubes. A factor of $4\zeta/R$ was included in the Poiseuille formula to satisfy this condition which leads to an increased flow. Here ζ is called the "coefficient of slip" and is considered to be proportional to the mean free path.[3] Thus, $4\zeta/R$ is large when the pressure is low or the tube very narrow.

2.3 The Effusion Studies of Martin Knudsen

(a) The Transition from Molecular to Viscous Flow

In the early part of this century, Martin Knudsen published a series of important papers having considerable influence on the concepts and development of the theory of the behavior of attenuated gases. These papers discussed and defined such familiar topics as molecular effusion, thermal effusion, thermal accommodation, and the cosine law of molecular reflections. The first two of his papers are discussed in this section, since they delineate the theory of what Knudsen defined as "molecular flow" and the conditions for which it obtains.

For his first study[13] Knudsen investigated the flow behavior of a pure gas which flowed through a long and narrow circular tube under a small pressure difference. The basic experimental system, constructed of glass, consisted of two large reservoirs separated by a circular tube of known length L and radius R. A gas at a pressure p_1 was contained in one of the reservoirs of volume V_1, and the same gas at a lower pressure p_2 was contained in the other reservoir of volume V_2. Vacuum pumps, manometers and McLeod gauges were attached to the reservoirs. The flow behaviors of the three gases, hydrogen, oxygen, and carbon dioxide were studied.

The gaseous flow rates were obtained indirectly from several measurements of the change in pressure over a known time period.

Since these experiments were carried out at constant temperature, the flow rate was designated by the volume of gas effused per unit pressure difference, which sometimes is called the "specific flow rate" and which Knudsen denoted by "T." Thus,

$$"T" = -V_1 \frac{dp_1}{dt} \frac{1}{p_1 - p_2} = V_2 \frac{dp_2}{dt} \frac{1}{p_1 - p_2} \quad . \tag{2.3-1}$$

The description of Knudsen's observations and deductions is given here in the more readily understood notation of mass flow rate, dw/dt. Knudsen's "T" function is related to the mass flow rate by the definition

$$"T" = \frac{dw}{dt} \frac{1}{p_1 - p_2} \frac{kT}{m} \quad , \tag{2.3-2}$$

where m, k and T have their usual definitions.

The flow rates of the various pure gases studied were tested as to dependence on the average pressure, defined by the expression

$$\bar{p} = \frac{p_1 V_1 + p_2 V_2}{V_1 + V_2} \quad , \tag{2.3-3}$$

as well as dependence on the pressure difference Δp. The average pressure as defined was constant during a series of measurements of the pressure change in the two reservoirs. It therefore proved to be a useful check on the reliability of the measurements, for example as an indication on the gas-tightness of the equipment.

The effect of four different tubes was studied. These had length-to-radius ratios from 1200 to 429. The experiments covered an average pressure range of about 10^{-3} to 140 mm Hg.

The experimental results showed a behavior which resembled the observation by Graham and others on the "transpiration" of gases through porous substances. At the lowest pressures, the mass flow rate was proportional to the pressure difference, inversely proportional to the square root of the density, and independent of the average pressure. At high average pressures, several mm Hg, the rate became nearly proportional to the average pressure multiplied by

the pressure difference and inversely proportional to the molecular density, in agreement with Poiseuille's law for viscous flow. At intermediate pressures the flow rate exceeded the rate predicted by Poiseuille's law in accordance with Kundt and Warburg's[3] ideas on the slippage of the gas along the walls of the tube, and exceeded the described flow rate at lowest pressure.

The flow rate divided by the pressure difference plotted as a function of the average pressure showed that, as the average pressure was decreased from the Poiseuille region of flow, the quantity proceeded through a minimum which with respect to the average pressure depended principally on the radius of the tube. At even lower average pressures, which were always less than twice the pressure p_1, the mentioned quantity increased as the pressure decreased and appeared to become nearly independent of the average pressure, as initially described.

Since Knudsen dealt with tubes having measurable dimensions, he was able to evaluate the observations in terms of absolute parameters in relation to some theoretical deductions. For the lowest pressures he supposed that, since the mean free path was very large compared with the dimensions of the tube, the molecules rarely collided with one another but progressed independently through the tube and made frequent encounters withthe wall. Such a behavior Knudsen called "molecular flow."

With these described conditions, the entire pressure difference at the ends of the tube could be related to the momentum imparted by the molecules to the wall. A quantitative analysis, however, required an assumption as to the change in momentum of the molecules on restoration to the gas. Knudsen analyzed this situation and decided that both complete path reversals and total specular reflections would be contrary to innumerable experimental observations, but that a reflection which was completely random, independent of the incident velocity of the molecule, was in accordance with the concepts of the size of the molecule in relation to the relatively large surface

imperfections of the solid boundary. Thus, Knudsen postulated that molecular emissions were random and that the emission rate of molecules from the wall, similar to the emission of light from radiating substances, followed the cosine law.

The so-called molecular flow law was deduced by two methods which, by accident,[14] gave identical and "correct" expressions. The first method employed a momentum balance, as mentioned, in which the gaseous molecules were assumed to have a Maxwellian average speed $\bar{c}$ and a uniform average flow velocity. In the second method a constant density gradient along the tube was ascribed to the gas and the cosine law was applied as an expression for the probability of the molecular flux following an arbitrary path between two surface elements on the wall of the tube. The net flux of molecules through a cross-sectional area of the tube could thus be calculated.

These calculations led to the flow rate expression

$$\frac{dw}{dt} = \frac{16R^3}{3m\bar{c}} \frac{dp}{d\ell} \quad , \tag{2.3-4}$$

which Knudsen preferred to write in a form similar to the formula

$$\frac{dw}{dt} = \sqrt{\frac{m}{2\pi kT}} \, (p_1 - p_2) \frac{\sqrt{2\pi}}{W} \quad , \tag{2.3-5}$$

for which W is the "resistance" of the tube and is expressed as

$$W = \frac{3}{8}\sqrt{\frac{\pi}{2}} \int_0^L \frac{O}{S^2} d\ell \quad , \tag{2.3-6}$$

where O is the periphery of the tube, S is the cross-sectional area, and $d\ell$ an element of length. This depends, therefore, upon the geometrical configuration of the flow tube and, as such, was considered to be a general expression applicable to arbitrary shapes.

For a circular tube, $\sqrt{2\pi}/W$ has the value $(\pi R^2)\,(8R/3L)$. The first factor is, of course, the cross-sectional area of the tube and $8R/3L$ is variously known today as the transmission coefficient or Clausing

factor for a long tube. Knudsen considered this "resistance" to be analogous to electrical resistance and thus subject to the same kind of laws, as for example Kirchoff's law. This is, of course, an intriguing idea and one popularly used in engineering considerations of the vacuum flow of gases,[15] but for quantitative work it is not a valid rule.

Knudsen decided that the flow rates over the entire average pressure range could be expressed by an empirical equation of the form

$$\frac{dw}{dt} = \left(a\bar{p} + b\,\frac{1 + C_1\bar{p}}{1 + C_2\bar{p}} \right) \frac{dp}{d\ell} \quad , \tag{2.3-7}$$

which at the high and low-pressure limits would reduce to

$$\frac{dw}{dt} = \left(a\bar{p} + b\,\frac{C_1}{C_2} \right) \frac{dp}{d\ell} \tag{2.3-8}$$

and

$$\frac{dw}{dt} = b\,\frac{dp}{d\ell} \quad , \tag{2.3-9}$$

respectively. Since these were known theoretical limits, the constants could be assigned partly by correspondence. For example, the first equation (2.3-8) could be correlated with Kundt and Warburg's[3] expression for Poiseuille's law modified for the "slip effect:"

$$\frac{dw}{dt} = \frac{\pi}{8}\,\frac{mR^4\bar{p}}{\mu kT} \left(1 + \frac{4\zeta}{R} \right) \frac{dp}{d\ell} \quad , \tag{2.3-10}$$

for which ζ was known as the "coefficient" of slip. Kundt and Warburg found ζ to be nearly equivalent to the mean free path of the gas, and accordingly Knudsen takes it to be equal to $k'\lambda$, where k' is an unknown constant of the order of unity or less and λ is the mean free path.

From the above correspondence, and using Maxwell's expression for the relationship between the viscosity μ and mean free path,[16] Knudsen found theoretically that $C_1/C_2 = 0.95\ k \leq 0.95$. The experimental data allowed him to make the choice $C_1/C_2 = 0.81$. The absolute values C_1 and C_2, which determine the location of the minimum

flow rate with respect to the average pressure, were decided upon first in a theoretical analysis of the effect of gas-phase collisions on the momentum balance and then, specifically, to fix the value of one unknown proportionality constant, by relating a theoretical expression for $C_1 - C_2$ to the previously fixed value of the ratio C_1/C_2. This analysis gave

$$C_1 = 2.00\sqrt{\frac{m}{kT}}\,\frac{R}{\mu} \quad , \qquad C_2 = 2.47\sqrt{\frac{m}{kT}}\,\frac{R}{\mu} \quad , \tag{2.3-11}$$

with the pressure in cgs units. These values, in accord with the experiments, fixed the minimum at a mean free path of about 2.5 times the diameter of the tubes. In this region the flow rate is about 5 percent less than that predicted by the molecular effusion formula.

Therefore, aside from small numerical corrections by which the experimental data are required to fit the equation, the constants are theoretically determined. Knudsen emphasized, however, that the equation was empirical because the general structure is arbitrary and chosen merely to effect a continuous coupling of two distinctly different flow laws. Besides, the theory used in these analyses must be considered in itself as strictly qualitative.

The data appear to adhere to the semi-theoretical formula in spite of some of the tenuous assumptions used in its derivation. Knudsen pointed out that more precise experiments, however, would probably show systematic deviations from the formula. The average pressure as defined is not that pressure required for Poiseuille's law; the required value has the form $\overline{p} = \frac{1}{2}(p_1 + p_2)$. Since the volumes V_1 and V_2 differ by about 8 percent, the constants then contain a systematic error.

(b) Effusion of Gases through Thin-edged Orifices

In a second paper[17] Knudsen reported the results of a study of the flow of dilute gases through thin orifices whose dimensions could be considered as small compared with the mean free path. It

could be suspected naturally from the previous study that similarly simple relations hold true under these conditions. The results confirmed this for hydrogen, oxygen, and carbon dioxide.

The experimental system was essentially identical to that used in the earlier study, except that the long tube was replaced by a tube of wider dimensions, at the end of which a thin platinum disk pierced with a small hole was attached. The same type of measurement and the same quantities were measured. These were ostensibly constant temperature measurements. The effects of two nearly circular orifices were studied. These had areas of about 5.21×10^{-6} and 66.0×10^{-6} cm^2, respectively. The ratio of thickness to radius appears to have been less than 0.25.

The values of flow rate measured for pressures of about 0.25 mm Hg or less corresponded within about 3 percent with those calculated from the molecular effusion expression (2.3-5) for an infinitesimally thick orifice for which the "resistance" W was given the value $\sqrt{2\pi}/S$, where S is the area of the orifice. The results at low pressures were stated to be independent of the average pressure and depended only on the pressure difference, whether small or nearly equal to the source pressure. At average pressures of the order of 1 to 3 mm Hg, the flow rate became dependent on both the average pressure, and on the relative values of p_1 and p_2. At even higher pressures, for the condition that the source pressure p_1 was larger than about one-half the exit pressure p_2, the flow was exactly that predicted for isothermal effusion of a gaseous fluid without beam contraction, that is, the flow agreed with the formula (2.2-3) in which S_2 is given the value of the orifice area.

These results for the first time confirmed and "explained" the transition from one kind of flow behavior, molecular flow, to another kind of flow behavior, the then well-known isothermal effusion behavior. The reason for the occurrence of these distinctly different processes was considered to be related to the length of the mean free path of the gas in comparison with the orifice dimension.

For large free paths, the gas equilibrium was considered by Knudsen to be unaffected by the occasional disappearance of a molecule through the orifice; molecules in their random motions in the gas escape independently of one another because they occasionally are knocked randomly into paths having collision-free trajectories leading through the orifice. At high pressures, collisions would occur in and near the orifice and set up a mass movement of the gas in the direction of the orifice. Such conditions led to the bulk effusion of the gas according to the laws of fluid behavior.

Using an approximate expression for the mean free path,

$$\lambda\,(\text{cm}) = 75 \times 10^{-5}/\bar{p}(\text{cm}) \quad , \qquad (2.3\text{-}12)$$

Knudsen summarized his data for oxygen in a manner equivalent to the following:

$$p_1 > 2p_2 \quad ; \quad \lambda/2R \ll 1/10 \quad ,$$

for the flow rate calculable from the isothermal effusion formula, and

$$0 < p_2 < p_1 \quad ; \quad \lambda/2R \geq 10 \quad ,$$

for the flow rate calculable from the molecular effusion formula. At intermediate ratios of the mean free path to diameter, the flow rate was intermediate between the prescribed limits.

These experiments were considered by Knudsen to be an excellent confirmation of Maxwell's velocity distribution law. Because of the direct and simple relationships of the various parameters in the molecular effusion expression, he suggested its application to the measurement of low vapor pressures and dissociation pressures.

2.4 Some Additional Studies

Several others[18,19,20] have taken up the problem of the transition from molecular to viscous flow in long tubes. The experimental studies principally substantiate the results obtained by Knudsen. Gaeda,[18] however, with longer tubes than Knudsen used found the minimum value of the ratio of the flow rate to pressure difference to

occur at low pressure for hydrogen corresponding to a mean free path of about 50 times the tube diameter. The occurrence of this minimum at a pressure of an order of magnitude lower than that observed by Knudsen presented quite an interesting problem which could not be attributed entirely to experimental error. This problem recently recieved some attention both theoretically and experimentally.[21,22]

Before mention is made of the results of these recent investigations, it is appropriate to present some brief comments on the mean free path concepts. This is a convenient and physically satisfying picture of the collisional behavior of a gas. Mathematically, it leads to easily handled equations, but clearly at the sacrifice of rigor. The mean free path, in fact, has limited quantitative meaning for a gas at equilibrium and is subject to nearly complete ambiguity for a gas in flow, especially when the various gradients are large. Therefore, when one discusses some phenomenon on the basis of the mean free path picture, he describes only a qualitative behavior, which, admittedly is easily visualized without cumbersome reference to detailed mathematical expressions. Moreover, the mean free path description of some aspects of gaseous flow has been adapted with reasonable success to a study of the onset of the departure from Knudsen's molecular flow.

Such theoretical analyses of this problem have dealt with the effect of the development of a drift velocity as a result of gas-phase collisions at low pressures[21,22] and the effect of gas density on the rate of transport of molecules by self-diffusion.[14] The conclusions drawn from these studies have some bearing on the occurrence of the minimum flow between the molecular and Poiseuille flow limits.

If the mean free path is much larger than the length of the tube, which in turn is larger than the radius, then the molecules travel through the tube along paths interrupted only by collision with the walls of the tube. DeMarcus,[23] for example, has shown that on the average a typical molecule makes about $(L/R)^2/12$ collisions with the wall in unit time for a long tube.

If the density of the gas is increased to a value for which the mean free path is intermediate between the length and radius of the tube, the molecules collide in the gas phase as well as with the walls. This would decrease the number of molecules by interrupting those having trajectories of lengths equivalent to the mean free path; but on the other hand there would be a gain in momentum in the direction of flow. There occur, then, two competing effects whose relative magnitudes should depend on the length of the tube compared with the radius for a fixed pressure. The longer the tube the lower need be the density to produce the initial decrease in the flow rate. For a short tube, the effect of the gain in momentum in the direction of flow would be expected to predominate and therefore a minimum may not occur. This conclusion seems to be borne out by various experiments.(24)

These comments and ideas apply principally to the flow of gases through tubes of length greater than their radius under small pressure differences. The discussion of the problem of unilateral flow has not been studied, as far as this author is aware. And there is yet no kinetic theory which considers the entire transition from molecular to Poiseuille flow.

CHAPTER 3
THE COSINE LAW AND MOLECULAR FLOW

It was not long after Knudsen published his first paper that the molecular effusion phenomenon was employed to produce molecular beams for the study of molecular and atomic properties, as for example it was notably used by Stern and his group. The phenomenon has been and continues to be used for the measurement of very low vapor pressures and in this respect has proved to be an invaluable tool for thermodynamic investigations.

In this chapter a brief examination is made of the flow of gases and vapors through thin orifices and of the cosine law distribution of the effusing molecules. Particular attention is directed to the cosine law because of its fundamental importance to many applications of molecular flow and its bearing on the studies reviewed here. The cosine law is a geometrical expression of the spatial distribution of molecular flux in an equilibrium system. It is derivable from the second law of thermodynamics. The cosine law, however, has been applied to some aspects of irreversible flow, and such applications are described here and in the next chapter.

3.1 The Cosine Law of "Molecular Radiation"

According to the second law of thermodynamics, the entropy of an isolated system can only increase; given enough time, it reaches a sensibly constant maximum value. This maximum defines the equilibrium state.

Kinetic theory postulates that a gas is composed of molecules continually in motion, and there is a degree of randomness about these motions which, statistically, is a measure of the configurational entropy. In the equilibrium state, however, provided there are no external forces acting on the molecules, all directions of motion are equally probable; if this were not so, then one could devise methods of showing that the entropy will continue to increase.

The statement that all directions of motion are equal probable may be reduced easily to a mathematical statement which expresses the probability of directions as a ratio of an arbitrary direction to all directions. Thus, the probability that a molecule with speed c, or even a group of molecules with average speed $\bar{c}$, has a trajectory whose direction lies within an arbitrary solid angle $d\omega$ is simply $d\omega/4\pi$. The cosine law may now be derived from this probability in the process of deducing the flux of molecules from some arbitrary surface.

If there are ν molecules per unit volume in the gas at equilibrium, then the number of these having trajectories located within an elemental solid angle $d\omega_j$ and inclined at any angle θ_{ij} measured, for convenience, from the normal to a face of a random volume element is $\nu\, d\omega_j/4\pi$. The rate at which these pass through this face of area ds_i and in the specified direction is the rate at which they generate the volume element $\bar{c}\cos\theta_{ij}ds_i dt$. Consequently, the flux of molecules from the surface ds_i in the direction of $d\omega_j$ is

$$Z_{ij}ds_j = \frac{\nu\bar{c}}{4\pi}\cos\theta_{ij}d\omega_j\, ds_i \quad . \tag{3.1-1}$$

This is the cosine law of "molecular radiation," so called in the early German literature because of its analogy with Lambert's law for light radiation from glowing solids. The cosine law has a particularly simple interpretation: the probability that a molecule leaves a surface ds_i in a direction specified by $d\omega_j$ is $d\omega_j/4\pi$; the probable frequency of this event is $\nu\bar{c}\cos\theta_{ij}ds_i$.

The above method of deducing the cosine law is not rigorous. A number of questions on soundness might come to mind, but these may be avoided by starting a derivation from the viewpoint of a Maxwellian velocity distribution.[25] The present description, however, yields a satisfactory physical picture, and most importantly delineates

the relationship between the idea of equal probabilities of motion and the cosine law derived therefrom, a relationship which is easily overlooked and possibly at times misunderstood.

The application of the cosine law to molecular effusions problems is direct but depends on the one assumption that a small hole with negligible thickness pierced in the wall of a container having initially a gas at equilibrium does not disturb the equilibrium state. Knudsen presumably verified within his precision that this was a realizable situation. The cosine law may now be applied to the orifice, since, as the law is derived, the element ds_i in equation (3.1-1) represents any real or mathematical surface arbitrarily located. In fact, by the statistical principle of detailed balancing,[26] the law applies also to reflections from an elemental area located on the wall of a containing vessel. We will return to this point, however, in the subsequent chapter.

Provided the gas densities in both the container in question and the recipient vessel are sufficiently low, according to Knudsen's experiments collisions will not occur in the region of the orifice to interrupt the trajectory of a molecule passing through the orifice. Consequently, the molecules leaving the orifice will travel in any of the solid angles a distance nearly equivalent to a mean free path before they are knocked out of that particular beam. Since the solid angle widens, the beam is increasingly attenuated and, by the definition of the solid angle, has a density proportional to $1/\ell^2$, where ℓ is the length of the trajectory within the solid angle $d\omega$ measured from the orifice to a location at which a sampling of the beam is made. The more highly evacuated is the recipient vessel, the longer becomes the collision-free trajectory. It is thus convenient that a good vacuum be maintained in the recipient vessel. Unless otherwise specified, this will be an assumed condition.

For total flow measurements, the efflux rate is the total molecular flux in the total 2π solid angle above the orifice. An integration of the cosine law gives the value,

$$\nu\bar{c}/4 = Z_e \qquad (3.1\text{-}2)$$

for the total rate at which molecules leave the container. If ν and $\bar{c}$ may be uniquely defined by the above-mentioned assumption of equilibrium, then the ideal gas law and the Maxwellian average velocity are used to transcribe (3.1-2) into the effusion formula (2.1-1).

Since the cosine law prescribes a measurable geometrical relationship between the total efflux rate Z_e and a part of the flux in some arbitrary direction, it is presumably possible to sample only this directional flux and from it obtain the total. Such is the case in the production of molecular beams. A portion of the flux may be totally condensed on a cooled intercepting target in the forward direction. The mass condensed per unit time may be considered as the intensity of the beam in the forward direction, and it is by formula (3.1-1) proportional to the pressure in the container, which pressure is called the source pressure. The container is often referred to as a Knudsen cell or oven. The question of realizable maximum beam intensity and therefore of the realizable maximum pressure, for molecular effusion and the validity of the cosine law of effusion are more detailed questions related to the problem of the upper limit initially studied by Knudsen for total flow.

3.2 Experiments on Molecular Beam Intensities

Professor Stern[27] writes that the characteristic features of the molecular beam method are "its directness and (in principle at least) its primitiveness." These arise from the fact that the beam defines a collection of virtually isolated molecules capable of directly exhibiting absolute molecular properties without an aura of statistical obscurity.

Many of the problems in the study of material structure require as intense a beam as possible with a narrow cross section. The latter condition is easily achieved by a collimation of the beam in the forward direction with narrow "image" slits and the use of slit-shaped rather than circular orifices. The former becomes a problem of ensuring that the highest source pressure used does not produce a fluid jet instead of a collision-free beam. The jet, of course, may produce distributions not in accordance with the cosine law but more in the character of turbulent interactions. The transition between the two behaviors, though, is not sharp, and it becomes of importance then that the necessary conditions for the maximum beam production become known.

(a) Some Experiments by Knauer and Stern

An analysis of the conditions for the realization of intense beams was reported in 1926 by Knauer and Stern.[28] These investigators studied experimentally the effects of changes in exit pressure, vapor pressure, and slit width on the quantitative detection of molecular beams by visible deposits or visible traces arising from the chemical activity between the beam molecules and a substance deposited on an intercepting target. This required some intensive study because a theoretical analysis was not possible. The minimum time t_m required for the appearance of the trace multiplied by the source pressure p was used as a definitive parameter. As may be seen from formula (2.1-1), with assumptions that all molecules impinging on the collector condense, that the deposit always becomes visible at the same layer thickness, and that the pressure in the recipient vessel is zero, the product pt_m is constant for a fixed geometrical arrangement under molecular flow conditions.

A number of experimental difficulties arise in this type of examination, and each was studied as far as possible. Scattered molecules due to reflection of peripheral parts of the beam from the

vacuum apparatus, and any gas evolution would cause a decrease in the beam intensity. The reflection problem proved more severe than gas evolution, but a detailed test satisfied Knauer and Stern that they could achieve sufficient cooling with a large cold-finger to condense the peripheral molecules.

They proceeded to study the influence of the source pressure and slit width, and the nature of the deposit on the detector efficiency, and the limit of the occurrence of molecular flow. The influence of these various effects could not be experimentally separated, although it was presumably possible to accumulate evidence allowing these to be understood independently. We are concerned principally with their analysis of the effect of the source pressure on the extent of molecular flow. One might expect this to be done in terms of the mean free path concept, but these investigators placed no great reliance on such a treatment because their studies in other connections indicated, as they state, that the kinetic theory atomic diameters are not definitive for molecular beam studies and that mean free paths found from gas kinetics are very inexact.

The results of the vapor pressure and trace characteristics effects for both water and mercury vapor supplied from the condensed phase were outlined. Qualitatively, the experiments demonstrated that departures from molecular flow occurred as the source pressure became larger, although the investigators were led to deduce that at higher and higher pressures collision between molecules in the region of the orifice or slit resulted in congestion in the orifice and a consequent cloud formation above the slits. Thus scattering of the beam in a region in and above the slit caused a decrease in the beam intensity over that predicted by the theory.

For rectangular slits of dimensions of 6 x 0.022 mm, the pressure at which this effect became significant occurred at about 0.5 mm Hg, for which they attribute a mean free path of 0.06 mm.

This is deduced principally from the observations of the effusion of the water which, with no great precision, showed nearly a constant value of the pressure-time product at low pressures up to 0.5 mm and then above this pressure an unmistakable increase in the product arising from increase in the appearance time and thus an intensity decrease. The mercury experiments were ambiguous, since no real constancy of the pt_m product was observed at low pressures; a plausible explanation for this could be devised on the hypothesis of re-evaporation of the condensate and surface migration effects occurring at rates which exceeded the arrival rate of the beam molecules.

One may have in mind here innumerable effects which might negate the conclusions and interpretations cited. One must not, however, discount these workers entirely, because it is apparent from their descriptions of the study that they devoted considerable attention to detail, with the recognition that the detection scheme was subject to large errors; they estimated these errors to be about 10 percent. It is important to keep in mind, however, that source pressures were calculated from the measured source temperatures and may be in error. Therefore, an estimate of the mean free paths may be in error. The question whether the "congestion" postulated occurred in the region of the same transition from molecular to hydrodynamic flow noted by Knudsen cannot be equivocally answered, since only a part of the total flow was measured.

One may deduce by inference, however, that molecular effusion occurred down to a mean free path of about 3 times the width of the slit; this is less than but of the order of magnitude of the mean free path-to-orifice diameter ratio cited by Knudsen. Further, one might infer from all evidence that, at smaller mean free paths, the total flow rate increases, but that at least in the direction normal to the orifice the molecules are strongly scattered and lead to a decreasing beam intensity at several centimeters distance from the orifice. These conclusions are subject to question by the inferences

drawn from the later results of at least two other investigators. Knauer and Stern, however, have subsequently criticized these inferences.

(b) The Molecular Beam Experiments of T. H. Johnson

Some experiments by Johnson[29] on the applicability of an ionization gauge for the detection of molecular beam intensities were reported shortly after the above-mentioned investigation by Knauer and Stern. This study was ostensibly an examination of a detection method rather than that of the upper limit of molecular effusion, but the results have bearing on this problem and on the interpretation of Knauer and Stern's observations.

Molecular beams of mercury vapor effusing from an oven were detected in a direction normal to the plane of the orifice, which was a slit of dimension 0.1 x 1 mm. An ionization detector was suspended several centimeters above the slits and consisted of a chamber containing the usual electrodes of such a gauge. The mercury effusing from the oven slit passed through an image slit into the gauge chamber. Liquid nitrogen completely surrounded the walls of the space between the slits, an arrangement which must have been more efficient than the cold-finger condensation surface used by Knauer and Stern.

The gas pressure within the ionization chamber for steady-state processes may be related to the beam intensity, and therefore to the source pressure, provided that outgassing of the detector parts was nearly eliminated and that the beam intensity is proportional to the source pressure. The ratio of the ionization and electron currents may be simply related to the source pressure, as shown by Johnson.[29] The measurement of the currents for various mercury saturation pressures calculated from the measured temperature of the condensed mercury extended over a range of pressures from 0.2 to 143 mm Hg.

The data were presented only in graphical form, with a current ratio plotted against the source pressure. The plot showed a linear increase of current ratio with increasing pressure up to 35 mm Hg, and above this showed a gradual decrease of slope until at 100 mm Hg the current ratio began to decrease with increasing pressure.

According to the interpretation of Knauer and Stern, one would expect a decrease in the current ratio beginning at only a fraction of one mm Hg pressure due to the formation of a diffuse cloud arising from frequent collisions of the molecules in the orifice region. The data here, however, showed a continuous increase of intensity up to 100 mm Hg pressure. Examination of the intensity at some distance to the side of the beam showed that scattered molecules at these higher pressures were significantly detectable.

A plausible explanation of these latter observations in relation to those of Knauer and Stern, as Johnson suggested, is that the beam passing through the region between the two collimating slits decreased in intensity due to collisions with molecules reflected from the uncooled portions of the walls and the scattered molecules from the beam. More efficient cooling between the slits would explain the occurrence of a maximum beam intensity at higher source pressures. The decrease above the 35 mm Hg source pressure could be attributed to saturation and adsorption effects in the ion guage, as well as to the scattered molecules.

The pressure range from 0.2 to 35 mm Hg covers approximately the range of mean free paths of 0.2 to 0.0002 mm, and thus ratios of mean free paths to slit width from 2.0 to 0.002. That over this range of numbers the flow is molecular may be drawn by inference, although the results do not give positive confirmation. In the hydrodynamical flow and even in the transitional regions, the beam intensity

in the forward direction may be a linear function of the source pressure. In fact, the measurements themselves may not be precise enough nor sufficient in themselves to offer detectable differences which would be apparent in total flow measurements or total distribution measurements. Consequently, there is little information which can be unequivocally drawn from Johnson's study except that it is contradictory to previous observations. This, of course, leads one to question the fundamental validity of the cosine law itself.

3.3 Mayer's Confirmation of the Cosine Law of "Molecular Radiation"

The most sensitive test of the validity of the molecular effusion cosine law should be the measurement of the distribution of the molecular flux from a Knudsen cell. Measurements of this kind, however, were not made until after numerous other applications of the effusion method were devised. The previously described molecular beam studies constituted only a minor examination of the distribution and were generally limited to regions normal to the orifice.

The experiments of Herbert Mayer[30,31] in 1928 are the first direct test of the distribution of molecularly effusing molecules through a variety of orifice shapes. The question of the effect of an appreciably thick orifice, the nonideal orifice, was not well understood except for long, cylindrical tubes as a result of Knudsen's early investigation and Smoluchowski's[32] theoretical analysis. Thus, Mayer's investigation of the flow through tubes of length comparable with or greater than the radius were particularly appropriate.

Mayer reported in a series of two papers on a torsion method for measuring the momentum of molecules effusing at an arbitrarily selected angle measured from the normal to the orifice. Since the cosine law is easily and directly transformed into a momentum distribution expression, the measurements could be used to test the cosine law. As Mayer points out, his study regarding the validity of the cosine law was of especial significance in regard to questions arising from the previously discussed molecular beam investigations.

The apparatus consisted of the usual vacuum components, a source chamber containing one of the experimental gases (air, hydrogen, carbon dioxide, and oxygen), the orifice (which was of prescribed dimensions and shape, depending on the particular experiment), and a chamber into which the gas effused from the orifice. In this recipient chamber, a small aluminum foil, of 0.01-mm thickness and about 3-mm diameter, was suspended from a long, thin quartz fiber in such a way that molecules colliding with the vane caused a torsional displacement against the restoring force of the twisting fiber. Consequently, this deflection was a measure of the molecular impulse on the small vane. It is easy to deduce the impulse given this vane if the effusing molecules obey the cosine law.

In a collision-free beam the molecules travel straight-line trajectories ending only at a physical boundary which may be considered to be a small element of area ds_j. This area projected in the (arbitrary) direction of the trajectory may be written as $ds_j \cos\theta_{ji}$, where θ_{ji} is the angle between the normal to the surface ds_j and the trajectory of length ℓ_{ij}. The projected area and trajectory length define a solid angle

$$d\omega_j = ds_i \cos\theta_{ji} / \ell^2_{ij} \quad . \tag{3.3-1}$$

If the flux of molecules in this solid angle is that prescribed by the cosine law, then the collision rate at the intercepting surface ds_j of the molecules leaving the surface ds_j is given by the required substitution.

If the molecules on collision with the surface ds_j rebound randomly, then the change in momentum at the surface ds_j is simply $m\bar{c} \cos\theta_{ji}$, where these symbols represent the usual quantities. Thus, the impulse given the elemental surface ds_j becomes

$$dI = \frac{\nu \bar{c}}{4\pi} m\bar{c} \frac{\cos^2\theta_{ji} \cos\theta_{ij} ds_i ds_j}{\ell^2_{ij}} \quad . \tag{3.3-2}$$

In Mayer's experiments the surface ds_j represents an elemental surface on the detector vane and the source surface ds_i represents the orifice, which is assumed to be small compared with ℓ_{ij}.

The detector was constructed so that an integral impulse both parallel with and normal to the orifice axis could be measured at varying distance from the orifice. This is necessary since the impulse, being proportional to the square of the cosine of the angle, falls off more rapidly at large angles, even more than does the intensity or flux. Thus, the momentum component in a direction normal to the axis of the orifice is greater at the high angles than is the component parallel with the axis, and at small angles the reverse is true.

In his first paper,[30] Mayer described the results of trial experiments with the apparatus. The orifice in these studies was nearly circular, with a diameter of 0.3 mm and a thickness of 0.01 mm. This was sealed to a 1-cm diameter tube, which appeared in a drawing to be about 10 cm in length. This tube was fused to a larger spherical chamber which, including the tube up to the orifice, was considered the source chamber I. The vane in the recipient chamber II was located at variable distances of several mm from the orifice. The trial experiments demonstrated that the deflection is independent of the nature of the gas and is rigorously proportional to the pressure difference.

The impulse observed at various distances from the orifice gave excellent agreement with that predicted by the cosine law. Individual measurements of the deflection appear to be within 10 percent of the theoretical, but the overall precision must be judged in reference to the extent to which the distributions agree with the predictions. On this basis, the precision and agreement are probably of the order of 4 percent. These results therefore experimentally confirm within small limits the cosine law of molecular effusion through very thin orifices.

In his second paper,[31] Mayer reported on his studies of the effect of the increased pressure p_2 in chamber II, to the extent that gas-phase collisions come to have a significant influence, the effect of increased source pressures under high vacuum in chamber II, and the distribution of molecules through channels of various lengths. Air, oxygen, and argon were used in these experiments.

The observations demonstrated that even at pressures of about 4.5 mm Hg under conditions of high vacuum in the recipient chamber, the cosine law holds for a thin slit, 0.01 by 0.05 mm. This pressure would correspond to a mean free path of slightly less than 0.01 mm, which is comparable with slit width. As the pressure p_2 became comparable with the source pressure p_1, the intensity in the forward direction decreased from that predicted by the cosine law. These observations confirmed those of Johnson that inefficient pumping or condensation in the recipient chamber leads to scattering of the beam rather than, at least at the higher measured pressures, a congestion in the orifice.

The experimentally observed distributions for orifices of various thicknesses showed a more pronounced beam formation in the forward direction. For a circular orifice of thickness equal to the diameter, the cosine distribution appeared to hold up to angles of about 45° to the sides of the normal, but a decreased intensity over that predicted by the cosine law occurred at larger angles. For circular orifices of thickness-to-diameter ratios greater than about 8, the shape of the beam was found to be nearly independent of the capillary length. The data confirmed Knudsen's observations of the dependence of the flow resistance on R^3/L.

Mayer's and Johnson's observations appear to contradict the conclusions of Knauer and Stern regarding the upper pressure limit to molecular flow. Both seem to indicate that the decrease in beam intensity noted by Knauer and Stern was due to insufficient cooling of the walls of the recipient chamber. Knauer and Stern, however,

suggested[33] that a cloud formation, as postulated for their experiments, would be more unlikely with a slit of smaller length than their own. Moreover, since Mayer's detector measured a rather large portion of the beam in contrast to the narrow, collimated beam sampled by Knauer and Stern, the impulse corresponded to a total intensity of the postulated cloud; that is, the detector responded to the momenta of the molecules arriving from all points throughout the volume of the cloud. In their estimation, the possibility of finding a cosine law distribution in the cloud is not excluded.

The first suggestion is plausible; the second is rather weak. It would be very unlikely that a diffuse cloud above the orifice and supplied by the gas effusing only from the orifice would lead to a cosine distribution. A more plausible explanation would be that the cloud, if it existed, contributed only a negligible number of molecules to the vane and that the integral impulse was more representative of the flux directly from the orifice. This, however, would suggest that Knauer and Stern's detector was more sensitive to the missing molecules; but their data do not yield support to such a conclusion. That the large area of the vane detector might have contributed some ambiguity, however, is suggested by the disagreement of one of the measured distributions with a theoretical calculation by Clausing,[34] derived from an application of the cosine law.

CHAPTER 4
THE COSINE LAW OF DIFFUSE REFLECTIONS

We now briefly discuss an extended application of the cosine law, an application which is fundamental to the solution of boundary value problems in the kinetic theory of rarefied gases. Specifically, this is an application of the cosine law as a law of reflection of molecules from condensed surfaces under irreversible conditions, as Knudsen first suggested.

It is quite important, of course, that one have available some kind of law for handling the effect of gas-boundary interactions in the flow of dilute gases, because their behavior, in contrast to that of dense gases, depends markedly on the boundary conditions. In fact, this situation decidedly led to the perplexing conflicts prior to Knudsen's studies and most unfortunately still plagues a number of more recent experiments. The geometrical arrangement of a particular apparatus and the conditions of the surfaces of the apparatus and experimental sample (for example, the extent of cleanliness or the effect of surface temperatures) become as much variables in the execution of a gas theory experiment as do the parameters unique to the gas itself. Consequently, generalizations of experimental results may lead to contradictory conclusions, and one can cite here as an example the difficulties arising in measurements of thermal accommodation.(35)

4.1 Application of the Cosine Law to Reflections

The deduction of a law of gas-solid interactions from basic principles indeed is a formidable task. As a result, there is no completely satisfactory theoretical deduction from this approach, so that it is not particularly fruitful to undertake here a more fundamental examination of the problem. There are, however, a number of interesting discussions available elsewhere for this point of view.(36,37)

The only a priori reflection law which may be deduced from considerations of the gas-phase alone is the cosine law. This is deduced again from equilibrium consideration, but given justification for application to an irreversible process. The cosine law represents the flux of molecules through an arbitrary area in an equilibrium gas. Necessarily, it represents at equilibrium the rate at which molecules collide with the wall of the container at an arbitrary surface element. Therefore, it represents the rate at which molecules leave that surface, since conditions are time invariant. Thus, for the equilibrium state, the cosine law represents the directional emission rate of molecules from any kind of a surface, whether it be an inert surface or a surface made up of the condensed phase of the gas in question.

At equilibrium the rate at which molecules from all parts of the gas collide with the element of wall ds_i is

$$(\nu\bar{c}/4)\, ds_i = Z_e\, ds_i \qquad (4.1\text{-}1)$$

molecules per second, which is the same as the total molecular effusion rate. Also at equilibrium, the rate at which molecules leave the surface ds_i in the direction specified by $\cos\theta_{ij}d\omega_j$ is the previously deduced cosine law expression:

$$Z_{ij}ds_j = Z_e\,(1/\pi)\cos\theta_{ij}d\omega_j ds_i \quad . \qquad (4.1\text{-}2)$$

This last formula is easily interpretable as an emission rate expression, for Z_e has the proper dimensions to be called a collision density or flux per unit area; and indeed this is exactly what it is. In the steady state, of course, to satisfy material balance, it is likewise the total emission density. Therefore $Z_e ds_i$ may be taken as the total emission flux and the factor $(1/\pi)\cos\theta_{ij}d\omega_j$, which is dimensionless, represents the fraction of the total flux having the specified direction. It consequently may be taken naturally to be an emission rate probability, which, as easily seen, is already normalized to unity with respect to total spatial integration. It must be especially noted, however, that

here we have merely re-defined terms and have not violated the condition originally discussed that all directions of motion are equally probable. We have only emphasized that the flux probability is proportional to the cosine of the specified angle.

The cosine law as an emission or evaporation law is merely the result of the application of the statistical principle of detailed balancing; concerning the real mechanism of reflections, nothing may be deduced. Therefore, whether a fraction ξ condenses and is re-evaporated randomly and the fraction ζ is reflected specularly, the sum $(\xi + \zeta)$ is unity in all directions of molecular restitution. Therefore, the cosine law makes no distinction on detailed occurrences, and this is the immediate difficulty incurred in its application to an irreversible process.

One now removes the restriction of equilibrium, but in doing this it is supposed that the reflection mechanisms, whether the gas be at equilibrium with the wall or not, are the same. This is only a plausible assumption and not a unique consequence of the equilibrium reasoning; the only condition really required is that the reflection mechanisms have a continuous transition from a nonequilibrium state to the cosine law for the equilibrium state. This is satisfied certainly if a fraction ξ of all molecules arriving at a surface element ds_i are reflected randomly with the probability $d\omega_j/2\pi$, with the cosine frequency, and with the temperature of the wall as would be specified by $\bar{c}$, the average Maxwellian molecular speed. The remaining molecules may reflect specularly to the extent only that at equilibrium the sum of all emissions from the wall add up to the cosine law with a coefficient of unity.

The cosine law of diffuse reflections, therefore, is a postulate that of all the molecules leaving an element of solid surface a fraction ξ is randomly emitted as a Maxwellian distribution characterized by the temperature of the surface. The question as to the reflection law for a nonisothermal system will not be discussed, for it is a problem

requiring more detailed analysis than is presently necessary. Furthermore, since it is impossible to decide a priori on the extent of the various possible reflection mechanisms, we shall assume that all reflections are diffuse. As justification for this, one takes the experimental verifications of this law by others.[38,39]

For a steady-state process, the cosine law for the transport of matter from one surface ds_i to another surface ds_j in unit time, as represented in Figure 4.1, may be written as

$$Z_{ij}\, ds_j = Z(ds_i) \left\{ (1/\pi) \cos\theta_{ij} d\omega_j ds_i \right\} \qquad (4.1\text{-}3)$$

molecules per second, where $Z(ds_i)$ is the emission density of the area ds_i and $Z_{ij}ds_j$ is the arrival rate at ds_j. The quantity $Z(ds_i)$ may be expressed equivalently by $\nu(ds_i)\bar{c}/4$, where $\nu(ds_i)$ is an "effective" gas density. Thus cosine law emission behaves as if it were emission from a surface in equilibrium with a gas of density $\nu(ds_i)$ and with an average molecular speed of $\bar{c}$.

4.2 Clausing's Integral Equation

When the orifice of a Knudsen cell is of appreciable length compared with the cross-sectional dimensions of the orifice, some of the molecules passing into the tube are returned again to the gas within the cell as a result of collisions with the walls of the tube and with other gas molecules. Knudsen tried to take this into account by attributing to the tube a conductance which, by the application of the cosine law of reflection and under the assumption that gas-phase collisions are entirely negligible, he deduced to be proportional to $(8R/3L)(\pi R^2)$.

Smoluchowski[32] deduced the above factor by a similar but more accurate application of the cosine law of reflection and the choice of a uniform pressure gradient. A rigorous formulation of the so-called conductance is possible, however, in which the only assumptions required are the cosine law and the absence of molecular gas-phase collisions. The problem then reduces to one involving a solution of an integral equation for the emission density rate at the walls of the tube.

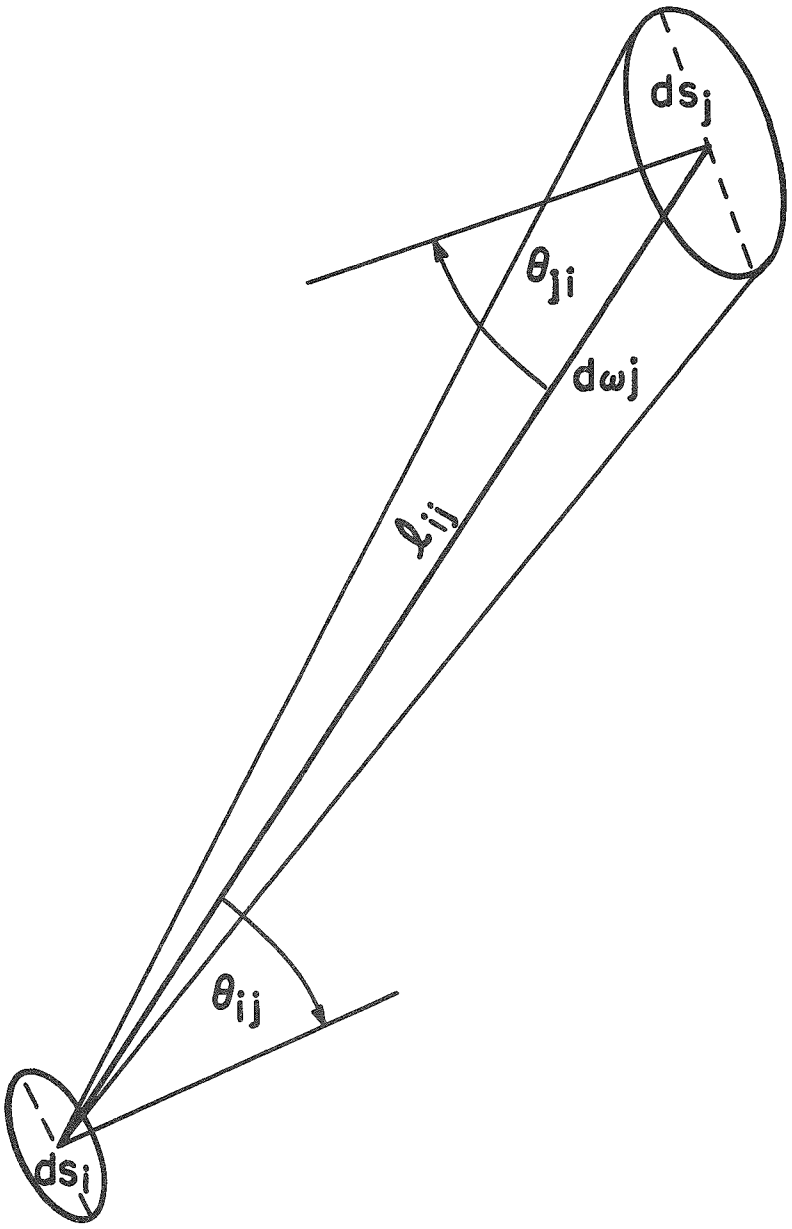

Fig. 4.1 Projected Surfaces

As DeMarcus[40] has recently shown, this formulation is a strict solution of the distribution function $F(\vec{v},\vec{r},t)$ of Boltzmann's integro-differential equation with the gas-phase collision frequency taken as zero. Thus, by its definition, once the distribution function is known, all the properties of the gas may be deduced.

Peter Clausing[41] was the first to consider this exact formulation of the molecular flow problem on the basis of Knudsen's theory of diffuse reflections. The approach taken by Clausing is, as far as the author is aware, the only approach by which angular distributions, as for example those measured by Mayer's methods, may be computed theoretically.

The molecules which finally escape the end of a tube considered as a channeled orifice of a large reservoir are those which have had their last collision with a portion of the walls of the tube or with another molecule in the gas and subsequently have followed collision-free paths to the exit into a recipient vessel. The rate at which a typical molecule executes this collision-free step depends on its velocity from the point of its last encounter. The total effusion rate is a time average of all such occurrences.

If the gas is of such a low density that gas-phase collisions are virtually absent, then the molecules which leave the tube have had their last encounters with the walls or somewhere in the reservoir, which is considered as a source of equilibrium gas at the same uniform temperature as the walls. The gas or vapor in the reservoir under these conditions, provided the density and temperature are known, is in a known, presumably equilibrium, state. Thus, as a result of the prescribed conditions, the gas in the reservoir emits molecules into the tube according to the cosine law at each elemental area ds_i in the cross section of its entrance. This cross section of area S_1 is taken as the source of the molecules. At each of these elements of the area in question the gas density is known and identical. Furthermore, the average

speed is Maxwellian and, as a consequence of the cosine law, subsequent collisions of molecules with the wall destroy only the character of the incident directions but not the Maxwellian speeds. Consequently, in principle at least, since we assume a steady state, whereby statistically all processes in any small unit of time occur simultaneously, we have knowledge enough to trace out the probable paths of each molecule and combine these to give the total effusion rate or the total collision rate at an elemental area of the wall. This is easily formulated by an integral equation.

At a small element of area ds_2 located arbitrarily on the wall of the tube, the total collision or arrival rate, $Z(ds_2)\, ds_2$, at this area is the sum of the numbers of molecules which arrive in unit time at ds_2 from every other part of the flow system, namely, the source and walls. The contribution from the source, by application of the equilibrium cosine law, is

$$Z_{12}\, ds_2 = Z_e \int_{S_1} \frac{1}{\pi} \cos\theta_{12} d\omega_2 ds_1 \quad , \tag{4.2-1}$$

in which the integration is taken over the entire area S_1 of the entrance cross section of the tube, θ_{ij} is the angle between the normal to the area ds_2 and the trajectory of length ℓ_{12} of a molecule between the two surfaces ds_1 and ds_2. The solid angle $d\omega_2$ is easily prescribed by the projection of the area ds_2 in the direction of the trajectory; thus

$$d\omega_2 = \frac{\cos\theta_{21}\, ds_2}{\ell_{12}^2} \quad , \tag{4.2-2}$$

as is represented pictorially in Figure 4 1.

The only other molecules arriving at ds_2 on the wall, provided that the recipient vessel is completely evacuated, are those arriving from all other portions of the wall in accordance with the cosine law. Thus, from another typical area of the wall, ds_2', the contribution to ds_2 may be written as

$$Z_{2'2}\, ds_2 = Z(ds_2')\, (1/\pi)\, \cos\theta_{2'2}\, d\omega_2\, ds_2' \quad . \tag{4.2-3}$$

Of course, in evaluating the contribution from the source the emission density Z_e is known. In the last expression, $Z(ds_2')$ is unknown at present, but its contribution to another surface may be formally expressed. It is now easy to add in the contributions to ds_2 from other portions of the wall to give the formal total collision density $Z(ds_2)$ and thus the total emission density at the area in question. Therefore,

$$\begin{aligned} Z(ds_2)\, ds_2 &= Z_{12}\, ds_2 + Z_{2'2}\, ds_2 + Z_{2'''2}\, ds_2 + \cdots, \\ &= Z_{12}\, ds_2 + \sum_{S_2'} Z_{2'2}\, ds_2 \quad , \end{aligned} \tag{4.2-4}$$

where S_2' represents the total wall surface of the flow boundary. This equation may be expressed equivalently as

$$\begin{aligned} Z_2(ds_2)\, ds_2 = Z_e \int_{S_1} \frac{1}{\pi} \cos\theta_{12}\, d\omega_2\, ds_2 \\ + \int_{S_2'} Z\, \frac{(ds_2')}{\pi} \cos\theta_{2'2}\, d\omega_2\, ds_{2'} \end{aligned} \tag{4.2-5}$$

Other equations could be written for the elements ds_2', ds_2'', and so forth, but formally these are all similar. Hence, the solution to the above integral equation, if possible, as a continuous function of the surface variables and geometrical parameters would give an expression for the emission density at an arbitrary surface element.

As to whether the equation has a solution, one can say this. The equation represents a physical situation which has a solution. Moreover, the equation may be disintegrated term by term into an iterative equation which is exactly the sum of all the single, double, and multiple collisions a molecule makes after it has left the source and finally collides at the elemental area ds_2. The cosine terms will not contribute here any indeterminate or infinite terms.

Once the prescription of the wall emission density $Z\ (ds_2)$ is known, the total rate of effusion is easily deduced. Thus, if the exit opening of the tube is denoted by an area S_0, then, as before, one writes that the arrival rate and thus the leaving rate into the recipient vessel at an elemental area in the opening is

$$Z\ (ds_0)\ ds_0 = Z_e \int_{S_1} \frac{1}{\pi} \cos\theta_{10}\ d\omega_0\ ds_1 + \int_{S_2} Z(ds_2)\ \frac{1}{\pi} \cos\theta_{20}\ d\omega_0\ ds_2 \quad , \tag{4.2-6}$$

which expresses the rate as a flux contribution directly from the source and contributions directly from the wall. The total effusion rate is simply obtained by an integration over the exit area S_0; thus,

$$\frac{dn}{dt} = Z(S_0)\ S_0 = \int_{S_0} Z\ (ds_0)\ ds_0 \quad . \tag{4.2-7}$$

These equations (4.2-5), (4.2-6) and (4.2-7), comprise Clausing's formulation of molecular flow through tubes of arbitrary shape

4.3 The Clausing Factors

The rate of molecular effusion of a gas from a reservoir into a vacuum through a thin orifice of arbitrary cross-sectional area S_0 may be expressed as

$$\frac{dn}{dt} = Z_e S_0 \quad . \tag{4.3-1}$$

If the cross-sectional shape is maintained but given an extension so that the orifice is a tube of appreciable length, the effusion rate is less than the above value by a fraction which may be denoted as W.

This factor W is variously known as the Clausing factor or transmission coefficient and is derivable from the equations just presented. The effusion rate in terms of the cosine functions is expressed as

$$Z(S_0)\,S_0 = Z_e \int_{S_0}\int_{S_1} \frac{1}{\pi}\cos\theta_{10}\,d\omega_0\,ds_1$$

$$+ \int_{S_0}\int_{S_2} Z(ds_2)\,\frac{1}{\pi}\cos\theta_{20}\,d\omega_0\,ds_2 \quad . \qquad (4.3\text{-}2)$$

By equating this to the expression (4.3-1) multiplied by W, one obtains the definition

$$W = \frac{Z(S_0)S_0}{Z_e S_0} = \frac{1}{S_0}\int_{S_0}\int_{S_1} \frac{1}{\pi}\cos\theta_{10}\,d\omega_0\,ds_1$$

$$+ \frac{1}{S_0}\int_{S_0}\int_{S_2} n(ds_2)\,\frac{1}{\pi}\cos\theta_{20}\,d\omega_0\,ds_2 \quad , \qquad (4.3\text{-}3)$$

in which the ratio $Z(ds_2)/Z_e$ is denoted as $n(ds_2)$; this ratio may be considered a normalized emission density.

The wall emission density equation also may be expressed simply in terms of $n(ds_2)$ by the above definition. In this way, the Clausing equations may be reduced to probability equations with known kernels which depend only on the geometrical arrangement of the flow system.

Exact solutions to the integral equation have not been found, but by various methods Clausing obtained approximate solutions which allowed him to calculate values of W for certain geometrical arrangements. For tubes of circular cross section, W is a function only of the ratio of the length L to radius R of the tube. Values of W for various L/R ratios have been tabulated in a number of available sources.[15] Recently, DeMarcus[42] has re-investigated the problem of molecular flow on the theoretical basis described. He was able to obtain values of these functions more accurate than those Clausing calculated.

Once an expression is known for the wall emission density, the cosine law may be applied to derive the distribution of flux of molecules emitted from the end of the flow tube with reference to the polar variables of the 2π solid angle above the exit of the tube. Mayer's

reported observations on the impulse distributions of molecules effusing from a circular orifice of length L = 2R induced Clausing to publish a paper[34] in which the flux distribution was theoretically calculated by the methods described above.

For a circular orifice with length L = 0, the flux is the cosine law value given by

$$\frac{dn}{dt}(\theta) = \frac{Z_e}{\pi} \cos\theta \, d\omega ds. \qquad (4.3\text{-}4)$$

In contrast, Clausing demonstrated that for a circular tube the flux becomes

$$\frac{dn}{dt}(\theta) = \frac{Z_e}{\pi} \cos\theta \, d\omega ds \cdot T(\theta, L, R) \qquad (4.3\text{-}5)$$

where $T(\theta, L, R)$ is unity normal to the orifice and decreases with increase in the angle θ. He evaluated $T(\theta, L, R)$ for the case L = 2R.

A comparative graph of the flux given by each of the expressions showed that the effect of the channeling was to produce a more pronounced beam in the forward direction. This agrees qualitatively with Mayer's observations. However, at an angle of 45°, the departure from the cosine law value given by (4.3-5) amounted to about 40 percent, whereas Mayer detected no appreciable departure at this angle.

In so far as the writer is aware, this discrepancy has never been explained. But as Clausing suggested, one could understand it if a significant number of molecules had been specularly reflected. Another possibility is that the wall collision density used by Clausing in his derivation was not accurate enough to reproduce faithfully the angular dependence of the molecular beam. This possibility is plausible because a very crude estimation of the wall emission density will give the nearly correct total flow value. For example, a simple two-parameter density equation may be used to deduce reasonably good transmission coefficients for all values of the L/R ratio.[42]

Nevertheless, this is only a possible source of discrepancy and would require further detailed analysis. The evidence for a variety of experiments is in favor of diffuse scattering at solid boundaries, with only negligible, if any, specular reflections occurring.

4.4 Geometry Factors and Probability Interpretation of the Cosine Law

Some useful and important distinctions and definitional interpretations of the various factors in the cosine law have been emphasized in the previous discussions. It is useful now to review certain of these and extend the concepts to encompass a probability formalism amenable to a subsequent analysis. A probability interpretation allows one to use the cosine law without detailed and cumbersome mathematics, at least up to the point at which numerical computations are required.

(a) The Geometry Factors

A probability prescription of the cosine law begins most naturally with a description of the geometrical quantities explicitly contained in the cosine law. This so-called law has been expressed as a product of the total emission flux $Z(ds_i)ds_i$ from a surface element multiplied by the flux probability $\left(d\omega_j/\pi \cos\theta_{ij}\right)$. Another interpretation, and one which emphasizes the equal probability of an emission direction, is expressed as the product of the random probability of a direction, $d\omega_j/2\pi$, multiplied by the number frequency of the event, $2Z(ds_i)ds_i\bar{c} \cos\theta_{ij}$. The form of the first factor arises from the physical limitation to a reflection through the boundary surface ds_i, that is, a solid boundary eliminates the remaining 2π directions otherwise possible. This second interpretation would be useful in those applications where a boundary value problem is solved by random walk procedures. The first interpretation, however, leads directly to the amenable formulations useful in an analytical prescription.

One may write the cosine law in the form

$$Z(ds_i)g(ij)ds_ids_j \quad , \tag{4.4-1}$$

in which the factor g(ij) is defined by the expression

$$g(ij) = \cos\theta_{ij} \cos\theta_{ji} / \pi \ell_{ij}^2 \quad . \tag{4.4-2}$$

One will notice that g(ij) is totally symmetrical with respect to the choice of the source and receiving surfaces and that it is purely a geometrical expression. As such, the quantity $g(ij)ds_i ds_j$ is often referred to as the emission geometry factor, both for effusion and light radiation problems. More generally, since real problems deal ultimately with macroscopic surfaces and their total emission densities an integral geometry factor is employed. Thus,

$$G(S_i S_j) = \int\int g(ij) ds_i ds_j \quad , \tag{4.4-3}$$

where the integration may be carried out partially or totally over the surfaces as might be required.

As an example of the use of such a quantity, we may consider the problem of determining the fraction of the total effusate which might arrive in a measured time at a condensation target intercepting a molecular beam some distance above an orifice of a Knudsen cell This is a typical problem encountered in vapor pressure measurements by the effusion method.[43] We assume that the vapor in the oven is saturated so that the orifice, considered as a mathematically thin, circular opening of area $S_0 = \pi R_0^2$, is a source having uniformly the cosine law flux at each of its elements ds_0. The total rate of emission or effusion is $Z_e S_0 = S_0 \nu_e \bar{c}/4$. If a circular disk of area $S_1 = \pi R_1^2$ is placed parallel to and coaxially with the orifice at a perpendicular distance L, then it is easily derived that the appropriate geometry factor is expressed by the symmetrical quantity

$$G(S_0 S_1) = \frac{\pi}{2} \left\{ L^2 + R_0^2 + R_1^2 - \sqrt{(L^2 + R_0^2 + R_1^2)^2 - 4R_0^2 R_1^2} \right\} \tag{4.4-4}$$

This result may be found in texts on light radiation theory;[44] for completeness it is derived in Appendix 1. If L and R_1 are large compared with R_0, the expression above may be expanded in powers of

$4R_0^2R_1^2/(L^2 + R_0^2 + R_1^2)^2$ to yield the familiar result

$$G(S_0S_1) \simeq S_0 R_1^2/(L^2 + R_1^2) \qquad (4.4\text{-}5)$$

in which the higher terms have been neglected.

The total rate of effusion in molecular units is Z_eS_0 and the condensation rate at the receiver, if it is sufficiently cooled to effect a total condensation of all intercepted molecules, is $Z_eG(S_0S_1)$. Consequently, the fraction intercepted is $G(S_0S_1)/S_0$. A probability interpretation of this fraction now follows directly, for the probability that a molecule in unit time arrives at S_1 a distance L away is precisely $G(S_0S_1)/S_0$.

(b) A Probability Interpretation

A variety of useful geometry factors may be derived according to the definition (4.4-3), and each of these may be reduced similarly to an easily interpretable probability. It is convenient to define these probabilities by some unique notation. Accordingly, for any surface ds_i having an emission density $Z(ds_i)$, the probability that a molecule leaving this surface will in unit time arrive at a macroscopic or elemental surface S_j is simply

$$K(ds_is_j) = \int_{S_j} Z(ds_i)g(ij)ds_ids_j \Big/ Z(ds_i)ds_i = \int_{S_j} g(ij)ds_j \quad , \qquad (4.4\text{-}6)$$

and the probability that a molecule leaving the surface S_i will in unit time arrive at the surface S_j may be expressed as

$$K(S_iS_j) = \int_{S_i}\int_{S_j} Z(ds_i)g(ij)ds_ids_j \Big/ \int_{S_i} Z(ds_i)ds_i \qquad (4.4\text{-}7)$$

In these, the convention has been used that the first symbol S_i in K represents the source and S_j the recipient surfaces, respectively. This convention is necessary in this case because, whereas the geometry factor is symmetrical with respect to the two surfaces in question, the probability factor is not. In all the situations hereinafter in which a probability interpretation is used, the emission density will be

independent of the variables of the surface over which a partial or total integration is carried out. Thus, under this restriction, for example, the probability $K(S_iS_j)$ above becomes

$$K(S_iS_j) = \frac{1}{S_i}\int_{S_j}\int_{S_i} g(ij)ds_ids_j \quad . \tag{4.4-8}$$

Consequently, the probability appropriate to the effusion problem previously outlined becomes

$$K(S_0S_1) = (1/S_0)\, G(S_0S_1) \quad . \tag{4.4-9}$$

Now to illustrate the nonsymmetry of the probability function, we may consider that the surface S_1, which previously was the recipient surface, is the source and S_0 the receiver. The probability that a molecule leaving S_1 will in unit time arrive at S_0 is

$$K(S_1S_0) = (1/S_1)\, G(S_1S_0) \quad . \tag{4.4-10}$$

However, since $G(S_1S_0) = G(S_0S_1)$, then

$$K(S_1S_0) = (S_0/S_1)\, K(S_0S_1) \quad . \tag{4.4-11}$$

Especial attention will now be devoted to this probability $K(S_1S_0)$ since it plays a leading role in applications of the cosine law to reflections from cylindrical surfaces, and we shall subsequently make extensive use of it in discussing the molecular effusion kinetics of a cylindrical cell. In particular, it is of interest to demonstrate that certain probabilities are derivable from $K(S_1S_0)$ by differentiation of its related geometry factor. We consider in illustration that a large circular disk of area $S_1 = \pi R_1^2$ is located parallel to and coaxial with a disk of area $S_0 = \pi R_0^2$ at distance L above S_1, as diagrammed in Figure 4.4.

If the disk S_0 is considered as a uniform source of particles having a cosine law emission rate, which in total is Z_eS_0, then the flux at S_1 is $Z_eG(S_0S_1)$. But it is convenient explicitly to state the fact that the geometry factor (4.4-4) is a continuous function of the three

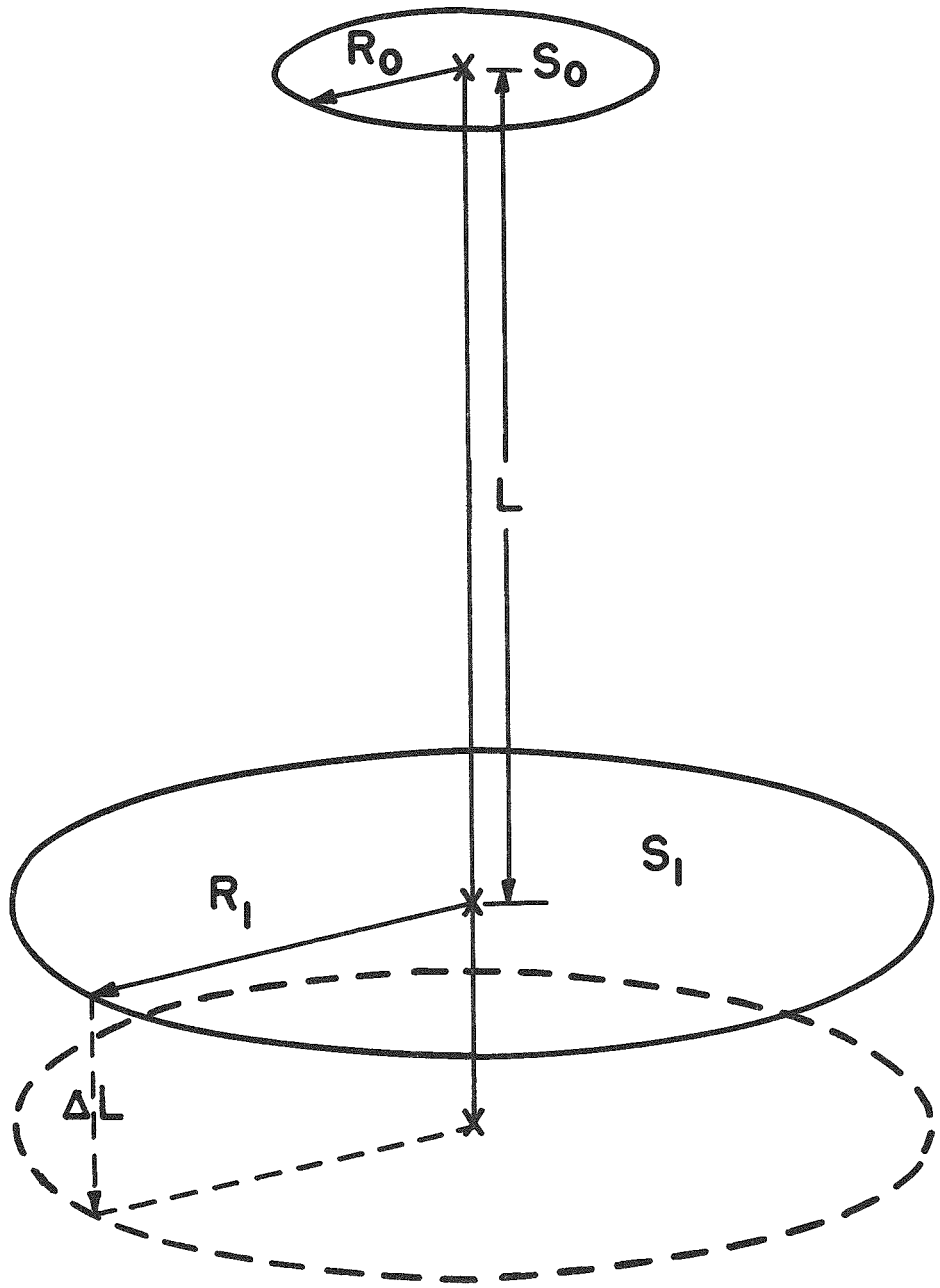

Fig. 4.4 A Geometrical Arrangement of Radiating Surfaces

parameters L, R_0 and R_1, and thus we express the flux at S_1 as $Z_e G(L,R_0R_1)$. The flux at S_1 accordingly would become $Z_e G(L+\Delta L,R_1R_0)$ if the recipient surface S_1 were moved down along the axis a distance ΔL. Since $G(L,R_0R_1)$ decreases in value for an increase in the length parameter, the second flux is slightly less than the first. It now must be emphasized that the geometry factor applies to a rate process such that the first and second fluxes represent arrival rates at either of the disks S_1 from S_0 in the same unit of time. Consequently, the difference in the two fluxes.

$$G(L,R_0R_1) - G(L + \Delta L,R_0R_1) \quad , \tag{4.4-12}$$

must be the flux at the ring element $2\pi R_1 \Delta L$. Because of the symmetry of the geometry factors, it might be supposed that the flux at S_0 from the ring element $2\pi R_1 \Delta L$ would be given by the same difference. However, in the event that the emission density at an elemental surface ds in this ring might vary with the small change in distance ΔL, but be independent of the location about the circumference, one may proceed to take the limiting differences. Thus, as ΔL is reduced to an infinitesimal, the difference (4.4-12) becomes

$$-\frac{\partial}{\partial L} G(L,R_0R_1)\, dL.$$

Therefore, if the disk S_0 were the source and the ring $2\pi R_1 dL$ were the receiver, or if the ring $2\pi R_1 dL$ were the source and S_0 the receiver, the geometry factor applicable to both under the condition that either source has uniformly the cosine emission rate is

$$G(2\pi R_1 dL,S_0) = -\frac{\partial}{\partial L} G(L,R_0R_1)dL = G(S_0,2\pi R_1 dL). \tag{4.4-13}$$

Hence, the probability that a molecule leaving the ring $2\pi R_1 dL$ will in unit time arrive at S_0 is

$$K(2\pi R_1 dL,S_0) = -\frac{1}{2\pi R_1}\frac{\partial}{\partial L} G(L,R_0R_1) = -\frac{R_1}{2}\frac{\partial}{\partial L} K(S_1S_0) \ . \tag{4.4-14}$$

In illustration, the above geometry factor is derived by integration in Appendix 1. Later we shall find it convenient to define and use the probability

$$K\left(\frac{L}{R_1}, \frac{R_0}{R_1}, \frac{R_1}{R_1}\right) = \frac{1}{2} \frac{G(L,R_0R_1)}{S_1} \tag{4.4-15}$$

to eliminate the factor $\frac{1}{2}$ arising in probabilities similar to (4.4-14) and state the explicit parametric dependence of the probability.

Another probability function could be derived by a second differentiation of (4.4-13) with respect to R_0 to obtain the geometry factor applicable to radiation between the ring $2\pi R_1 dL$ and an annular surface $2\pi R_0 dR_0$ at the disk S_0. Again, only the limiting difference is required, and the limiting operations are permissible because the factor $G(L,R_1,R_0)$ is continuous and well behaved in all defined regions of the parameters.

CHAPTER 5
VAPOR SATURATION IN A KNUDSEN CELL

The effusion of vapor from a Knudsen cell is an irreversible process. Consequently, the question regarding the extent of departure from vapor saturation within the cell is a question of the unique definition of the pressure p in the molecular effusion formula if it is to be an accurate prediction of the rate of effusion. It is this problem which is discussed in this chapter. The problem is intimately associated with the question of the flux distribution of molecules, for only under the condition of complete vapor saturation is the orifice a source having at each of its surface elements an equilibrium cosine law emission rate which a priori is applicable both to the prediction of the flux intensity at an arbitrary location outside the cell and to the usual calculation of the transmission coefficient or Clausing factor of an orifice of appreciable thickness.

In the fifty years since Knudsen first examined the molecular flow behavior of gases, evidence has been accumulated to demonstrate within the precision of innumerable experimental measurements that the vapor within a properly designed cell is practically saturated. Equivalently, this means that the precision of effusion experiments heretofore performed is insufficient to attribute real discrepancies to undersaturation effects arising from normal density gradients in the gas phase, for it is the more general occurrence of thermal gradients and depletion effects at evaporating surfaces[45] which predominantly lead to the majority of difficulties and experimental errors. Yet it is of interest both for the practical application and for the design and execution of precision effusion experiments, and of interest in connection with the extent of the validity of flux distribution calculations and experiments dependent upon the assumption of saturation at the orifice, that the question of undersaturation effects be examined rigorously. A number of inadequate previous discussions[46,47,48,49,50] of this problem,

however, indicate that the fundamental aspects of the kinetics of effusion either are not clearly understood, or not properly employed. It is the intention here not to condemn these previous discussions, but rather to examine the problem from a more reliable, consistent, and complete viewpoint in order to clarify the misconceptions which have been unfortunately promulgated. For example, the rate of effusion appears to have been viewed in terms of supposedly known flow "impedances" of the cell wall and orifice in a manner similar to the popular, but entirely qualitative, treatment of vacuum system design. But apparently it is not entirely understood that such a concept has only limited generality, is inaccurate, and, most seriously, is not strictly applicable without a rigorous justification to provide a priori corrections to experimental data.(48,51)

The problem of deducing under an arbitrary set of conditions the extent of vapor saturation in a Knudsen cell from basic principles is a naturally difficult task, first because basic principles of gas-solid interaction phenomena are not well understood and, secondly, because density conditions leading to molecular flow may be appreciably different. The effusion process may occur under conditions in which gas-phase collisions are negligible and also under conditions in which gas-phase collisions are frequent. A complete formulation of the problem would prescribe the behavior of the gas under either of these limiting conditions and be capable of predicting the departure at higher pressures from molecular flow. The present examination considers the problem only for the low-density limit in which gas-phase collisions are negligible. This is not an unimportant situation, however, for the effusion method is used extensively in the pressure region of 10^{-4} mm Hg and lower, and at this pressure one may deduce from a simple mean free path treatment that less than five percent of the molecules leaving the orifice of a Knudsen cell have been involved in a gas-phase

collision.[52] Furthermore, previous treatments ostensibly have been limited to this pressure region, and the problem is formidable enough even under this density specification.

It is the present intention that only limited aspects of the kinetics of effusion at low densities be discussed in relation to the extent of departure from vapor saturation to show within the framework of a few simple consistent assumptions and conditions that a formal expression for this departure may be deduced rigorously. The equations developed herein permit certain valid conclusions of general applicability to be deduced by inspection. The results of this treatment are briefly compared with those of previous treatments to assess their reliability. Only those aspects derived from the steady-state application of the conservation laws and statistical thermodynamical principles to an isothermal enclosure are included here. Some consequences of a nonisothermal enclosure and concentration gradients at interfacial boundaries have been discussed by others elsewhere.[45,53]

5.1 Previous Analyses of the Extent of Vapor Saturation

Before the rigorous treatment of the problem of vapor saturation in a Knudsen cell is presented, the assumptions and results of two previous descriptions of the extent of vapor saturation are outlined here for a model in which the vapor within the cell is supplied by the molecules evaporating in the steady state from a condensed phase. The analysis here conveniently allows one to assess a part of the limitations of these treatments and outline questions of a general nature which a more detailed and rigorous formulation might hope to answer.

(a) A Classical Derivation[54]

Assuming explicitly only a conservation of mass, one can write that the rate of effusion in the steady state equals the rate of evaporation minus the rate of condensation. Furthermore, if one assumes that the three rates are described by the classical kinetic expressions and that the pressure $p(0)$ throughout the cell is uniform but less than

the equilibrium pressure p_e, then the conservation statement may be expressed by the equation,

$$\frac{p(0)S_0}{\sqrt{2\pi mkT}} = \frac{\alpha p_e S_1}{\sqrt{2\pi mkT}} - \frac{\alpha p(0) S_1}{\sqrt{2\pi mkT}} \quad , \tag{5.1-1}$$

in which S_0 and S_1 are the orifice area and evaporation areas, respectively, and α is the vaporization coefficient. From this equation one finds that

$$p(0) = p_e \Big/ \left(1 + \frac{S_0}{\alpha S_1}\right) \quad . \tag{5.1-2}$$

The validity of this expression, of course, depends on the validity of the assumption of a uniform pressure throughout the gas phase; as will be shown indirectly in subsequent discussions, this is not generally valid for a cell of an arbitrary shape. The assessment of its validity, moreover, requires certainly a more detailed analysis.

(b) The Analysis by Whitman and Motzfeldt.

There have been reported[46,48] at least two attempts to derive an expression for the extent of undersaturation on the basis of the explicit assumption of a conservation of mass and a pressure gradient of a presumably unspecified nature. Whitman[46] and Motzfeldt[48] consider a cylindrical effusion cell with an evaporating sample located at the base of the cell and an orifice located coaxially at the top of the cell. The effect of gas-phase collisions is considered to be negligible. Whitman's analysis consists of summing the numbers of molecules which leave the evaporating surface and finally escape from the orifice after all possible reflections, but the method of accounting for these reflections, however, leads to the same result as Motzfeldt's more amenable analysis.

Motzfeldt considers the equations derivable from four rate processes. First, he writes that the rate of evaporation equals the rate of condensation plus the rate of effusion; the latter is assumed to be equal to the total collision frequency at the top of the effusion cell

multiplied by the ratio of the orifice area to the cross-sectional area of the cell, S_0/S_1. The second equation is a valid one in which the total emission rate from the evaporation surface is expressed as the sum of the rate of direct evaporation plus the rate at which molecules are reflected from the same surface without condensation. A third equation expresses the assumption that the reflection rate of molecules at the top of the cell equals the collision rate at the top surface minus the assumed rate of effusion. The fourth equation assumes that the collision frequency at the top of the cell is given by the emission rate from the evaporation surface multiplied by a probability W_A minus the reflection rate at the top of the cell multiplied by the probability $(1 - W_A)$. This presumes a symmetrical system in which the fraction $(1 - W_A)$ of the molecules heading toward the bottom of the cell are reflected by the walls of the cell back to the top. These four rate processes lead to the equation,

$$p(0) = \frac{p_e}{1 + \frac{S_0}{S_1}\left(\frac{1}{\alpha} + \frac{1}{W_A} - 2\right)} \qquad (5.1\text{-}3)$$

in which the symbols represent already defined quantities. Since $p(0)$ represents the pressure which is contained in the molecular effusion formula, then the expression (5.1-3) presumably uniquely defines this pressure provided W_A is known.

Both Whitman and Motzfeldt apparently accept W_A to be the usual Clausing factor calculated for a right circular cylinder of the same radius R and length L as the Knudsen cell in question, but both realize that this rests on the strictly erroneous assumption that the collision densities are independent of the radial variables of the surfaces. Whitman tried to assess the limitations of this assumption by returning to an examination of Clausing's derivation. In doing this he had to make additional assumptions to evaluate the errors in the denominator of expression (5.1-3). His analysis indicated that errors of

two to seven percent might arise from the invalid assumptions in the derivation, but since the undersaturation effect calculable from the derived equation amounts to only a percent for a Knudsen cell of normal dimensions, the derivation becomes decidedly superficial and of questionable quantitative value. Whitman's analysis of the derivational errors should have shown him that it is necessary to return to basic principles from which only a rigorous formulation is capable of quantitatively treating the problem he wished to attack.

(c) Limitations and Questions

The foregoing treatments have the virtue of apparent simplicity at the sacrifice of rigor. They serve qualitatively to illustrate the degree of saturation in a Knudsen cell and its dependence on the geometrical parameters of the cell. But because they are of a rather superficial nature they can be of little or no value in answering quantitatively the questions on flux distribution and the consequent validity of the cosine distribution at the orifice of a Knudsen cell. There are related additional questions of interest:

1. What errors occur and what is the spatial distribution of the effusate when the walls of the cell are a sink for the vapor?
2. What is the effect of the location of the evaporation surface?
3. Which is the more reliable measurement of the equilibrium pressure, that of the total rate of effusion or that of the rate measured in the forward direction?
4. What are the effects of the cell shape and dimensions on the rate of effusion?
5. What is the most important limitation to the orifice dimensions ?

These and others are questions to which one using the effusion method must seek an answer. Therefore, a rigorous derivation which yields an expression permitting even a semiquantitative discussion of these is of value. Because all the theoretical framework for such a treatment exists, at least for limited conditions, one feels

especially compelled to present such an analysis, even though it appears elementary and in part redundant.

The principal difficulty which must be properly circumvented can be easily illustrated. Certainly for a mass conservation, one may state that the rate of effusion must be equal to the rate of evaporation minus the rate of condensation. Further, one may define the pressure $p(0)$ as the unique pressure contained in the formula for the rate of effusion, so that this may be written as

$$\frac{dn}{dt} = \frac{p(0)\, S_0}{\sqrt{2\pi mkT}} \quad . \tag{5.1-4}$$

Probably there is no serious error in accepting that the rate of evaporation as given by the classical cosine law expression:

$$\frac{dn}{dt_{vap}} = \frac{\alpha\, p_e S_1}{\sqrt{2\pi mkT}} \quad , \tag{5.1-5}$$

especially since any error may be absorbed in the nebulous quantity α, which is usually thought of as the vaporization coefficient. However, it is not possible to write a similar expression for the condensation rate, especially in terms of $p(0)$, without having a knowledge of the dependence of the vapor density upon the coordinates within the cell. What one assumes for this will determine the final expression. In the classical derivation the vapor density was assumed to be a constant corresponding to $p(0)$. In the derivation by Whitman and Motzfeldt it was assumed to have certain values at the top and bottom of the cell, and these were related to each other by the factor W_A and the ratio of areas, S_0/S_1.

It is the purpose of the subsequent analysis to derive the correct density dependence, although indirectly, for a simple set of consistent, basic assumptions and conditions, in fact the same ones which tacitly were taken in the analysis by Whitman and Motzfeldt. These basic prescriptions, which are derivable from kinetic theory

and were used rigorously by Clausing in his problem, are sufficient to effect a formal solution without accepting additional and more tenuous assumptions.

5.2 Assumptions Necessary for a Limited but Consistent Analysis of the Kinetics of Molecular Effusion

Although it may at first appear redundant to return to a discussion of the basic assumptions necessary for the analysis of the kinetics of effusion - and these are the assumptions which have been carefully outlined in the foregoing chapters - one can cite two reasons for doing this. First, one must emphasize that a complete set of assumptions must be consistent with and contain all the laws of thermodynamics. Second, one must remember that if all directions of evaporation and reflection are assumed a priori to be equally probable, then the cosine law follows as a consequence and must be used consistently. This consistency, however, has been violated at the outset of the previous treatments, with the result that errors incurred in the derivations can be assessed only by returning to an initially consistent formulation. For example, the Clausing factors for circular cylinders are derived under the assumption of equally probable directions of reflection applied to a geometrical arrangement of surfaces in which the added reflecting surface corresponding to the lid of an effusion cell is not included. To take these factors so calculated to be applicable to a foreign geometrical arrangement without adequately compensating for this new arrangement leads to the inconsistency. As will become apparent, the lid surface of the cell changes the complexion of the problem to such an extent that the usual Clausing factor has no direct bearing on the problem whatever, and in fact the solution to the problem may be thought of as one of evaluating a new Clausing factor for a geometrical arrangement different from those heretofore considered.

For completeness, we cite here the two assumptions and their consequences which enable one to effect a complete and consistent analysis of the vapor saturation problem under an admittedly limited condition to a restricted system.

Assumptions: (1) We assume that all direction of gas-phase motion, reflection and evaporation are equally probable in an isothermal enclosure. (2) We assume that the conservation laws, i.e., conservation of mass and energy, are applicable.

Consequences: From these assumptions one can derive all of the consequences of kinetic theory of interest to the problem under consideration: These are (1) that the average thermal speed $\bar{c}$ of the molecules is $(8\ kT/\pi m)^{\frac{1}{2}}$, (2) that the pressure at a physical boundary is $\nu_e kT$, where ν_e is the uniform molecular density, (3) that the directional rate of evaporation is the cosine law expression, $\alpha\ (\nu_e \bar{c}/4\pi)\ \cos\theta_{ij} d\omega_j$, which gives a total rate of $\alpha\ \nu_e \bar{c}/4$, both per unit area of evaporating surface with α representing an indeterminate factor having a value between zero and unity, and (4) that the directional rate of emission from a wall surface of the enclosure or the directional flux at a mathematical surface in the gas phase is the cosine law expression $(\nu_e \bar{c}/4\pi)\ \cos\theta_{ij} d\omega_j$, which gives a total unilateral flux of $\nu_e \bar{c}/4$ both per unit area.

We now wish to apply these assumptions and their consequences under one limited condition to a restrictive system, as follows.

Condition: Gas-phase collisions are absent, and molecules move and behave independently.

System: We consider a totally closed, isolated, and isothermal container, whose shape will be specified in terms of amenable geometrical parameters, filled with a noninteracting gas specified in the above condition and in equilibrium with its condensed phase.

These three specifications allow one to proceed with an analysis which is thermodynamically consistent. The statement of the assumptions applied to the closed system under consideration ensures complete thermal accommodation of the gas with the reflecting and evaporating surfaces and, in so far as the physical analysis is concerned, avoids the troubles associated with heat losses in an open system. The quantity α, which one will recognize as a so-called vaporization coefficient, with the present system becomes a quantity having no thermal dependence, a situation which may or may not have an equivalence for the real vaporization coefficient. The nature of the explicit assumptions is to preclude the occurrence of other than random reflections. This is done first for simplicity and second because there is no a priori knowledge as to the extent of other possible types of reflections. The consideration of a noninteracting gas is cited here as a condition rather than an assumption because it appears to be within one's ability to attain this as an experimental condition at low vapor pressures.

One now may ask how this admittedly limited system pertains to the loss of vapor in an effusion experiment even in accepting the other restrictive consequences of the closed system. It does, however, correspond exactly to this situation if one proceeds with the correct bookkeeping, for, since the system is in the steady state and the gas molecules are considered to be independent particles, then it is possible to effect a scheme whereby one separately accounts for those molecules which in a unit of time arrive by all possible single and multiple reflections and by direct evaporation at a preselected area which would correspond to the orifice in an open system, without having been reflected previously at this area. We take the trouble to proceed in this manner only for the sake of complete thermodynamic consistency, although the analysis would proceed identically if the statement had been made that we consider an open system under the

assumption that the reflection mechanism and isothermal properties of the system are identically those of the closed system. However, the scheme chosen allows one at the outset to prescribe exactly those conditions which one must evaluate in transferring this analysis to a real and thus irreversible effusion process.

5.3 Mathematical Formulation

The necessary assumptions, condition, and specification of the nature of the system under consideration have been prescribed in such a way that the analysis to be effected follows identically the logical steps which Clausing considered in his special problem of the transmission coefficient of an orifice of appreciable extent. It is possible to proceed, then, on this basis to modify his formulation to include the additional reflecting surface of a lid with a small and now imaginary orifice, and to make immediate use of the probability interpretation of the cosine law. It is felt that such an attack, however, obscures some of the interesting and important aspects of the derivation, so that the procedure chosen here follows a more detailed, but descriptive, path which relies on the concepts outlined in section 4.4.

First, it is desirable that we explicitly define the problem again and as much as possible prescribe the form of solution and at the outset define a few symbols and shorthand designations which are convenient. These may be defined generally quite independently of the shape of the cell. Secondly, the variables specific to a cylindrical Knudsen cell are defined and employed in deriving the equations to effect a formal solution of the initial prescription. It will become readily apparent, if it is not so already, that the problem numerically becomes more formidable than that studied by Clausing. It is not the intention at present to obtain exact numerical information, but rather to exploit the formalism to answer some of the questions initially posed.

(a) An Explicit Statement of the Problem and Its Solution, and Some Definitions

Principally, we wish to obtain a unique definition for the pressure p occurring in the effusion formula, and this pressure shall be defined as p(0). It is of use to determine this pressure only if it may be related to the equilibrium pressure, p_e, of an isothermal enclosure, and this will depend generally on the geometrical parameters of the Knudsen cell. If the orifice of the cell is sufficiently small, the pressure p(0) would be expected to be nearly the equilibrium value p_e, so that in effect one would wish to derive a quantity Δ, which is nearly zero and dependent, if necessary, on the cell geometry. Therefore, we shall try to define the value of Δ consistent with the previously stated restrictions and applicable to a hypothetical effusion process in which the effective pressure may be defined in terms of p_e by the relation

$$p(0) = p_e (1-\Delta) \quad . \tag{5.3-1}$$

As a result of the previously stated assumptions, restriction, and condition, the total (equilibrium) wall collision density and emission density in units of number per unit time per unit area is $Z_e = \nu_e \bar{c}/4$, and these are the only density quantities of direct interest. We shall formally account separately for the emission or collision density at an element of area ds_i on the physical boundaries by considering (1) the density $Z(ds_i)$ due to those molecules which in a unit of time arrive at an area under consideration from the evaporating sample by all possible reflections without having at any time previously collided at a specified area, S_0, equivalent in the open system to the orifice of the enclosure, and (2) the density $Z(ds_i)_0$ due to those molecules which have collided with the orifice and returned to the area ds_i without having been condensed and re-evaporated at the evaporation surface S_1. In effect if this were an open system, these definitions would be equivalent in the first case to considering the evaporating

surface as the real source and the orifice as the real orifice, and in the second case to considering the orifice as the real source and the evaporation surface as the real orifice. For S_0 much less than S_1, the value of $Z(ds_i)_0$ should be much less than that of $Z(ds_i)$. Since these two emission densities are uncoupled by definition, then at all times

$$Z_e = Z(ds_i) + Z(ds_i)_0 \quad ,$$

and

$$1 = n(ds_i) + \delta(ds_i)_0 \quad , \qquad (5.3\text{-}2)$$

in which the latter equation is derived from the former by division by Z_e. The quantities n and δ may be considered normalized emission or collision densities, and since both are positive, they have values only between zero and unity, and vary in general from one to another surface element. It should be apparent by analogy with Clausing's problem that the only important quantities are the emission densities at the physical boundaries, so that gas densities are immaterial but may be derived if desired.

The geometry factor representing the geometrical variables of the surfaces for a particular coordinate system is employed as previously defined. Thus,

$$g(ij) = \frac{1}{\pi} \frac{\cos\theta_{ij}\cos\theta_{ji}}{l_{ij}^2} \quad , \qquad (5.3\text{-}3)$$

for which the symbols will be taken to specify generally defined surface elements. It must be remembered that the emission rate from one to another surface element in the same plane perpendicular to both surface normals is zero because both cosines are zero. The first symbol in the quantity g(ij), namely i, defines the general location of the "source" surface and the second, j, defines the terminal surface. This is only a convenience, however, since g(ij) is symmetrical with respect to these surfaces.

(b) Derivation of the Kinetic Equations for a Cylindrical Cell

We shall consider a circularly cylindrical enclosure as specified in the Figure 5.3. The evaporating material is distributed uniformly over the surface S_1 at the base of the cylinder. A hypothetical circular orifice of area S_0 is located coaxially at the top of the cylinder. The remaining area of the top is denoted as $S_1 - S_0 = S_1'$, and the walls of the cylinder are defined as the area S_2. At arbitrary "points" on the various boundaries, the surface area elements ds_1, ds_1', ds_2 and ds_2' are selected, and it should be noted that ds_2' represents an area equivalent to ds_2 but at another arbitrary location. The length of the cylinder measured from the base is denoted by L, the radius of the cylinder by R_1, and the radius of the hypothetical orifice by R_0. A cylindrical coordinate system allows one to define the surface variables conveniently as follows, with r taken as a radial variable, β as an angular variable, and ℓ as a length variable measured from an origin on the axis at the base of the cylinder:

$$
\begin{aligned}
ds_0 &= r_0 d\beta_0 dr_0 \\
ds_1 &= r_1 d\beta_1 dr_1 \\
ds_1' &= r_1' d\beta_1' dr_1' \\
ds_2 &= R_1 d\beta_2 d\ell \\
ds_2' &= R_1 d\beta_2' d\ell' \quad .
\end{aligned}
$$

The "vaporization coefficient" α is taken as unity, so that the normalized rate of evaporation is unity at every element on the surface S_1.

The molecules which arrive in unit time at the hypothetical orifice S_0 without having previously been reflected at this surface have had their last encounter with the wall elements ds_2 or have evaporated from the surfaces ds_1, and in a unit of time have followed a collision-free trajectory whose extremes intersect the surfaces ds_2, ds_0 and ds_1, ds_0, respectively. The emission rate from one to another surface both at the top of the cylinder is zero since the applicable cosines are

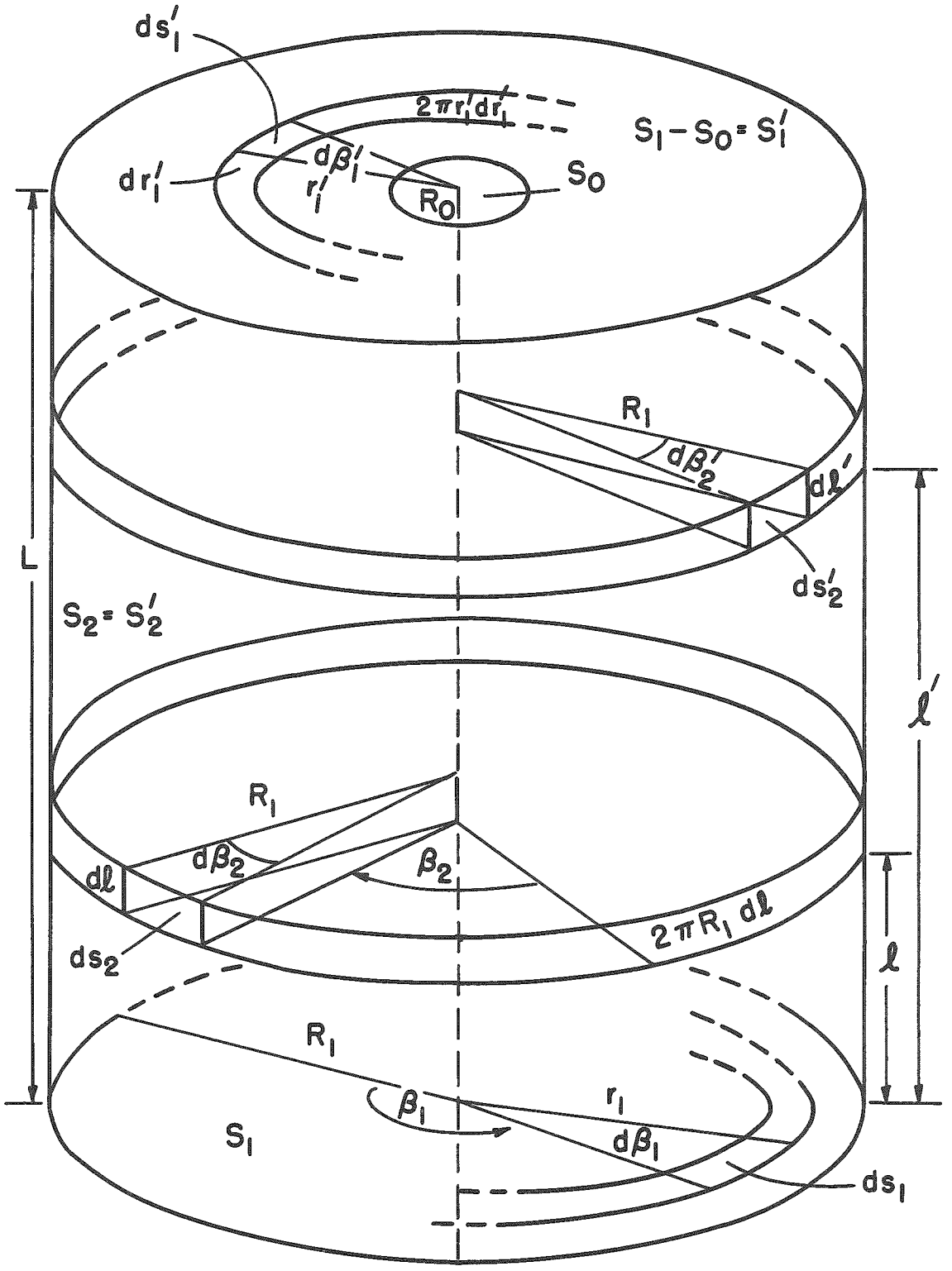

Fig. 5.3 Geometrical Variables of a Cylindrical Knudsen Cell

identically zero. Consequently, the normalized rate of arrival at an element ds_0 may be expressed in generalized cosine law variables by the definitional equation,

$$n(ds_0)ds_0 = \int_{S_1} g(10)ds_1ds_0 + \int_{S_2} n(ds_2)\, g(20)ds_2ds_0 \quad . \tag{5.3-5}$$

Therefore, an integration over the surface S_0 defines the total arrival rate or hypothetical effusion rate,

$$\frac{dn}{dt} \equiv Z(S_0)S_0 = Z_e \int_{S_0} n(ds_0)ds_0 \quad ,$$

$$= Z_e \int_{S_0}\int_{S_1} g(10)ds_1ds_0 + Z_e \int_{S_0}\int_{S_1} n(ds_2)g(20)ds_2ds_0 \, . \tag{5.3-6}$$

This equation can be evaluated only if $n(ds_2)$ is known as a function of the cylindrical variables, and it should be especially noted that once the wall emission density is known the problem is solved without resorting to an artifical mass balance relation in which the effusion rate is equated to the net rate of evaporation. A mass and energy-balance relationship is accounted for at the outset by the steady-state equivalence of the emission and collision densities at all elemental surfaces.

The wall emission density is derived similarly by equating the collision density due to those molecules which have had their last encounters with all but the elements of the hypothetical orifice area S_0. It should be remembered, incidentally, that a molecule arriving at the evaporation surface is considered to condense and on re-evaporation be unidentifiable as anything other than one of many evaporating molecules. Thus one may write,

$$\begin{aligned} n(ds_2)ds_2 = & \int_{S_1} g(12)ds_1ds_2 \\ & + \int_{S_2'} n(ds_2')g(2'2)ds_2'ds_2 \\ & + \int_{S_1'} n(ds_1')g(1'2)ds_1'ds_2 \quad . \end{aligned} \tag{5.3-7}$$

The first term in the above equation represents the density due to directly evaporated molecules, and the second term represents the contribution of single and multiple reflections from other parts of the wall. The last integral term represents the contribution to the wall density due to the presence of the top reflecting surface S_1-S_0, which is the "lid" of the enclosure. If this last term were absent, the equation would exactly represent Clausing's problem, and it is easily seen that the inclusion of the last term ensures a more nearly saturated enclosure and simultaneously vastly modifies the Clausing formulation.

Another equation is now demanded by the presence of the top surface emission density, $n(ds_1')$. Its form follows immediately by similarity with equation (5.3-5). Thus,

$$n(ds_1')ds_1' = \int_{S_1} g(11')\, ds_1 ds_1' + \int_{S_2} n(ds_2) g(21') ds_2 ds_1' \quad . \qquad (5.3\text{-}8)$$

These comprise a complete set of equations consisting of two simultaneous equations (5.3-7) and (5.3-8), which prescribe the emission densities at the reflecting surfaces, and an equation (5.3-6) representing the total arrival rate at the hypothetical orifice S_0.

It is now possible to make considerable simplifications by exploiting the rigid symmetry of the system. A moment's consideration will show that the normalized surface emission densities are independent of the angular coordinates, so that, for example, $n(ds_2)$ has identical values at every element ds_2 in the cylindrical ring element $2\pi R_1 d\ell$ because the geometrical environment of each of such elements in this ring is identical. This is a situation which would not be true if the hypothetical orifice were located asymmetrically. Identical reasoning also demonstrates that the emission density $n(ds_1')$ has identical values in the annular element $2\pi r_1' dr_1'$ located at the top of the cell, and the reasoning extends naturally to the quantity $n(ds_2')$.

One may explicitly express this angular independence of the surface emission densities by defining them as a function of ℓ or r alone. Thus, we write

$$\begin{aligned} n(ds_2) &\equiv n(\ell) \\ n(ds_2') &\equiv n(\ell') \\ n(ds_1') &\equiv n(r_1') \end{aligned} \tag{5.3-9}$$

We may now carry out the angular partial integrations over the surfaces. For the $n(\ell)$ and $n(r_1')$ equations, these operations consist of integrating over the angular variables of both surfaces ds_2 and ds_2' and as well of the surface ds_1'. For example, the integration of the left side of the $n(\ell)$ equation (5.3-7) yields the result

$$\int_{\beta_2} n(\ell)\, ds_2 = n(\ell)\ 2\pi R_1\, d\ell \quad . \tag{5.3-10}$$

For the equation (5.3-6) expressing the total arrival rate at S_0, a single partial integration is made over the angular variable of ds_2 in the second term; the first term in the equation is presumably known, so that we need not be concerned here with its detailed integration. However, it should be noted that the first term, if divided by $S_1 = \pi R_1^2$, represents exactly the probability that a molecule leaving any point on the evaporating surface will arrive in unit time at any point on the surface S_0 without having previously been reflected at this surface. Consequently it is completely analogous to the similar probability (4.4-9). This suggests that the three kinetic equations of interest, (5.3-6), (5.3-7), and (5.3-8) be divided through by the area S_1. The angular partial integrations and the division by S_1 yield the following set of equations:

$$\begin{aligned} \frac{Z(S_0)S_0}{Z_e S_1} &\equiv W(L, R_0, R_1) \\ &= \left\{ \frac{1}{S_1} \int_{S_1} \int_{S_0} g(10)\, ds_1 ds_0 \right\} \\ &\quad + \int_{\ell} n(\ell) \frac{2}{R_1} \left\{ \frac{1}{2\pi} \int_{S_0} \int_{\beta_2} g(20)\, ds_0 d\beta_2 \right\} d\ell \ , \end{aligned} \tag{5.3-11}$$

$$n(\ell)\frac{2d\ell}{R_1} = \left\{\frac{1}{\pi R_1}\int_{S_1}\int_{\beta_2} g(12)ds_1 d\beta_2 d\ell\right\}$$

$$+\int_{\ell'} n(\ell')\frac{2}{R_1}\left\{\frac{R_1}{2\pi}\int_{\beta_2}\int_{\beta_2} g(2'2)d\beta_2 d\beta_2' d\ell\right\} d\ell'$$

$$+\int_{r_1'} n(r')\frac{2r_1'}{R_1^2}\left\{\frac{R_1}{2\pi}\int_{\beta_2}\int_{\beta_1'} g(1'2)d\beta_2 d\beta_1 d\ell\right\} dr_1' \quad , \qquad (5.3\text{-}12)$$

and

$$n(r_1')\frac{2r_1'dr_1'}{R_1^2} = \left\{\frac{r_1'}{\pi R_1^2}\int_{S_1}\int_{\beta_1'} g(11')ds_1 d\beta_1' dr_1'\right\}$$

$$+\int_{\ell} n(\ell)\frac{2}{R_1}\left\{\frac{r_1'}{2\pi}\int_{\beta_2}\int_{\beta_1'} g(21')d\beta_2 d\beta_1' dr_1'\right\} d\ell \qquad (5.3\text{-}13)$$

Some of the terms in the above equations may be divided out, of course, but the form chosen here is the most convenient because the bracket terms may be demonstrated to be related to one another in a most simple way. Consider the first equation (5.3-11) of the last set. In it $Z_e S_1$ represents the total rate of evaporation and $Z(S_0)S_0$ represents the total rate of effusion. The ratio of these must represent the previously described probability. Accordingly, this ratio is analogous to the usual Clausing factor and would be identical to it if the hypothetical orifice had the area of S_1.

The second term in equation (5.3-11) is as easily interpreted. Since $Z(dS_2)2\pi R_1 d\ell$ represents the total flux, exclusive of the hypothetical orifice contribution, at the ring element $2\pi R_1 d\ell$ and $Z_e \pi R_1^2$ represents the total rate of evaporation, then the ratio $n(\ell)(2/R_1)\, d\ell$ of these fluxes represents the probability that a molecule evaporating from the surface S_1 will arrive in unit time at the ring surface $2\pi R_1 d\ell$ by all possible reflections, exclusive of those

involving the hypothetical orifice S_0, and the surface element in question. The bracket term in the integral consequently must represent the probability that in a unit time a molecule emitted from the wall element $2\pi R_1 d\ell$ will arrive by a collision-free path at the hypothetical orifice S_0. Thus, the $W(L,R_0,R_1)$ equation (5.3-11) merely expresses the proper addition of continuous, independent probabilities. It is easy to verify these statements by considerations analogous to those presented in section 4.4. In fact, these considerations lead directly to the idea that the bracket terms in all three of the equations are related by differentiation to the geometry factor $G(S_0S_1)$ as defined by equation (4.4-4), because the present equations define differences in the flux, for example, at S_0 from two hypothetical emitting disks of area πR_1^2 located a distance $d\ell$ apart, which flux difference is that attributable to the ring element $2\pi R_1 d\ell$. Similarly, the annular element $2\pi r_1' dr_1'$ is merely the difference in the coaxial disks of radii r_1' and $r_1' + dr_1'$, respectively, so that the geometry factor in question is readily deduced by a differentiation of $G(S_0S_1)$. The bracketed terms involving two elemental surfaces, for example the elements $2\pi r_1' dr_1'$, $2\pi R_1 d\ell$ and $2\pi R_1 d\ell'$, $2\pi R_1 d\ell$, involve two partial differentiations of the geometry factor.

The considerations outlined above enable one to proceed in a straightforward fashion to arrive at more useful but entirely equivalent relationships without the necessity of carrying out the tedious indicated integrations. However, because the general form of the integration requirements has been established at the outset, it is not difficult mathematically to verify these relationships. Before these are presented, however, it is convenient first to exploit the fact that the equations and functions developed are all presentable in terms of the ratios R_0/R_1, r_1'/R_1, ℓ/R_1, R_1/R_1, and so forth, a result which means that it is very natural to reduce the variables and parameters by

appropriate symbols to represent these dimensionless quantities. Thus, we define the reduced variables

$$\eta = \frac{\ell}{R_1} \; ; \quad d\eta = \frac{d\ell}{R_1} \quad ,$$

$$\rho' = \frac{r_1'}{R_1} \; ; \quad d\rho' = \frac{dr_1'}{R_1} \quad , \tag{5.3-14}$$

and let the equivalent capital Greek letters represent the appropriate cell parameters:

$$H = L/R_1 \quad ,$$

$$P = R_0/R_1 \quad . \tag{5.3-15}$$

With these definitions, it follows that

$$G(S_1S_0)/S_1 = \frac{1}{2}\left[H^2 + P^2 + 1 - \sqrt{(H^2 + P^2 + 1)^2 - 4P^2} \right]$$

$$\equiv 2\,K(H,P,1) \quad . \tag{5.3-16}$$

Since all of the probabilities may be related to an equivalent expression, we may state the general definition

$$K(h,a,b) = \frac{1}{4}\left[h^2 + a^2 + b^2 - \sqrt{(h^2 + a^2 + b)^2 - 4a^2 b^2} \right] \tag{5.3-17}$$

and assign to the symbols h, a, and b the appropriate, specific significance required.

Accordingly, one finds,

$$\frac{1}{S_1}\int_{S_1}\int_{S_0} g(10)ds_1ds_0 = 2K(H,P,1)$$

$$\frac{1}{2\pi}\int_{S_0}\int_{\beta_2} g(20)ds_0d\beta_2 = \frac{\partial}{\partial\eta} K(H-\eta, P, 1)$$

$$\frac{1}{\pi R_1}\int_{S_1}\int_{\beta_2} g(12)ds_1d\beta_2d\ell = -2\frac{\partial}{\partial\eta} K(\eta,1,1)d\eta \qquad (5.3\text{-}18)$$

$$\frac{R_1}{2\pi}\int_{\beta_2}\int_{\beta_{2'}} g(2'2)d\beta_2d\beta_2'd\ell = +\frac{\partial^2}{\partial\eta\partial\eta'} K(|\eta-\eta'|,1,1)d\eta$$

$$\frac{R_1}{2\pi}\int_{\beta_2}\int_{\beta_1'} g(1'2)d\beta_2d\beta_1'd\ell = \frac{1}{\rho'}\frac{\partial^2}{\partial\eta\partial\rho'} K(H-\eta,\rho',1)d\eta\ ,$$

$$\frac{r_1'}{\pi R_1^2}\int_{S_1}\int_{\beta_1'} g(11')ds_1d\beta_1'dr_1' = 2\frac{\partial}{\partial\rho'} K(H,\rho',1)d\rho'\ ,$$

and

$$\frac{r_1'}{2\pi}\int_{\beta_2}\int_{\beta_1'} g(21')d\beta_2d\beta_1'dr_1' = \frac{\partial^2}{\partial\eta\partial\rho'} K(H-\eta,\rho',1)d\rho'\ .$$

These exactly represent a consistent set of probabilities. The negative sign arises in these terms only because the flux from one surface to another decreases as the distance ℓ or η increases. Each of the terms, however, is - and must be - positive with the sign included. The absolute term, $|\eta - \eta'|$, in the fourth equation of this set arises because the difference in the two variables may change signs depending on their respective relative positions.

The differential functions may now be replaced in the kinetic equations, the excess terms divided out (for example, $2d\ell/R_1$), and the remaining variables and parameters reduced according to the

previous prescriptions (5.3-14) and (5.3-15) to yield the following simplified equations representing the kinetic aspects of effusion. In these equations, however, we have taken the following definitions:

$$Z(ds_1')/Z_e = n(\rho') \quad ,$$

$$Z(ds_2)/Z_e = n(\eta) \quad . \tag{5.3-19}$$

Thus, we obtain

$$W(H,P,1) = 2K(H,P,1) + 2\int_0^H n(\eta)\,\frac{\partial}{\partial\eta}\,K(H-\eta,P,1)d\eta, \tag{5.3-20}$$

$$n(\eta) = -\frac{\partial}{\partial\eta}K(\eta,1,1) - \int_0^H n(\eta')\,\frac{\partial^2}{\partial\eta\partial\eta'}K(|\eta-\eta'|,1,1)d\eta'$$

$$+\int_P^1 n(\rho')\,\frac{\partial^2}{\partial\eta\partial\rho'}\,K(H-\eta,\rho',1)d\rho' \quad , \tag{5.3-21}$$

$$n(\rho') = \frac{1}{\rho'}\,\frac{\partial}{\partial\rho'}K(H,\rho',1) + \frac{1}{\rho'}\int_0^H n(\eta)\,\frac{\partial^2}{\partial\eta\partial\rho'}K(H-\eta,\rho',1)d\eta, \tag{5.3-22}$$

and

$$\frac{dn}{dt} = Z_e S_1 W(H,P,1) \quad . \tag{5.3-23}$$

If $P \to 1$, then $n(\rho') \to 0$, and the equations reduce to the Clausing problem for a circularly cylindrical tube. These equations do not appear to give the desirable result initially stated. This result, however, is conveniently found from the fact that the normalized wall emission density is unity if the total equilibrium flux is considered.

5.4 The Extent of Saturation and Some General Conclusions

(a) A Formal Solution

In the foregoing analysis we have considered only those aspects of molecular behavior attributable to reflection processes at all surfaces of the enclosure except the hypothetical orifice of area S_0. The neglect of part of the reflections within the equilibrium enclosure

required no detailed analysis, for the scheme involved merely a formal accounting of the emission densities, which in total are unity at every surface element. A consideration of only a part of these densities attributes to them necessarily a dependence on the geometrical variables of the enclosure unless it may be proved otherwise, and one may easily demonstrate that a constant value for each of the densities $n(\eta)$ and $n(\rho')$ exists only for $P = 0$.

We now wish to exploit the fact that an equilibrium enclosure has at its boundaries normalized emission densities of unity. If the development has been entirely consistent, the equations appropriate for those molecules interacting at the hypothetical orifice of area S_0 are derivable from the present equations by a substitution of the quantities

$$n(\eta) = 1 - \delta(\eta) \quad ,$$

$$n(\rho') = 1 - \delta(\rho') \quad , \tag{5.4-1}$$

which are the same as those given by (5.3-2). For the transmission coefficient $W(H,P,1)$, one obtains the result

$$W(H,P,1) = 2\,K(0,P,1) - 2\int_0^H \delta(\eta)\,\frac{\partial}{\partial\eta}\,K(H-\eta,P,1)\,d\eta \quad . \tag{5.4-2}$$

An examination of the function (5.3-16) shows that

$$K(0,P,1) = \frac{1}{2}\,P^2 = \frac{1}{2}\,S_0/S_1 \quad , \tag{5.4-3}$$

since the positive root is that required. Hence,

$$W(H,P,1) = \frac{S_0}{S_1} - 2\int_0^H \delta(\eta)\,\frac{\partial}{\partial\eta}\,K(H-\eta,P,1)\,d\eta \quad , \tag{5.4-4}$$

and thus

$$\frac{dn}{dt} = Z_e S_1\,W(H,P,1)$$

$$= Z_e S_0 \left\{1 - 2\frac{S_1}{S_0}\int_0^H \delta(\eta)\,\frac{\partial}{\partial\eta}\,K(H-\eta,P,1)\,d\eta\right\} \quad . \tag{5.4-5}$$

Consequently, it follows directly from the formula (2.1-1) that

$$p(0) = p_e\,(1 - \Delta) \tag{5.4-6}$$

if one defines the positive function

$$\Delta = \Delta(H,P) = 2\frac{S_1}{S_0}\int_0^H \delta(\eta)\,\frac{\partial}{\partial\eta}\,K(H-\eta,P,1)\,d\eta \quad . \tag{5.4-7}$$

Therefore, we have a formal consistent solution to the problem of the unique definition of the quantity $p(0)$ occurring in the "molecular effusion formula" under admittedly restrictive conditions. A numerical answer, however, rests on a solution for the quantity $\delta(\eta)$.

The transformations of the emission density equations are easily made. In evaluating the integrals, one makes use of the following values of the functions:

$$K(0,\rho',1) = \rho'^2/2 \quad ,$$

$$K(H,\rho',0) = 0 \quad , \tag{5.4-8}$$

and

$$\int_0^H \frac{\partial^2}{\partial\eta\partial\eta'}\,K(|\eta-\eta'|,1,1)\,d\eta' = 1 + \frac{\partial}{\partial\eta}\,K(\eta,1,1) - \frac{\partial}{\partial\eta}\,K(H-\eta,1,1) \quad .$$

The last integral function is evaluated by splitting it into an integral from 0 to η and an integral from η to H. An indefinite integration is made, the derivatives of $K(\eta-\eta',1,1)$ and $K(\eta'-\eta,1,1)$ are taken with respect to η, and then the result is evaluated for the limits of η' to yield the stated result.

The transformations yield the following equations, which one will observe to be those derived assuming the hypothetical orifice to be the source and the evaporation surface to be the hypothetical orifice:

$$\delta(\eta) = \frac{\partial}{\partial\eta}\,K(H-\eta,P,1) + \int_0^H \delta(\eta')\,\frac{\partial^2}{\partial\eta\partial\eta}\,K(|\eta-\eta'|,1,1)\,d\eta'$$

$$+ \int_P^1 \delta(\rho')\,\frac{\partial^2}{\partial\eta\partial\rho'}\,K(H-\eta,\rho',1)\,d\rho' \tag{5.4-9}$$

$$\delta(\rho') = \frac{1}{\rho'} \int_0^H \delta(\eta) \quad \frac{\partial^2}{\partial\eta\partial\rho'} \quad K(H-\eta, \rho', 1)d\eta \quad . \qquad (5.4\text{-}10)$$

Although the collision density at the evaporation surface does not enter into the problem, it is possible to deduce the equation defining this rate simply by analogy with the foregoing development. Thus, for this collision density defined by $n(\rho) + \delta(\rho) = 1$, one obtains

$$n(\rho) = -\frac{1}{\rho}\int_0^H n(\eta) \quad \frac{\partial^2}{\partial\eta\partial\rho} \quad K(\eta,1,\rho)d\eta$$

$$+ \frac{1}{\rho}\int_P^1 n(\rho') \quad \frac{\partial^2}{\partial\rho\partial\rho'} \quad K(H, \rho', \rho)d\rho' \quad . \qquad (5.4\text{-}11)$$

For the transformed equation, one has

$$\delta(\rho) = \frac{1}{\rho}\frac{\partial}{\partial\rho}K(H,P,\rho) - \frac{1}{\rho}\int_0^H \delta(\eta) \quad \frac{\partial^2}{\partial\eta\partial\rho} \quad K(\eta,1,\rho)d\eta$$

$$+ \frac{1}{\rho}\int_P^1 \delta(\rho') \quad \frac{\partial^2}{\partial\rho\partial\rho'} \quad K(H, \rho', \rho)d\rho' \quad , \qquad (5.4\text{-}12)$$

where ρ is the reduced radial variable at the surfaces S_1.

It should be clear from this development that the function $\Delta(H,P)$ has the significance that if the area S_0 were open, but of mathematical thinness, and the thermal restrictions for a closed system were applicable to the open system, then the extent of undersaturation is due entirely to the molecules which otherwise would have been reflected from S_0 back to other parts of the wall.

(b) Simple Conclusions Derivable from the Kinetic Equations

It is not the intention here that extensive numerical results be presented, for such would require a more detailed examination of the collision density equations with respect to methods involved in treating integral equations. These additional more detailed remarks will be presented elsewhere.[55] It is possible, however, by inspection of the equations and the initially stated assumptions,

condition, and specification of the nature of the system to demonstrate certain valid conclusions of a general nature. In addition, a slightly more detailed evaluation is possible from simple considerations on the properties of the integral equations.

(1) Some General Conclusions

The equations necessary for the complete description of the restricted system make no direct use of the mass balance relationship in which the arrival rate at the hypothetical orifice is equated to the net rate of evaporation. It is, of course, possible to state this equivalence from the equations developed, but it would be of little value in solving the equations. Yet, all necessary mass and energy balances are accounted for by the equivalence of the emission and collision densities at the reflecting surfaces, and the collision density $n(\rho)$ at the surface of the condensed phase bears no simple relationship to the arrival rate at the hypothetical orifice of area S_0. Consequently, the classical derivation of the extent of saturation in a cylindrical oven is entirely qualitative.

One may easily demonstrate that the wall collision densities are necessarily functions of the height and radial variables, η and ρ', since if constants are substituted in the right-hand members of the density equations, the result generally is not a constant. On the other hand, it follows that there is a unique solution to these equations for $S_0 = 0$ in which the densities are unity at all surface elements, and this is a necessary requirement for a set of valid equations. Two of the assumptions necessary to the derivation by Whitman and Motzfeldt require that $n(\rho')$ be a constant: (1) the assumption that the rate of effusion is the fraction S_0/S_1 of the total arrival rate at the top of the lid, and (2) the assumption that of the molecules moving toward the bottom the fraction $[1 - W(H,1,1)]$ are reflected back to the top. These are assumptions which are true only for the trivial case that the orifice were of zero area. It follows then that the extent of

saturation calculable from their equation is either less than or greater than the rigorous value calculable from the present equations.

One will notice that the foregoing equations are applicable to the Clausing problem when S_0 is given the value S_1. Consequently, the Clausing factor is $W(H,P,1)_{P=1;\alpha=1}$, and it bears no direct relation to the problem under consideration. Indeed the present problem involves that of deducing the quantity $W(H,P,1)$ for general values of H and P including, in a broad sense, the value P = 1. Therefore, a derivation based upon the use of $W(H,1,1)$ totally obscures the real problem.

The first four of the questions posed earlier may be answered by simple considerations. First, if the walls are a sink for the vapor molecules, the emission densities are zero, whereas the collision densities are due only to those molecules which evaporate and proceed directly to the area under consideration. Consequently, the molecules arriving in unit time at the orifice come directly from the evaporation surface S_1, and by equation (5.3-20) the arrival rate at the orifice becomes

$$\frac{dn}{dt} = Z_e S_1 \cdot 2K(H,P,1)$$

$$= Z_e G(S_1 S_0) \quad . \qquad (5.4\text{-}13)$$

This result illustrates the fact that the location of the evaporation surface with respect to the orifice influences the directional arrival rate at the orifice, for the normalized emission densities in general are less than unity except, by assumption, at the evaporation surface. Therefore, with the particular geometrical arrangement considered in the present analysis, in the directions of molecules having trajectories intersecting the orifice and evaporation surface, the vapor behaves as if it were saturated, but in all other directions at the orifice the vapor would behave as if it were undersaturated.

The effect of the location of the evaporation surface may be illustrated in another way. If the entire enclosure were covered uniformly with the evaporating substance, then $n(\eta)$ would be unity. Consequently, $\Delta = 0$, and $p(0) = p_e$. For this reason, it is advisable that the evaporation surface in a Knudsen cell cover as large an area as possible.

If we consider for a moment that the orifice were real but that all other specifications of the problem were unchanged, then it follows from the previous considerations that a measurement of the vapor pressure of the evaporating substance by a sampling of the molecular beam in directions normal to the orifice would correspond more directly to a measure of a saturation pressure than would a measurement of the total rate of effusion. For example, if the condensation receiver above the orifice, as discussed in section 4.4, were arranged such that it had a direct view only of the evaporating sample, then the source of saturated molecules could be taken as the orifice, and the cosine law could be applied to the orifice - receiver geometrical arrangement to yield the correct flux at the receiver and consequently, the correct value for p_e, despite the fact that the vapor in cell is undersaturated. On this basis, one could state that the sampling of the molecular beam in directions normal to the orifice gives a more reliable measure of the saturation pressure than does a total rate of effusion measurements.

It is not difficult to demonstrate the effect of the geometrical parameters H and P. For example, the leading term in the equation (5.3-21) for $n(\eta)$ comes close to zero for large values of η. The integral term compensates considerably for this decrease, but nevertheless $n(\eta)$ probably departs most significantly in the upper regions of the enclosure. The combined effect of the various functions leads one to the natural conclusion that the larger is H the more undersaturated the vapor becomes and the greater the value of $\Delta(H,P)$ becomes. The δ equations illustrate most clearly the effect

of P. Because each of the terms in the equation (5.4-9) for $\delta(\eta)$ is positive, the leading term is a minimum contribution:

$$\delta(\eta) \geq \frac{\partial}{\partial\eta} K(H-\eta,P,1) \quad . \tag{5.4-14}$$

This function is nearly zero for small values of P and the behavior of this function may be considered as a strictly qualitative picture of the variation of the depletion of the emission density. In general, $\delta(\eta)$ increases as P increases.

(2) A Minimum Value for the Extent of Saturation

It is instructive and admittedly more satisfying that we obtain now a direct indication of the extent of saturation, and it is possible to do this without detailed numerical considerations by employing some simple properties of the integral equations. One will remember that the emission density equations are bounded, so that

$$0 \leq \delta(\eta) \leq 1 \quad ,$$

and

$$0 \leq \delta(\rho') \leq 1 \quad . \tag{5.4-15}$$

Consequently it should be possible to find a solution, within these defined regions, which we know to be a maximum value for the function $\delta(\eta)$. We wish to consider, in fact, the iterate properties of the equations in order to construct such a function, and it is most convenient to search for a constant value, $\delta(H,P) \geq \delta(\eta)$ over $0 \leq \eta \leq H$.

The iterate, $I\left\{f(\eta)\right\}$, of the arbitrary function $f(\eta)$ is defined by the equation

$$\begin{aligned} I\left\{f(\eta)\right\} = & \frac{\partial}{\partial\eta} K(H-\eta,P,1) \\ & + \int_0^H f(\eta') \frac{\partial^2}{\partial\eta\partial\eta'} K(|\eta-\eta'|,1,1)d\eta' \\ & + \int_P^1 f(\rho') \frac{\partial^2}{\partial\eta\partial\rho'} K(H-\eta,\rho',1)d\rho', \end{aligned} \tag{5.4-16}$$

where

$$f(\rho') = \frac{1}{\rho'} \int_0^H f(\eta') \quad \frac{\partial^2}{\partial\eta\partial\rho'} \quad K(H-\eta, \rho', 1)d\eta \quad . \qquad (5.4\text{-}17)$$

From this definition, it follows that

$$I \quad \left\{\delta(\eta)\right\} \quad = \delta(\eta) \quad . \qquad (5.4\text{-}18)$$

In Appendix I it is demonstrated that if the condition

$$I \quad \left\{f(\eta)\right\} \leq \quad f(\eta) \qquad (5.4\text{-}19)$$

is satisfied, then

$$\delta(\eta) \quad \leq \quad I \quad \left\{f(\eta)\right\} \quad \leq \quad f(\eta) \qquad (5.4\text{-}20)$$

over the range $0 \leq \eta \leq H$. We may employ this to construct a constant function $\delta(H,P)$ which satisfies the condition

$$\delta(\eta) \quad \leq \quad \delta(H,P) \quad \text{for} \quad 0 \leq \eta \leq H \qquad (5.4\text{-}21)$$

to obtain a minimum value for the extent of saturation.

First, we assume that

$$I \quad \left\{\delta(H,P)\right\} \leq \quad \delta(H,P) \quad , \qquad (5.4\text{-}22)$$

and determine then the conditions necessary numerically to satisfy this requirement. From the equations (5.4-9) and (5.4-10), and the above assumption, one obtains the equations,

$$\delta(H,P) \geq I \left\{\delta(H,P)\right\}$$

$$0 \geq [1 - \delta(H,P)] \frac{\partial}{\partial\eta} K(H-\eta,P,1) + \delta(H,P) \frac{\partial}{\partial\eta} K(\eta,1,1)$$

$$- \delta(H,P) \frac{\partial}{\partial\eta} \int_P^1 \frac{1}{\rho'} \frac{\partial}{\partial\rho'} K(H,\rho',1) \frac{\partial}{\partial\rho'} K(H-\eta,\rho',1)d\rho' \quad , \qquad (5.4\text{-}23)$$

and it is only necessary to maximize this to find a value for $\delta(H,P)$ which ensures that the condition (5.4-21) be true. The integral term

presents little difficulty if one does not require an exact procedure for maximizing. It is easily demonstrated that

$$\frac{1}{\rho'} \frac{\partial}{\partial \rho'} K(H, \rho', 1)_{\text{min. on } \rho'} = \frac{1}{2} \left[1 - \frac{H}{\sqrt{H^2 + 4}}\right]$$

$$= \left\{\frac{1}{\rho'} \frac{\partial}{\partial \rho'} K(H, \rho', 1)\right\}_{\rho' = 1} \equiv G(H,1) \quad . \qquad (5.4\text{-}24)$$

Thus, the integral term in equation (5.4-23) is greater than

$$G(H,1) \left\{\frac{\partial}{\partial \eta} K(H-\eta, 1, 1) - \frac{\partial}{\partial \eta} K(H-\eta, P, 1)\right\} \quad . \qquad (5.4\text{-}25)$$

The second term of (5.4-25) goes through a maximum in the region of $H - \eta < 1$ so that a choice in the minimum value becomes difficult. However, if we restrict our consideration to values of H greater than unity, we may take

$$\frac{\partial}{\partial \eta} \int_P^1 \frac{1}{\rho'} \frac{\partial}{\partial \rho'} K(H, \rho', 1) \frac{\partial}{\partial \rho'} K(H-\eta, \rho', 1)$$

$$\geq G(H,1)[F(H,1) - F(H,P)] \quad , \qquad (5.4\text{-}26)$$

where

$$F(H,1) = \left\{\frac{\partial}{\partial \eta} K(H-\eta, 1, 1)\right\}_{\eta=0} ,$$

$$F(H,P) = \left\{\frac{\partial}{\partial \eta} K(H-\eta, P, 1)\right\}_{\eta=0} . \qquad (5.4\text{-}27)$$

Also, we may take

$$\frac{\partial}{\partial \eta} K(H-\eta, P, 1) \leq \frac{P^2}{2} \quad ,$$

$$\left.\begin{array}{l} \frac{\partial}{\partial \eta} K(H-\eta, 1, 1) \\ - \frac{\partial}{\partial \eta} K(\eta, 1, 1) \end{array}\right\} \geq \left\{\frac{\partial}{\partial \eta} K(H-\eta, 1, 1)\right\}_{\eta=0} \equiv F(H,1) \quad . \qquad (5.4\text{-}28)$$

We then have

$$\delta(\eta) \leq \delta(H,P) \leq \frac{P^2}{2F(H,1) + 2G(H,1)[F(H,1) - F(HP)] + P^2}$$

for

$$0 \leq \eta \leq H \text{ and } H \geq 1 \quad . \qquad (5.4\text{-}29)$$

This value for $\delta(\eta)$ is, therefore, the maximum value of the extent of undersaturation; that is, the wall emission density $n(\eta)$ is greater than 1 - $\delta(H,P)$ at each elemental surface area.

This function $\delta(H,P)$ faithfully, although not accurately, reproduces the effect of the geometrical parameters. The term multiplied by G(H,1) represents part of the contribution of the "lid" to the saturation. For Knudsen cells of normal dimensions, reasonable values for the geometrical parameters would be

$$P = 0.1 \quad ,$$
$$H = 2 \quad .$$

Thus, from the Figure 5.4, in which is represented the parametric dependence of the functions (5.4-24) and (5.4-27), we obtain

$$F(H,1) = 0.0607 \quad ,$$
$$F(H,P) = 0.0008 \quad ,$$
$$G(H,1) = 0.1465 \quad .$$

Consequently,

$$\delta(H,P) = 0.067 \quad .$$

From the formula (5.3-16), we find for the above parameters

$$K(0,P,1) = \tfrac{1}{2}P^2 = 0.005 \quad ,$$
$$K(H,P,1) = 0.001 \quad .$$

These yield

$$\Delta(H,P) = 0.054 \quad .$$

Therefore, the extent of saturation is at least 94 percent of the equilibrium value. It should be emphasized that in this analysis we have not accrued unknown numerical errors to the extent of 6 per cent, but we know on the basis of the initial specification of the problem that 94 percent is a minimum value for the extent of saturation in a cell of the above dimensions. A value of P equal to 0.01 leads to a saturation of 99 percent for the same value of H.

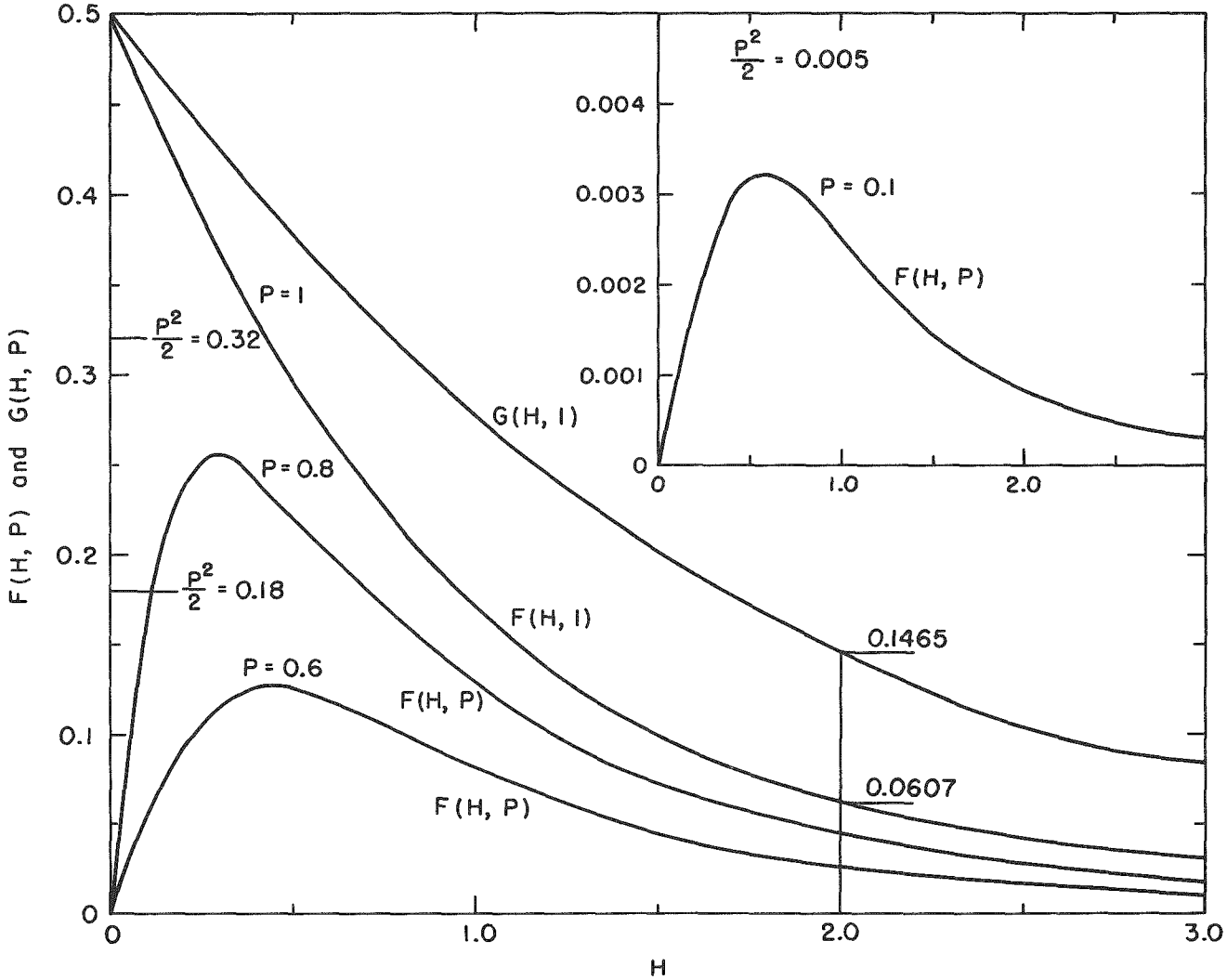

Fig. 5.4 Parametric Dependence of Certain Probability Functions Derived from the Cosine Law

(c) The Open Cell

We have demonstrated that, beginning with a consistent formulation, one may deduce certain kinetic aspects of the behavior of molecules in an equilibrium enclosure. Admittedly, the formal results appear to be mathematically cumbersome with respect to numerical results, but a direct analysis of the properties of the equations enables one to retain the initial consistency in obtaining a result having known limitations. We now inquire into the applicability of this analysis to the real effusion process. Immediately we are confronted with the fact that the present analysis is based entirely on equilibrium considerations of the gas phase whereas the real effusion process is irreversible, and there are no rigorous principles presently known to permit one to make a valid transformation from the equilibrium to the general steady state.

One must recognize two general limitations in the application of the equilibrium analysis to a description of the irreversible processes. First, the thermal characteristics of the equilibrium enclosure are decidedly not those of an open system. Second, considerations of the equilibrium gas phase alone do not permit one to choose a priori the complete description of reflection and evaporation phenomena. Moreover, these limitations are not entirely separable since our present knowledge of irreversible phenomena indicate that the thermal and gas-solid interaction characteristics are coupled for the open system. The thermal properties of an open cell depend principally on the experimental conditions, but one cannot entirely avoid the occurrence of thermal gradients in the cell, for the orifice is a heat sink. Consequently, in answer to the last question posed in section 5.1, the most important limitation to the orifice dimensions is the tolerable extent of temperature inhomogeneity. The reflection and evaporation processes in the open cell depend on the thermal characteristics of the enclosure, and this should be obvious from the

details of the mathematical analysis, since the thermal speeds of the molecules are an intimate part of the cosine law. One may illustrate this in a manner which emphasizes the coupling of the thermal and reflection processes for an arbitrary value of the quantity α, which is known generally as the vaporization coefficient.

In the foregoing analysis the quantity α was taken as unity, so that the normalized emission rate at the evaporation surface was unity. The equations developed as a result of this specification are easily modified for an unspecified value of α, which in a closed system necessarily equals the condensation coefficient. Thus, in addition to taking the normalized emission density as α for the directly evaporated molecules, one must add to each of the equations a term accounting for the fraction $(1 - \alpha)$ of the molecules reflected without condensation. Since the collision density at the evaporation surface is $n(\rho)$, then presumably $(1 - \alpha)$ of these reflect. Consequently, the total emission density from surface S_1 is $\alpha + (1 - \alpha)n(\rho)$ at each elemental area. The equations then may be developed similarly to the present analysis, but the numerical evaluation of the wall emission density depends on the solution of three simultaneous equations, for the collision density $n(\rho)$ directly enters the problem. The quantity α, moreover, does not simply factor out of the equations, but becomes a complicated part of the prescription of the emission densities. Now, an analysis on this basis if transferred to the description of the real effusion process leaves this question to be answered: if a fraction $(1 - \alpha)$ of the molecules does not condense, is this fraction thermally accommodated or not ? If it is not, then the equilibrium cosine law is certainly not applicable and the nature of the problem becomes more complicated.

It must be argued further for the sake of consistency that, if one attributes a vaporization coefficient to the evaporating material, then he should probably attribute a vaporization coefficient, although not necessarily the same one, to the wall emission densities, for an

initially clean surface exposed to a vapor condenses at least a monolayer of the vapor molecules.[56] Since one of the mechanisms which may lead to the phenomenon of random reflections is the condensation-evaporation mechanism, it therefore follows that if a fraction of molecules reflects without condensation one must inquire whether reflections are random or according to some other specification, and whether thermal accommodation is nevertheless obtained. The complications arising here are due to the fact that considerations of the equilibrium gas phase alone permit only general aspects to be deduced. Specifically, there can be placed no more importance from these equilibrium considerations alone on the arbitrary coefficient α than there can be placed on the arbitrary selection of totally random directions of reflection. Since at equilibrium reflected and evaporated molecules cannot be distinguished one from the other, α cannot be measured under true equilibrium conditions. Therefore α has no useful significance for an equilibrium system. Only under the conditions of an irreversible process can α be measured, but then α necessarily is dependent upon the irreversible conditions. These are the conditions which must be scrutinized before a useful, generally applicable significance may be attributed to the quantity α and to the assumption of equal probabilities of reflection in an open system.

In spite of the difficulties associated with the application of this analysis to a real effusion process, one nevertheless may take the analysis to be a qualitative indication of the extent of saturation attributable to the size and shape of the Knudsen cell for very low gas densities. The limitations, however, must be recognized, so that a rigorous solution of the kinetic equations should not and clearly cannot be used to deduce a priori corrections to measured values of the vapor pressure of the condensed substance. Nor can meaningful vaporization coefficients be measured by the effusion method, since there is no justification for believing that the aspects of the problem are those

used in these deductions. It is these last two remarks which the writer wishes to emphasize in particular, for as Prüger[37] has remarked, only an analysis which begins with the fundamental aspects of the condensed state is capable of yielding a rigorous and unique concept of the vaporization coefficient and the mechanism of gas-solid interactions. The present analysis clearly demonstrates this fact because an arbitrarily unique concept was necessarily assumed in the initial specification of the problem.

CHAPTER 6

INTRODUCTION TO THE EXPERIMENTAL STUDY

This chapter concludes the review of the published experimental studies of effusion behavior, some of its basic theory, and an analysis of the Knudsen cell.

The discussions in the previous chapters have been given in slightly more detail than usual. This was done not only because of their bearing on the present study, but because of their importance to an understanding of the effusion methods of measuring physico-chemical properties. These topics have been reported only piecemeal in sources other than the original papers. The particular emphasis on the cosine law was given in part as an introduction to its application in the analysis of vapor saturation.

The experimental aspects of effusion are briefly summarized in the following pages. Also, some additional remarks are made which seem particularly appropriate at this time. Following this summary, a brief prospectus of the experimental work is outlined to coordinate the background material and present experimental work. A description of the principal experiments of the present study are presented, and finally the results of some preliminary experiments are reviewed.

6.1 Summary Aspects of Effusion

At very low pressures the flow of a gas through a thin orifice from one reservoir to another presumably is given by the molecular flow formula (2.1-1), derivable from equilibrium kinetic theory. Under these same pressure conditions but with an orifice of appreciable length, the flow is reduced by a factor which, on the basis of diffuse scattering of molecules from the wall, is calculable under isothermal conditions from the geometrical configuration of the orifice.

As the source pressure is increased, the flow progresses through some kind of a transitional behavior into a fluid behavior which depends again on the geometrical aspects of the orifice and the expansion processes of the gas in question. For flow into a vacuum through a thin orifice, the rate presumably is predictable by the usual hydrodynamic formula, for example, the so-called isothermal effusion formula (2.2-3) such as Knudsen applied in his studies. The flow through orifices of appreciable extent depends on frictional and viscous effects. For long circular tubes the flow is viscous and predictable from Poiseuille's law with appropriate corrections for slip and expansion of the gas.

(a) Flow through Thin-edged Orifices

From the various experiments reported, one finds no definitive evidence concerning the conditions leading to the transition from molecular flow to viscous flow. Knudsen, on the one hand, indicated that for flow through thin orifices the transition sets in at an average pressure corresponding to a mean free path-to-diameter ratio of about 10 for an average pressure. This corresponds to a ratio of 5 for unilateral (vacuum) flow. The studies of Knauer and Stern and of Mayer lead to comparative ratios in order-of-magnitude agreement with Knudsen, whereas Johnson brings evidence to support an argument in favor of molecular flow occurring at a mean free path-to-diameter ratios much less than a tenth, which is well within the region of gas densities at which Knudsen observed isothermal effusion.

Knudsen was the only one of these experimenters to study the total flow behavior of gases. Knauer and Stern, and Johnson measured beam intensities in a direction normal to the orifice. Mayer measured the distribution of momentum up to angles of 80° from the normal and at a pressure of 4.5 mm Hg he observed a distribution corresponding to the cosine law value. If all of these observations except those of Johnson are taken to be in agreement within an order

of magnitude, one then concludes that molecular effusion occurs at least up to a pressure corresponding to a mean free path comparable with the orifice dimensions. Beyond this pressure the evidence is decidedly contradictory. The data for permanent gases in Knudsen's studies indicate the occurrence of hydrodynamical flow at a much lower source pressure than those pressures which for mercury, according to Johnson, yielded a beam apparently in accordance with the cosine law. Even accepting the the fact that classical mean free path calculations may not be definitive for molecular beam studies, it is difficult to reconcile these data. We shall return again to this problem after the present experimental data are presented.

It should be said here that vapor pressure measurements by methods of molecular effusion are carried out both with total flow measurements and by molecular beam procedures, whereby a portion of the vapor beam in a direction normal to the orifice is condensed and weighted by appropriate methods. Molecular beam methods such as this may be plagued, however, by the transition of the flow from the known molecular effusion behavior. It is quite useful to extend vapor pressure measurement to the highest possible pressures by these methods, since at high temperatures, and thus at higher vapor pressures, ordinarily minor vapor species may occur in measureable quantities. Thus the "upper limit" becomes important in the design of such experiments.

Therefore the upper limit problem has two aspects; not only that concerning the vapor density conditions at which the transition sets in, but the problem concerning the effect of this occurrence on the intensity or flux of the molecular beam. For example, Ackermann, Gilles, and Thorn[43] recently have carried out vapor pressure measurements with uranium dioxide by these methods up to pressures corresponding to a mean free path of about one-tenth of the orifice diameter. They observed an increase in the measured pressure from that

attributable to a vapor corresponding to a single molecular species. They attributed this to the existence of additional vapor species having a larger sublimation heat. These conclusions, however, have subsequently proved to be incorrect, and other thermodynamical reasoning has not proved to offer satisfactory explanations.[57] These investigators had analyzed the evidence concerning the upper limit and concluded that the evidence, principally Johnson's experiments, seems to favor the idea that a transitional flow region did not occur at least at pressures well within the region of their measured pressure increase.

(b) Flow of Gases through Orifices of Appreciable Length

The effect of an orifice having appreciable length on the molecular flow behavior of a gas or vapor presumably is correctly taken into account by the so-called Clausing factor, which is dependent only on the macroscopic geometrical arrangement of the orifice. The experimental evidence predominantly seems to favor a totally diffuse reflection behavior, so that it has been a general practice to use Clausing's factors, which are based on this assumption. In a few experiments there has been evidence for the occurrence of specular reflections. One may cite here the suggestion by Clausing[34] that some of Mayer's results are explainable on this basis.

Some recent work by Huggil[58] and by Berman and Lund[59] seems to indicate that path-reversal reflections occur. Berman and Lund present what they claim to be evidence that the transmission coefficient for molecular flow is gas dependent and offer a graphical representation of various flow measurements in support of this claim. The flow data were obtained from experiments similar to those of Knudsen. A transmission coefficient was calculated on the basis of the molecular flow formula from their measurements of the pressure change with time as gas flowed from one to another reservoir through an orifice. These calculated coefficients were plotted against a function

of the pressure which is, on the basis of classical kinetic theory, proportional to the reciprocal of the mean free path. The coefficients were then extrapolated to zero pressure.

A diffuse reflection mechanism of gas-solid interactions should have shown at low pressures an independence of the gas and pressure. Berman and Lund's data, on the other hand, at average pressures from several mm Hg down to values corresponding to mean free paths of about 10 times the orifice diameter showed a nearly linear dependence of the calculated transmission coefficient with the average pressure for both a thin-edged orifice and an orifice having a length equal to about three times the radius. No pressure-independent values were obtained. The straight lines were extrapolated to zero pressure and the intersection at the ordinate was taken as the zero-pressure transmission coefficient.

For the thin-edged orifice, the data all fell on the same line. For the above-mentioned tube, the various gases defined different lines and thus had different intersections, some of which, if not all, lay below Clausing's value of the transmission coefficient. Even if one assumes that this coefficient may be gas dependent, it is difficult to see how it might be pressure dependent at very low pressures in the same way that it is under effusive conditions at higher pressure. It is more plausible to suppose that their lowest pressure data were not in the molecular flow region and that extrapolation to zero pressure was not justifiable. The dependence of the extrapolated coefficients on the gas could easily be a result of viscous flow effects and thus indicate nothing fundamental in regard to the molecular reflection mechanism at the wall. Indeed, viscous effects on the flow of gases become quite important for tubes of appreciable length, and for very long tubes, as Knudsen and others have shown, there is a continuous change from molecular flow to Poiseuille flow. At very low pressures Knudsen observed a flow dependent on diffuse reflection within the limit of his precision of about 3 percent.

6.2 Prospectus

The experimental study to be reported is concerned now with the aspects reviewed in the previous discussion, principally the departure from molecular effusion and the study of the transition flow of vapor through tubes of appreciable length. The experiments are designed so that, as much as possible, data of good precision may be obtained to answer unequivocally some of the questions concerning these aspects and to demonstrate the possibilities of carrying out precision effusion measurements.

The experimental substance used for this study was mercury, and it was chosen principally because the requisite physical properties are reasonably well established, as is discussed subsequently. But it is of interest that mercury be studied because it was the substance used by Johnson in his molecular beam investigation which yielded results having considerable discrepancies with those of others. The present investigation is concerned only with total effusion rates, so that all of the questions related to the upper limit may not be answered. But even this limited aspect has not been answered unequivocally, and thus a partial understanding is of value. The experiments and equipment were designed so that the measurements could be extended well into and beyond the transitional regions, so that an adequate picture may be drawn of these aspects. A study of the unilateral flow of mercury vapor through channels of appreciable extent has some interest in relation to whether at least an estimation of the viscosity of the effusing vapor might be obtained by such a technique. Methods of measuring vapor viscosities at temperatures above 1000°C are quite limited, but information of this nature is of value. Effusion techniques, although subject to limitations, are easily carried out in principle, so that conditions might be found which enable one to determine the vapor viscosity of the effusing substance.

In spite of the criticism that the writer may appear to be inconsistent, the question of saturation of vapor within the effusion cells used in the subsequent study is not examined with respect to the formalism described in Chapter 5. The data probably do not extend to low enough vapor densities to ensure the requisite pressure condition specified in the analysis, and besides, more detailed numerical computations would be necessary to make the analysis of sufficient precision to permit adequate conclusions to be drawn. In addition, there are those mentioned aspects of the correspondence of the theoretical analysis to a real process which without some serious, detailed considerations would yield precisely those inconsistencies which we tried to avoid at the outset of the discussion by the acceptance of a rigidly limited system.

6.3 Design of the Principal Experiments

The principal experiments were similar to those used to measure vapor pressure by molecular flow methods. A condensed substance, in these experiments mercury, is maintained at a constant temperature, and its presumably saturated vapor is allowed to effuse from a reservoir through an orifice of known dimensions into a highly evacuated chamber. The weight loss of material from the reservoir in a measured period of time is determined by appropriate methods.

These experiments differ from those with unsaturated gases principally in that the pressure in the source reservoir is determined by the temperature with the advantage that, in principle, a virtual steady-state flow is easily obtained by the maintenance of a constant temperature. Other advantages and disadvantages, too, are common to this method, but the interest in this kind of experiment is its direct relationship with the effusion methods for the study of the vapors of condensable substances.

The experimental variables in the flow measurements are weight loss, time, and temperature. The flow rate parameters are derived from these variables. Since the experiments were directed to the

measurement with high precision of both the molecular and fluid flow behaviors, and as well the transition between them, it was necessary to design the equipment and methods consistent with the following requirements:

(1) A reliable, sensitive, and absolute technique for measuring flow rates over several orders of magnitude;

(2) A good vacuum system;

(3) A constant, uniform temperature of the source reservoir or oven;

(4) An experimental substance whose vapor is monatomic and has well established equilibrium and transport properties.

(a) Mercury as the Experimental Substance

Mercury was chosen as the experimental substance because as a metal and as a substance having vapor pressures up to one atmosphere at moderate temperatures, heating requirements would be no severe problem and temperature gradients would be relatively minor compared with those possibly incurred with the use of substances of low thermal conductivity. The vapor pressure and vapor viscosity of mercury are reasonably well established; mercury, in fact, is the only metal whose vapor viscosity has been measured over a reasonably extended temperature range. There is a small amount of viscosity data for zinc and cadmium[60] and no measured viscosity data for other metals.

The vapor pressure and viscosity data and appropriate equations are summarized in Appendix 2. The vapor pressure equation used in the analysis of the flow data is derived from the data of Busey and Giauque:[61]

$$\log p(\text{mm Hg}) = 10.80644 - \frac{3322.183}{T} - 0.95768 \log T + 0.073859 \times 10^{-6} T^2. \qquad (6.3\text{-}1)$$

Mercury vapor at one atmosphere has gas imperfections of less than 2 percent, so that dimerization has an entirely negligible effect in these experiments. The reliability of the vapor pressures derived from the

equation (6.3-1) may be taken as about 2 per cent over the temperature range of the present experiments.

The vapor viscosity equation is taken from the data of Braune, Basch, and Wentzel:[60]

$$\mu(10^{-7} \text{ poise}) = -43.7883 \sqrt{T} + 11.472\ T. \qquad (6.3\text{-}2)$$

Unfortunately, values derived from this equation have rather large uncertainties for the various reasons outlined in Appendix 2. However, one may assume a reliability of about 10 percent over the temperature range of the present experiments.

(b) Outline of the Basic Experiments

The mercury was contained in especially designed effusion ovens constructed of stainless steel. The orifices of these ovens were either knife-edged, circular small holes, or circularly cylindrical channels cut from steel hypodermic needles and welded to the oven. Except for the orifices, these ovens were welded vacuum-tight.

Several methods of measuring the mass flow rate of mercury were initially considered before a final choice was made. There are two principal types of methods available. The first and more direct method is the measurement of the loss in weight of the effusion oven. The second consists of condensing the effusate and determining the mass by direct weighing or chemical assay. The latter is a method having considerable problems, however, for if the distribution of the effusate is not known it is necessary that the total effusate be condensed. For these experiments the first method seemed most appropriate because of its directness.

Consequently, the first two mentioned requirements on the equipment were reasonably well satisfied by the use of a semimicro vacuum balance designed for measuring losses of weight in vacuum from one milligram to 100 grams. The balance, which was an ordinary chainomatic-type, simply modified for these experiments, was maintained

in a vacuum system as an integral part of the experimental apparatus. The effusion oven was suspended on long rods supported from the stirrup of one arm of the beam and centered within a liquid nitrogen-cooled, evacuated glass envelope.

The oven was heated by induction-heating equipment controlled by a thermocouple fused to the effusion oven and maintained by a control circuit to within 0.25°C. The temperature controller, which basically was a null balance potentiometer device, behaved sufficiently reproducible to allow the oven to be taken rapidly to a predetermined temperature and then maintained at this temperature with the above precision for a long period of time.

The details of these various components are described in subsequent chapters.

6.4 Some Preliminary Studies

Prior to a final decision on the specific design of the primary apparatus, a number of preliminary studies were made to answer questions on techniques, procedures, and design. These were concerned with the problems of eliminating temperature gradients, measuring reliable temperatures, and avoiding clogging of the orifice. Three series of experiments were carried out in these studies with equipment which was not used for the primary sets of experiments. The designs of this equipment and results of these studies are outlined in this section.

(a) Series 1

The most troublesome problem associated with measurements on saturated vapors is that of ensuring uniformity, reliability, and precision of temperature measurements. Gradients and errors in temperature yield large uncertainties in the vapor pressure calculated from an erroneously measured temperature. The first problem studied in this regard was that of temperature uniformity. The series 1 experiments and associated equipment were designed for this study.

Specifically, the problem of concern was whether the orifice as a long, narrow tube could be heated uniformly to the same temperature as that of the body of the oven and the contained mercury sample to avoid troublesome condensation of the effusing vapor in this channeled orifice. An effusion oven was therefore designed so that the orifice could be heated independently of the body of the oven.

(1) The Apparatus

Figure 6.4 illustrates the principal features of the apparatus, which, except for the oven, was constructed initially from existing components. The oven was constructed of welded stainless steel in the same way as subsequent ovens which are later described. It was circular with a diameter and length of about $1\frac{1}{4}$ inches. The orifice consisted of a hypodermic needle of 0.03-mm radius and 3-cm length welded slightly off-set along the diameter of the front face of the effusion oven. On the opposite face of the oven a kovar-glass window fused to a kovar metal ring of about $\frac{1}{4}$-inch diameter was welded coaxially with the cylindrical orifice.

The oven and orifice were wrapped separately with insulated nichrome heating wires having a common junction with an outer steel jacket supported at the end of a steel rod, as shown in the figure. Chromel-alumel thermocouples of 0.003-inch diameter were spot-welded, one to the oven body and the other to the orifice near its outer end. The heating wires and thermocouples were led to a brass plate to which the oven support rod was silver soldered and out of the vacuum system through Stupakoff seals. The heating power was supplied from two variable-voltage isolation transformers. The thermocouple voltages were measured with a potentiometer.

The brass plate containing the oven-support rod was sealed by an "O" ring to a brass collar which was sealed with Apiezon wax w to a lip on the pyrex glass vacuum chamber. This plate could be rotated to align the orifice with the optical window on the sight tube

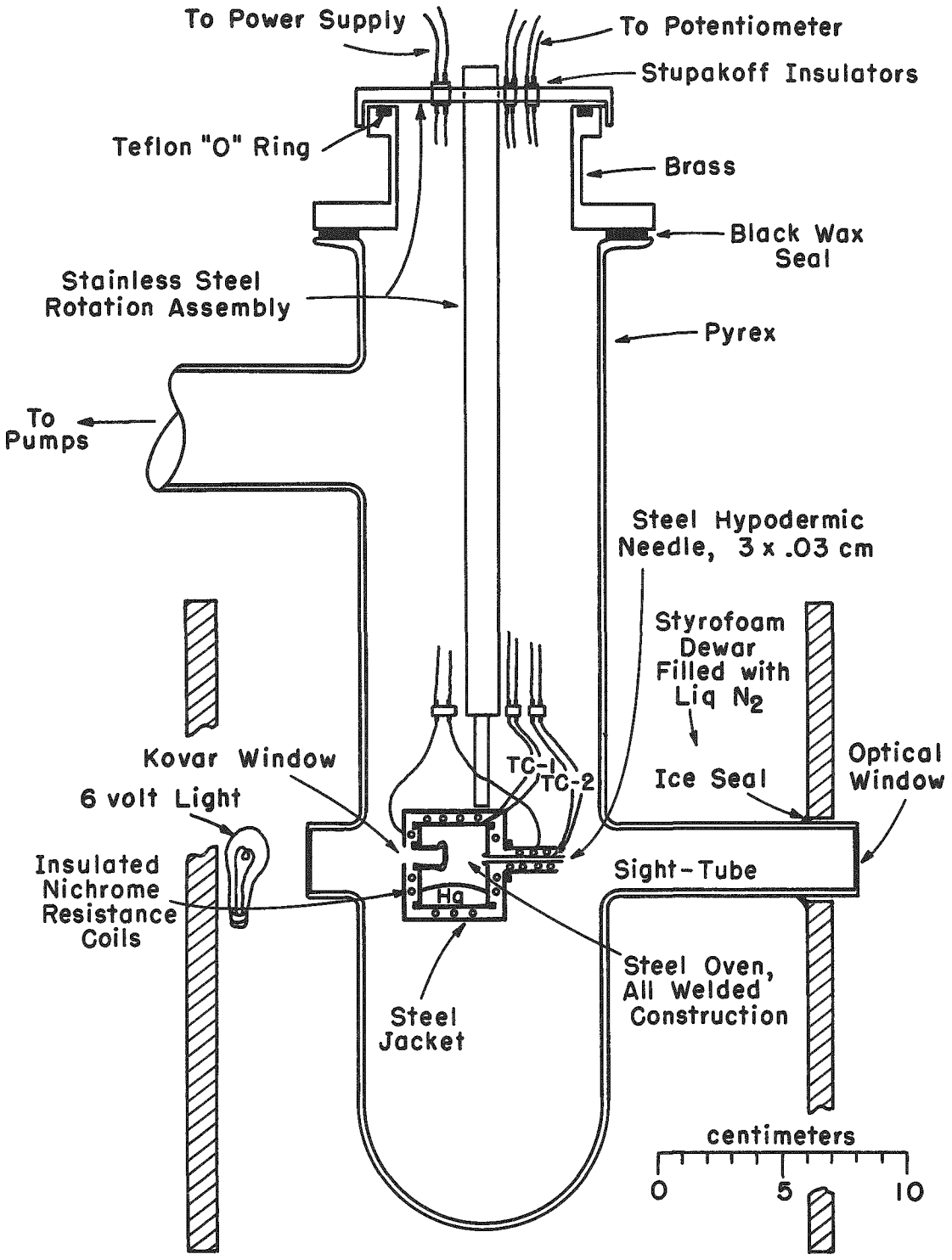

Fig. 6.4 Apparatus Used for Series 1

and the beam of light from a 6-volt lamp. The vacuum chamber was evacuated with the usual pumping equipment and immersed in liquid nitrogen nearly up to the evacuation tube.

The liquid nitrogen was contained in a styrofoam Dewar. The sight tube projected out of the Dewar and was sealed to it by an ice layer. The optical window on the sight tube was warmed by a blast of air to prevent condensation there of the effusing mercury.

(2) Methods and Results

Eleven experiments were made with the apparatus described. Five of these comprised trial heatings and temperature calibrations, and six consisted of actual flow measurements. Some effort was made to obtain quantitative data by weighing the entire support rod, oven, and associated parts before and after an experiment, but these efforts were futile and only the temperature information, for which these experiments were actually designed, was useful. The methods and results are descriptively summarized here.

The oven was filled with pure mercury through the orifice with a syringe and hypodermic needle and assembled in the vacuum system. The orifice was aligned with the window of the sight tube and the small lamp so that a beam of light illuminated the interior of the orifice channel, which could then be viewed from the window of the sight tube.

Various methods of heating the oven to a constant temperature were tried. In one experiment, the power to both the orifice and body was slowly increased to maintain a uniform temperature; in the others, the power to both was rapidly applied. In all cases the interior of the orifice was continually observed for the occurrence of adverse condensation effects. No untoward behavior, however, was noted, even for orifice temperatures of about 1°C less than the body temperature and at a vapor pressure of nearly 30 mm Hg.

The mercury condensed on the liquid nitrogen-cooled walls of the vacuum chamber was in appearance nearly uniform up to 90° measured from the axis of the cylindrical orifice. At 90° there was a sharp drop in the deposit thickness and beyond this the walls of the vessel were fairly clean. Thus it was concluded that the mercury was satisfactorily condensed on the walls with negligible occurrence of scattering.

A final experiment in this series showed that even with the cylindrical orifice being 50°C cooler than the body, the condensation in the channel was negligible at a source pressure of 20 mm. There appeared to be an occasional rapid decrease in the intensity of the light as viewed through the orifice, and it was inferred that this was due to the formation of small droplets which after formation fell back into the liquid mercury. At no time was the orifice completely clogged.

After the oven had attained a constant temperature, helium was rapidly admitted to the vacuum system to a pressure of 400 mm Hg. The oven cooled from 200°C to 0°C in about one minute, but the effusion of vapor was stopped almost immediately and no mercury froze in the orifice. This appeared to be an excellent procedure for quickly stopping an experiment. A vacuum of 10^{-6}mm Hg could be attained again in about 20 minutes after the oven was cooled.

Several disturbing occurrences were noted in these experiments, and these ultimately led to the final design of the ovens and heating procedures. First, there was a severe heat lag in the oven assembly and this caused considerable warm-up troubles. For example, it required nearly a half-hour to attain a constant, uniform temperature. Second, it was found that however desirable in principle it was to heat the orifice separately, in practice the adjustment problems became so cumbersome as to negate its usefulness. However, these experiments seemed to indicate that the vapor itself effected some warming of the orifice, and that effect along with thermal conduction decreased the external power requirements for the orifice.

Based on the knowledge gained from these experiments an oven of a different design was constructed.

(b) Series 2

It was apparent that an induction-heating procedure would be advisable, because with a properly designed oven it would allow for increased heating response and cumbersome radiation shielding could be eliminated to reduce much of the heat lag which occurred with the previous heating method. Moreover, the induction method appeared to be quite amenable to an oven designed on the basis of experience gained from the initial series. In addition to the heating problem, there were those of weighing the oven and measuring its temperature. Although these might appear to be separate problems, they were at first dependent on one another. Since it was necessary to condense out the effused mercury vapor, the oven could not be placed in an isothermal enclosure.

After some consideration, feasible procedures were devised for the use of a vacuum balance in the flow studies. The experiments comprising the series 2 set were designed for testing these procedures to enable a vacuum balance to be adapted to the principal investigation with a minimum of trouble.

(1) The Apparatus

The oven was similar to that previously described, but it had a re-entrant tube orifice. The tube was of the same length and diameter as the one previously described, but in this new design it projected into the oven, and its exit was welded into the face of the oven coaxially with the cylinder walls. The oven was about $1\frac{1}{2}$ inches in height and about $\frac{3}{4}$ inch in diameter.

The oven was supported on long tungsten rods from a vacuum balance which had been used previously in this laboratory for a number of volatility experiments. The oven and vacuum balance and the experimental methods used in this series are basically identical with those to be discussed in subsequent chapters, so the details of these are not outlined here. The oven was oriented so that the orifice opened

downward, and inside the oven it projected about $\frac{1}{2}$ cm above the mercury sample. In this way the mercury served as a warming bath which, in principle at least, ensured that the channel would be as warm as the mercury and therefore at the same temperature as the presumably saturated vapor.

A single thermocouple was spot-welded to the rear of the oven and brought up along side the support rods and taken across the balance by special contactors which made contact during the heating and disengaged the thermocouple leads during the weighing operations. This procedure, which will be described later in detail, proved quite successful and eliminated a potential problem in adapting a vacuum balance to these studies.

(2) Summary of the Results

The experimental results of this second set of experiments were similar to, but less refined than those of a later series 6 group carried out with the final apparatus. The experiments demonstrated that the vacuum balance with a few new features was adaptable to this investigation and was potentially capable of yielding precision data. The experience gained from these experiments, however, demonstrated the need for a temperature controller and one additional refinement in the design of the oven.

It was discovered that a thermocouple spot welded to the oven did not respond reproducibly for these experiments. It required extremely careful handling after its preparation and offered no assurance of reliability until much time had been invested in carrying out a series of experiments concerned with this problem. The rapid heating and cooling of the oven often caused enough thermal strain at the oven-couple junction to loosen the weld. Consequently, the oven used in series 2 was modified by the additionof a deep thermocouple well which was adequately immersed in the mercury sample. The modified oven was experimentally examined in the series 3 study.

(c) Series 3

The use of thermocouples to measure temperatures of materials heated in vacuum may lead to grave problems, for radiation and conduction losses of heat occur in the region of the couple junction. The previously outlined experiments delineated some of the temperature problems to be solved. The oven modified by the addition of a deep thermocouple well proved to be successful only after an experimental investigation demonstrated the need for especial attention to the placement of the couple in the well.

It was pointed out that a couple spot-welded to the oven was found not to be reliably reproducible and, in fact, proved to be rather fragile as a result of frequent thermal stresses. Therefore, a thermocouple well was designed for the oven; but in a study comprising the series 3 experiments it was found that even under the most nearly ideal conditions the lag in thermal response and the large conduction losses were more severe than anticipated. Although the well was over $1\frac{1}{2}$ inches in depth and the oven was presumably at uniform temperature, the couple placed in the oven measured a temperature about 20°C too low.

Several techniques to improve the thermal response of the couple were tried, but only one proved to be successful. This technique consisted of placing the junction of the thermocouple into a pool of molten silver at the bottom of the well and then allowing the silver to freeze. The frozen silver stuck tightly to both the couple junction and the walls of the well and provided an adequate stable, thermal conductor.

CHAPTER 7
EXPERIMENTAL APPARATUS AND EQUIPMENT

The principal components of the apparatus and equipment used in this experimental study consisted of a specially designed vacuum balance and a temperature controller capable of maintaining temperature constant within 0.25 °C. Measurements were made of the rate of effusion of mercury vapor supplied from the liquid contained in stainless steel ovens. These various components are described in detail in this chapter.

7.1 The Vacuum Balance

The basic design of the vacuum balance was taken from an original design proposed by Ackermann, Rauh, and Thorn of this laboratory and constructed in the Argonne Shops. The principal modifications consisted of additional components which allowed for the use of thermocouples, a wider range in measurable weight changes, and zero-load referencing. Only recently have vacuum balances become commercially available, but none at present will handle the weight range of the present balance nor have its versatility.

(a) General Description

(1) The Balance and Associated Components

A Christian Becker semimicro chainomatic balance, style 16, cleaned of all paint and lacquer, was mounted on a brass platform cut to accommodate the beam-rest lowering mechanism. This platform was centrally anchored to an 18-inch diameter, one-inch thick brass plate, grooved for an "O" ring on which rested a bell jar having a 12-inch diameter base and a height of 18 inches. A chain-weight scale runner was mounted on a similar platform anchored to the base plate in a position nearly relative to that it occupies in a normal case-mounted analytical balance.

These platforms corresponded to the base plate of a case-mounted balance, and, similarly, the gears translating the necessary motions to the beam-rest lowering mechanism and sliding vernier scale of the chain weight were mounted below the platforms. The various gears were fixed to $\frac{1}{4}$-inch shafts which passed through the base plate with "O" ring seals. The beam was lowered and the chain weight set manually for the weighing operations by a rotation of the shafts under the base plate. Except for the removal of paint and lacquer, the balance proper was not modified.

The right-hand end of the beam supported an ordinary balance pan to which was attached a rack for holding Ainsworth wire weights. Ordinary pan weights from 0 to 200 grams could be added to the pan by a simple rack and pinion device. The left-hand stirrup of the beam supported a hanger arrangement which held the rods leading up from the oven. The hanger was designed so that the oven, oven support rods, and associated parts could be disengaged from the beam so that a zero-load rest could be determined. This operation was essential to realizing the semi-micro capabilities of the balance. The mechanism which removed the load was a simply constructed lift operated through "O" ring seals by a shaft projected below the base plate.

The usual kind of pan rest pads was not used. There was no rest pad for the weight pan. A rest mechanism on the oven hanger, however, served a double purpose: it maintained the oven motionless during the heating and quenching operations, and made electrical contact between the thermocouple leads from the oven and the external leads from the temperature-measuring and controlling circuitry. This rest and contactor arrangement was operated from the beam-rest release mechanism.

(2) The Vacuum System

A schematic representation of the balance and vacuum system is given in Figure 7.1-1. The glassware was attached to the balance base plate by machined brass, standard-taper joints bolted to the plate and sealed with "O" rings. The glass-to-metal joints were sealed with Apiezon wax W.

The oven hung from the left arm of the beam into a Pyrex vacuum jacket which served as a condenser. This jacket was immersed in liquid nitrogen to condense the mercury vapor effusing from the oven. Below the right-hand pan was mounted a liquid nitrogen-cooled vapor trap. This had a high conductance compared with usual re-entrant tube traps, but had their pumping efficiency. The vacuum pressure was found to be quite insensitive to the nitrogen level over wide limits since there was no direct path that a molecule from the diffusion pump could follow without striking a cooled surface.

Directly below the trap was an air-cooled Eimac three-stage oil diffusion pump. Oil was used rather than mercury because of the tendency of the latter to "bump" during its heating and thus to jar the balance during a weighing operation. The diffusion pump was backed by a Welch Duo Seal mechanical pump.

The pyrex tubing joined at one end to the condenser union just below the balance and to the stopcock leading to the mechanical pump at the other end was used to admit purified helium to the vacuum system. Attached to this were a mercury manometer and inlet tube. The effusion experiment could be stopped by admitting the helium to the high vacuum side through the condenser union with the stopcocks to the mechanical pump closed. In this way the vacuum system could be flooded with helium without transporting hot oil from the diffusion pump. The liquid nitrogen-cooled re-entrant tube trap condensed out most of the mercury vapor from the manometer, which was used to gauge reproducibly the amount of helium admitted to the system.

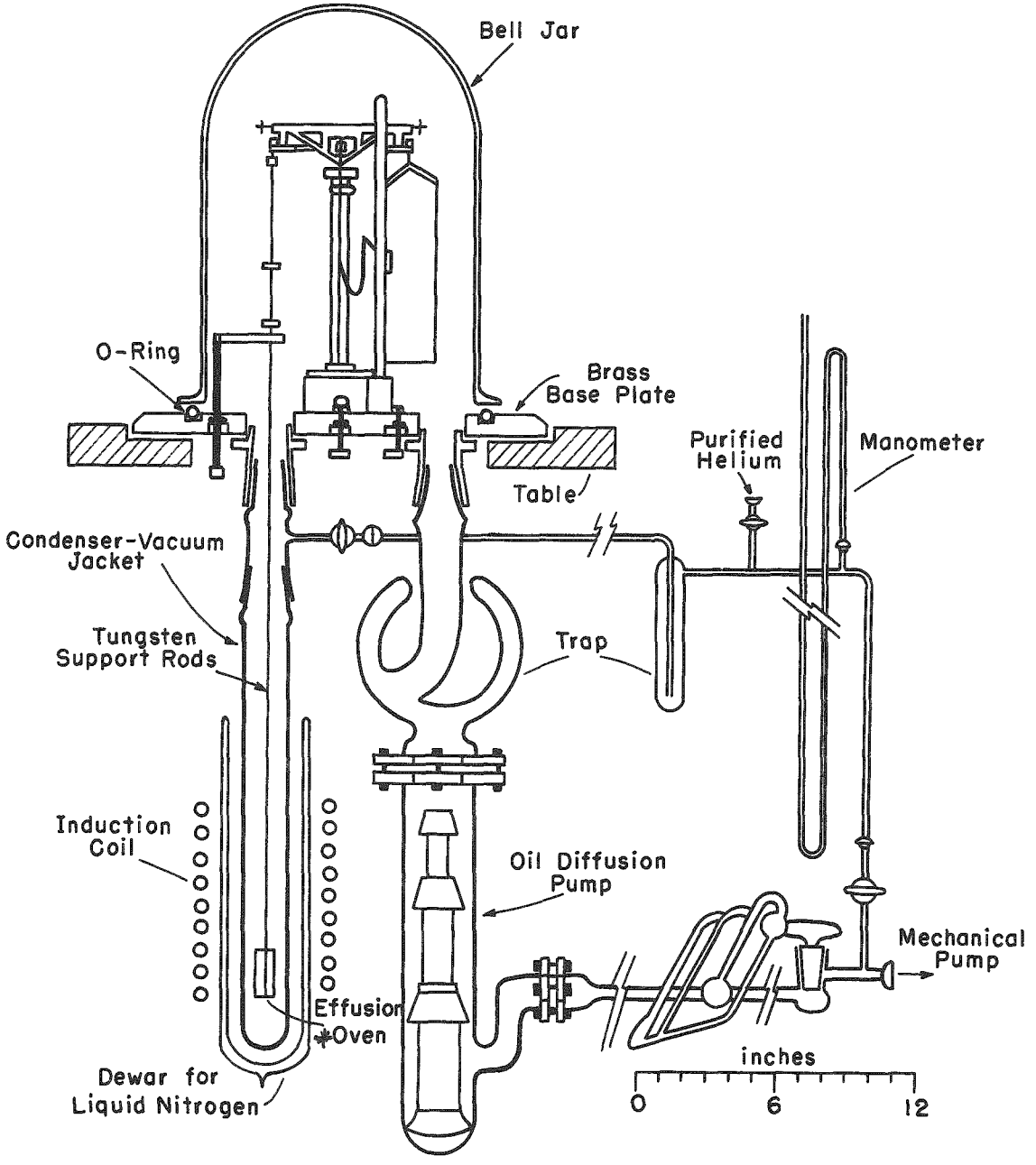

Fig. 7.1-1 Schematic Representation of the Balance Vacuum System

* NOTE:

The effusion oven should be located in the mid-region of the induction coil.

The balance base plate, vacuum system glassware and other associated parts were supported from a table constructed of Unistrut steel beams. This table had leveling screws for adjusting the level of the balance.

The figure illustrates the salient features of the vacuum system. The high vacuum pressure gauge, however, is not shown. This gauge was an ordinary Phillips ionization gauge attached to the base plate behind the balance by a standard tapered brass joint bolted on the underside and sealed with an "O" ring.

(b) The Weight-moving Mechanism

The weight-moving mechanism was a very simple, although versatile apparatus designed to add or subtract ordinary pan weights on the right-hand pan of the balance. The mechanism consisted of a rack-and-pinion-operated fork which slipped under the knobs of the class S pan weights located in pockets machined into brass blocks, as shown in Figure 7.1-2.

The device has three degrees of freedom. Horizontal motion was accomplished with the rack-and-pinion and vertical and rotary motion by the movement of a shaft through greased ring seals from beneath the base plate. The rotary and horizontal movements did not affect the vacuum of about 10^{-6} mm, but the vertical motion caused an order of magnitude pressure increase for about four seconds.

The "L"-shaped piece at the inner end of the fork was used to raise or lower any one of the lever arms of the wire weight holder.. This holder was taken from an Ainsworth keyboard balance and fitted with a shaft attached to the balance column. A nickel saw-tooth rack was supported on the pan rods. When the lever on the weight holder was raised by the "L"-shaped piece on the mover, the selected wire weight was transferred to the rack.

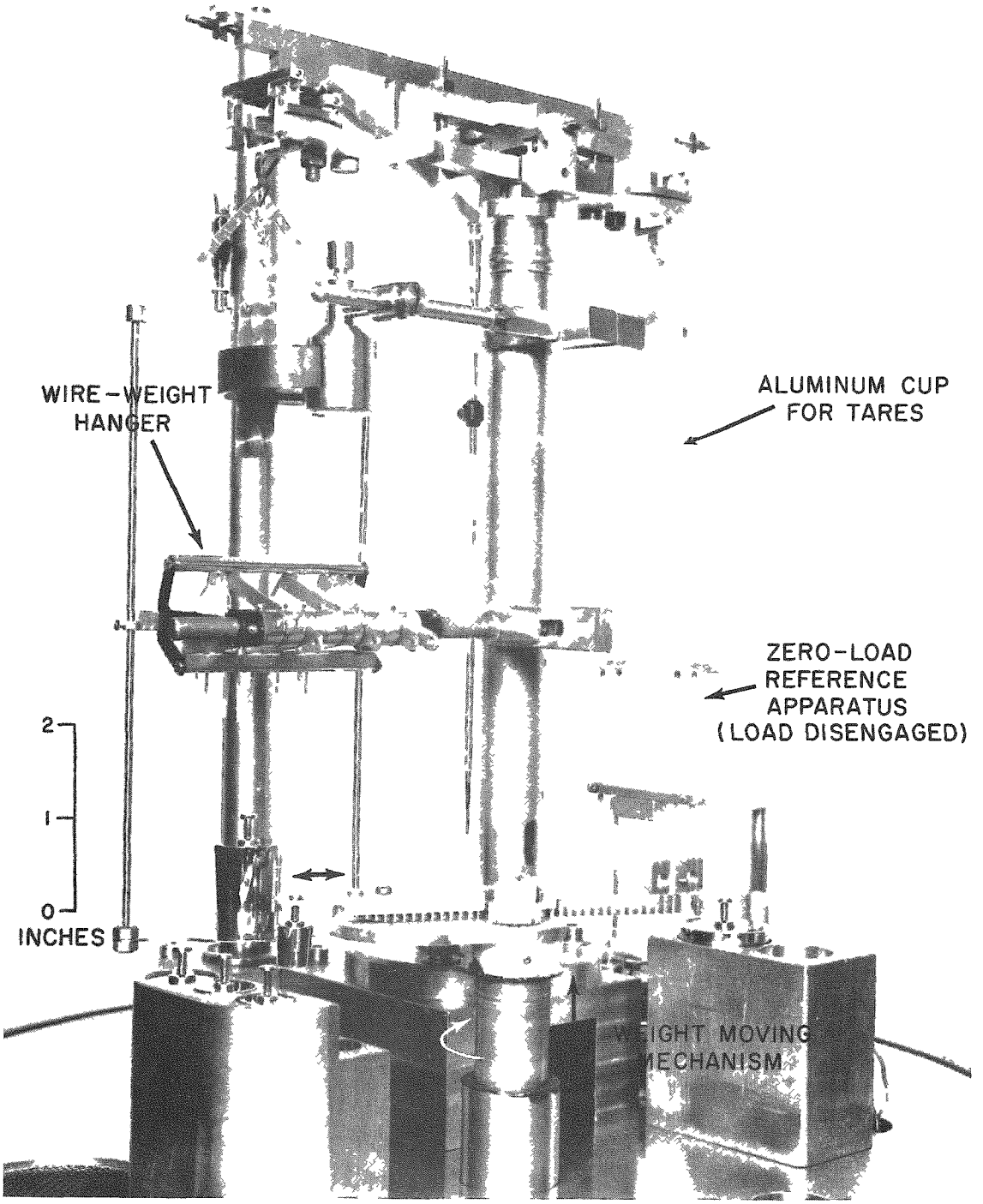

Fig. 7.1-2 Rear-View of Balance

(c) The Zero-load Reference Apparatus

Figure 7.1-2 shows the zero-load reference apparatus with the load disengaged from the balance. The apparatus consisted of a flat brass paddle, as shown in Figure 7.1-3, fixed to a steel shaft which traveled through the base plate of the balance. On being lifted, the paddle engaged the lower brass support bar to which was attached two steel shafts having tapered stops at the top ends. These stops slipped into corresponding tapered holes in the top brass support bar. The taper on the stops and holes served as a semikinematic positioning device.

When the stops were moved out of the positioning holes, the beam of the balance was free to swing independently of the lower support bar and attached load. Consequently this allowed a rest to be determined for a constant reference load.

The aluminum cup hanging under the arch served to contain various tare weights so that a reference load would give a rest point occurring at about the zero point on the scale.

(d) Load Rest and Thermocouple Contactors

The load rest and thermocouple contactors consisted of insulated copper cylinders having finely machined flat surfaces for maximum surface area of contact. The arrangement of the mechanism is shown in Figure 7.1-3. It was screwed to the base plate of the balance below the left extremity of the beam.

A brass T-shaped piece fixed to the forward oven support rod held the two cylindrical contactors to which were attached the ends of the thermocouple leads from the oven. These leads, not shown in the figure, were 32 gauge chromel and alumel wires, each held tightly to a polished side of the contactor with a brass screw. Each contactor was anchored to the T-shaped piece by a nylon screw and was insulated from the piece by a nylon washer, as shown in the inset diagram of Figure 7.1-3.

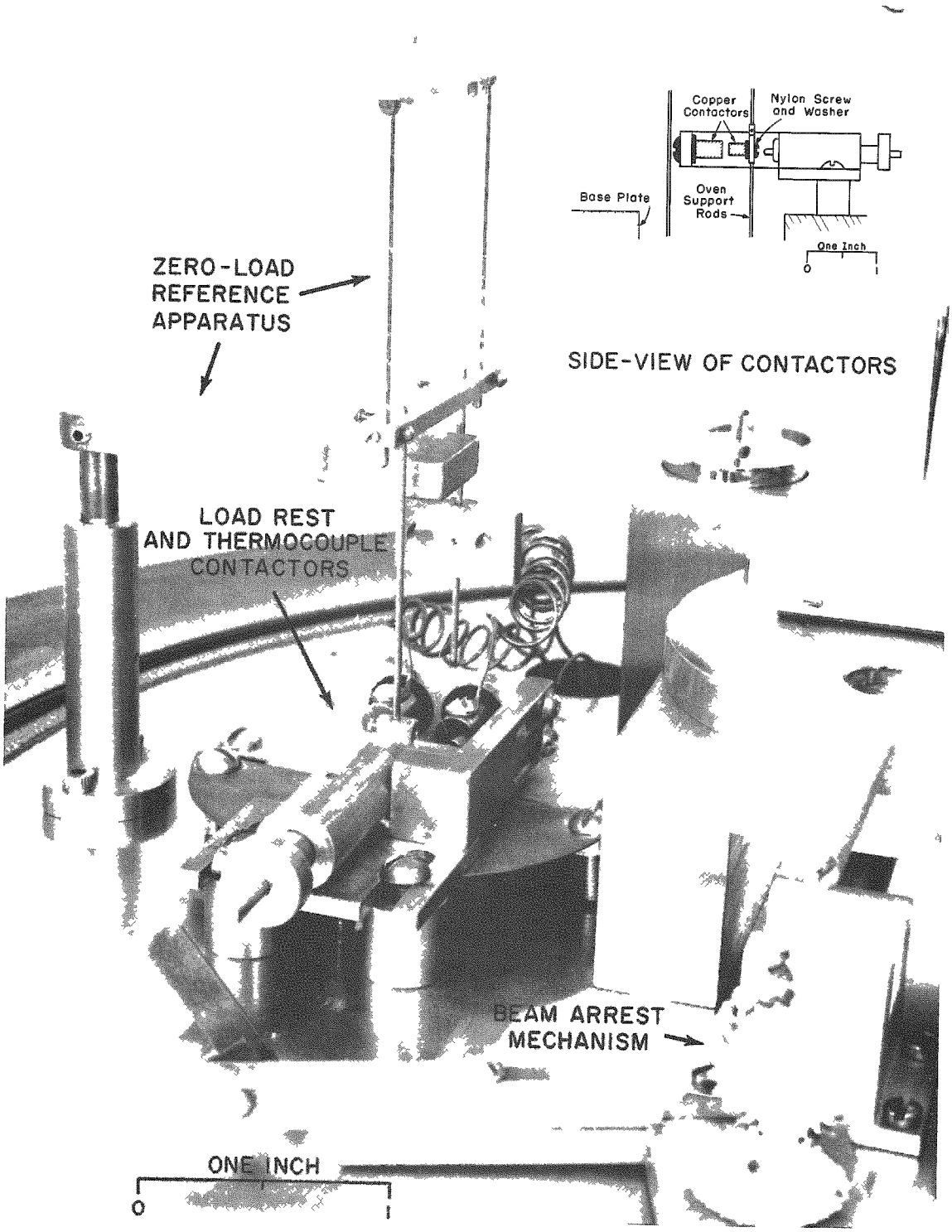

Fig. 7.1-3 Front-View of Balance from the Left Side

The immobile mate contactors were similarly insulated and fixed to a plate which was screwed to the end of an "L"-shaped support attached to the platform of a spring-loaded plunger. Copper wire of 20 gauge was screwed to polished sides on these contactors and was threaded through and soldered to Stupakoff hollow-core insulators sealed to the balance base plate.

The oven and associated parts supported on the left side of the beam normally hung so that the movable contactors cleared their mates by about 2 mm during the weighing operations. An arm having attached at its extremity a strip of phosphor bronze spring was bolted to the rotary gear which operated the beam-arrest mechanism. When the shaft was rotated to arrest the beam, the arm swung up to the plunger and forced the plunger to press the movable contactors firmly against their mates. When the beam was lowered for weighing, the arm moved back and the spring within the cylinder forced the shaft of the plunger away from the contactor to break the electrical contact.

This arrangement of the contactors has proved to be quite satisfactory and apparently solved the biggest problem connected with the use of a vacuum balance for this investigation. The possibility was considered initially that the contactors could be machined from chromel and alumel metals. However, it would still have been necessary to join these to copper leads to reduce the impedance of the thermocouple circuitry.

Admittedly there are several aspects to be criticized and and questioned. For example, contact potentials and uneven heating of the contactors could lead to serious problems; but these are points which may be answered only by the experimental work.

Uneven heating of the contactors was reduced in several ways. First, the natural arrangement of the oven and liquid nitrogen coolant placed these at a considerable distance from the contactors. Since the closest radiating surfaces contribute the majority of radiant energy to the contactors, it appeared to be desirable that a radiation

shield of large surface area be placed under the contactors. Consequently, such a shield was constructed of copper sheet and placed under the contactors and supported above the circular opening in the base plate in such a way that the pumping rate of residual gases within the condenser was not unduly reduced.

7.2 Effusion Ovens

Several ovens were used in this investigation, but the basic design of each was the same. The ovens were designated as 2-A, 3, 7, and 9. Except for the oven used in series 1, which will not be further described, these differed principally in the length-to-radius ratio of the cylindrical orifice. Diagrams of typical ovens are shown in Figure 7.2.

The oven and thermocouple well were fabricated from 304 stainless steel, and the cylindrical orifice was made from a section of a rustless steel hypodermic needle. Stainless steel #304 is not the best material for use with mercury, but it is more easily machined and welded than other types of stainless steels. The first oven constructed and tested showed no visible corrosion damage, and analysis of the mercury sample after use showed only traces of impurities. Insofar as the writer is aware, no trouble was encountered except possibly in series 8, as will be mentioned later.

The cylindrical bodies, 7/8 inch in diameter, were machined from tubing to an approximate length of 2 inches and a wall thickness of 1/16 inch. The ends were constructed to accommodate the circular end plates which were machined from flat stock to avoid the microscopic fissures common to cylindrical stock. A circular groove whose outer edge was inset 1/32 inch from the periphery of the end plate was machined to a depth of 1/16 inch. This groove and the machined end of the cylindrical body formed lips, as shown in the figure, which subsequently were heliarc welded together.

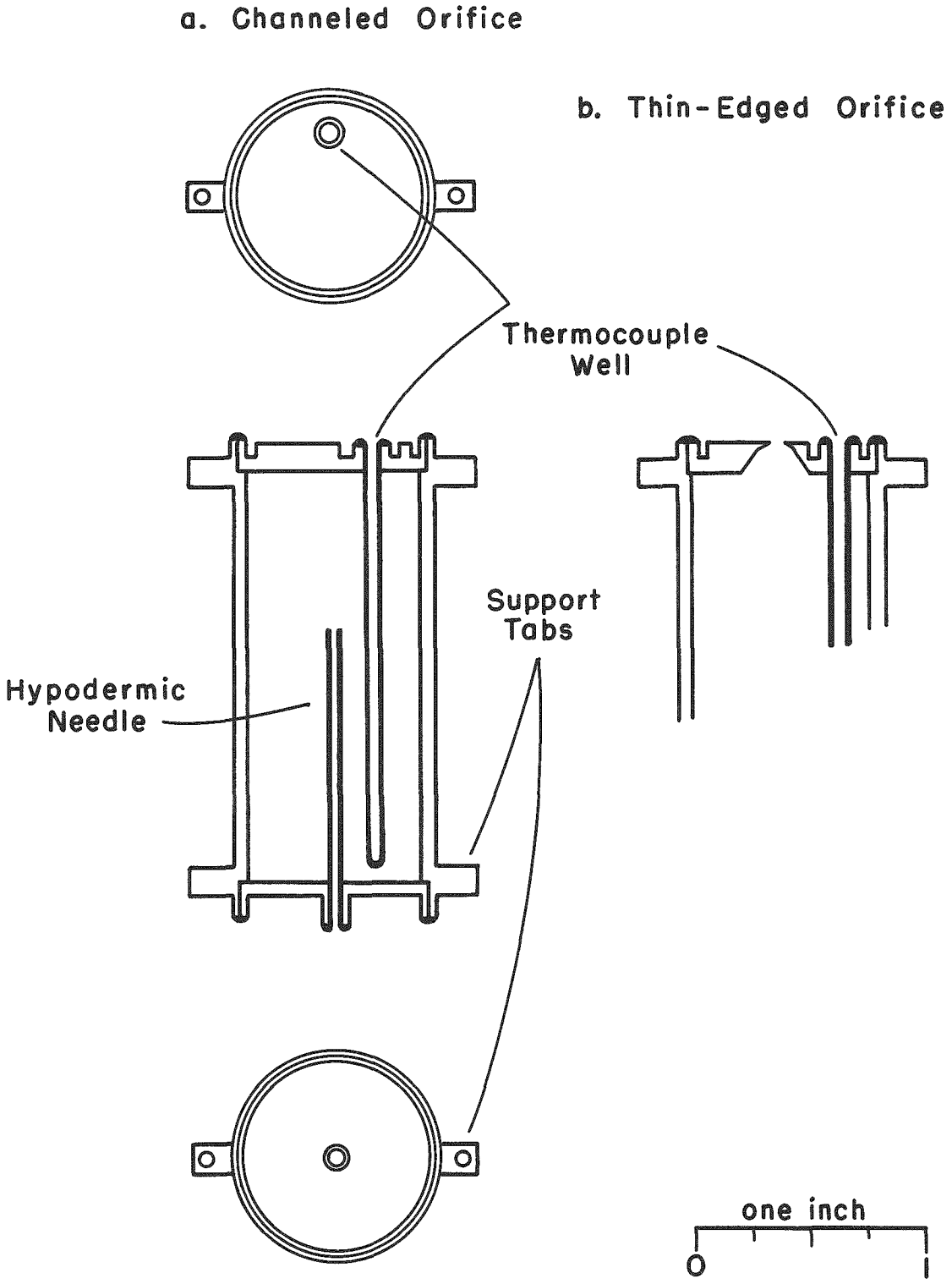

Fig. 7.2 Effusion Ovens

Welding lips for the orifice and thermocouple well were machined as shown in the figure, and had wall thicknesses of slightly less than twice the wall thickness of the orifice and thermocouple well tubing, respectively.

The cylindrical orifices made from the hypodermic needles appeared to have a fairly uniform cross section. A length was cut from the needle, the ends were filed smooth, and after cleaning it was placed in a cylindrical channel in the center of the end plate so that it protruded about 0.005 inch above the outer end of the channel. The fit was snug but not so tight that the needle was distorted. The tip was then heliarc welded to the channel.

With the first ovens constructed there was no evidence that the welded seam at the orifice tip constricted the opening. However, after the series 5 experiments with oven #3, it was discovered that there was a severe constriction at the welded end of the orifice. If these ovens were to be re-designed, it would be best to have the end flared out slightly to avoid this problem, although the original intention was to construct the orifices so that they would have no distortion.

The end of the cylindrical orifice tube protruded slightly above the plane of the peripheral lips to avoid having the vapor beam intercepted by these lips and also to allow the placement, if necessary, of radiation shields in front of the end plate. Although such a protrusion is not good from a heating standpoint, apparently the arrangement gave no troubles and radiation shielding proved to be unnecessary.

The orifice radius and length were measured after the needle had been welded to the front plate. In the assembling of the oven each piece after welding was tested with a helium-sensitive mass spectrometric leak detector. This continual check assured that the orifice was the only opening in the oven.

The thermocouple well was cut from a length of steel tubing of 1/8-inch outer diameter. The one end was crimped, heliarc welded, and leak tested. The other end was then welded into the end plate in

the same manner as was the orifice. The bottom of the well during an experiment was adequately immersed in the mercury sample which had an initial depth of about two centimeters.

The support tabs were either machined as a part of the cylindrical body or cut from 1/8-inch diameter rod and welded to the cylinder. These tabs had holes of 0.05-inch diameter aligned along the plane of the diameter of the oven. These tabs held the tungsten support rods hanging from the balance arm.

7.3 Temperature Controller

The control and measurement of the temperature was accomplished with the same equipment. This simplified the thermocouple circuitry and, more importantly, eliminated the added weight on the balance due to another thermocouple and associated contactor components.

The thermocouple in the well of the oven had insulated leads extending to the balance contactors. From the mate contactors copper wires led through Stupakoff seals in the base plate.

One wire ran to a chromel-alumel 18 gauge thermocouple which was immersed to a depth of 8 inches in an ice-water bath. The lead from this couple and the second lead wire from the Stupakoff seal joined with shielded two-conductor wire connected with the control circuitry. The junction of the couple was grounded through the metal support rods to the balance base plate when the beam was arrested.

The temperature control and measurement circuitry, shown in Figure 7.3, essentially comprised a potentiometer device. The various units were purchased from the Wheelco Instruments Division of the Barber Coleman Company. The circuit consisted of a stable millivolt reference source (Model 350), a capacitrol stepless control galvanometer and amplifier chassis (Model 417), a magnetically modulated current output amplifier (Model MMC), and another magnetic amplifier (Model 610A) which controlled a 4-KVA saturable-core reactor. The saturable reactor was used to vary the output of a 4-KVA induction heater.

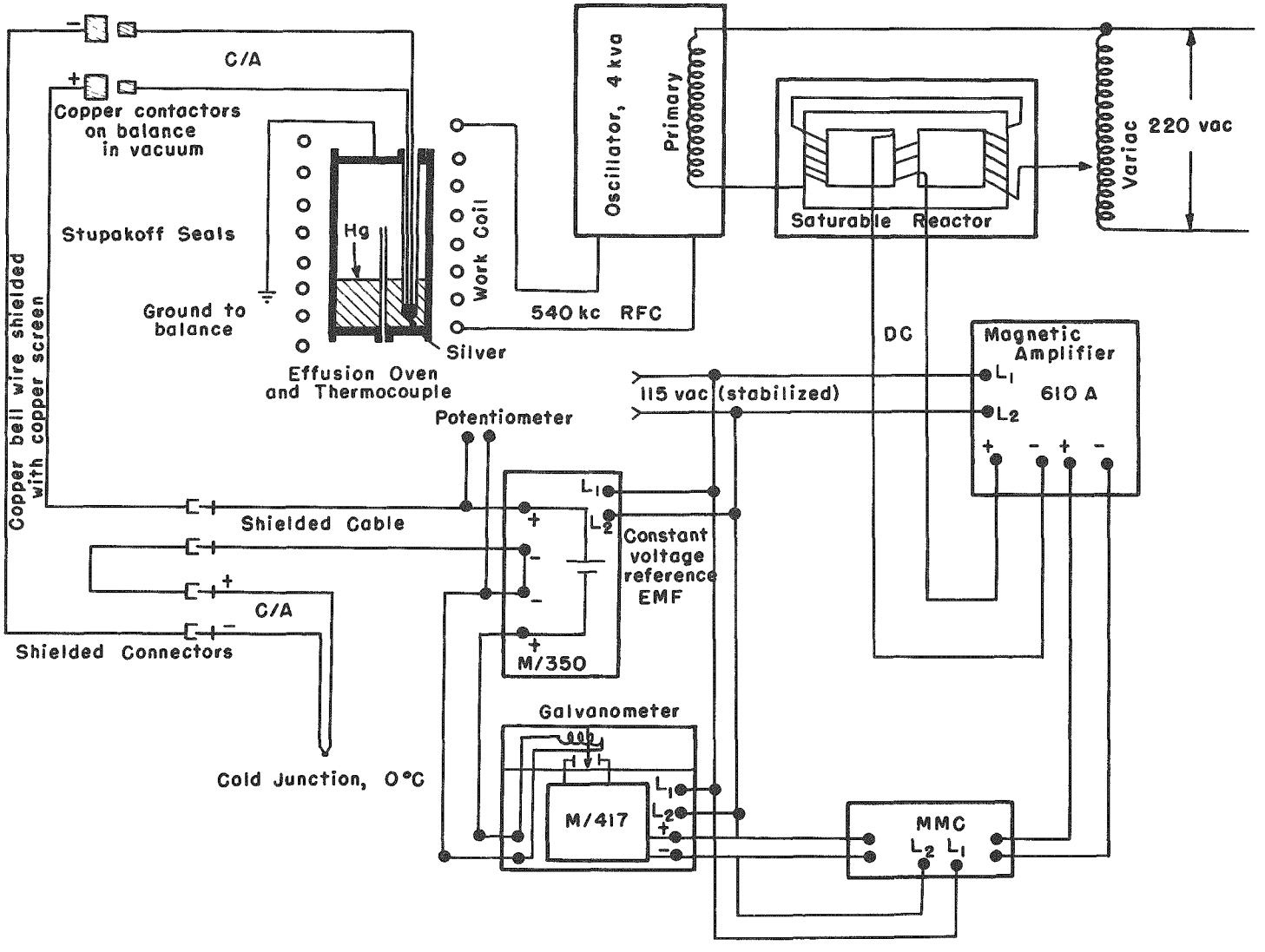

Fig. 7.3 Schematic Diagram of the Temperature Controller and Heating Equipment

The millivolt reference source was a zener diode stabilized, line-powered EMF-reference wired to oppose the thermocouple signal. The unit had a 0 to 80-millivolt adjustable range and a stability of at least two microvolts over a 48-hour period after warm-up. As a general practice, the power to the instrument was maintained continuously to retain its stability.

An output signal from the EMF reference source was selected prior to an experiment. The unbalanced signal due to the difference in the thermocouple and reference voltages was fed to the galvanometer, which had a 3-mv range each side of zero-center and a sensitivity of about 1/10°C for a chromel-alumel couple. The scale of the galvanometer was calibrated over a 20° range about the zero-center in divisions of 0.04 mv per mm.

The galvanometer carried a vane which moved between two pancake oscillator coils and thereby continuously changed the tuning of an oscillator circuit fed by the Model 417 amplifier chassis. The change in the unbalanced thermocouple signal in the range of -0.20 mv to + 0.20 mv caused the output of the amplifier to change from a maximum of 10 volts direct current to zero. With further amplification, this changed the power input to the oven from the induction heater from maximum to minimum power. This, along with the other components, caused the heat input to the oven to attain a steady-state value such that there was a null balance of the thermocouple and reference voltages. The range of the unbalanced signal effective in varying the heat input was referred to as the "proportional band," which signified that the heat input was proportional to the unbalanced signal in this band. On either side of the band, the heat input was constant and independent of the signal.

The 10 to 0-volt output of the Model 417 chassis was fed to the MMC unit, which further amplified the signal and, by various feedback features, added to or subtracted from the signal in anticipation of undesired changes of the heat input to the original source, that is, the oven.

Thus, occasional fluctuations in the temperature of the oven were rapidly compensated to maintain a nearly continuous null balance and therefore a reasonably constant temperature.

The 610A amplifier boosted the MMC output to that voltage required to control the impedance of the 4-KVA saturable-core reactor. This reactor was a variable choke with an impedance that was continuously variable over ranges sufficient to change the line voltage to the primary transformer of the induction heater from about 5 to 200 AC volts. The reactor was wired in series with the primary of the power transformer of the induction oscillator.

The line power input to the induction heater-reactor circuit was fed from a 220-volt Variac. This was used to adjust the maximum heating power so that the MMC unit operated at about 50 percent of its output at null balance. At this output value, it had been found that the oven heating and cooling recovery times were about equal, which conditions ensured the most sensitive control.

This equipment has performed most satisfactorily and has given control of the temperature often within better than 0.25°C. Since the unbalanced signal was nearly zero within small limits, the temperature in terms of chromel-alumel voltages may be taken as the potential of the reference source. The output of this source was measured before and after an experiment with a Leeds and Northrup type 8662 Potentiometer. A more detailed description of the use and operation of the controller is described in Chapter 8.

7.4 Heating Equipment

As mentioned, the ovens were heated by induction. The induction oscillator was a General Electric Model 4F 5A12 electronic heater having a maximum output of about 4 KVA. Although an old model, it served quite well and had more than sufficient power necessary to meet the heating requirements for this investigation.

The induction coil of 27 turns of 1/4-inch diameter copper tubing had a diameter of 5 inches and a length of 10 inches. To ensure the most uniform heating of the oven, the coil should have been longer, but, since the diameter was fixed by the dimensions of the Dewar flask for the liquid nitrogen, the length was somewhat restricted by the efficiency desired and the requisite impedance match to the oscillator circuitry. This work coil, however, appeared to be entirely adequate.

CHAPTER 8

EXPERIMENTAL METHODS

The methods, procedures, and techniques used in the primary experiments were the same for each of the four series to be reported, and these are summarized in this chapter. The first section on techniques outlines the preparational procedures prior to the execution of an experimental series or set of experiments. The second section describes measurements and methods used in deriving the basic flow rate quantities from the experimental measurements. The third section summarizes the standardizations of various components of the apparatus and some miscellaneous details.

8.1 Techniques

(a) Treatment of the Oven and Thermocouple

The oven just prior to use was outgassed at 1000°C for about one hour. This was more than sufficient to remove any of the impurities volatile in the temperature region of the effusion experiments, about 0 to 300°C. The oven was then checked for vacuum-tightness with a helium-sensitive mass spectrometric leak detector. All the ovens used were found to be tight. The oven was then again briefly outgassed prior to the fusing of the thermocouple into the well.

A small slug of silver having a diameter slightly less than that of the thermocouple well, 2 mm, and a length of 5 mm, was prepared by melting and solidifying a weighed amount of silver in a thin, round-bottomed, fused silica tube of the desired inner diameter. The silver slug when cooled was broken out of the tube, rinsed with acetone and dried, and then dropped into the well of the oven.

A thermocouple was prepared of 32 gauge chromel-P and alumel wires of about one meter in length. The couple junction was fused in a flame with a fluoride flux to form a clean spherical tip. The wires were threaded through an eight-inch length of $\frac{1}{16}$-inch diameter,

two-conductor ceramic insulator which extended to within $\frac{3}{16}$ inch of the junction.

The oven was supported in an outgassing vacuum chamber. The thermocouple was placed in the well so that the tip of the junction rested on top of the silver slug. The leads of the couple were fastened to leads coming into the vacuum chamber from a potentiometer, and the top end of the insulator was clipped to a magnetically operated shaft. The chamber was evacuated and the oven heated to about 25° above the silver melting point of 960.8°C. The movable shaft clipped to the thermocouple insulator was forced down with a magnet until the couple junction tip rested on the bottom of the well. The silver was then allowed to freeze.

After the cooled oven had been removed from the vacuum system, the continuity of the couple was checked. The insulator was broken off at the top of the well and the excess piece was discarded. The remaining portion of the insulator in the well was broken at the midpoint to reduce heat losses by conductivity. It was easy to determine from the performance of the couple in subsequent heatings whether or not the leads had shorted in the well, and such an occurrence rarely happened.

(b) Support of the Oven and Thermocouple on the Vacuum Balance

The ends of two tungsten rods of 0.05-inch diameter and 28-inch length were arc melted to form small spherical tips on which the oven support tabs would rest. These were slipped through the support tabs on the sides of the oven and anchored to a brass bar above the thermocouple contactors, as shown in Figure 7.1-3. Very thin-walled silica sheaths drawn from larger tubing were slipped over the thermocouple leads to insulate them from the support rods. The ends of the leads were cut to a desired length and screwed tightly to the polished sides of the contactors. It would have been more satisfactory

to have spot-welded these to the contactor, but so many adjustments and interchanges of ovens with their couples were required that it would have been too restrictive.

The contactors were polished to rid the surfaces of oxide. The oven with its assembled components was placed into the condenser by lowering it through the hole in the base plate and then was attached to the semikinematic support from the balance. The balance post could be rotated on its base to locate the oven in the center of the condenser.

(c) Design and Construction of the Condenser-Vacuum Jacket

The long channeled orifice of the oven opened downward into the condenser-vacuum jacket, and thus only a minimum of vapor could reach the balance chamber since the mercury was adequately condensed on the liquid nitrogen-cooled surfaces of the condenser. The condenser used for the ovens with these channeled orifices consisted of a Pyrex tube 18 cm long rounded at the bottom, and sealed at the top to a 50/50 standard taper joint. With the oven having a thin-edged orifice, which necessarily opened upwards, a different condenser having a side arm Dewar was used. The Dewar fitted between the supporting rods and thermocouple leads without rubbing them. This Dewar was kept filled with liquid nitrogen. Occasionally between experiments the condensed mercury on this Dewar was allowed to warm and drip off a spout at its end to prevent the mercury from falling on the oven.

Cooling rates in vacuum of heated substances below red heat are very slight and as a consequence, temperature control becomes difficult because of the slow approach to a steady-state temperature. The temperature controller was essential in alleviating most of this difficulty. But it was found in the preliminary series 2 that the cooling rates could be slightly increased by using a blackened condenser. A colloidal dispersion of graphite was prepared by mixing about one cc of Aquadag, obtained from the Acheson Colloids Company, with about 40 cc of distilled water and 10 cc of sodium silicate solution.

The proportions are not critical, but the dilution of the Aquadag must be done slowly with constant stirring to avoid destroying the colloidal dispersion.

The solution was then painted on the outside of the cleaned condenser while it was continuously rotated on a glass lathe. The layer was air dried and then baked with a heat lamp. About two coats of solution were found to be sufficient without giving a layer so thick that it flaked off with repeated immersions in liquid nitrogen.

(d) Procedures Preparatory to an Experimental Series

The oven with its associated parts was fixed on the balance and was outgassed at 600°C in vacuum to age the thermocouple and test its performance. The oven assembly was removed then from the balance and the oven was filled with a measured quantity of triply distilled mercury manufactured by F. W. Berk and Company. This filling was done without having to disturb the thermocouple and support assembly by causing the liquid mercury to flow into the oven through the orifice from a syringe and hypodermic needle.

The oven assembly was again supported on the vacuum balance, the proper tares were added to the tare cup, and the radiation shield below the contactors was set in place. One or two trial heatings were carried out to test and adjust the weighing apparatus and temperature controller.

8.2 Measurements, Methods, and Calculations of the Flow Parameters

(a) Experimental Requirements

Each experiment was carried out in a pattern similar except for minor modifications to the description given below. Many of the techniques, however, which finally yielded precision data were developed only by trial and error methods based on the requisite procedures demanded by the kind of experiment carried out and the equipment used.

The temperature controller performed quite well, but it was initially somewhat tricky to induce it to operate exactly in the

desired way. It was necessary to measure a steady-state constant-temperature mass flow rate, and this required a procedure for rapidly warming up the oven to the desired temperature, maintaining it at this temperature for a given period of time, and then quenching the flow processes. Weighings could be made before and after the heating. For several reasons this could not be generally accomplished by attaining the steady-state temperature and then weighing the oven periodically at temperature. First, some of the mass flow rates measured amounted to several milligrams per minute or more, and the balance was not constructed for rapid or continuous weighings. Secondly, the reason that the balance was not so constructed is that the magnetic field effects and static charges were known to severely affect such weighings with substances heated by induction, at least at high power inputs. Also, the thermocouple contactors had to be closed during the heating of the oven.

The problem with rapid warm-ups at relatively low temperatures is that the cooling rate is not sufficient to prevent an overshoot of the temperature and rapid attainment of the steady state. The temperature controller, however, led to a sufficiently reproducible warm-up pattern that it could be used to duplicate the warm-up cycle of an initial experiment. Therefore, initial weight loss corrections could be experimentally determined, and this is illustrated in the description below.

It was discovered during one of the experimental series that the temperature controller was sufficiently stable that contact to the couple during the heating could be broken, and consequently weighings could be made at temperature while the effusion process was occurring without having the temperature drop outside the normal small fluctuations. Several tests, as described later, showed only negligible, if any, effect of the induction field at the low power inputs. This ability to weigh at temperature and to avoid the additional troubles of measuring a correction was discovered too late to be used for all of the experiments, but it was fully exploited in series 8.

The flow processes were quenched by the admission of helium to the vacuum system while the oven and diffusion pump oil were hot. This necessitated purification of the helium, which was very simply done by allowing the helium stream to flow over clean uranium chips heated to about 500°C.

(b) Experimental Procedures

The vacuum system was evacuated to a pressure of 10^{-6} mm and liquid nitrogen was placed in the Dewar surrounding the condenser. The level of this liquid was maintained to within about four to six centimeters from the top of the Dewar flask. The reference millivolt source was set at an approximately desired value, and, with the thermocouple contactors open, its EMF was accurately measured with a potentiometer. The galvanometer of the control unit was adjusted to correspond closely to zero millivolt on the scale. The oven was then weighed. A check on the reference load rest was made if the weight loss was to be small enough to warrant a rest-point correction.

The thermocouple contactors were closed, and with the power to the induction heater off the Variac was set at a high voltage sufficient to warm the oven to temperature in about three to six minutes. the galvanometer needle with the contactors closed was against the stop at the left-hand end of the scale, which corresponded to about -3.0 mv, although the temperature of the oven was generally lower than indicated by this differential value.

The power to an electrical timer and the oscillator was turned on by the activation of a relay system. When the unbalanced signal reached about -3.0 mv, the galvanometer needle began to move up the scale. The time t_i at which this movement began was recorded. As the needle moved into the lower region of the proportional band, frequent time and millivolt readings were recorded. At a reading of -0.20 mv, the Variac was adjusted to a lower voltage sufficient to maintain, as previously described, a moderate balance in the heating and cooling rates at the steady state. The control unit took full control

at this point, and after about two cycles of over and under-shooting by a few degrees brought the heating process to a nearly steady state at which the needle registered about zero millivolt. When the steady state was achieved, the time t_0 was recorded.

Time, millivolt, and vacuum pressure readings were recorded at intervals of two to thirty minutes, depending on the length of the heating period. The controller continuously adjusted the heating power over small limits and, consequently, a slight periodic cycling of the temperature occurred over about $\frac{1}{4}$ to $\frac{1}{8}$°C about the null point. The periodicity of this cycle was frequently altered as true power fluctuations demanded automatic compensations. This required the frequent but random recording of the galvanometer readings so that reasonably accurate averages of the temperature could be obtained.

After a sufficient heating period the steady-state flow process was quenched by the rapid admission of purified helium to the vacuum system to a pressure of about 400 mm Hg. This caused the ionization gauge to trip a relay when the vacuum pressure exceeded 10^{-4} mm Hg and cut the power to the induction heater and diffusion pump and stop the timer. This time was recorded as the final time t_f. The oven was allowed to cool for about 3 minutes before the diffusion pump was again started.

The operating vacuum of 10^{-6} mm Hg was attained again after about 15 to 20 minutes, and the oven was then weighed. The initial warm-up procedure was repeated up to the time at which the steady-state process set in. The flow was then quenched by the admission of helium. The time registered on the stopped timer was recorded as t_f'. A weighing was again made. This second heating was carried out to obtain an experimental warm-up weight loss correction.

In so far as possible the various manipulations involved in these experiments were carried out with reproducible procedures. For example, the time allowed for the cooling of the oven after the quenching

operation was the same for both the primary and warm-up correction experiments. If the apparatus had remained inactive for any extensive period of time, the oven was heated up and then quenched prior to the flow experiment.

The warm-up corrections appeared to be reproducible to within 25 percent and since the actual warm-up weight loss correction amounted to about 5 to 10 percent of the total loss in weight in the primary experiment, the corrected loss had a precision of about 2 to 3 per cent.

For those experiments for which it was found possible to weigh the oven at temperature during the heating, either the flow rate was slight enough that a weighing easily could be made before perceptible changes in the rest point of the balance could be noted, or for slightly higher flow rates the weight pan could be overloaded and the time at which the indicator needle passed zero on the index scale could be measured. Both procedures were found to be reproducible. The cooling rate was sufficiently slight that the oven temperature did not change by more than $\frac{1}{4}$ degree during the weighing operation. Several tests indicated that the induction field gave no problem in weighing.

(c) Calculation of the Flow Parameters and Mass Flow Rate

Figure 8.2 gives a schematic representation of a typical experiment. In this figure, w represents a weighing, and its position at the top of the graph represents the time in the heating sequence with which it is associated. The symbol t denotes time as registered on a timer. The subscripts i and f refer to initial and final values of the respective variables, and t_0 represents the time at which the steady-state heating sets in. The primed symbols represent the variables of the secondary experiment which measured the warm-up corrections; the unprimed symbols represent the variables measured in the primary experiment.

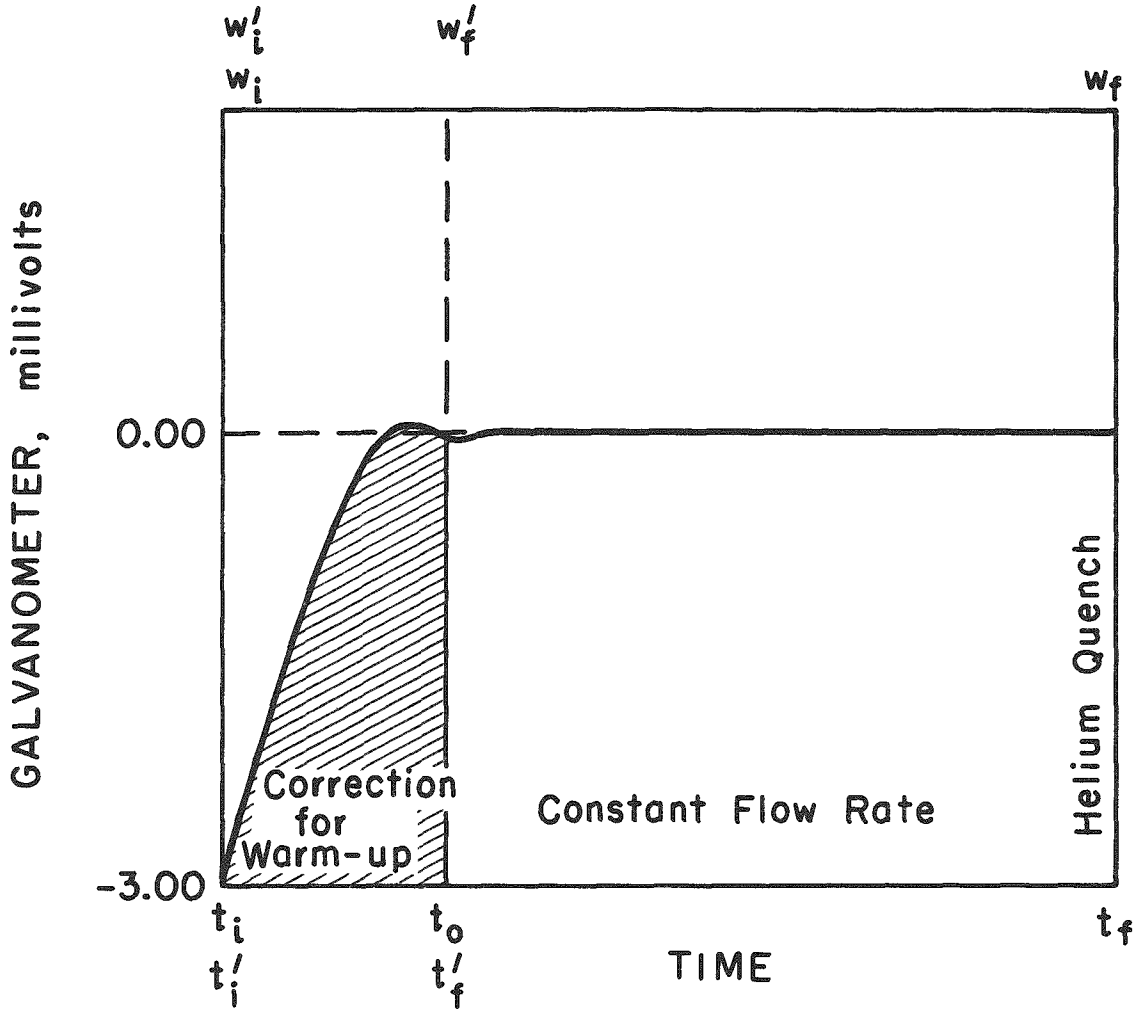

Fig. 8.2 Schematic Representation of an Experiment

From these experimental variables, the constant-temperature weight loss was derived as follows. For the primary experiment, the heating period and total weight loss were given by

$$t_1 = t_f - t_i, \text{ minutes}$$
$$w_1 = w_i - w_f, \text{ milligrams;} \qquad (8.2\text{-}1)$$

and for the secondary experiment,

$$t_2 = t'_f - t'_i ,$$
$$w_2 = w'_i - w'_f . \qquad (8.2\text{-}2)$$

Therefore

$$\frac{dw}{dt} = \frac{w_1 - w_2}{t_1 - t_2}, \text{ mg min}^{-1} \quad . \qquad (8.2\text{-}3)$$

The quantity t_0 does not directly enter these expressions but is used merely as a check on the duplication agreement in the coupled experiments.

The apparent temperature of the oven in millivolts was derived as the sum of three quantities: the galvanometer zero reading E_0, the EMF of the reference source E_r, and the EMF of the average galvanometer readings, E_a. Thus

$$E_{apparent} = E_r + E_a - E_0 \ , \qquad (8.2\text{-}4)$$

where all values are algebraic millivolt readings. The EMF of the reference source was measured both before and after an experiment. Examination of all the data showed this EMF to be constant within the precision of the potentiometer, ± 0.002 mv. The galvanometer rest at zero-input signal, that is, the galvanometer zero reading, was measured both before and after the experiment, and these agreed within better than a deviation of ± 0.003 mv.

The EMF of the thermocouple during an experiment was taken as the group average of all the recorded, ostensibly steady-state millivolt readings, which were about ten or more in number. Some kind of a weighted time average would appear to have been better. However, the fluctuations were small enough certainly that this would have been wasteful of time and effort. The fluctuations were rather taken as a measure of the error so that account is taken of the fact that real but small fluctuations occurred.

The apparent temperature was obtained from the apparent EMF for a corresponding voltage listed in a standard conversion table.[62] The true temperature was taken as the apparent temperature plus a correction term obtained from a plot of correction values vs apparent temperature, as discussed in the next section.

8.3 Mercury Analysis, Standardizations, and Orifice Dimensions

(a) Mercury Analysis

The same stocks of mercury and materials for the construction of the ovens were used in all the effusion experiments. A test of the purity of the mercury both before and after a series of experiments should be indicative of the purity for all experiments. After the preliminary series 1, the mercury was removed from the oven and analyzed spectroscopically for trace elements. Both the initial and residual mercury had detectable traces of cobalt, nickel and manganese of the order of less than 0.00002 percent Accordingly, no further purificiation prior to the principal experiments was deemed necessary.

(b) Standardization of the Temperature Controller and Thermocouples

(1) The Galvanometer

Since the galvanometer indicator of the temperature controller was used for the measurement of the temperature as well as for control purposes, the scale was standardized against a potentiometer. It was found that a scale division of one millimeter corresponded to 0.04 millivolt over the usable range of the galvanometer scale under

a circuit impedance identical to that of the thermocouple circuit. Consequently, the scale calibrations were taken as 0.04 millivolt per millimeter. The voltage of the reference source was directly measured with a potentiometer prior to and at the completion of every experiment.

(2) Reliability Tests, Experiments 60 and 61.

Because of the method used in transferring the oven's thermocouple signal through contactors to the external detectors, it seemed desirable that some direct test be made of the reliability of the measured temperatures. Experiments 60 and 61 were carried out for this purpose at the completion of a set of experiments denoted as series 5. For experiment 60, two thermocouples were fused into silver in a well drilled into a steel cylinder having dimensions similar to those of the effusion ovens. The leads of one couple were joined with the contactors and the leads of the other were taken through a side arm in the condenser and directly to a reference junction and potentiometer. The temperatures of the two couples were compared at several steady-state temperatures. The leads and reference junctions were then reversed and similar comparisons made so that the combined results would be independent of the standardization corrections. The results were not definitive for several reasons, however. Kinks and bends in the leads taken through the side arm were difficult to avoid because of the limited space available for manipulations required in the assembling of the cylinder and associated parts in the condenser. In one case the contact between the silver and junction changed enough to affect the comparison during the experiment. The results indicated that the measurement of the temperature by the controller was reliable at least within 0.40 degree. A more detailed experiment would have been necessary to determine whether the reliability was better. The series 8 set of the experiments, however, would indicate that absolute errors were less than 0.40 degree. Since the thermocouple circuitry effectively had additional hot and cold junctions due to the junctions between the chromel-to-copper and alumel-to-copper connections, an error equal to the temperature difference between

the contactors and external connections will occur. This should have been corrected, but these experiments just described indicate that no serious trouble occurred. The present experiments indicate that if the error is real, it is such that the apparent temperature is too low in the low-temperature regions around 50°C.

In experiment 61 a test was made of the effect of both the radiated energy from the heated oven and the radiofrequency field of the induction coil on the thermocouple signal. Various radiation shields were placed below the contactors to shield them from the thermal radiation of the oven, but no changes in the signal were detectable. Measurements of a steady-state temperature of the oven, both with the heating power on and momentarily off, showed no differences at various values of the input power. One must conclude that these effects were negligible for the experimental conditions prevailing in the present experiments and that temperatures measured by the control units were reliable within 0.40 degree or better.

(3) Thermocouples

The thermocouples were standardized in situ by intercomparison with a platinum-platinum, 10 percent rhodium couple which was standardized against the freezing points of metal samples certified by the National Bureau of Standards. After all experiments had been completed, the oven with its thermocouple and the standard couple was placed in the cavity of a thick cylinder of copper, which was heated under a hydrogen atmosphere in a controlled tube furnace. Intercomparisons of the thermocouple voltages were made at three temperatures over the temperature range of the experiments. Direct measurements at the ice point gave a fourth standardization point for each of the thermocouples. Corrections to the apparent temperature as taken from a table[62] of standard voltage versus temperature on the International Centigrade Scale, 1948, were obtained from a smooth curve of the correction values plotted against the apparent temperature.

The cavity of the copper cylinder initially was found to have a temperature change of no greater than 0.25 degree from one to the other end, a length of about four inches. The junction of the standard thermocouple was placed on the outside of the oven at a position corresponding to that of the junction of the oven couple. The data for the four ovens are cited in Table 8.3-1. The two sets reported for oven 9 correspond to two different positions of the standard couple: set 1 for the standard couple placed on the outside of the oven, as was done in the other measurements, and set 2 for the standard couple placed within the oven. The orifice of oven 9 was drilled out so that the standard couple could be placed within the oven. The two sets agreed substantially in the low-temperature regions but disagreed at the highest temperature. The data show that the furnace was changing temperature fairly rapidly in this last measurement of set 2, so that this measurement may be invalid. The smoothed curve was drawn as an average of these, however. For the most part, the reported corrections are an average of three groups of three measurements of the comparative

TABLE 8 3-1

Thermocouple Standardization Data

Thermocouple for Oven Number	Experimental Series	Apparent Temperature (°C)	True minus Appar Temp (°C)(Measured by Intercomparison)	True minus Appar Temp (°C) (smooth Values)	True minus Appar Temp (°C)(Freezing-Point Standardization)
2-A	6	-0 20	0 20	0 16	0 20
		73	0 34	0 23	0 20
		163	0 38	0 49	0 26
		329	1 47	1 40	0 80
3	5	-0 15	0 15	0 10	
		59	0 15	0 17	
		162	0 58	0 58	
		318	1 81	1 81	
7	7	-0 08	0 08	0 08	
		59	0 23	0 23	
		162	0 74	0 76	
		317	2 16	2 15	
9 (Set 1)	8	-0 15	0 15	0 14	
		61	0 19	0 20	
		168	0 55	0 59	
		303	1 75	2 04	
(Set 2)	8	58	0 17	0 18	
		157	0 52	0 52	
		263	1 75	1 46	

temperatures. The precision of these averages is between 0.05 and 0.15 degree. It is believed that the reliability of the smoothed corrections is about 0.25 degree or better at the lower temperatures and about 0.5 degree or better at the higher temperatures in the region of 300 degrees. The residual voltage at the ice point appears to be due to a slight composition difference between the oven couple and reference junction.

After the thermocouple of oven 2-A was standardized by intercomparison, it was removed from the well by melting the silver in vacuum; the junction was removed free of silver. The couple was then standardized with freezing point samples. The resulting standardization gave values from which are obtained those reported in the penultimate column of the data for oven 2-A. These values are lower than those resulting from the intercomparison. The latter, however, are applicable to the couple junction as it existed in the silver within the well, and thus the intercomparison in situ is probably the more applicable to the conditions unique to the effusion experiments. It would have been more satisfactory, admittedly, if the standardization could have been carried out in the vacuum balance under conditions similar to those of the effusion experiments. Most of the freezing-point standards, however, are corrosive to stainless steel. Bismuth appeared to have some chance of success, but since the orifice dimensions needed to be measured and since large quantities of solidified metal surrounding the orifice would have made this difficult, this line of investigation was not pursued.

(c) Standardization of the Balance Weights

The class S pan weights, class 2-S wire weights, and chain were compared with a set of weights recently standardized by the National Bureau of Standards. The small differences in the weights were combined appropriately with buoyancy corrections to obtain the required corrections. Some of the small weights and the chain and a few of the pan weights were checked at the end of each series of experiments

to determine whether they had reacted with traces of mercury vapor in the vacuum system. No appreciable changes were detected. The chain weight gave some difficulties in calibration attempts since the balance was not sufficiently sensitive nor stable to provide the small corrections necessary for precision measurements of the smallest changes in weight. Consequently, for series 7 and subsequent experiments the balance was tared so that both the zero and ten-milligram scale readings of the chain could be compared in vacuum with the ten-milligram wire weight. This proved to be quite satisfactory since the balance stability and its sensitivity under vacuum conditions were good. The chain then could be calibrated in vacuum at any time before or after an experiment.

(d) Orifice Dimensions and Clausing Factors

The dimensions of the cylindrical orifices were measured by various techniques, but only one of these yielded the precision requisite to this study. Measurements of the cross-sectional diameter of the ends of the orifice appeared to give unreliable results because of apparent distortions. The method which gave reproducible results involved the measurement of the volume of the cylinder and from this could be directly calculated the average square of the radius. The orifices were cut out of the oven and weighed both with and without mercury, and the volume of the orifice was determined from a volume-temperature equation[61] for liquid mercury.

One end of the orifice was sealed with a small piece of masking tape, and then the orifice cylinder was filled by a fine hypodermic needle. Great care was taken to ensure that air bubbles were not trapped in the cylinder. Before each weighing and after the filling with mercury, the ends were microscopically examined for the extent of the meniscus. In only one determination was it necessary to correct for a meniscus, and this correction was less than 0.5 percent of the total weight. Several determinations of the volume gave excellent mutual agreement. The lengths of the cylindrical orifices were measured with a micrometer. The results of the measurements and some

derived quantities are recorded in Table 8.3-2. The errors cited are standard deviations converted to percentage values. Only the largest errors in these measurements are listed; several of the determinations gave even smaller errors, but since these merely are statistical errors, one must acknowledge possible absolute errors of perhaps twice these values. The absolute error, however, certainly must be less than one percent.

TABLE 8.3-2

Orifice Dimensions and Clausing Factors
Derived from Volume Measurements

Oven	Series	Cross-sectional Area (cm^2), ±0.2%	Length (cm); ± 0.2%	Radius (cm), ± 0.1%	Length: Radius, ±0.3%	Clausing Factor, ±0.3%
3	5	0.001296	2.495	0.02031	122.8	0.02077
2-A	6	0.002849	2.997	0.03011	99.54	0.02540
7	7	0.002953	2.036	0.03066	66.41	0.03726
9	8	0.001440 (0.6%)	0.00156 (±20%)	0.02141 (±0.3%)	0.0729 (±20%)	0.965 (±2%)

The dimensions of the thin-edged orifice were measured microscopically with a standardized scale located in the eye-piece of the microscope, and these measurements indicated that the opening was quite circular. The thickness of the orifice was measured at an angle of forty-five degrees and then converted to the value of the true length. Because of its extreme thinness, the length corresponded to only one-third of the smallest scale division, so that there is uncertainty of perhaps twenty percent in the measured value. The Clausing factor or transmission coefficient derived from the length to radius ratio, however, varies only about three percent over these limits, so that a standard deviation of about two percent appears to be a reasonable choice in the error for this quantity. It was planned that the length would be more accurately measured subsequent to the experiments, but the orifice was irreparably damaged before this could be done. Apparently the

mercury so affected the grain structure in the thin portions of the orifice that it became brittle and soft, and in the refilling of the oven for a second set of experiments, the hypodermic needle bent the edges of the orifice. The flow rate measurements, however, were carried out in such a way that the data support the contention that the orifice was not significantly injured, if at all, during the effusion experiments.

The Clausing factors listed in the table were calculated from the equation deduced by DeMarcus[42] and reported in this thesis in Appendix 1. It should be noted that the expression 8R/3L is not applicable as the transmission coefficient for the long channels used in this study. The above expression yields coefficients several percent too high, and as DeMarcus has shown,[42] 8R/3L is correct only for an infinite value of the length-to-radius ratio.

The orifice radii listed in Table 8.3-2 are applicable, of course, only as a measure of an average cross section of the orifice. There is, then, the question of the uniformity of the channels and the extent of the effect of nonuniformity on the interpretation of the subsequent measurements of flow rates particularly under molecular flow conditions. The Clausing factor is a function principally of the square of the radius, so that a measure of the average of the cross-sectional area would appear to be the most meaningful measurement. The problems arising from a nonuniform channel are common to all experiments such as the present ones, and they are most troublesome for extremely thin channels.

Various measurements of the radii showed that these channeled orifices were of uniform cross section to an extent of one or two percent, and the orifice of oven 2-A appeared to be the least uniform of the three channeled orifices. The orifices of ovens 2-A and 7 were made of sections of a 20 gauge hypodermic needle and the orifice of oven 3 was made from a length of a 22 gauge needle. A microscopic measurement of the radius of two such needles randomly selected

gave reasonable agreement with the orifices of ovens 7 and 3, but showed that the average radius of that of oven 2-A was several percent smaller. These observations are summarized in Table 8.3-3. A microscopic examination of the welded ends of the orifices showed that there was not constriction in the end of the orifice of oven 2-A, a possible constriction of much less than one percent of the area for the orifice of oven 7, and a severe constriction in the welded end of the orifice of oven 3. These constrictions would tend to lower the theoretical molecular flow limits

TABLE 8.3-3

Comparison of Radii for Channeled Orifices

Oven or Needle Number	Series	Radius (cm) by Volume Measurement	Radius (cm) by Diameter Measurement of Welded End	Extent of Constriction by Percent of Area by Volume Measurement	Cross-sectional Area of Constricted End (cm^2)
Oven 2-A	6	0.03011(±0.1%)		0.0%	
Oven 7	7	0.03066(±0.1%)		$<1.0\%$	
Oven 3	5	0.02031(±0.1%)	0.01788(±0.84%)	$\sim 22.5\%$	0.001004
Needle 20			0.03084(±1.47%)		
Needle 22			0.02032(±1.47%)		

For the comparisons of theoretical predictions employing the orifice dimensions with the experimentally measured quantities, the thermal expansion of the orifices has not been accounted for. Neglect of the expansion leads to errors no larger than one percent in series 8 and no larger than two percent in the other series of experiments. These are errors within the precision of the measurements of the mass flow rates.

CHAPTER 9
MASS FLOW RATE DATA

In this chapter the data obtained in the experiments comprising four series are reported. The basic data including a priori estimates of the statistical errors are presented in the first section. The measurements extend over a temperature range of 300° and a flow rate range of a factor of ten million! A discussion of some preliminary experiments is given in a second section. A third section outlines the methods used in deriving the a priori statistical errors.

9.1 Tables of Basic Data

(a) Description of the Table Format

Four tables of data on the weight losses and temperatures measured in the experimental series 5,6,7 and 8 are reported here. The few experimental results comprising a series 4 are not reported since they were obtained with an oven having a severe leak in the thermocouple well. When the leak was discovered, these experiments were discontinued.

A single constant-temperature mass flow rate value is obtained generally from two experiments: the primary total weight loss experiment and the secondary warm-up weight loss experiment. These are combined as previously described to give the steady-state flow rate. These data are assembled in the tables of this section. In the first column the number of the experiment is cited. The primary and associated secondary or warm-up correction experiments are grouped together with the experimental number enclosed in parentheses representing the secondary experiment. Also, it should be noted that there are a few groups of experiments for which the secondary experiment was made prior to the primary one.

The faulty series 4 experiments ended with experiment 28. Experiment 29 of set A, series 5, begins the listing of the results of the

principal experiments which end finally with experiment 158 of Series 8. Some of the experiments between these numbers are not cited in the four tables in this section because either they require some detailed comment or are not flow experiments. These missing experiments are described later. In those cases where the heating period was sufficiently long, within the precision of the data, no warm-up correction was necessary, so that a secondary experiment was not carried out. Its absence for this circumstance is denoted by a dash in place of an experiment number. In other cases where weighings at temperature during the flow process were made, no warm-up correction, of course, was necessary. But to distinguish these from the previous ones, for which the helium quench method was used before the weighing operations, an appropriate symbol, as will be mentioned, denotes these in the second column under "remarks." These latter experiments allowed for several weighings at temperature within a single experiment. Data for each of these are denoted by a dash and sequential number. The quantities for the total experiment are distinguished by the symbol "-T" following the experiment number.

The total group of experiments within a series was carried out with a single oven, and thus each of these experiments is unique to a given orifice. Within a series, the experiments are grouped in alphabetically denoted sets comprising natural divisions arising from some feature unique to that set. For example, several experiments could be carried out with one filling of the oven and these may define a set, or for some of the large flow rate experiments a set was carried out in which the oven was filled prior to each experiment.

The third, fourth, and fifth columns contain the basic data on the weight losses w_1 or w_2 and heating times t_1 or t_2, as described, and the steady-state mass flow rate, dw/dt, calculated from these data. The last two columns present the temperatures derived as previously prescribed. Errors are listed along with these data, and the basis of the calculation of these is described later.

The symbol codes listed in the "Remarks" column are defined in Table 9.1-1. These comprise certain a priori predictions and

TABLE 9.1-1

Definition of the Symbols used in the Tables 9.1-2.

Distinguishing Notations:

mv. . . . . Millivolts
C/A. . . . . Chromel/Alumel Thermocouple

( ) . . . . . Secondary Experiment
F. . . . . Oven filled prior to the experiment
T. . . . . Oven weighed at temperature
R. . . . . Temperature recorded overnight
[ ] . . . . . Enclosed remark or datum uncertain.
OFL. . . . . Overflow of mercury occurred.
{ } . . . . . Mass flow rate in error due to overflow

A Priori Prediction Notations:

HHH. . . . . Weight loss much too large
HH. . . . . Weight loss too large
H. . . . . Weight loss slightly too large

L. . . . . Weight loss slightly too low
LL. . . . . Weight loss too low
LLL. . . . . Weight loss much too low.

IND . . . . . Conflicting events make choice in predictions indeterminable.

distinguishing remarks which will be useful in discussing the data. An examination of the originally recorded data shows that although the duplication of the initial warm-up behavior in the secondary experiment is generally satisfactory, it is possible to judge in some cases whether the measured weight loss is too small or too large because of over or under shooting in the temperature. For example, if the weight loss correction is too large, the calculated steady-state mass flow rate

would be too low. In some cases conflicting events made a predication impossible and in other cases, in so far as they can be judged, the duplication is completely satisfactory.

These a priori predictions, however, are not to be construed as indicating necessarily any failure or unreliability in the associated data, but merely represent qualitative information. The "overflow" notation will be described later in detail. In some of the experiments, the progress of the temperature overnight was monitored by recording the MMC input voltage (0-10 volts, DC). Nothing unusual was noted in these measurements, however.

(b) Basic Data Tables

The data presented in the following tables are given with more significant digits than the precision appears to warrant. This is done, first, to retain accuracy in the derived quantities and, second, because these data are taken from the intermediate output of a programmed series of calculations with the IBM 610 digital computer, which handles internally more than 15 significant digits. As a result of the rounding off in the reported data, some of the derived quantities may disagree slightly with such quantities derived from the recorded data, but these discrepancies should be negligible.

The weight loss and time data are measured data and consequently are given to the smallest measured decimal fraction rather than being rounded to the extent demanded by the magnitude of the cited errors.

9.2 Incidental Experiments and Preliminary Inquiries

Following experiment 56 at the end of the series 5, set A group, five additional experiments not directly concerned with the measurement of flow rates were carried out. The last two of these, experiments 60 and 61, have been discussed in connection with the standardization of the temperature control unit; the remaining three have bearing on the interpretation and reliability of the flow measurements and consequently are outlined in this section. In addition to these,

TABLE 9.1-2A

Basic Data for Series 5 (Oven 3)

Experiment	Remarks	Weight Loss (w, mg)	Heating Period (t, min)	Mass Flow Rate (dw/dt, mg/min)	Apparent Temperature (mv, C/A)	True Temperature (T, °K)
Set A						
29	F	30.90	123.88			
(30)		2.42	11.79	0.2540 ± 0.0061	6.036 ± 0.012	421.3 ± 0.3
31		31.78	124.51			
(32)	L	2.06	11.65	0.2633 ± 0.0052	6.040 ± 0.008	421.4 ± 0.2
33		4.46	279.24			
(34)	HH	0.53	28.81	0.01570 ± 0.00083	4.047 ± 0.005	372.3 ± 0.1
35		548.94	118.29			
(36)		27.46	9.90	4.811 ± 0.071	8.031 ± 0.005	471.4 ± 0.1
37		4424.45	77.50			
(38)	H	316.61	7.71	58.86 ± 1.3	10.025 ± 0.016	521.4 ± 0.4
39		11.75	208.15			
(40)		0.68	15.79	0.05755 ± 0.0011	5.034 ± 0.008	396.4 ± 0.2
41		1786.17	99.41			
(42)		95.29	7.26	18.35 ± 0.29	9.029 ± 0.004	496.6 ± 0.1
43		162.57	146.57			
(44)	HH	10.08	10.57	1.121 ± 0.024	7.035 ± 0.004	446.4 ± 0.1

TABLE 9.1-2A (Cont'd.)

Basic Data for Series 5 (Oven 3)

Experiment	Remarks	Weight Loss (w, mg)	Heating Period (t, min)	Mass Flow Rate (dw/dt, mg/min)	Apparent Temperature (mv, C/A)	True Temperature (T, °K)
45		10695.12	67.84			
(46)		672.15	6.39	163.1 ± 3.1	11.030 ± 0.005	546.0 ± .1
47		642.76	128.28			
(48)	H	29.88	8.01	5.096 ± 0.070	8.034 ± 0.013	471.5 ± 0.3
49		2.51	2879.63			
-		-	-	0.0008699 ± 0.00003(	2.043 ± 0.005	323.9 ± 0.1
50		4.23	254.69			
(51)	LL	0.37	12.14	0.01590 ± 0.00056	4.042 ± 0.009	372.2 ± 0.2
52		2 45	604.11			
-		-	-	0.004052 ± 0.00012	3.040 ± 0.007	348.1 ± 0.2
53		4669.24	78.75			
(54)	L	211 05	7 60	62.66 ± 0 83	10.027 ± 0.006	521 5 ± 0.2
55		12678.56	50.72			
(56)	L	834.89	5 56	262 3 ± 5 6	11 635 ± 0.004	561.0 ± 0 1

TABLE 9.1-2A (Cont'd.)

Basic Data for Series 5 (Oven 3)

Experiment	Remarks	Weight Loss (w, mg)	Heating Period (t, min)	Mass Flow Rate (dw/dt, mg/min)	Apparent Temperature (mv, C/A)	True Temperature (T, °K)
Set B						
130-1	F, RT	1.37	1495.51	0.0009161 ± 0.000020	-	-
130-2	R, T	0.67	716.31	0.0009353 ± 0.000042	-	-
130-T	R, T	2.05	2211.82	0.0009268 ± 0.000014	2.048 ± 0.004	324.0 ± 0.1
131-1	T	1.50	371.56	0.004037 ± 0.000081	-	-
131-2	T	0.90	226.53	0.003973 ± 0.00013	-	-
131-T	T	2.40	598.09	0.004013 ± 0.000050	3.046 ± 0.006	348.3 ± 0.2
132-1	R, T	0.55	1403.40	0.0003919 ± 0.000021	-	-
132-2	R, T	0.41	1159.55	0.0003536 ± 0.000026	-	-
132-T	R, T	0.95	2562.95	0.0003718 ± 0.000012	1.524 ± 0.009	311.4 ± 0.2
Set C						
133	[OFL]	29759.23	37.60			
(134)	(H)	745.48	1.84	({811.3 ± 3.6})	13.034 ± 0.029	594.9 ± 0.6
135	F,[OFL]	58377.63	29.99			
(136)	(H)	2055.83	2.12	({2021. ± 76.})	14.512 ± 0.017	631.0 ± 0.4
137	F,[OFL]	55934.34	28.38			
(138)	(L)	1704.56	1.64	({2028. ± 20.})	14.556 ± 0.017	632.0 ± 0.4

TABLE 9.1-2B
Basic Data for Series 6 (Oven 2-A)

Experiment	Remarks	Weight Loss (w, mg)	Heating Period (t, min)	Mass Flow Rate (dw/dt, mg/min)	Apparent Temperature (mv, C/A)	True Temperature (T, °K)
Set A						
62	F	109.45	132.17			
(63)	HH	9.95	14.00	0.8420 ± 0.025	6.050 ± 0.011	421.6 ± 0.3
64		2530.48	137.30			
(65)	L	58.62	6.29	18.87 ± 0.13	8.038 ± 0.006	471.5 ± 0.2
66		5326.11	84.41			
(67)	HH	301.97	7.48	65.3 ± 1.1	9.040 ± 0.035	496.7 ± 0.9
68		38.83	210.27			
(69)	[H]	1.50	13.03	0 18931 ± 0.0022	5.049 ± 0.006	396.8 ± 0.2
70		48651.06	49.96			
(71)	HHH	2476.62	10.16	1160. ± 22.	12.056 ± 0.069	570.7 ± 1.7
Set B						
72	F, OFL	55451.97	49.31			
(73)	L	3972.16	5 34	1171. ± 28.	12.032 ± 0.013	570.1 ± 0.3
74		577.29	135.74			
(75)		41.71	11.85	4 323 ± 0.094	7.046 ± 0.005	446.6 ± 0.1
76		7.77	614 40	0 01265 ± 0 000079	3.048 ± 0 011	348.4 ± 0.3

TABLE 9.1-2B (Cont'd.)
Basic Data for Series 6 (Oven 2-A)

Experiment	Remarks	Weight Loss (w, mg)	Heating Period (t, min)	Mass Flow Rate (dw/dt, mg/min)	Apparent Temperature (mv, C/A)	True Temperature (T, °K)
77		9.39	202.92			
(78)		0.27	11.83	0.04773 ± 0.00047	4.044 ± 0.006	372.2 ± 0.1
79		62.06	153.09			
(80)		4.92	14.15	0.4113 ± 0.010	5.542 ± 0.007	408.9 ± 0.2
81	LL	3.62	3034.75			
-		-	-	0.001193 ± 0.000012	1.535 ± 0.031	311.7 ± 0.7
82	H	3.58	1267.80			
-		-	-	0.002824 ± 0.000051	2.055 ± 0.005	324.2 ± 0.1
84		17449.26	86.38			
(85)	IND	1535.28	10.03	208.4 ± 6.0	10.050 ± 0.011	521.8 ± 0.3
86		1113.95	136.17			
(87)		19.27	4.59	8.320 ± 0.041	7.529 ± 0.023	458.7 ± 0.6
Set C						
88	F, T	6.67	1106.84	0.006026 ± 0.000036	2.547 ± 0.006	336.3 ± 0.2
89	T, (L)	14.32	563.51	0.02541 ± 0.00012	3.535 ± 0.026	360.2 ± 0.6

TABLE 9.1-2B (Cont'd.)
Basic Data for Series 6 (Oven 2-A)

Experiment	Remarks	Weight Loss (w, mg)	Heating Period (t, min)	Mass Flow Rate (dw/dt, mg/min)	Apparent Temperature (mv, C/A)	True Temperature (T, °K)
90	T,R,[L]	3.88	2450.31	0.001583 ± 0.000014	1.730 ± 0.014	316.4 ± 0.4
91		63.65	315.50			
(92)	H	0.81	8.51	0.2047 ± 0.00082	5.043 ± 0.010	396.6 ± 0.2
93		26.15	258.81			
(94)	L	0.93	13.97	0.1030 ± 0.0011	4.545 ± 0.007	384.4 ± 0.2
95		517.45	227.00			
(96)	LL	12.14	9.16	2.320 ± 0.021	6.604 ± 0.010	435.5 ± 0.2
97		3527.20	99.93			
(98)		240.76	9.66	36.41 ± 0.75	8.541 ± 0.005	484.1 ± 0.1
99		7681.07	65.48			
(100)		387.60	5.25	121.1 ± 1.8	9.538 ± 0.005	508.9 ± 0.1
101		20213.38	66.08			
(102)	HH	1036.51	5.13	314.6 ± 5.3	10.495 ± 0.022	532.7 ± 0.5
Set D						
(103)	F, OFL	14245.97	4.50			
104	HH	40451 61	21.95	{1502. ± 290.}	13.019 ± 0.022	594.0 ± 0.5

TABLE 9.1-2B (Cont'd.)
Basic Data for Series 6 (Oven 2-A)

Experiment	Remarks	Weight Loss (w, mg)	Heating Period (t, min)	Mass Flow Rate (dw/dt, mg/min)	Apparent Temperature (mv, C/A)	True Temperature (T, °K)
105	F, OFL	37971.38	55.00			
(106)	[LL]	1726.52	4.57	{718.7 ± 13.}	11.259 ± 0.017	551.5 ± 0.4
107	F, OFL	92115.10	40.47			
(108)	L	6057.39	3.95	{2356. ± 50.}	13.037 ± 0.071	594.4 ± 1.6
Set E						
140		55000.	27.05			
(141)		2050.	1.66	2085. ± 17.	13.021 ± 0.024	594.1 ± 0.5
145		50710.30	12.08			
(147)		6764.60	2.09	4399. ± 140.	14.539 ± 0.025	630.9 ± 0.6

Experiments 83, 139, 142, 143, and 144 presented later.

TABLE 9.1-2C

Basic Data for Series 7 (Oven 7)

Experiment	Remarks	Weight Loss (w, mg)	Heating Period (t, min)	Mass Flow Rate (dw/dt, mg/min)	Apparent Temperature (mv, C/A)	True Temperature (T, °K)
109	F	28.16	98.46			
(110)	L	2.70	11.84	0.2939 ± 0.0094	5.037 ± 0.014	396.6 ± 0.4
111		1966.20	71.28			
(112)	IND	210.68	10.01	28.65 ± 1.0	8.044 ± 0.013	472.1 ± 0.3
113		186.98	129.81			
(114)		8.93	8.46	1.467 ± 0.018	6.054 ± 0.005	421.9 ± 0.1
115		6705.62	70.30			
(116)	[H]	462.90	7.07	98.73 ± 2.1	9.051 ± 0.011	497.4 ± 0.3
117		603.72	93.24			
(118)		50.09	9.29	6.595 ± 0.15	7.049 ± 0.012	447.0 ± 0.3
119		12561.17	47.82			
(120)		876.82	5.49	276.0 ± 5.2	10.051 ± 0.011	522.4 ± 0.3
121	T, [L]	6.15	332.11	0.01852 ± 0.00012	3.048 ± 0.009	348.4 ± 0.2
122	T	12.32	166.05	0.07419 ± 0.00042	4.043 ± 0.018	372.3 ± 0.4
123	T, R	5.34	1244.69	0.004290 ± 0.000028	2.051 ± 0.013	324.1 ± 0.3

TABLE 9.1-2C (Cont'd.)
Basic Data for Series 7 (Oven 7)

Experiment	Remarks	Weight Loss (w, mg)	Heating Period (t, min)	Mass Flow Rate (dw/dt, mg/min)	Apparent Temperature (mv, C/A)	True Temperature (T, °K)
124	T, R	3.91	2592.98	0.001508 ± 0.000013	1.451 ± 0.008	309.6 ± 0.2
125	T	6.47	333.76	0.01939 ± 0.00012	3.036 ± 0.011	348.1 ± 0.3
126	T	6.56	333.83	0.01965 ± 0.00011	3.044 ± 0.009	348.3 ± 0.2
127	T [L]	36.55	121.76	0.3002 ± 0.00051	5.053 ± 0.013	397.0 ± 0.3
128 (129)	L	3136.47 311.05	59.32 7.50	54.52 ± 1.7	8.554 ± 0.013	484.9 ± 0.3

TABLE 9.1-2D
Basic Data for Series 8 (Oven 9)

Experiment	Remarks	Weight Loss (w, mg)	Heating Period (t, min)	Mass Flow Rate (dw/dt, mg/min)	Apparent Temperature (mv, C/A)	True Temperature (T, °K)
148-1	F,T	1.74	30.87	0.05637 ± 0.0011	2.049 ± 0.004	324.1 ± 0.1
148-2	T	2.32	40.41	0.05741 ± 0.00087	2.048 ± 0.004	324.0 ± 0.1
148-3	T	1.74	32.18	0.05407 ± 0.0011	2.048 ± 0.005	324.0 ± 0.1
148-T	T	5.80	103.46	0.05606 ± 0.00034	2.049 ± 0.005	324.1 ± 0.1
149-1	T	35.48	31.69	1.120 ± 0.0051	4.046 ± 0.005	372.2 ± 0.1
149-2	T	35.17	30.68	1.146 ± 0.0054	4.045 ± 0.004	372.2 ± 0.1
149-T	T	70.62	62.37	1.132 ± 0.0026	4.046 ± 0.004	372.2 ± 0.1
150-1	T	1.65	160.06	0.01031 ± 0.00022	1.125 ± 0.009	301.4 ± 0.2
150-2	T	1.75	168.30	0.01040 ± 0.00021	1.124 ± 0.009	301.4 ± 0.2
150-T	T	3.43	328.36	0.01045 ± 0.00011	1.124 ± 0.010	301.4 ± 0.2
151-1	T	7.83	31.04	0.2523 ± 0.0016	3.046 ± 0.006	348.3 ± 0.2
151-2	T	8.40	31.94	0.2630 ± 0.0017	3.048 ± 0.005	348.3 ± 0.1
151-T	T	16.22	62.98	0.2575 ± 0.00087	3.047 ± 0.005	348.3 ± 0.1
152-1	T	1380.00	34.68	39.79 ± 0.81	7.109 ± 0.014	448.3 ± 0.4
152-2	T	1500.00	36.76	40.81 ± 0.79	7.108 ± 0.010	448.2 ± 0.2
152-T	T	2880.00	71.44	40.31 ± 0.40	7.109 ± 0.009	448.3 ± 0.2
153-1	T	227.04	32.53	6.979 ± 0 060	5.438 ± 0.010	406.3 ± 0.2
153-2	T	210.53	30 27	6.955 ± 0 064	5.439 ± 0.005	406.3 ± 0.1
153-T	T	437.57	62.80	6.968 ± 0.031	5.439 ± 0.008	406.3 ± 0 2

TABLE 9.1-2D (Cont'd.)
Basic Data for Series 8 (Oven 9)

Experiment	Remarks	Weight Loss (w, mg)	Heating Period (t, min)	Mass Flow Rate (dw/dt, mg/min)	Apparent Temperature (mv, C/A)	True Temperature (T, °K)
154-1	T	4.15	31.94	0.1299 ± 0.0012	2.575 ± 0.019	337.0 ± 0.5
154-2	T	4.03	30..88	0.1305 ± 0.0013	2.573 ± 0.011	337.0 ± 0.3
154-T	T	8.19	62.82	0.1304 ± 0.00063	2.574 ± 0.011	337.0 ± 0.3
155		25738.14	38.71			
(156)		887.56	2.88	693.6 ± 7.2	11.132 ± 0.024	548.8 ± 0.6
157		8491.12	45.61			
(158)	H	270.64	3.14	193.6 ± 1.8	9.131 ± 0.009	499.2 ± 0.2

mention is made of the result of experiment 83, which was carried out toward the end of the series 6, set B group. These various experiments comprise a study of two broad questions, the one concerned with some aspects of the reliability of the weight loss measurements, and the other bearing on the question of the occurrence of thermal effects during the effusion process. Therefore, these experiments in question are described in this framework.

(a) Some Questions Concerning the Flow Rate Measurements

The kind of experiments presented in the previous sections and the techniques used suggest five questions on the reliability of the weight loss measurements:

(1) Has progressive oxidation of the mercury in the oven occurred to introduce some systematic error?

(2) Do the helium quench experiments agree with those in which the oven was measured at temperature?

(3) Has a transpiration effect due to the evacuation of the helium from the oven introduced some error?

(4) Were there volatile impurities from the oven and associated parts which invalidate the small flow rate measurements?

(5) Has the radiofrequency induction field interfered with the weighings?

The first question is most easily answered in an examination of the entire group of experiments. However, it should be noted that the experiments in a given series were carried out somewhat randomly; that is, especially in the first two series, a large flow rate and a small flow rate were usually measured in succession, so that some trend should appear on examination of the data. Also, several sets beginning with fresh mercury were carried out. As mentioned, the helium was purified by passing it over hot uranium chips and through a liquid nitrogen-cooled trap. This should have been quite an efficient purification. It was noted, incidentally, that the oven, after removal from the

vacuum system at the completion of set C of series 6, was as clean as it initially appeared after its outgassing. Severe oxidation would have visibly tarnished the steel oven after repeated quenchings. The experiments of set B, series 5, and the first three of set C, series 6, were carried out specifically to investigate the present question; the latter three will be examined later, and the former set are cited below.

The second question is related, of course, to the first. To test for the agreement between the helium quench experiments and those in which weighings at temperature were made, one can compare the three pairs of experiments cited in Table 9.2-1 which should agree because of their close temperature correspondence.

TABLE 9.2-1

Comparison of the Two Techniques for the Measurement of Mass Flow Rates

Series-Set	Experiment	Temperature (°K)	Mass Flow Rate (mg. min)	Technique	% Deviation
5-A	49	323.9	8.699×10^{-4} (±4.1%)	He Quench	-3.2
5-B	130-T	324.0	9.268×10^{-4} (±1.5%)	At Temperature	
5-A	52	348.1	4.052×10^{-3} (±3.0%)	He Quench	+0.5
5-B	131-T	348.3	4.013×10^{-3} (±1.3%)	At Temperature	
7	109 (110)	396.6	2.939×10^{-1} (±3.2%)	He Quench	-1.1
7	127-T	397.0	3.002×10^{-1} (±0.2%)	At Temperature	

The percent deviations were calculated as the percent ratio of the difference between the measurements and the average in a pair to the mean value, with the positive sign taken if the first member is the larger. Since the deviations are within the cited errors, which are discussed later, one must conclude that the two techniques give identical values within the precision of the measurements. Incidentally, it is seen that the second technique, involving the weighings at temperature, gives more precise values. This is due to refined techniques in weighing operations and a reduction of the warm-up correction error.

The third question may be answered experimentally. Experiment 83 was carried out to see if a transpiration effect produced a noticeable decrease in the weight of the oven. The oven was weighed, helium was admitted to the system, then the oven was re-weighed after the vacuum pressure of 10^{-6} mm Hg was regained. The two weighings gave agreement within the balance sensitivity and stability, ± 0.025mg. Therefore, one concludes that this effect presented no problem.

In connection with this question, however, it should be remarked that the quenching and re-evacuation procedures were carried out reproducibly. The manometer was used to gauge the amount of helium put into the system, and a timer was used to gauge and reproduce the cooling period and the time elapsed before the weighing in vacuum was made. Thus, any unsuspected errors should have been common to both the initial and final weighings and consequently should have cancelled in the difference. However, the method of weighing at temperature should have been much more satisfactory, provided, of course, that the induction field of the work coil caused no trouble, and thus when this method was found to be satisfactory it was used exclusively for the low volatility experiments.

Question four was answered experimentally by the result of experiment 59 of series 5. The oven was previously emptied of mercury by total evaporation and used in experiments 57 and 58 with some unavoidable manual handling. The oven was heated to 600°C for 3 hours and found to have lost no weight. Consequently, the weight loss measurements may be assumed to be unique to the mercury volatilization.

In three of the flow rate experiments, 127 of series 7, and 150-T and 154-T of series 8, the weighings were checked both with the heating power on and off. In the first two experiments no difference was detected; in the third the difference was less than 0.02 mg, which is well within the sensitivity of the balance. Apparently the weighings at temperature are reliable.

(b) A Study of the Thermal Effects Occurring during Effusion

Experiments 57 and 58 comprise a brief study of the thermal effects occurring during the effusion process at various temperatures for the series 5 measurements. In these experiments a thermocouple of 32 gauge chromel-P and alumel wires was spot-welded to the top end of the oven 3 used in series 5. This is the end of the oven opposite the orifice, which opens downward into the condenser-vacuum jacket. In experiment 57 the welded couple obviously was not adequately welded to the oven, in comparison with the results of experiment 58, for the top temperature measured from 4 to 10 degrees colder than the well temperature. This couple was replaced by another and especial care was devoted to the welding of the couple firmly to the oven. Microscopic examination indicated it to be fairly well anchored.

The oven was filled with mercury, and the thermocouple leads from the well were brought out of a side arm of the condenser to a potentiometer, and the spot-welded couple leads were connected to the balance thermocouple contactors and thus to the control unit. This arrangement was used because several measurements with the oven empty were to be carried out, and it had been found that the heat lag in the well is too severe with an empty oven for the controller to operate properly with its natural fluctuations. This effect made it easy to determine whether mercury was still in the oven during the principal experiments. The oven was brought to a steady-state temperature at about 50-degree increasing intervals, and at each of these temperatures the temperature difference between the rear and well was measured during the steady-state effusion. At the highest of these temperature intervals the oven was taken rapidly to the desired temperature, and after a slight settling-out period the difference in the two temperatures was measured as a function of time as the mercury completely effused from the oven. Then with the oven empty, temperature differences for similar temperatures at decreasing intervals were measured. These data are summarized in Figures 9.2-1 and 9.2-2.

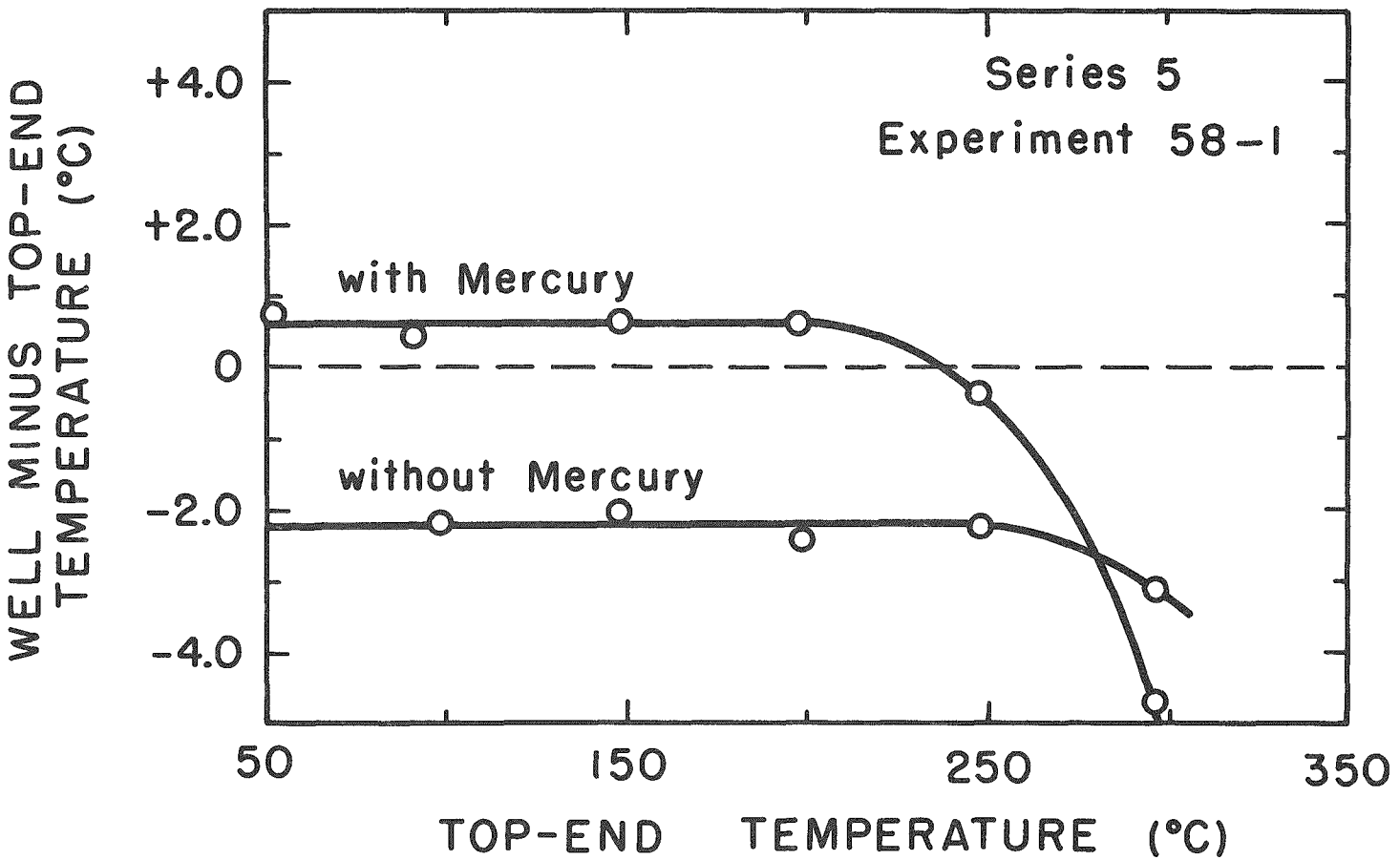

Fig. 9.2-1 Comparison of the Well and Top-End Temperatures for Experiment 58-1 of Series 5

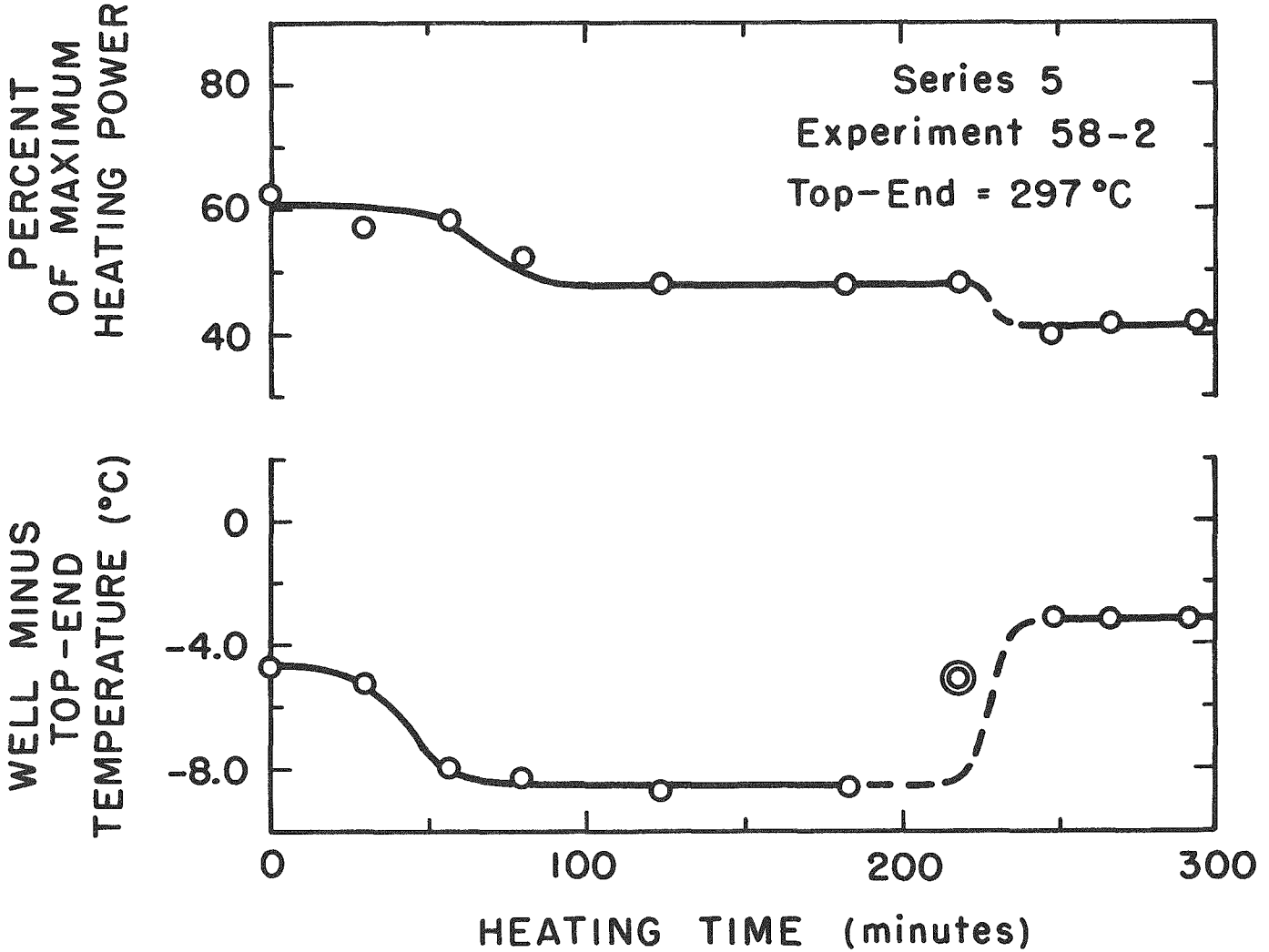

Fig. 9.2-2 Progress of the Thermal Effects during Effusion for Experiment 58-2 of Series 5

The fact that the well measured a temperature lower than the rear plate with an empty oven, as shown in Figure 9.2-1, was a frustrating effect which was noticed in some of the earliest preliminary experiments. It seems to be common to the low temperatures used in this experimental investigation. Apparently it is due to conduction losses from the well which cannot be compensated by radiation to the well from the interior walls of the empty oven. Especial care had been taken to keep these conduction losses to a minimum without introducing other troubles. Smaller thermocouple wires would have been more satisfactory, of course, but they are subject to strain and in use proved to be too fragile for the manipulations required in assembling the oven in the apparatus. With the oven filled with mercury, the well measures apparently a more reliable temperature. Aside from possible calibration error differences, the only way the well temperature of the couple immersed indirectly in the mercury can be in error is by measuring a temperature which is too low. The fact that it is greater than the top temperature at the lower temperatures seems to indicate that the thermal conductivity of the mercury is sufficient to compensate for the conduction heat losses.

Figure 9.2-2 shows that the temperature difference decreases at about 220°C, becomes negative above this, and reaches a value of -5 degrees at the highest temperature of 297°C. This indicates that a significant heat effect arises from the mass transport at the large mass flow rates, which is in agreement with such concepts of mass transport phenomena.(63)

Figure 9.2-2 shows an interesting behavior. The difference in the two temperatures negatively increases for about 50 minutes, becomes constant during the effusion for about 250 minutes, and then decreases to another steady-state value for the empty oven. The "percent of maximum power" value is that indicated by the MMC control unit. In principle, this quantity is the percent of the maximum power

available to heat the oven and therefore is proportional to the power input to the oven. This power input appears to follow the trend in the temperature difference. The power requirement falls off fairly sharply to a lower value for the empty oven. Again, this is evidence that some of the power is measurably used to vaporize and transport the mercury in this effusion process. This would suggest that a calorimetric technique might be used to measure the heat of transport in this process. The point doubly circled on the graph in Figure 9.2-2 is not an erroneous measurement, but refers to an experiment in which the mercury level in the oven was probably near the bottom tip of the well or below it; there was about a 2-millimeter difference between the tip and the bottom of the oven. This temperature difference is between that of the empty and full oven, probably because the vapor effects some warming of the well. The power requirements for the oven during the effusion process appear, then, to be nearly independent of the level of the mercury inside the oven. Since the well is somewhat shielded from the vapor in the orifice, the well probably measures more nearly the liquid mercury temperature at all times.

The reason for the initial high values of the power input and temperature difference is obscure. In part, such high values may arise from the reflectance change in the film of condensed effusate as it builds up below the plane of the orifice exit, and partly to the slow attainment of a steady state under these conditions. In the principal experiments the power input responded to the temperature of the well, and this steadied out quite rapidly in these cases. Of course, it is unknown what happens to the temperature of the wall during these effusion experiments at higher temperatures.

(c) The Problem of Overflow.

The maximum volume available to the mercury sample within the ovens was not precisely enough known prior to the experiments to permit one properly to gauge the maximum quantity of

mercury which could be introduced without overflowing on expansion at higher temperatures. Moreover, before the experiments were undertaken, it was not known to which temperatures and pressures the experiments could and would be extended; for various reasons the capabilities of the temperature controller and balance were unknown for conditions of mass flow rates of several grams per minute. The large flow rates were obtained by trial-and-error and brute-force methods; the measurements were extended to higher and higher pressures after the nature of the flow rate in these regions and the capabilities of the equipment were more clearly understood from the experimental data. It was discovered however, in series 6, set E, that the flow rate data indicated that the mercury was overflowing. The first evidence for this was obtained from the combined experiments 103, 104 and 107, 108, both pairs of which should have yielded similar flow rates. However, the combination 103, 104 gave low results, and 107, 108 gave high results. The secondary or warm-up correction experiment for the former combination was carried out first and for the latter second; an initial overflow of mercury would account for these discrepancies. Thus, if one assumes identical conditions for both sets, namely, that the oven was filled to the same initial volume prior to experiments 103 and 107, then the combinations 108, 107 and 104, 108 should have yielded results in mutual agreement, and they did so reasonably well; an overflow of approximately 10 grams in the experiments 103 and 107 would make the combinations 103, 104 and 107, 108 agree with the results of experiments 140, 141 for which the results are known to be reliable.

The orifices of ovens 2-A, 7 and 3 were oriented downward so that overflow of some mercury could have occurred in the experiments with these containers. The oven 9 of series 8 had an orifice oriented upwards, and therefore no similar trouble could have occurred in this series. Set E of series 6 was carried out expressly to study the problem of overflow. This set consists of experiments 139 through 147,

four of which are reported in Tables 9.1-2. The remaining experiments demonstrate the problem and the reliability of those previously mentioned experiments. For set E of series 6 the oven was filled to capacity, the secondary or warm-up correction experiment 139 was carried out, then the primary experiment 140 was made, followed by a duplicate secondary experiment 141. The oven was refilled and two repetitions, experiments 142 and 143, were made of the secondary experiment. The results recorded in Table 9.2-2 show an initial loss in weight which

TABLE 9.2-2

Data on the Examination of the Loss in Weight Due to the Overflow of Liquid Mercury, Set E of Series 6.

Experiment	Remarks	Weight Loss (grams) (Secondary Experiments)	Time (min) Required for the Oven to Attain the Steady-State Temperature	
(139)	Oven Filled	10.060	1.45	
140	Primary Experiment, Table 9.1-2B			Difference = 8.010 *
(141)		2.050	1.66	
(142)	Oven Filled	10.352	1.48	Difference
(143)		2.082	1.42	= 8.270 *
(144)		7.536	1.87	
145	Primary Experiment, Table 9.1-2B			
(146)		4.896	1.58	
(147)		6.765	2.09	

obviously is too high by about 8 grams. Also, the data illustrate that the measurements were reproducible, both in the initial loss and in the subsequent experiments, and that the flow rate appeared to be independent of the mercury level after the initial loss of 8 grams. Consequently, these data indicate that the initial loss of 8 grams was due to overflow of liquid and the loss of 2 grams was due to the effusion of the vapor.

* NOTE: The term difference = 8.010 applies to the difference in weight losses of experiments (139) and 140. The second term difference = 8.270 applies similarly to the experiments (142) and (143).

A similar group of experiments was carried out for the higher temperature measurements of set E. The experiments 144, 145, 146 and 147 were carried out immediately after experiment 143 and without a refilling of the oven. The data in Table 9.2-2 seem to indicate that no overflow occurred. The fluctuations in the weight losses are understandable as the normal variation in the measurement due to experimental conditions. The flow rate calculation arbitrarily employed the result of experiment 147 for the warm-up correction: this result seems to be a reasonable compromise among the three possible corrections for the loss in weight in the warm-up procedure.

The results of these experiments certainly seem to demonstrate that overflow of the liquid leads to the abnormally high results. Since the specific volume of mercury is calculable, one ought to be able to examine the present data with the knowledge of the experimental volumes determined from the weight of the oven both empty and full, the temperature, and the measured maximum volume available to the liquid. The usable capacity of the ovens 2-A, 3, and 7 was between 7.5 and 4.5 cm^3, and the experimental data indicate that overflow could have occurred only in the experiments of set D and E of series 6 and set C of series 5. For these particular experiments, however, the data can account for only about one-half of the overflow loss in weight experimentally measured in the set E experiments of series 6. The trouble here seems to be associated with the severe temperature gradients near the walls of the oven on the rapid warm-up procedure. During this procedure, large amounts of power are applied to take the oven from nearly zero degrees to the steady-state temperature in only a few minutes. Since the well senses only the temperature of the liquid near the orifice, it is possible that the liquid near the wall of the oven becomes momentarily hotter by many tens of degrees, and perhaps a fountain effect occurs. However, whatever happens, it appears that it must lead to an overflow of the liquid. Other effects, such as the

boiling of liquid and the formation of bubbles, are possible, but it is difficult to conceive how these could be so reproducible. Since a priori predictions of the extent of the overflow are not possible, the experiments 105, 106 of series 6 and the set C experiments of series 5 must be considered to be too high by an indeterminate amount. All other experiments appear to be reliable. In further analyses and considerations, the experiments 103, 104, 107 and 108 of set D of series 6 will be taken in the combinations 103, 107 and 104, 108.

9.3 Calculation of A Priori Errors in the Basic Data

(a) Errors in the Weight Losses

The primary and secondary weight losses, w_1 and w_2, respectively, are differences in initial and final weighings of the oven. The errors in these quantities are derived using the propagation of error formulation for statistically independent measurements.(64) In so far as possible, these errors are deduced on the basis of standard deviations assumed or calculated for the actually measured quantities.

(1) The Error in the Primary Weight Loss w_1

The quantity w_1 is derived from the initial and final weight differences in the primary experiment. Thus,

$$w_1 = w_i - w_f \quad , \tag{9.3-1}$$

and if ϵ_i and ϵ_f represent the standard deviations for the initial and final weighings, then the error in w_1 is given by the expression

$$\epsilon_{w_1} = \pm \sqrt{\epsilon_{w_i}^2 + \epsilon_{w_f}^2} \quad . \tag{9.3-2}$$

The weight w_i or w_f is the sum of the pan weights, rest point correction, and weight standardizations, and the last two quantities contain the errors propagated to the calculated weight loss. Since a number of calibrations of a single weight were made and since the NBS certificate supplied with the standard reference weights contained information concerning the limits of uncertainty in the absolute mass, an assumption could be made as to the possible "absolute" standard deviation in

the standardization corrections. The total calibration error was derived as the root of the sum of the squares of the individual errors for those weights actually involved in the weight differences; the remaining weights served only as tares.

The error in the rest point correction is somewhat involved and was calculated by various methods, depending on the way the rest correction was determined. In some of the experiments the method of "swings" was used to determine the rest point; in others it was found to be more convenient and, for vacuum weighings, equally or more reliable to employ a magnetic damping method. The standard deviation for the rest correction was calculated by the propagation procedures with the same function as used to derive the value of the rest correction from the rest point determinations. All of the rest point measurements in a given series were analyzed to determine the balance sensitivity and error in a single measurement under the conditions prevailing. This was used in the propagation formulas as required to determine the error in the rest correction, which error depends on the magnitude of the correction. For example, in series 5 the rest correction error in milligrams, with some convenient simplifying assumptions, was found to be given by the formula

$$\epsilon_R = \pm K\sqrt{2}\ \epsilon_f \sqrt{1 + \left(\frac{R}{0.3}\right)^2 + \left(\frac{R}{0.3}\right)}\ , \qquad (9.3\text{-}3)$$

where K and ϵ_f are the balance sensitivity, milligrams per scale division, and error in a rest point measurement in units of scale divisions, respectively, and R is the rest correction in milligrams. The constant 0.3 represents a tare weight and is a natural result of the particular method used in determining the correction R. The values of K and ϵ_f were determined, as stated, by analysis of all of the data, so that the rest point error represents a fairly rigorous standard deviation of a single measurement.

These calculated errors were used to determine the errors in w_i and w_f, and finally the standard deviation in the weight loss w_1. Some of these tedious calculations would not have been attempted in hand calculations, but the availability of a computer made it convenient to carry these out as part of the general scheme of the calculations.

(2) The Error in the Secondary Weight Loss w_2

The error in the quantity w_2 was not calculated in the same way as that for w_1 because this error needed to be derived with respect to the extent of its agreement with the warm-up loss in weight in the primary experiment. The principal error in the steady-state flow rate, in fact, where the coupled experiments were carried out, is that attributable to the error in w_2. An a priori determination of this error was strictly impossible, but pseudo-errors were determined from an examination of the series 5 data. A group of four nearly duplicate experiments were carried out and the secondary weight losses were compared in order to obtain some idea of the reproducibility of the warm-up correction procedure. The pertinent data are assembled in Table 9.3. The data in this table are taken from the Table 9.1-2A.

Examination of the Table 9.3 shows that, except possibly for the first set, these secondary weight losses should agree in the group if each of the two were carried out under identical conditions. For various reasons they were not so carried out, but nevertheless the fractional deviations from the mean should indicate the reproducibility of the secondary experiment, and the root mean square value appears to be a reasonable choice for the fractional error attributable to a single secondary weight loss. Consequently, the error in w_2 generally was taken for all experiments as

$$\epsilon_{w_2} = \pm\ 0.28\ w_2. \qquad (9.3\text{-}4)$$

TABLE 9.3

Comparison of Secondary Correction Experiments

Secondary Experiment	Temperature (°K)	Secondary Weight Loss (mg)	Heating Period (min)	Fractional Deviation from the Mean
34	372.3	0.53	28.81	0.35
51	372.2	0.37	12.14	
30	421.3	2.42	11.79	0.16
32	421.4	2.06	11.65	
36	471.4	27.46	9.90	0.08
48	471.5	29.88	8.01	
38	521.4	316.61	7.71	0.40
54	521.5	211.05	7.60	

Root-Mean-Square

Fractional Deviation = 0.28

(b) Errors in the Time

Errors in recorded values of the time were quite small. An examination of all the data showed that a conservative value for standard deviation of an individual time reading would be ±0.03 minute. This error was occasionally adjusted by a small amount as the data warranted. These errors were propagated to other derived quantities in the usual way.

(c) Errors in the Mass Flow Rate dw/dt.

The standard deviations in the mass flow rates dw/dt were calculated by the propagation procedures from the basic errors discussed in the above sections.

(d) Errors in the Temperature

(1) The Error in the Apparent EMF of the Thermocouple.

The apparent thermocouple temperature of the oven is derived, as previously described, from the sum of three measurements:

the EMF of the reference voltage source, the galvanometer scale reading in the absence of any applied voltage (that is, the galvanometer zero reading), and the average of the galvanometer readings for the steady-state flow measurement. The error of the total apparent EMF is the root of the sum of the squares of the three errors associated with these independent measurements.

An examination of all the data indicated that the standard deviation error of the galvanometer zero reading could be taken as ± 0.003 mv and that an error in the reference voltage measured by the potentiometer could be given the value ±0.002 mv. The error in the average of the galvanometer reading for the steady-state process was taken as the statistical standard deviation of a single measurement as calculated in the usual way by the root-mean-square average of the differences between the calculated mean and the single readings. This error, of course, does not represent a true standard deviation because the fluctuations are real rather than apparent. Thus the error in the apparent temperature represents more nearly a geometrically averaged fluctuation.

(2) Errors in the True Temperature

No errors attributable to the temperature corrections have been included in the tabulation of the data, since it would be difficult to assign meaningful errors of the nature of a prediction of the accuracy of the standardizations. The calibrations should be accurate to about 0.25 degree, and this would introduce uncertainties in the vapor pressures of about two percent or less. One might wish that the accuracy of the measurements could be prescribed more closely, but this study must be recognized to be limited by the strong temperature dependence of the vapor pressure. This is a problem common, of course, to all effusion studies of saturated vapors.

CHAPTER 10
DISCUSSION OF THE EXPERIMENTAL DATA

The basic experimental data presented in the previous chapter may be used to derive other quantities which are more amenable to a graphical representation and discussion of the general features of the observed effusive behavior of mercury vapor. These quantities are derived and reported in this chapter and analyzed with reference to the observed features of the present experiments and the general and specific previous concepts outlined in the initial chapters. As might be expected, these analyses illustrate that the previous concepts qualitatively predict many aspects of the effusive behavior observed in this investigation.

There is, however, only a limited quantitative correspondence, and this is examined here in as much detail as the data warrant. There is observed a quite interesting new feature of the effusive behavior of vapors flowing through channeled orifices from a source of vapor presumably at a pressure near one atmosphere. These conditions lead to a phenomenon superficially corresponding to a predictable limiting effusion rate, which apparently has not been observed previously nor would be expected for conditions similar, for example, to those employed in Knudsen's investigations.

10.1 Some Quantities Derived from the Basic Data

The physical constants in the molecular effusion formula (2.1-1) may be evaluated to yield the relation appropriate for monatomic mercury vapor:

$$\frac{dw}{dt}\ (\text{mg min}^{-1}) = 49571\ SW\ \frac{p(\text{mm})}{\sqrt{T(^{\circ}\text{K})}} \quad , \qquad (10.1\text{-}1)$$

in which S in square centimeters is the cross-sectional area of the orifice and W is the dimensionless transmission coefficient or Clausing factor. Since the mass flow rate dw/dt and temperature T are

experimentally measured quantities and the pressure is derivable from the temperature by equation (6.3-1), then it is natural to choose the experimental quantity

$$\frac{\sqrt{T(°K)}}{p(mm)} \frac{dw}{dt} \text{ (mg min}^{-1}\text{)}$$

for the representation of the data and comparison with the theoretically predicted molecular flow limit. A graphical representation of this quantity for the various experiments within the four series is plotted in Figure 10.2 against the variable $p(mm)/\sqrt{T(°K)}$. Since these two quantities cover a wide range of numerical values, a logarithmic plot is used.

Knudsen's semitheoretical formula (2.3-7) for the transition from molecular to viscous flow may be expressed for mercury vapor by the relation

$$\frac{\sqrt{T(°K)}}{p(mm)} \frac{dw}{dt} \text{ (mg min}^{-1}\text{)} = C\left(\frac{Rp}{\mu\sqrt{T}}\right)\left[\frac{\sqrt{T}}{p}\frac{dw}{dt}\right]_{mol} + \left[\frac{\sqrt{T}}{p}\frac{dw}{dt}\right]_{vis} \tag{10.1-2}$$

in which the average pressure has been taken as one-half of the source pressure p. In this expression,

$$C\left(\frac{Rp}{\mu\sqrt{T}}\right) = \frac{1 + 2.0709\,\dfrac{Rp}{\mu\sqrt{T}}}{1 + 2.5576\,\dfrac{Rp}{\mu\sqrt{T}}} \quad , \tag{10.1-3}$$

and

$$\left[\frac{\sqrt{T}}{p}\frac{dw}{dt}\right]_{vis} = 50525\,\frac{R^4 p}{\mu\sqrt{T}} \quad ; \tag{10.1-4}$$

further $\left[\dfrac{\sqrt{T}}{p}\dfrac{dw}{dt}\right]_{mol}$ has the value specified by the equation (10.1-1).

The quantities are appropriate to the units of pressure, temperature, mass, and time already specified, and R and L are the radius and length, in centimeters, of the channeled orifice and μ is the vapor viscosity of mercury.

Knudsen's semitheoretical formula is a coupling of Poiseuille's viscous flow term and the molecular flow term with a coupling coefficient represented here by the symbol $C(Rp/\mu\sqrt{T})$. This coefficient varies between 1 and 0.810. At high pressures, Knudsen's formula predicts that the quantity $\left[\frac{\sqrt{T}}{p}\frac{dw}{dt}\right]$ on the left side of the expression (10.1-2) is a function of $p/\mu\sqrt{T}$; at intermediate pressures it is dependent upon both of the coupled terms; at very low, decreasing pressures it proceeds through a minimum to a limiting value specified by the molecular flow term.

The basic data reported in the Tables 9.1-2 are converted to the appropriate quantities described and are listed along with other derived quantities, such as the vapor Pressure derived from equation (6.3-1). These quantities are arranged in Tables 10.1 according to increasing temperatures and consequently increasing pressures and increasing ratios of the pressure divided by the square root of the temperature, $p/\sqrt{T}$. Not all of the basic data are used; only the total flow rates of a given experiment are employed.

The errors recorded are those propagated from the errors in the basic data. The error in the temperature is propagated in two ways: by the direct error in the temperature and by the error in pressure as a result of the temperature error. The error ϵ_p in pressure p due to the error ϵ_t in the temperature T is taken as

$$\epsilon_p = \pm\, p\,(\Delta H/R_0T^2)\,\epsilon_t \quad , \qquad (10.1\text{-}5)$$

where ΔH and R_0 are the heat of vaporization and gas constant, respectively. For convenience, the value of $\Delta H/R_0$ is taken as one-half of 15,000 calories at all temperatures, and for an error of 0.25 degree in the temperature this yields an error in the pressure of 2 percent at 300°K, 1 percent at 450°K, and $\frac{1}{2}$ percent at 600°K. The true error calculable from the real heat at these temperatures is slightly smaller.

TABLE 10.1-1

Derived Flow Rate Quantities, Series 5 (Oven 3)

Orifice Dimensions:
Radius* = 0.02031 cm; Length:Radius = 122.8
Length = 2.495 cm; Clausing Factor = 0.02077

$$\left[\frac{\sqrt{T(°K)}}{p(mm)}\frac{dw}{dt}\ (mg\ min^{-1})\right]_{mol} = 1.334$$

Experiment	T(°K)	Pressure (mm Hg) [Eq. (6.3-1)]	$\left[\frac{\sqrt{T(°K)}}{p(mm)}\frac{dw}{dt}\ (mg\ min^{-1})\right]$		$\frac{p\ (mm)}{\sqrt{T(°K)}}$
			Experimental	Knudsen [Eq. (10.1-2)]	
132	311.4	0.00571	1.15 ± 0.04	1.324	0.000324 (1.6)†
49	323.9	0.0142	1.10 ± 0.04	1.312	0.000790 (0.8)
130	324.0	0.0143	1.16 ± 0.02	1.312	0.000797 (0.7)
52	348.1	0.0687	1.10 ± 0.04	1.279	0.00368 (1.1)
131	348.3	0.0695	1.08 ± 0.02	1.279	0.00372 (1.0)
50	372.2	0.269	1.14 ± 0.04	1.302	0.0139 (1.2)
33	372.3	0.270	1.12 ± 0.06	1.303	0.0140 (0.6)
39	396.4	0.888	1.29 ± 0.03	1.533	0.0446 (1.0)
31	421.4	2.64	2.04 ± 0.04	2.221	0.129 (0.9)
29	421.3	2.63	1.98 ± 0.05	2.217	0.128 (1.3)
43	446.4	6.94	3.41 ± 0.07	3.783	0.328 (0.4)
35	471.4	16.4	6.36 ± 0.10	6.932	0.757 (0.4)
47	471.5	16.5	6.72 ± 0.12	6.945	0.759 (1.1)
41	496.6	35.7	11.4 ± 0.2	12.77	1.60 (0.3)
37	521.4	71.2	18.9 ± 0.5	22.66	3.12 (1.1)
53	521.5	71.3	20.1 ± 0.3	22.68	3.12 (0.4)
45	546.0	132	28.8 ± 0.5	38.37	5.67 (0.3)
55	561.0	189	32.9 ± 0.7	51.87	7.96 (0.2)
133	594.9	390	50.8 ± 0.7	96.77	16.0 (1.4)
135	631.0	774	65.5 ± 2.5	174.1	30.8 (0.8)
137	632.0	789	64.6 ± 0.8	176.9	31.4 (0.7)

*Orifice is constricted.

†Percent error.

TABLE 10.1-2

Derived Flow Rate Quantities, Series 6 (Oven 2-A)

Orifice Dimensions:
Radius = 0.03011 cm Length: Radius = 99.54
Length = 2.997 cm Clausing Factor = 0.02540

$$\left[\frac{\sqrt{T(°K)}}{p(mm)}\frac{dw}{dt}\ (mg\ min^{-1})\right]_{mol} = 3.587$$

Experiment	T(°K)	Pressure (mm Hg) [Eq. (6.3-1)]	$\left[\frac{\sqrt{T(°K)}}{p(mm)}\frac{dw}{dt}\ (mg\ min^{-1})\right]$		$\frac{p(mm)}{\sqrt{T(°K)}}$
			Experimental	Knudsen [Eq. 10.1-2)]	
81	311.7	0.00584	3.61 ± 0.20	3.546	0.000330 (5.4)*
90	316.3	0.00828	3.40 ± 0.10	3.533	0.000465 (2.7)
82A	324.2	0.0146	3.49 ± 0.07	3.505	0.000809 (0.9)
88	336.3	0.0328	3.36 ± 0.04	3.455	0.00179 (1.0
76	348.3	0.0698	3.38 ± 0.06	3.425	0.00374 (1.7)
89	360.2	0.139	3.45 ± 0.12	3.464	0.00735 (3.4)
77	372.2	0.269	3.43 ± 0.04	3.632	0.0139 (0.8)
93	384.4	0.499	4.04 ± 0.06	4.003	0.0255 (0.9)
91	396.6	0.898	4.54 ± 0.06	4.668	0.0451 (1.2)
68	396.7	0.904	4.17 ± 0.06	4.677	0.0453 (0.7)
79	408.8	1.56	5.34 ± 0.14	5.747	0.0770 (0.8)
62	421.6	2.66	6.48 ± 0.21	7.499	0.130 (1.2)
95	435.5	4.62	10.5 ± 0.14	10.44	0.221 (1.0)
74	446.6	6.99	13.1 ± 0.29	13.83	0.331 (0.5)
86	458.7	10.7	16.6 ± 0.36	18.96	0.501 (2.1)
64	471.5	16.5	24.9 ± 0.21	26.47	0.758 (0.5)
97	484.1	24.6	32.6 ± 0.68	36.61	1.12 (0.4)
66	496.7	35.8	40.7 ± 1.3	50.03	1.60 (2.8)
99	508.9	50.8	53.8 ± 0.83	67.22	2.25 (0.4)
84	521.8	72.0	66.1 ± 2.0	90.54	3.15 (0.8)
101	532.7	95.4	76.1 ± 1.6	115.2	4.13 (1.4)
105	551.4	151	112 ± 2.4	171.1	6.43 (1.1)
72	570.1	231	121 ± 3.0	247.2	9.68 (0.7)
70	570.7	234	118 ± 5.4	250.0	9.81 (4.1)
104	594.0	383	121 ± 6.6	381.9	15.7 (1.1)
140	594.1	384	132 ± 1.9	382.3	15.7 (1.2)
107	594.4	386	136 ± 10	384.6	15.8 (3.5)
145,147	630.9	774	143 ± 4.7	698.8	30.8 (1.1)

*Percent error

TABLE 10.1-3

Derived Flow Rate Quantities, Series 7, (Oven 7)

Orifice Dimensions:
Radius = 0.03066 cm; Length: Radius = 66.41
Length = 2.036 cm; Clausing Factor = 0.0372o

$$\left[\frac{\sqrt{T(°K)}}{p(mm)}\frac{dw}{dt}\,(mg\ min^{-1})\right]_{mol} = 5.453$$

Experiment	T°K	Pressure (mm Hg) [Eq. (6.3-1)]	$\left[\frac{\sqrt{T(°K)}}{p(mm)}\frac{dw}{dt}\,(mg\ min^{-1})\right]$		$\frac{p(mm)}{\sqrt{T(°K)}}$
			Experimental	Knudsen Eq. (10.1-2)	
124	309.6	0.00497	5.33 ± 0.10	5.400	0.000283 (1.6)*
123	324.1	0.0145	5.34 ± 0.14	5.331	0.000804 (2.5)
125	348.1	0.0687	5.26 ± 0.09	5.214	0.00368 (1.7)
126	348.3	0.0696	5.27 ± 0.08	5.214	0.00373 (1.4)
121	348.4	0.0700	4.93 ± 0.07	5.214	0.00375 (1.4)
122	372.3	0.269	5.31 ± 0.12	5.558	0.0140 (2.3)
109	396.6	0.897	6.52 ± 0.24	7.201	0.0451 (1.7)
127	397.0	0.914	6.54 ± 0.10	7.246	0.0459 (1.5)
113	421.9	2.70	11.1 ± 0.15	11.77	0.131 (0.6)
117	447.0	7.09	19.7 ± 0.50	21.93	0.335 (1.1)
111	472.1	16.8	37.1 ± 1.4	32.32	0.771 (1.1)
128	484.9	25.1	47.7 ± 1.6	58.88	1.14 (1.1)
115	497.4	36.6	60.2 ± 1.3	80.46	1.64 (0.8)
119	522.4	73.1	86.3 ± 1.7	144.9	3.20 (0.8)

*Percent error

TABLE 10.1-4

Derived Flow Rate Quantities, Series 8 (Oven 9)

Orifice Dimensions:
Radius = 0.02141 cm; Length:Radius = 0.0729
Length = 0.00156 cm; Clausing Factor = 0.965

$$\left[\frac{\sqrt{T(°K)}}{p\ (mm)}\frac{dw}{dt}\,(mg\ min^{-1})\right]_{mol} = 68.88$$

Experiment	T(°K)	Pressure (mm Hg) [Eq. (6.3-1)]	$\left[\frac{\sqrt{T(°K)}}{p\ (mm)}\frac{dw}{dt}\,(mg\ min^{-1})\right]$ Experimental	$\frac{p\ (mm)}{\sqrt{T\ (°K)}}$
150	301.4	0.00261	69.5 ± 1 6	0.000150 (2.0)*
148	324.1	0.0144	70.1 ± 0.7	0.000799 (0.9)
154	337.0	0.0343	69.8 ± 1.3	0.00187 (1.8)
151	348.3	0.0696	69.0 ± 0.6	0.00373 (0.8)
149	372.2	0.269	81.2 ± 0.5	0.0139 (0.5)
153	406.3	1.39	101 ± 1.0	0.0690 (0.9)
152	448.3	7.43	115 ± 1.5	0.351 (0.8)
157	499.2	38.5	112 ± 1.3	1.72 (0.7)
155	548.8	141.8	114 ± 2.2	6.05 (1.6)

*Percent error

10.2 The General Behavior of the Flow of Mercury Vapor

Logarithmic plots of the derived quantities listed in Tables 10.1 are graphically represented in Figures 10.2. In these plots the horizontal lines at the left represent the value of the calculated ordinate derived from the molecular flow equation (10.1-1), the orifice parameters listed in both Table 8.3-2 and Tables 10.1. It should be noted that the representation of the data is similar to that used by Knudsen,[13] with his "T" function, and by others who plot an analogous quantity called the specific flow variable.[59] It is the general practice to represent these data normalized to unity for the molecular flow limit; this is avoided here because it obscures the relationship between the experimental and derived quantities. The present data, derived quantities, and the graphical representations consider the flow behavior of the mercury vapor in relation to the source pressure, which is assumed at present to be the saturation pressure of mercury corresponding to the measured temperature of the liquid.

The quantities derived from the data of the four series of experiments yield graphical representations having quite similar features. An examination of the Figures 10.2 show qualitatively that at the lowest pressure or value of the abscissa, log $p/\sqrt{T}$, the ordinates in all but the series 5 representation are nearly predictable by the molecular effusion formula with the Clausing factors derived by DeMarcus[42] and the measured parameters of the orifices. The discrepancy in Figure 10.2-1 for series 5 at the lower pressures appears to arise from the previously mentioned constriction in the orifice of the oven used in this series.

In the graphical representations of the series 5, 6 and 7 experiments on the flow of vapor through channeled orifices, the value of the ordinate, $\log\left(\frac{\sqrt{T}}{p}\frac{dw}{dt}\right)$, appears first to decrease and then to increase for increasing values of the source pressure. This is in agreement both with the predictions of Knudsen's semitheoretical formula and the

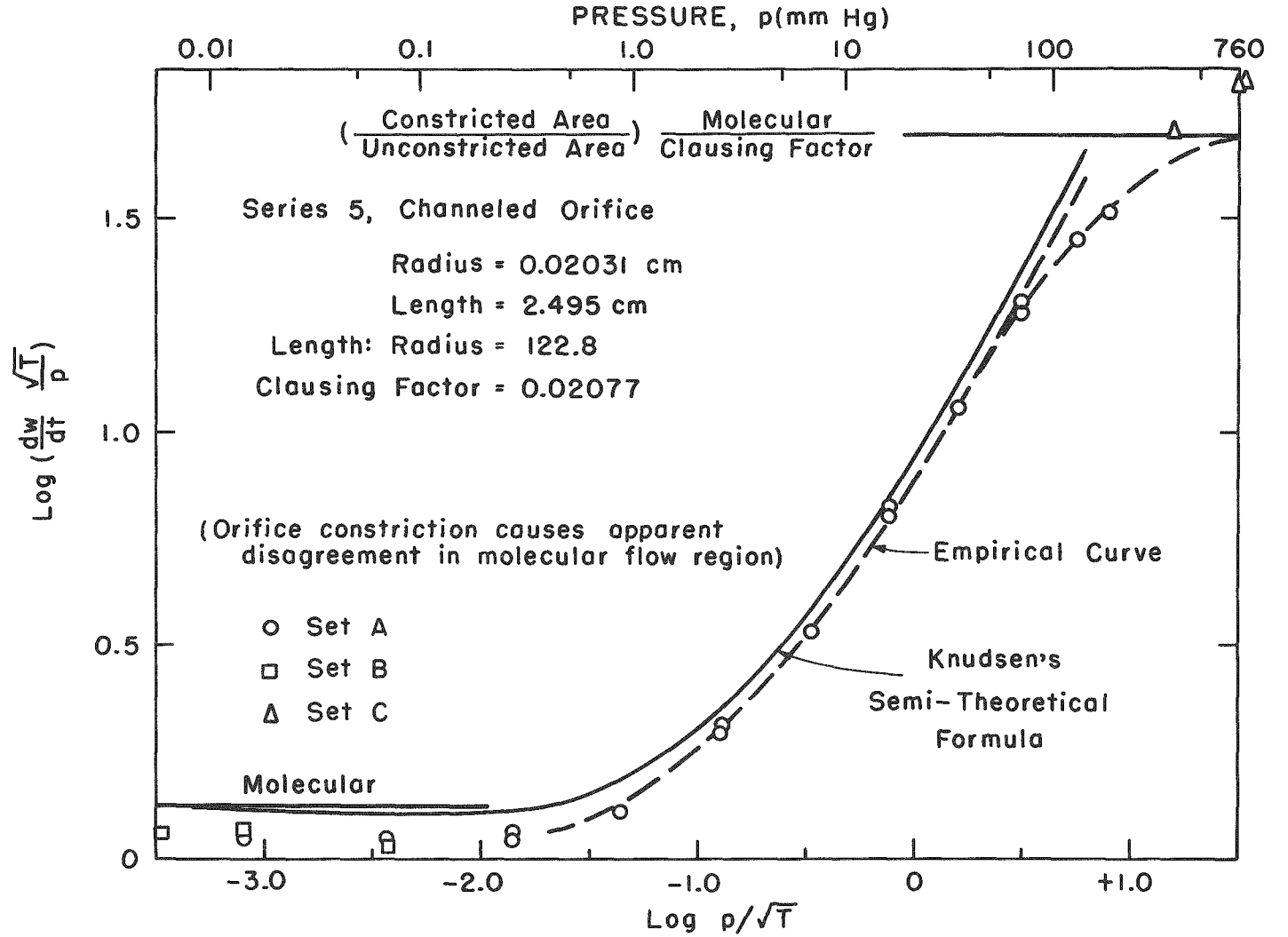

Fig. 10.2-1 Graphical Representation of the Experimental and Theoretical Flow Rates for Series 5

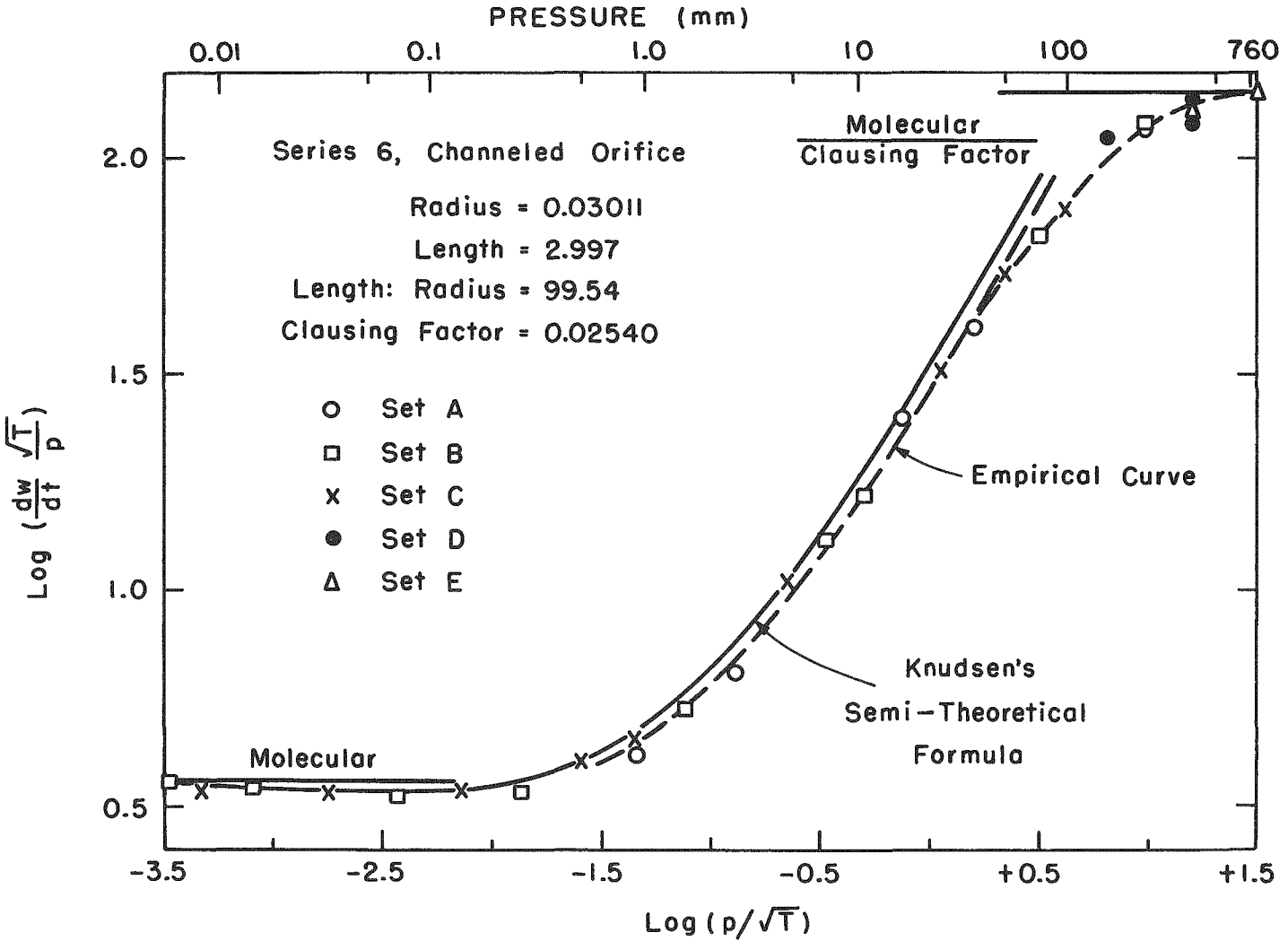

Fig. 10.2-2 Graphical Representation of the Experimental and Theoretical Flow Rates for Series 6

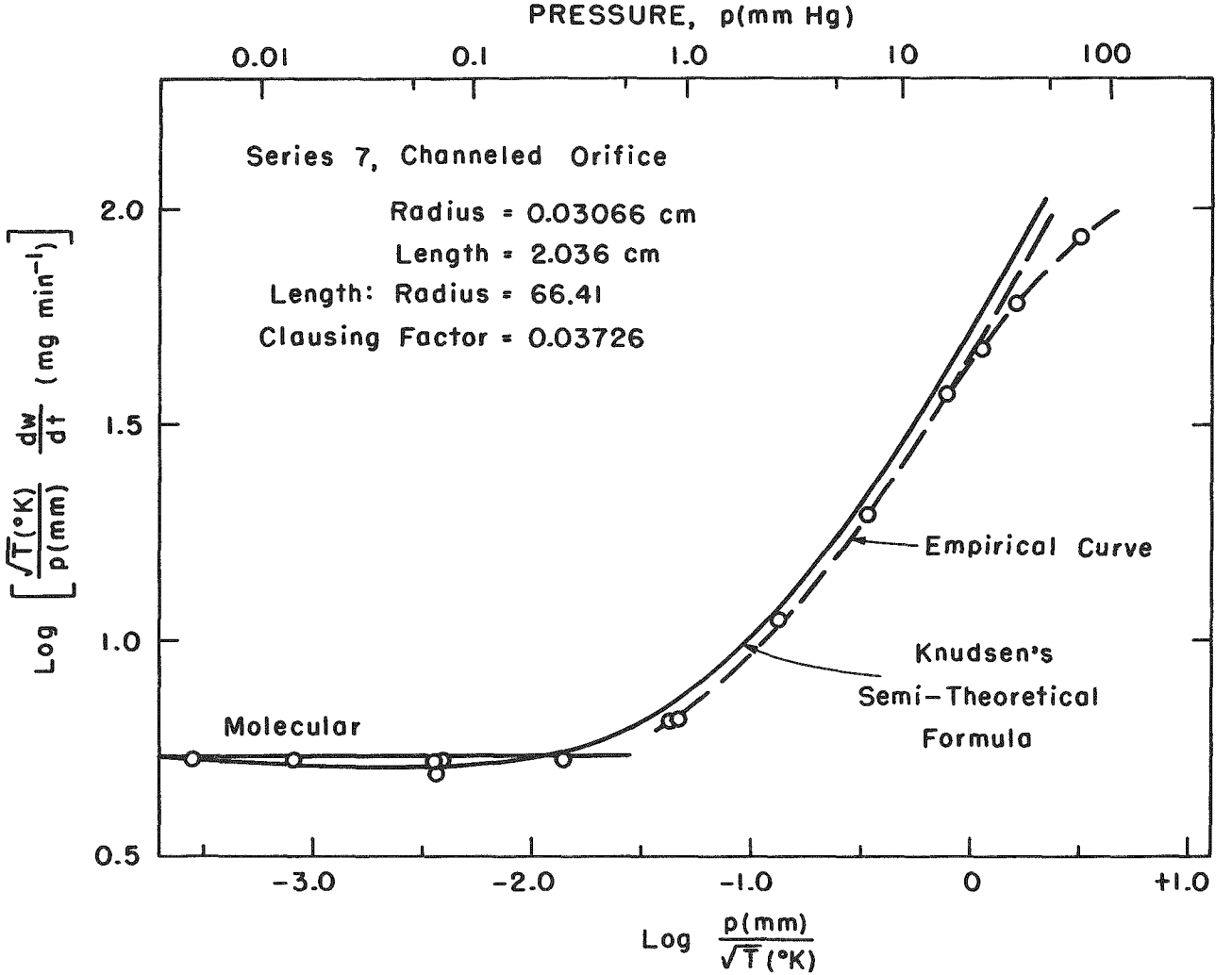

Fig. 10.2-3 Graphical Representation of the Experimental and Theoretical Flow Rates for Series 7

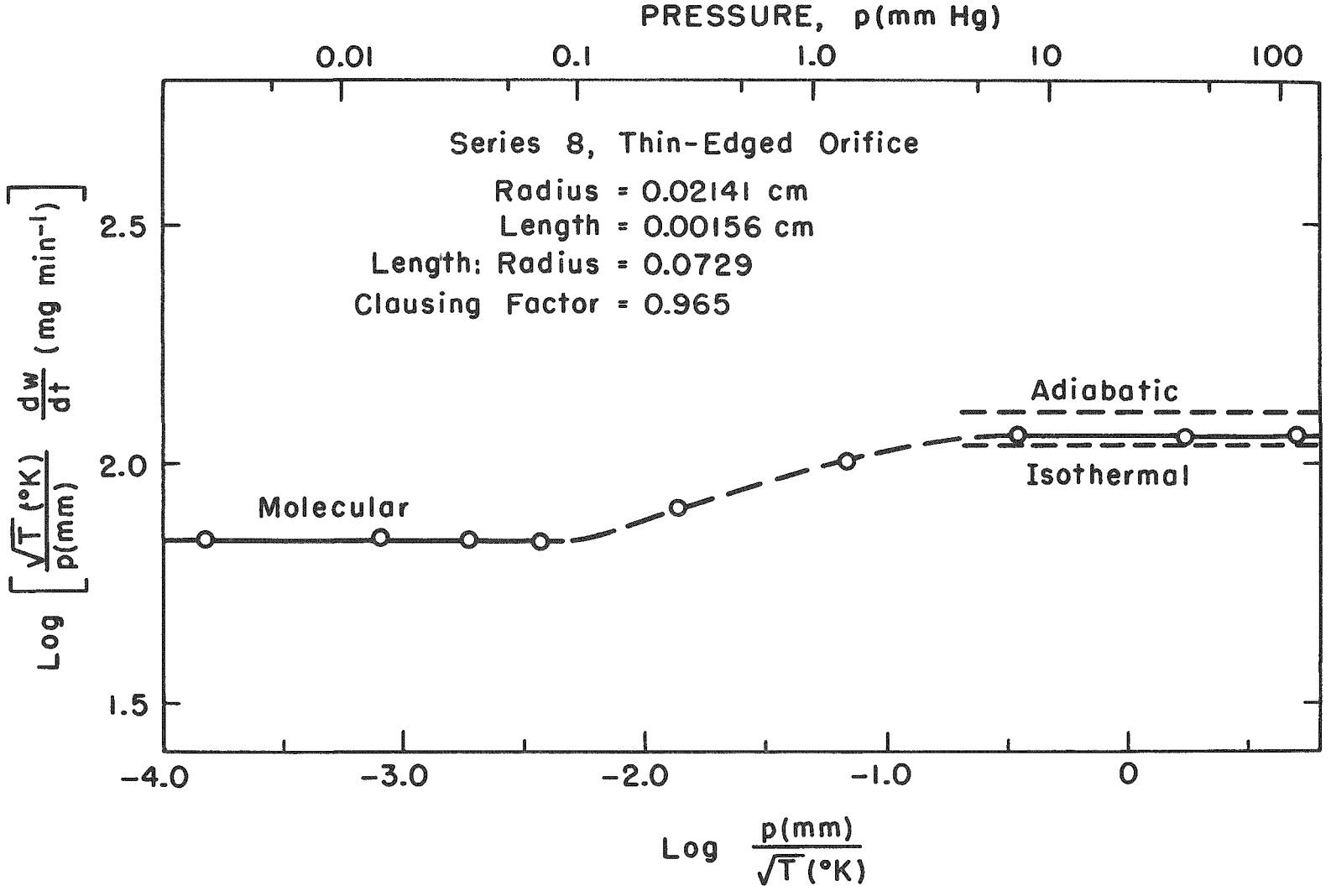

Fig. 10.2-4 Graphical Representation of the Experimental and Theoretical Flow Rates for Series 8

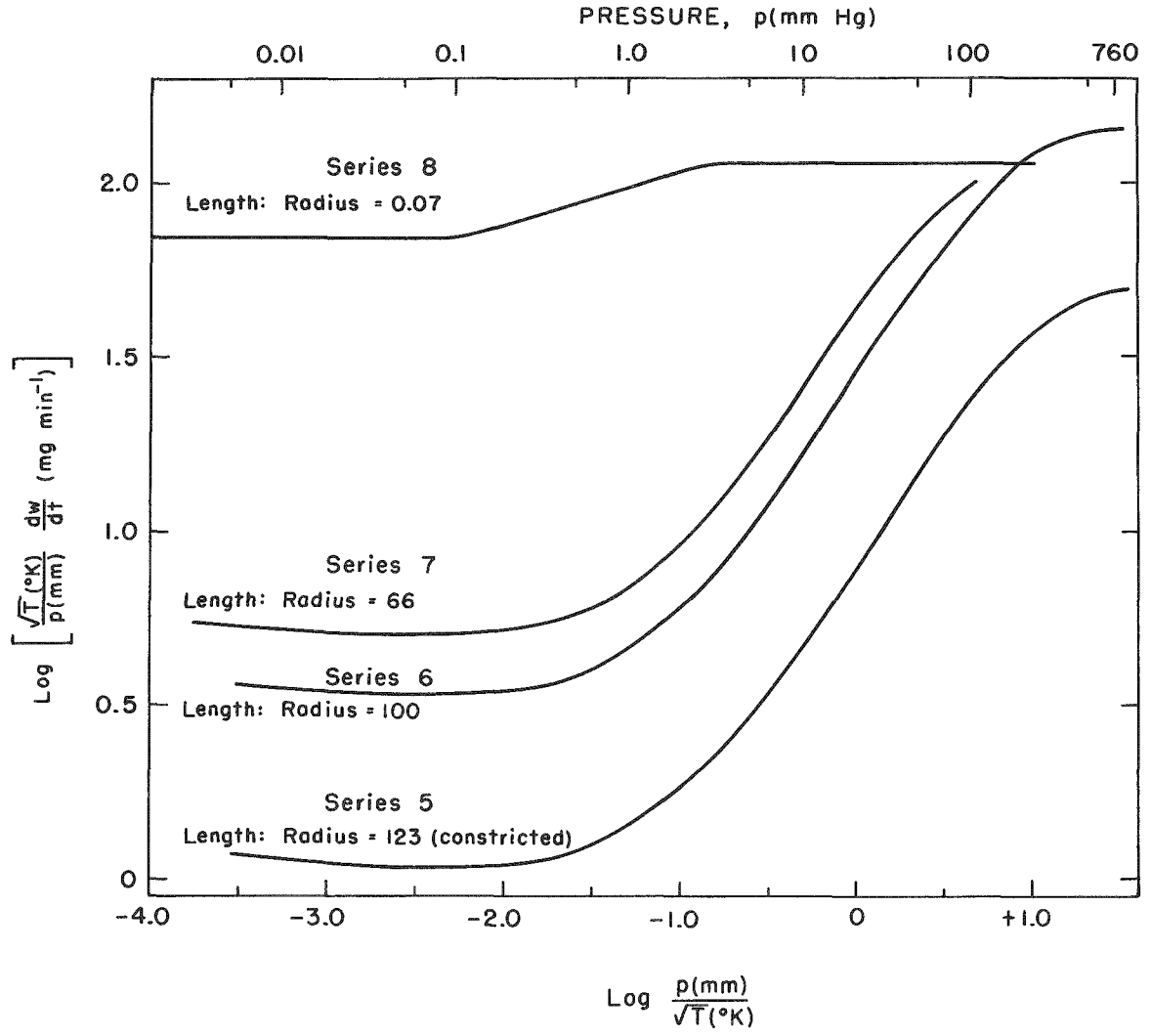

Fig. 10.2-5 Comparison of the Experimental Flow Rates for All Series of Experiments

results of similar experiments as outlined in the initial chapters. The solid curve drawn in the figures under consideration is derived from Knudsen's formula with the values of the viscosity, pressure, and orifice parameters recorded in Tables 10.1. In the pressure region of 0.5 mm Hg and above, the experimental values of the ordinate appear to follow the same general trend as predicted by Knudsen's formula, but are systematically lower. In the graphical representation of the Series 8 experiments on the flow of vapor through a thin-edged orifice, there is no minimum, but the ordinate does increase at a pressure of 0.1 mm Hg.

The series 6 representation shows that at source pressures of several tens of mm Hg, the values of the ordinate systematically and increasingly depart from the predictions of Knudsen's formula, and it appears that the flow approaches some kind of a limiting rate. The horizontal line drawn in the figure in this pressure region is the value of the ordinate derived from the molecular flow formula with the Clausing factor taken as unity or similarly the molecular flow value, $\left[\frac{\sqrt{T}}{p}\frac{dw}{dt}\right]_{mol}$, recorded in Table 10.1-2 divided by the Clausing factor. The reason this value appears to correspond to the limiting flow rate may be that at these high source pressures the channeled orifice behaves as if it were nearly saturated with vapor so that the virtual source of vapor is near the exit of the orifice. This phenomenon appears not to have been previously reported.

The effusive behavior at high pressures for the series 5 and 7 qualitatively agrees with the more detailed results of series 6. The effusive behavior at high pressures for the series 8 also shows a limiting flow rate, but this rate is expected on the basis of the previous experiments of Knudsen. The present experimental flow rates in the region of source pressures of 10 mm Hg and higher are nearly in agreement with the hydrodynamical isothermal effusion formula (2.2-3).

In the region of pressures of 5 mm Hg and above, the slope of the curve defined by Poiseuille's formula would be unity for a graphical plot similar to those of Figures 10.2 if the viscosity were independent of the temperature. The present experiments differ from those of Knudsen in that an increase in pressure necessarily requires an increase in temperature. Consequently, since the viscosity of the vapor increases with temperature, the slope of the curve in question would be slightly less than unity. On the other hand, Knudsen's formula predicts and the present data yield a slope much less than Poiseuille's formula because the viscous and molecular flow contributions are comparable. The purely viscous flow term of Knudsen's formula begins to predominate only in the high pressure regions in which the experimental curve commences to depart from the viscous flow behavior.

Consequently, except for the high-pressure limiting flow of vapor through channeled orifices, the effusive behavior of mercury vapor in the present experiments is in qualitative agreement with previous concepts and experiments. The results of the experiments of series 8 appear to be of sufficient precision and accuracy that they are unequivocal, and this should allow one to clarify to some extent the departure from molecular flow of the effusive behavior of vapors flowing through a thin-edged orifice. The experimental results of the effusive behavior of the vapors flowing through the channeled orifices are of less precision than desirable, but they should allow one to deduce some limited conclusions. The quantitative aspects are now considered.

10.3 The Flow of Mercury Vapor through Channeled Orifices, Series 5, 6 and 7

(a) The Molecular Flow Limit

(1) The Experimental Intercept

Because of insufficient precision and measurements it is not possible to conclude that the present observations extrapolate to the molecular flow limit. However, the experimental values of the ordinate for the low-pressure measurements and the theoretical molecular

flow values calculated from the measured orifice parameters are compared in Table 10.3-1. For experiment 127 of series 7, the experimental quantity is lower than the theoretical limit by about 2 percent, which is nearly within the limits of the a priori error. For series 6, experiment 81 yields a quantity in good agreement with the theoretical value, but the a priori error is large; experiment 90 yields a value which is low by about 5 percent, and the average of the two experiments yields a quantity which is within 2.2 percent of the theoretical value.

TABLE 10.3-1

Comparison of the Experimental and Theoretical Ordinates for the Molecular Flow Region of Pressures

Series	Experiment	$\left[\frac{\sqrt{T}}{p}\frac{dw}{dt}\right]$ (Experimental)	$\left[\frac{\sqrt{T}}{p}\frac{dw}{dt}\right]_{mol}$ (Theoretical)	Percent Difference
5	132-T	1.15 ± 0.04	1.334(a) 1.034(b)	-13 +12
6	81	3.61 ± 0.20	3.587	+ 0.6
	90	3.40 ± 0.10		- 5.0
	average	3.51 ± 0.11		- 2.2
7	124	5.34 ± 0.10	5.45	- 2.0

(a)Calculated for an unconstricted orifice.

(b)Calculated for the maximum extent of the effect of a constriction. Refer to text.

The results of series 5 in the low-pressure region are somewhat difficult to interpret, but one may show that the discrepancy is most likely caused by the constriction in the orifice at the exit. The idealized situation is similar to that discussed in Chapter 5 in regard to the extent of saturation within a cylindrical enclosure; the constriction in the exit end of the orifice tends to increase the wall emission

density. Accordingly, the problem becomes that of deducing the correct transmission coefficient or Clausing factor for the orifice. The theoretical low-pressure limit was calculated with the value of the cross-sectional area S_1 of the unconstricted portion of the channel and the Clausing factor derived from the radius defining this circular area. On the other hand, if we may consider the constricted end to define a reflecting surface similar to the lid portion of a Knudsen cell, then the correct transmission coefficient to be used to define the low-pressure limiting value of the ordinate in the series 5 experiments is that function W(H,P,1) defined by equation (5.4-4). Consequently, the molecular flow quantity desired is

$$\frac{\sqrt{T}}{p}\frac{dw}{dt} = 49571\ S_1\ W(H,P,1) \quad , \tag{10.3-1}$$

as is apparent from the equation (5.4-5), rather than the already calculated value

$$\frac{\sqrt{T}}{p}\frac{dw}{dt} = 49571\ S_1\ W(H,1,1)$$

$$= 1.334, \tag{10.3-2}$$

where

$$P^2 = \frac{\text{area of constricted cross section}}{\text{area of nonconstricted cross section}}$$

$$= 0.775 \quad . \tag{10.3-3}$$

We cannot calculate W(H,P,1) exactly without detailed numerical work, but we can demonstrate the extent of this transmission coefficient. Since the constricted exit contributes to the wall emission density, $n(\eta) = 1 - \delta(\eta)$, then $n(\eta)$ is larger than it would be for the present orifice if the constriction were absent. Therefore, if the quantity $\delta(\eta)_c$ were that leading to the Clausing factor W(H,1,1) for the tube having a uniform cross-sectional area S_1 throughout, and if the positive but small value $\delta(\eta)^*$ were a measure of the increase in the wall emission density, then one could write

$$\delta(\eta) = \delta(\eta)_c - \delta(\eta)^* \quad , \tag{10.3-4}$$

where $\delta(\eta)$ is the quantity needed to determine the present transmission coefficient.

One may show that

$$p^2 \frac{\partial}{\partial \eta} K(H-\eta,\ 1,\ 1) \geq \frac{\partial}{\partial \eta} K(H-\eta,\ P,\ 1) \quad . \tag{10.3-5}$$

Thus, the above expression (10.3-4) and equation (10.3-5) may be placed into the equation (5.4-4) to obtain the equation

$$W(H,P,1) \geq P^2 W(H,1,1) + 2 \int_0^H \delta(\eta) * \frac{\partial}{\partial \eta} K(H-\eta,P,1)\, d\eta. \tag{10.3-6}$$

Therefore, the correct transmission coefficient is larger than $P^2W(H,1,1)$, where $W(H,1,1)$ is the coefficient reported in Table (8.3-2). Hence, the limiting molecular flow quantity is greater than

$$\left[\frac{\sqrt{T}}{p} \frac{dw}{dt}\right] = (1.334)\ (0.775)$$

$$= 1.034 \quad . \tag{10.3-7}$$

As shown in Table 10.3-1, this value leads to a discrepancy between the theoretical and experimental values to the same extent as before. Consequently, it appears quite likely that the discrepancy principally is due to the effect of the constriction.

In summary, the present data demonstrate that the limiting values of the ordinate at low pressures for the two series 6 and 7, where a quantitative comparison may be made, are on the average within 3 percent of the theoretical values and within the precision of the data. The comparison for series 5 suggests an agreement within the extent of one's knowledge of the systematic error due to the effect of the constriction in the orifice. The accuracy of the data is another matter, and this point has bearing on whether values at low pressures are really less than or greater than the theoretical values. For series 6 and 7 the data superficially suggest that the experimental values of the ordinate at the low pressures are less than the theoretical molecular flow values.

There are two known possible sources of a systematic error. The first is that attributable to the possible error resulting from the thermocouple circuitry, as discussed in section 8.3. This error is such that, if it exists, the true low temperatures are less than those reported; consequently, the true pressures are less than those employed and the ordinates should be larger than those calculated. The second source of error is that arising from an error in the heat of vaporization of mercury. As discussed in Appendix 2, the error may be such that the pressures employed are too low by one or two percent, and the true experimental ordinate possibly should be larger. Consequently, both of the known possible sources of error could lead only to a decrease or to a change in sign in the apparent discrepancy. Another point which should be remembered is that one has no assurance that the experiments have been carried to low enough pressures that true molecular flow occurred.

(2) Comparison of the Intercept with Previous Observations

The known possible sources of a systematic error lead one to conclude that the discrepancies, if any, between the theoretical and experimental values of the intercept are no greater than 3 percent of the theoretical value. Berman and Lund[59] and Huggil,[58] on the other hand, suggest that the true limiting flow possibly should be of the order of 5 percent less than the theoretical molecular flow formula predicts with the use of Clausing's factor. The suggested reason for this occurrence is that the reflections at the wall of the channel are not random, but depend on the potential of interaction between the wall surface and the impinging molecules. This may indeed be the case, but the present data are not precise nor extensive enough to furnish any evidence bearing on this point. The only conclusion these present data permit one to draw is that the agreement between the experimental and theoretical values is within the experimental precision of about 3 percent.

(b) The Region of the Transition between Molecular and Viscous Flow

(1) The Minimum

Strict conclusions on the correspondence of the experimental data with the theoretical predictions in the transition region depend upon the reliability of the vapor pressure values employed in this study. The low-temperature data, however, indicate that at values of $p/\sqrt{T}$ of 10^{-2} and less there occurs in the quantity $\left[\frac{\sqrt{T}}{p}\frac{dw}{dt}\right]$ a very slight minimum value in accordance with those ideas outlined in Chapter 2. The minimum appears to be most significant in the series 5 experiments, and least significant in the series 7 experiments. This minimum as it occurs in series 5 may be the result of the constriction in the orifice, but the data for the other two series do not appear to be explainable on this basis unless it be a matter of the uniformity of the cross section of the channeled orifice.

The minimum in the ordinate $\left[\frac{\sqrt{T}}{p}\frac{dw}{dt}\right]$ for series 6 occurs in the region of experiment 88, and this experiment yields a value of the ordinate about 1.1 percent lower than that of experiment 90. The individually assigned errors propagated from the basic data are larger than this value, so that one must examine the data closely to decide upon the reliability of these observations. The difference in the ordinates of experiments 125 and 124 of series 7 amounts to about 1.3 percent, which is nearly comparable to the possible minimum in series 6.

In the low-temperature region of interest, gas imperfections in mercury vapor are insignificant. Thus, the quantity $\left[\frac{\sqrt{T}}{p}\frac{dw}{dt}\right]$ may be written in the form

$$\log\left[\frac{\sqrt{T}}{p}\frac{dw}{dt}\right] = \log\left(\sqrt{T}\frac{dw}{dt}\right) + \frac{\Delta H^{\circ}_{T}}{2.303\ R_0 T} - \frac{\Delta S^{\circ}_{T}}{2.303\ R_0} \quad . \quad (10.3\text{-}8)$$

The heat capacities of mercury appear to be sufficiently well established that the small uncertainties in the entropy and temperature dependence of the heat introduce no appreciable errors. Consequently, the error in $\log\left(\frac{\sqrt{T}}{p}\frac{dw}{dt}\right)$, aside from experimental systematic errors in the temperatures and random fluctuations in the mass flow rate measurements, is the error in ΔH_0°, and thus the percent error in the quantity $\left(\frac{dw}{dt}\frac{\sqrt{T}}{p}\right)$ is the error in

$$\Delta H_0^\circ / R_0 T \quad .$$

An error in the ΔH_0° value used in the vapor pressure equation introduces a systematic error in $(\sqrt{T}/p)(dw/dt)$ which will not cause the curve to pass through a minimum as observed experimentally. If the heat ΔH_0° employed is too high, then, consistent with the requisite entropy change, the effect would be to raise the lowest values of the ordinate and deepen the minimum. On the other hand, a value of ΔH_0° too low would tend to make the experimental minimum less pronounced. For a small adjustment in the heat ΔH_0°, however, the region under consideration will be affected primarily in the limiting value of the ordinate at the low temperatures with the general features of the transitional region remaining largely unaffected.

Both sources of a known possible systematic error, as previously described, would tend to obscure the minimum in these curves if the minimum exists; that is, if these errors are real and significant and could be accounted for, the present data would show a more pronounced minimum. But it is possible to analyze the data only as they now exist. In the region around pressures of 0.05 mm Hg, the experimental values of the ordinates compared with those at the lowest pressures indicate a minimum of the extent of 4 percent in series 5, 1 to 8 percent in series 6, and about 1.3 percent in series 7. In view of the a priori errors, however, the minimum appears to be real only in series 5; the data of the other two series could nearly define a straight

line having ordinate values of 3.43 for series 6 and 5.30 for series 7 with the experiment 121 discarded; this experiment appears to be in error. Therefore, if a minimum exists in series 7, it is 3.3 percent or less than the theoretical molecular flow limit, and may be about 1.3 percent less than the experimental ordinate at the lowest pressure. Similarly, if a minimum exists in the series 6 data, it is 6.1 percent or less than the theoretical molecular flow limit and may be about 4 percent less than the experimental ordinate at the lowest pressure. The minimum in series 5 appears to be real and about 4 percent of the experimental ordinate at the lowest pressure. These observations are summarized in Table 10.3-2.

TABLE 10.3-2

Extent of the Minimum

Series	Extent of Minimum
5	4%
6	<6% (Perhaps about 4%)
7	<3.3% (Perhaps about 1%)

(2) Comparison of the Minimum with Previous Observations

The problem in determining the existence of a real minimum in the curves for the present data is that the precision of the measurements is not sufficient and that it is quite possible that the extent of the minimum, if real, amounts to a very small percent of the limiting value of the ordinate at the lowest pressures. The present experimental data appear to follow a trend similar to Knudsen's formula, which is based on data for gaseous flow under conditions of smaller pressure gradients. The differences are not surprising. The minimum in the curve at low pressures may be less pronounced and thus qualitatively agrees with the idea that gas-phase collisions tend to cause the initial decrease. As the pressure gradient becomes large at a constant source pressure for a given channeled orifice, the total effect of gas-phase collisions becomes less. The constriction in the orifice of the oven 3

for series 5 would decrease the pressure gradient, and thus one might expect a consequent increase in the effect of gas-phase collisions and a more pronounced minimum; that is, the constriction would yield results more in agreement with the usual bilateral flow measurements.

The data for all of the ordinates of series 6 and 7 in the region of $p/\sqrt{T}$ equal to 10^{-2} and less agree on the average within better than 2 percent with Knudsen's semitheoretical formula.

(c) The Viscous Flow Region

In the strongly curved region at source pressures near and greater than 0.2 mm Hg the figures show an abrupt transition, and the experimental curve is nearly parallel to Knudsen's curve, the difference amounting to about 10 percent for experiment 117 of series 7. It is possible that the mercury viscosity is too low by this same percentage or more, so that too great a reliance on the difference might prove to be misleading. On the other hand, if Knudsen's formula were strictly applicable here, the present data might well be a reliable measure of the vapor viscosity. The correspondence is such that an estimate of the vapor viscosity by an effusion method similar to that of this study should yield viscosities within 10 to 20 percent in these pressure regions.

(1) The Extent of the Viscous Flow Behavior

The dashed curves drawn through the experimental data for each of the three series 5, 6, and 7 show a similar systematic departure from Knudsen's semitheoretical curve. The apparent parallelism between the curves is quite striking and suggests some kind of systematic error leading to a constant difference in the logarithms. An inspection of Knudsen's formula shows that a possible error in the radii of the channels could lead to such an effect. However, this does not appear to be the correct explanation for two reasons. First, Knudsen's equation contains two terms of nearly comparable magnitudes in the low-pressure region but of different magnitudes in the regions at higher pressure.

An error in only one of the terms would not generally lead to a constant error in the logarithm, and the molecular flow term appears to be sufficiently accurate that a large error cannot be attributed to this term. Secondly, we know there is an error of about 10 percent in the radius of the oven used for series 5, but this amounts to nearly a 40 percent error in the factor R^4 occurring in the viscous term of Knudsen's formula. However, since the results of series 5 in this viscous region show a trend nearly identical to those of the other two series, the difference between the experimental and semitheoretical curves appears to arise from some fundamental aspect of the flow. In fact, it would appear that the constriction in the orifice for series 5 has little effect, if any, on the flow behavior in this viscous flow region. This suggests that the end effects, such as beam contraction or expansion of the gas, are not sensitive to the uniformity of the channel at its exit.

One cannot ascribe any great significance to Knudsen's formula, as has been emphasized previously, first because the derivation is not rigorous and, secondly, because the formula as applied to the present study should contain terms to account for the expansion of the gas. For the relatively short channels used in this study the viscous flow formula is not applicable first without the usual end corrections and even less applicable to the present study because of the severe pressure gradients which necessarily existed. The irreversible character of the flow in this region probably is such that the expansion of the gas cannot adequately be treated by considerations of reversible isothermal or adiabatic expansions. This is suggested by the thermal effects studied in conjunction with series 5 and reported in section 9.2. We shall return to this point later. However, there cannot be any doubt that at least within a limited pressure region the flow is of a viscous nature, and the parallelism between the experimental and semitheoretical curves is such at the parameters in Knudsen's equation probably could be adjusted to effect a reasonably good fit to the experimental data.

In the upper pressure regions beginning in the region near 50 mm Hg, the curves begin to depart increasingly from Knudsen's equation, and these departures occur at pressures where the viscous term in Knudsen's equation becomes the principal term. Consequently, the length-to-radius ratios of the present orifices are too small to allow us directly to determine if viscosities within, for example, 10 percent of the true value could be measured by the effusion method employed here. It ought to be possible for a channel of about 30 cm or more in length to be coiled and placed within the present ovens. If the departure from the viscous behavior observed here at the upper pressures is restricted by the increased length, then it would be possible to extend flow measurements to higher pressures and temperatures. A problem associated with this, however, in regard to applying the technique to the measurement of viscosities would be the pressure effects. The coefficient of viscosity is not very sensitive to pressure at normal densities, but at several atmospheres the effect in a precision measurement might well be noticeable and obscure the normal viscous behavior. Nevertheless, one ought to be able to measure viscosities of saturable vapors to within 10 percent over a temperature region of nearly 50 degrees by such methods.

(2) The Upper Pressure Region

The upper pressure region is perhaps the most interesting aspect of these data. The experimental quantities define a curve which progressively departs from the viscous flow predictions and appears to approach some kind of a limit at about one atmosphere of pressure within the effusion cell. Surprisingly, though perhaps fortuitously, this limit in series 6 is exactly that predicted by the molecular effusion formula applicable to a thin-edged orifice. Of course, there must be some limit to the effusion rate; the viscous flow equation predicts continuously increasing rates, whereas the true rate cannot exceed the rate of evaporation of the liquid mercury. However, if it were true,

and it probably is not, that the oven was totally saturated with vapor under all conditions, then the rate of effusion would not exceed the arrival rate of molecules at the inner opening of the channel. The data indicate this to be the case for series 6. The situation in series 5 is complicated by the possibility that experiments (133, 134), (135, 136), and (137, 138) yield weight losses too high as a result of possible overflow of the liquid. Nevertheless, series 5 qualitatively agrees with the effects observed in series 6. Not enough mercury could be contained in the oven for series 7 to permit higher pressure measurements to be made, but the partial results of series 7 agree with the more detailed aspects of the flow behavior measured in series 6.

The true situation must be complicated; certainly there would be some effect analogous to a process leading to increasing saturation of the channel through turbulent interactions. But turbulence, expansion of the vapor, and thermal effects must be strongly associated at these high rates of effusion. The experiments 58-1 and 58-2, discussed earlier for series 5 in section 9.2, are probably generally applicable qualitatively to the three series. One will notice that the drop in the temperature difference between the well and the top-end temperature of the oven begins in the region where the curves begin to bend over and depart from the viscous flow behavior. The temperatures used in deriving the values of $\left(\frac{\sqrt{T}}{p}\,\frac{dw}{dt}\right)$ are those of the liquid, whereas the oven itself appears to be at a higher temperature, and the temperature of the vapor also may be higher. Consequently, the real nature of the flow is somewhat obscure. Probably turbulent effects begin to set in the region under consideration. The usual Reynolds number[65] [R] may be expressed in quantities appropriate to the experimental measurements by the relationship

$$[R] = 1.67 \times 10^{-5}\ \frac{dw/dt}{2\pi R\mu}\quad , \qquad (10.3\text{-}9)$$

where the symbols have their usual significance. For experiment 66 (67)

of series 6 one calculates a value of [R] of 12, whereas the usual value of the Reynolds number at which turbulent effects set in is [R] 7500 to 3,000.[65] Thus, the Reynolds number hardly seems appropriate here.

We have very little data on which to base decisions regarding the leveling off region near one atmosphere. We know that thermal effects are associated with this behavior but know little more. The only explanation presumably available is that a tendency might exist for the vapor to saturate the channel so that the virtual source of the vapor is near the exit of the tube. The question as to the reality of such an explanation is difficult to answer and would demand a more detailed experimental study. It was only the fortuitous choice of the particular orifice used in series 6 that permitted measurements to be made, although with difficulty, in the high-pressure region. In so far as the writer is aware, this effect has not been observed nor reported previously. Probably the usual hydrodynamic experiments would not demonstrate a completely analogous effect.

10.4 The Flow of Mercury Vapor through a Thin-edged Orifice

The data for series 8 depict a behavior almost identical to that observed by Knudsen.[17] The curve in Figure 10.2-4 shows the molecular flow behavior, a transition region, and some kind of a hydrodynamic behavior at the higher pressures. The writer wishes to emphasize that these present data are unusually precise for the method employed in this study and demonstrate an unequivocal behavior. The absolute values of the curve may be shifted slightly by small temperature or pressure errors, but the general behavior cannot be obscured by these errors.

(a) The Molecular Flow Limit

The data of series 8 compare favorably in the molecular flow region with the theoretically derived value of the ordinate, as can be seen in Figure 10.2-4. It is interesting, however, to compare the pressures calculated from the data by the use of the molecular effusion

formula (10.1-1) with the vapor pressures reported by Busey and Giauque[61] and derivable from the vapor pressure equation (6.3-1). Table 10.4-1 summarizes the appropriate data for series 8. The pressure p_1 (mm) is calculated from the molecular flow formula (10.1-1). The error in the calculated pressure is larger than the error in the mass flow rate $\frac{dw}{dt}$, but for the comparison of the internal consistency the percentage error in the pressure may be taken as the percentage error in the flow rate. The error of 2 percent in the Clausing factor in addition to the error in the flow rate yields an error in the pressure of more than 2 percent, and this is important in comparing the calculated pressure with those derivable from the vapor pressure equation (6.3-1), which comprises the pressures reported by Busey and Giauque.

The data summarized in Table 10.4-1 are assembled in three groups. Group 1 comprises the calculations which use the temperatures and weight losses experimentally averaged over the full heating period. Group 2 comprises the calculations which use the temperatures and weight losses measured at intermediate intervals during the experiment, as described in Section 9.1. Group 3 comprises the data covering the transitional and hydrodynamical flow regions. One will notice that the internal consistency of these data, both with respect to the a priori errors and agreement between the individual measurements, is excellent. The data of groups 1 and 2 in Table 10.4-1 show unusually good precision of about one percent or better, principally because the weight losses were large enough to be measured with ease. The data of group 3 show within a partial experiment less precision than that attributed to the data for a total experiment because the measured weight losses are smaller.

The pressures calculated from the molecular flow formula and assembled in group 2 agree within the precision of the data with the pressures reported by Busey and Giauque.[61] There may be systematic errors in the temperature, but the data show that up to a pressure of nearly 0.1 mm Hg the flow rate is calculable within at least 2 percent

TABLE 10.4-1

Pressures Calculated from the Data of Series 8

Radius (R) = 0.02141 cm (±0.3%) Length: Radius$\left(\frac{L}{R}\right)$ = 0.0729

*Length (L) = 0.00156 cm (±20%) Clausing Factor (W) = 0.965 (±2%)

Experiment	T(°K)	$\frac{dw}{dt}$ (mg min^{-1})	P_1(mm), calculated	P_2 (mm), Busey and Giauque	Percent Deviation $100\,\frac{P_1-P_2}{P_2}$	log p_1 (mm)	$\frac{10^3}{T(°K)}$
Group 1: Molecular Flow Region, Total Heating Periods							
150-T	301.4	0.01045(±1.05%)	0.00263	0.00261(±2.0%)	0.77	-2.580	3.318
148-T	324.1	0.05606(±0.61%)	0.0146	0.0144 (±0.86%)	1.75	-1.834	3.086
154-T	337.0	0.1304 (±0.48%)	0.0347	0.0343 (±1.8 %)	1.17	-1.459	2.968
151-T	348.3	0.2575 (±0.34%)	0.0698	0.0696 (±0.80%)	0.29	-1.156	2.871
Group 2: Molecular Flow Region, Partial Heating Periods							
150-1	301.4	0.01031(±2.1 %)	0.00260			-2.585	3.318
150-2	301.4	0.01040(±2.0 %)	0.00262			-2.582	3.318
148-1	324.1	0.05637(±2.0 %)	0.0147			-1.832	3.086
148-2	324.0	0.05741(±1.5 %)	0.0150			-1.824	3.086
148-3	324.0	0.05407(±2.0 %)	0.0141			-1.850	3.086
154-1	337.0	0.1299 (±0.95%)	0.0346			-1.461	2.968
154-2	337.0	0.1305 (±0.98%)	0.0348			-1.459	2.968
151-1	348.3	0.2523 (±0.64%)	0.0684			-1.165	2.871
151-2	348.3	0.2630 (±0.66%)	0.0713			-1.147	2.871

TABLE 10.4-1 (Cont'd.)

Pressures Calculated from the Data of Series 8

Radius (R) = 0.02141 cm (±0.3%) Length: Radius $\frac{L}{R}$ = 0.0729

Length (L) = 0.00156 cm (±20%) Clausing Factor (W) = 0.965 (±2%)

Group 3: Transition and Hydrodynamic Flow Region, Total Heating Periods							
Experiment	T (°K)	$\frac{dw}{dt}$ (mg min^{-1})	P_1 (mm), calculated	P_2 (mm), Busey and Giauque	Percent Deviation $100\ \frac{P_1-P_2}{P_2}$	log P_1 (mm)	$\frac{10^3}{T(°K)}$
149-T	372.2±0.1	1.132 (±0.23%)	0.317	0.269(±0.49%)	17.8	-0.499	2.686
153-T	406.3±0.2	6.968 (±0.44%)	2.039	1.390(±0.91%)	46.7	+0.309	2.461
152-T	448.3±0.2	40.31 (±0.99%)	12.39	7.427(±0.82%)	66.8	+1.093	2.231
157(158)	499.2±0.2	193.6 (±0.93%)	62.79	38.55(±0.66%)	62.9	+1.798	2.003
155(156)	548.8±0.6	693.6 (±1.0 %)	235.9	141.8(±1.5 %)	66.4	+2.373	1.822

by the molecular flow formula. Above this pressure the flow rate departs from the molecular flow prediction, and this will be analyzed subsequently. An unweighted least-squares analysis of the data assembled in group 1 yields for the heat and entropy of vaporization the values

$$\Delta H_0^\circ = 15{,}392 \pm 58 \text{ cal g-atom}^{-1}$$
$$\Delta S_{325}^\circ = 23.45 \pm 0.18 \text{ e.u.} \quad ,$$

and these agree within their errors with the values derived from the work of Busey and Giauque,[61]

$$\Delta H_0^\circ = 15{,}403 \text{ cal g-atom}^{-1}$$
$$\Delta S_{325}^\circ = 23.48 \text{ e.u.}$$

(b) The Transitional and Hydrodynamical Flow Regions

Figure 10.2-4 very clearly shows a departure from the molecular flow behavior at a source pressure of 0.1 mm or higher and a leveling off at a pressure near 5 mm Hg. Thus the figure shows two limiting flow behaviors and a transitional region extending over a pressure range differing by a factor of 50. The nature of this transition has never been clearly explained nor has the reason for the nature of the onset of the transition and the onset of the hydrodynamical behavior been unequivocally established. Nevertheless, this region, similar to the transition to viscous flow in channeled orifices, has the aspects of a progressive change in the bulk character of the gas from one of a discontinuous medium to one of a fluid medium.

In the pressure region of 5 mm Hg and higher, the flow rate appears to be slightly higher than the isothermal effusion formula predicts with no contraction of the issuing stream of vapor. From the expressions (2.2-2) and(2.2-3) one finds that

$$\frac{\left(\frac{\sqrt{T}}{p}\frac{dw}{dt}\right)_{\text{isothermal}}}{\left(\frac{\sqrt{T}}{p}\frac{dw}{dt}\right)_{\text{molecular}}} = \sqrt{\frac{2\pi}{e}}\frac{S_1}{SW} = 1.575\frac{S_1}{S} \quad , \qquad (10.4\text{-}1)$$

$$\frac{\left(\frac{\sqrt{T}}{p}\frac{dw}{dt}\right)_{adiabatic}}{\left(\frac{\sqrt{T}}{p}\frac{dw}{dt}\right)_{molecular}} = \left(\frac{2}{\gamma+1}\right)^{\frac{\gamma+1}{2(\gamma-1)}} \sqrt{\gamma 2\pi}\ \frac{S_1}{SW} \qquad (10.4\text{-}2)$$

$$= 1.886\ \frac{S_1}{S} \quad ,$$

where γ is the ratio of specific heats, which for mercury is 1.667, e is the base-number of the natural logarithms, S_1 is the cross-sectional area of the vena contracta, S is the orifice area, and W is the Clausing factor. The horizontal lines representing these hydrodynamic flows in the Figure 10.2-4 are drawn for S_1 equal to S.

The nature of the flow in this high-pressure region probably is complicated by several factors, such as the small extent of the channeling, thermal effects, contraction of the jet, and so forth. Therefore, it would be difficult to decide on the exact effusive behavior here. Nevertheless, the behavior clearly has the aspects of a truly hydrodynamical effusion process. It is interesting now to examine the data of series 8 on a log P vs $1/T$ plot, as in Figure 10.4. One can see that in the present experiments measurements were carried out to sufficiently high source pressures that the full effusive behavior could be ascertained. On the other hand, had the experiments been carried out only to pressures as high as 0.5 mm, such that only the first five of the lowest pressure points had been determined, then a plot such as that given in Figure 10.4 would suggest only the effect of large errors in the measurements rather than a fundamental violation of the conditions under which molecular flow occurs. This is exactly the reason why one wishes to establish as clearly as possible the necessary a priori conditions for the occurrence of molecular effusion, for rarely is a vapor pressure experiment capable of handling the excessive flow rates necessary to trace out the full experimental behavior. In the Argonne National Laboratory we have previously been confronted with this difficulty in

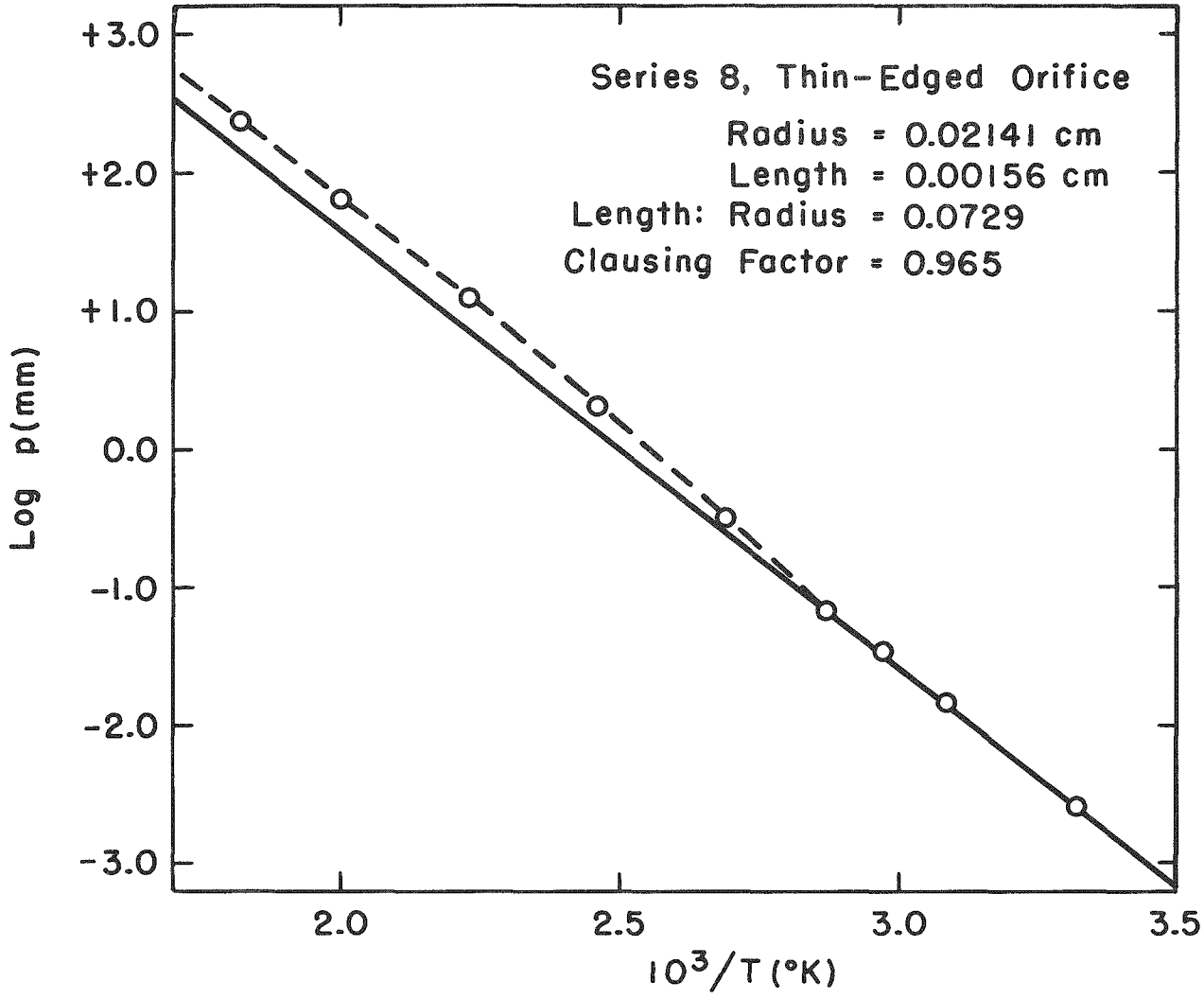

Fig. 10.4 Mercury Vapor Pressures Derived from the Experiments Compared with Pressures Reported by Busey and Giauque (Solid Curve)

connection with other less precise experiments[66] which yielded an entropy of vaporization several units too high for the substance under study. The present experiments, however, delineate the problem quite clearly.

(c) Comparison of the Effusive Behavior with Previous Concepts

We now come to the interesting but difficult questions regarding the comparison of these data with the concepts and experimental results of others. Specifically, one would wish to have these questions answered:

(1) How does one predict the onset of the departure from molecular flow?

(2) What is the behavior of the issuing stream of vapor in the transitional region ?

Clearly, the single series of experiments here is not capable of answering these questions unequivocally. Nevertheless these data combined with previous knowledge permit one to establish tentative conclusions, besides the one valid conclusion that molecular effusion occurs under present conditions up to 0.1 mm Hg. If the ratio of mean free path to orifice diameter or slit width is the defining quantity which predicts the onset of the departure, then the present data yield a ratio of about unity at this pressure. As discussed in Appendix 2, the mean free path may be calculated from the vapor viscosity, pressure and temperature by the formula

$$\lambda\ (\text{cm}) = 0.6064\ \frac{\mu(\text{poise})\sqrt{T(^\circ\text{K})}}{p(\text{mm})} \quad . \qquad (10.4\text{-}3)$$

Mean free path values and ratios of the mean free path to orifice diameter are tabulated in Table 10.4-2 for the various experiments of series 8.

Johnson's study[29] employed mercury, and the results of this study, as described in Chapter 3, lead one to infer that molecular flow occurs at mean free path-to-diameter ratios of less than unity.

The appropriate ratios for Johnson's study, on the basis of the same mean free path formula, are between 2.0 and 0.002 if the slit width of the orifice is used, or between 0.2 and 0.0002 if the slit length is used for the pressure range from 0.2 to 35.0 mm Hg. Consequently, the lowest pressure employed by Johnson is within the region where these present data begin to show the transitional regions. Since the same pressure ranges and nearly comparable orifice dimensions and same experimental substances were used in both the present study and Johnson's study, it seems reasonable to conclude that Johnson's experimental arrangement yielded, not molecular beams of mercury vapor, but rather fluid-like streams. These conclusions, of course, assume that the vapor pressures were correctly measured by Johnson.

TABLE 10.4-2

Mean Free Path Calculations for Series 8

Series 8

Orifice Radius (R) = 0.02141 cm

Experiment	T(°K)	p(mm)	$\mu(10^{-7}$ poise)	λ(cm)	$\lambda/2R$
150-T	301.4	0.00261	2698	**1.088**	25
148-T	324.1	0.0144	2929	**0.222**	5.2
154-T	337.0	0.0343	3062	0.0995	2.3
151-T	348.3	0.0696	3178	0.0517	1.2
149-T	372.2	0.269	3426	0.0149	0.35
153-T	406.3	1.390	3778	0.00332	0.078
152-T	448.3	7.427	4215	0.000729	0.017
157(158)	499.2	38.55	4749	0.000167	0.004
155(156)	548.8	141.8	5270	0.0000528	0.001

The conclusions derivable from the comparison of the present data with the results reported by Johnson could be extended further. For example, Johnson's data clearly show that the beam intensity in the forward direction was nearly proportional to the pressure up to 35 mm Hg. One concludes, then, that within the transitional and

hydrodynamic flow regions, contrary to the conclusions drawn by Knauer and Stern,[28] the beam intensity did continue to increase with the source pressure. Consequently, it may be true, but is not proven, that the intensity increased over that predicted on the basis of the cosine law, and this would explain the positive curvature in the results reported by Ackermann, Gilles, and Thorn[43] and discussed in section 6.1. This conclusion, of course, is only tentative, and further experimental study on this matter is warranted. Phipps and associates,[67] for example, are studying angular dependences of flux intensities of molecular beams at various source pressures.

Finally, we are confronted with the task of making a decision as to how one might accurately predict the conditions under which the departure from molecular flow occurs. The usual prediction is based upon the mean free path-to-orifice dimensions concept. The question arises now as to whether this is a proper parameter to permit an accurate prediction to be made. The values of the mean free path calculated from the present data cannot be considered to be any more reliable than 10 percent, if even that much. But it would appear that the present study in conjunction with the observations by Knauer and Stern[28] and Knudsen[17] indicate that the ratio of mean free path to cross-sectional length of the orifice defines the departure to occur at unity within a factor of 10.

10.5 Summary of the Conclusions

The experiments reported here have never before been carried out extensively for saturated vapors, although basically they are similar in concept to those experiments carried out by Knudsen[13] in 1909. In the low-pressure regions they yield results having features similar to those of Knudsen, and for the effusion of vapors through channeled orifices at source pressures near one atmosphere, yield results considerably different from those of the more usual experiment employing common gases flowing under small pressure gradients. The results of

the measurements of the effusive behavior of mercury flowing through a thin orifice yield for the first time unequivocal verification of the transition from the molecular to the hydrodynamical effusive behavior.

The experimental results of the study of the behavior of mercury vapor flowing through channeled orifices into vacuum from a region of nearly saturated vapor show a general agreement with Knudsen's formula, which expresses the transition from molecular to viscous flow behavior, except in one pressure region. The length-to-radius ratios of the channeled orifices employed were between 122 and 66. In the low-pressure regions of 10^{-3} mm Hg, the agreement of the experimental measurements with the predictions of the molecular effusion formula is about three percent. At increasing pressures there appears to be a very slight negative deviation of 5 percent or less from the molecular flow behavior, and in this region the data agree with the predictions of Knudsen's equation within 2 percent.

At source pressures beginning about 0.5 mm Hg, or greater, the effusive behavior of mercury vapor progresses into the viscous flow region, where there are systematic differences between the predictions of Knudsen's formula and the experimental results. This difference appears to be attributable to fundamental differences between the present unilateral flow experiments with short channels compared with the usual bilateral flow measurements with much longer channeled orifices. The present experiments indicate that viscosities of saturable vapors could be measured within 10 percent by methods similar to those employed in this study by some adjustment of the length of the channels.

At source pressures near 50 mm Hg and higher, the flow behavior progresses into a turbulent flow region which leads to an apparent saturation of the vapor within the channel. In one series of experiments the flow rates clearly begin to correspond exactly with this apparent effect at source pressures near one atmosphere.

The results of the study of the flow of mercury vapor through a thin-edged orifice show unusually good precision. The data demonstrate a molecular flow region, a transitional region, and a hydrodynamical flow region which has a flow rate only slightly higher than the isothermal flow reported by Knudsen. The pressure at which the departure from molecular flow occurs is slightly less than 0.1 mm, which corresponds to a mean free path-to-orifice diameter ratio of unity. On the basis of the same kind of analysis, the study by Johnson on the beam intensity of mercury vapor is applicable to the effusion of vapor under hydrodynamical conditions. This leads to the tentative conclusion that the positive curvature in the plot of the vapor pressure data of uranium dioxide reported by Ackermann, Gilles, and Thorn[43] may be due in part to the departure of the vapor from conditions under which molecular flow occurs. Different and more extensive studies are required, however, to decide the validity of the conclusions.

CHAPTER 11
SUGGESTIONS FOR FURTHER STUDIES

The present investigation comprises a study of two aspects of the effusive behavior of vapors. The first is concerned with questions related to the extent of vapor saturation at very low pressures, and the second is concerned with questions related to certain phenomena occurring at pressures for which the effects of gas-phase interactions are significant. These are limited aspects of an effusive behavior, which depends in general on a variety of conditions and on the effects of the molecular interactions. This suggests several possibilities for further investigation.

The equations and formalism developed for the problems of the extent of vapor saturation may be modified to include the effects of some gas-phase interactions. The problem, of course, becomes more difficult from a mathematical standpoint, but certain aspects of the departure from the molecular flow behavior might be handled in this way. The formalism should include terms which account for the termination of free paths in the gas by interactions of the gas-phase molecules. The usual mean free path treatment should be avoided in favor of a more rigorous formulation in terms of an intermolecular potential.

A systematic experimental investigation of the viscous behavior under the conditions used in these present experiments should be carried out. For example, the effusive behaviors of a group of elements such as the alkali metals could be studied to exploit the systematic differences in their potential functions. Since the viscosity of the vapor is intimately related to the intermolecular potentials, interesting differences in the viscous effusive behavior would be observed. Certainly some experiments should be designed to employ much longer tubes than those employed in the present study in order that a more extensive pressure range of viscous flow behavior be obtained.

The transitional flow region for the effusion of vapor from thin-edged orifices should be similarly investigated, for in such an investigation one might be able to determine the various factors leading to the departure from molecular flow. A systematic study should delineate the extent of the reliability of the classical mean free path as a parameter which predicts the pressure at which the transition from the molecular flow behavior occurs. In addition, similar experiments in which beam intensities are measured at various angles normal to the plane of the orifice should be carried out for source pressures covering the molecular and transitional flow regions. Such experiments are necessary to determine whether or not beam intensities relative to the intensities predicted by the cosine law increase in the directions normal to the orifice.

Finally, in view of the interesting discrepancies in the measured vapor pressure and the vapor viscosity of mercury, these properties should be remeasured. As yet there has been no precise measurement of this vapor pressure by effusion methods. The present apparatus seems admirably suited to an accurate determination of this in the low-pressure regions. Both the pressure and viscosity measurements should permit one to deduce a more reliable value for the dissociation energy of the dimer than presently exists.

APPENDIX 1

MATHEMATICAL DETAILS RELATED TO SOME FUNCTIONS DERIVED FROM THE COSINE LAW

A1.1 Two Geometry Factors

(a) A Circular Receiver and Source

The geometry factor is defined by the cosine law expression

$$G(S_iS_j) = \int_{S_i}\int_{S_j} \frac{\cos\theta_{ij}\cos\theta_{ji}}{\pi \ell_{ij}^2}\, ds_i ds_j \qquad (A1.1\text{-}1)$$

The quantity $G(S_0S_1)$ associated with the geometrical arrangement shown in Figure A1.1-1 is derived by making the following substitutions:

$$\begin{aligned}
\theta_{01} &= \theta_{10} \\
\cos\theta_{01} &= L/\ell_{01} \\
\ell_{01}^2 &= L^2 + q^2 \\
q^2 &= r_1 + r_0^2 - 2r_1r_0\cos(\beta_1 - \beta_0) \\
ds_1 &= r_1 dr_1 d\beta_1 \\
ds_0 &= r_0 dr_0 d\beta_0 \quad .
\end{aligned} \qquad (A1.1\text{-}2)$$

Therefore,

$$G(S_0S_1) = \frac{L^2}{\pi}\int_{S_0}\int_{S_1} \frac{ds_0 ds_1}{[L^2 + r_1^2 + r_0^2 - 2r_1r_0\cos(\beta_1 - \beta_0)]^2} \qquad (A1.1\text{-}3)$$

The integration over S_1 may be carried out first. For convenience, we define

$$\begin{aligned}
r_1^2 &= x \\
M &= L^2 + r_1^2 + r_0^2 \\
N &= -2r_1r_0 \\
\gamma &= \beta_1 - \beta_0 \quad .
\end{aligned} \qquad (A1.1\text{-}4)$$

Thus, one has

$$G(S_0S_1) = \frac{L^2}{2\pi}\int_{S_0} ds_0 \int_{x=0}^{R_1^2}\int_{\beta_1=0}^{2\pi} \frac{dx d\beta_1}{[M + N\cos\gamma]^2} \quad . \qquad (A1.1\text{-}5)$$

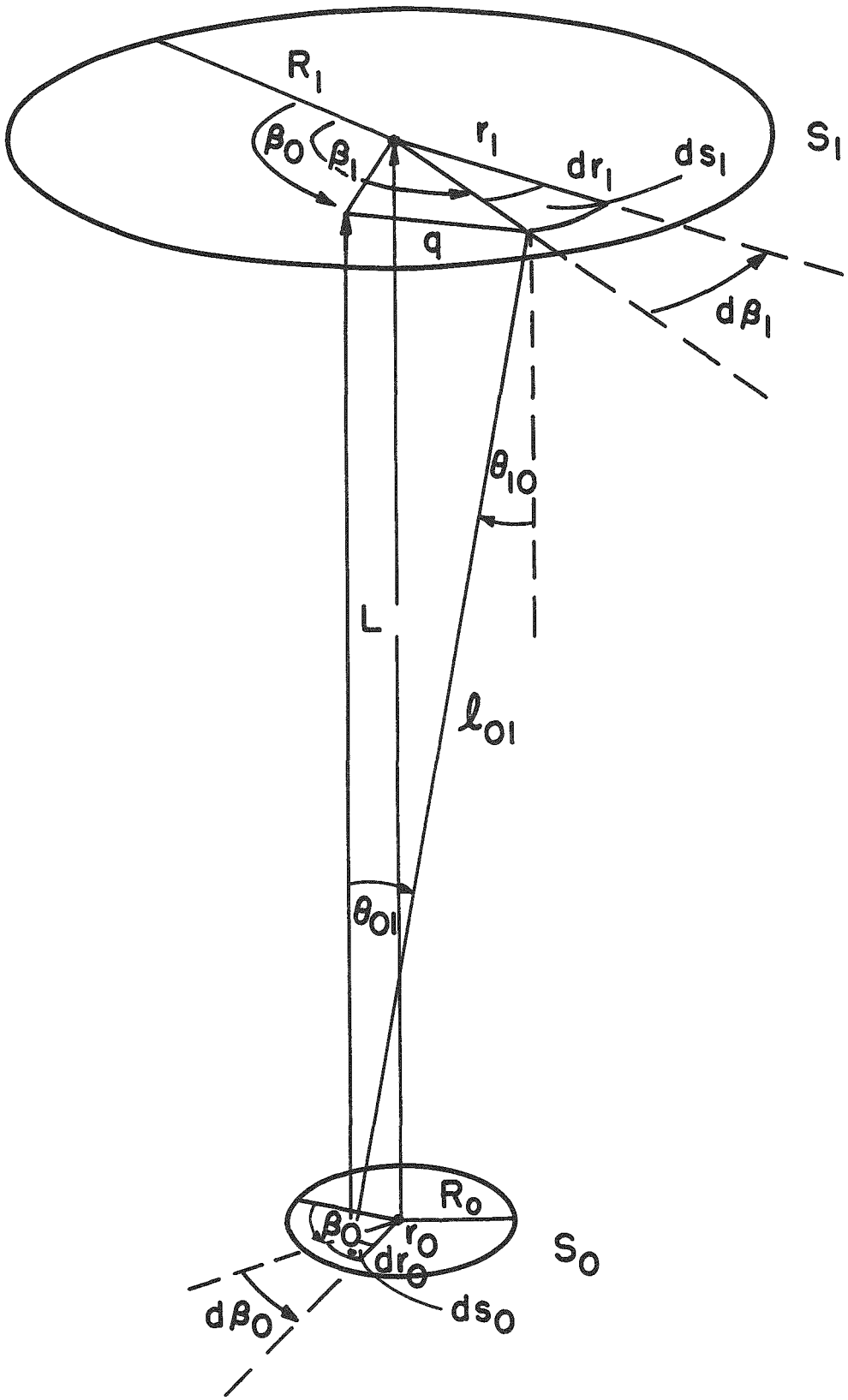

Fig. A1.1-1 Variables of the Geometry Factor for a Circular Receiver and Source

It may be demonstrated that

$$\int_{\beta_1=0}^{2\pi} \frac{d\beta_1}{[M \pm N \cos \gamma]^2} = \frac{2\pi M}{(M^2 - N^2)^{3/2}} \quad , \text{ for } M^2 > N^2 \quad , \tag{A1.1-6}$$

First, because of the symmetry, one can choose $\beta_0 = 0$ and $\gamma = \beta_1$. Second, one may find that all the conditions are satisfied to validate the operation[68]

$$\frac{d}{dM} \int_\beta \frac{d\beta}{M + N \cos\beta} = - \int_\beta \frac{d\beta}{[M + N \cos \beta]^2} \quad . \tag{A1.1-7}$$

Therefore, the value of (A1.1-5) may be derived from the standard integral[69]

$$\int \frac{d\beta}{M + N \cos \beta} \quad . \tag{A1.1-8}$$

We obtain the result

$$G(S_0S_1) = \int ds_0 L^2 \int_0^{R_1^2} \frac{M dx}{(M^2 - N^2)^{3/2}} \tag{A1.1-9}$$

The integration over R_1 proceeds in a straightforward manner. By making the substitutions

$$\begin{aligned} c &= (L^2 + r_0^2)^2 \\ b &= 2(L^2 - r_0^2) \\ a &= 1 \\ x &= r_1^2 \quad , \end{aligned} \tag{A1.1-10}$$

one obtains

$$G(S_0S_1) = \int ds_0 L^2 \int_0^{R_1^2} \frac{\sqrt{c} + x}{[ax^2 + bx + c]^{3/2}} \, dx \quad , \tag{A1.1-11}$$

which may be separated into two standard integrals.[69] The evaluation of these yields the result

$$G(S_0S_1) = \int_{S_0} \frac{ds_0}{2}\left[1 - \frac{L^2 + r_0^2 - R_1^2}{[(L^2 + r_0^2 + R_1^2)^2 - 4r_0^2R_1^2]^{1/2}}\right] . \quad (A1.1\text{-}12)$$

The integration over ds_0 proceeds by similar steps. The integration over β_0 follows immediately. The remaining constants and variable r_0 may be combined to yield integrals of a standard form. The desired result is

$$G(S_0S_1) = \frac{\pi}{2}\left[L^2 + R_0^2 + R_1^2 - \sqrt{(L^2 + R_0^2 + R_1^2)^2 - 4R_0^2R_1^2}\right] . \quad (A1.1\text{-}13)$$

In the process of deriving this final factor, we have derived also the useful geometry factor

$$G(2\pi r_0dr_0,S_1) = \pi r_0dr_0\left[1 - \frac{L^2 + r_0^2 - R_1^2}{[(L^2 + r_0^2 + R_1^2)^2 - 4r_0^2R_1^2]^{1/2}}\right] . \quad (A1.1\text{-}14)$$

(b) A Cylindrical Source and Circular Receiver

From Figure A1.1-2 one obtains the following:

$$\begin{aligned} J^2 &= r_1^2 + L^2 \\ &= R_0^2 + \ell_{01}^2 - 2R_0\ell_{01}\cos\theta_{01} \\ \cos\theta_{10} &= L/\ell_{01}\ ;\ \ell_{01}^2 = q^2 + L^2 \\ q^2 &= R_0^2 + r_1^2 - 2R_0r_1\cos\gamma \\ \gamma &= \beta_1 - \beta_0 \\ ds_1 &= r_1dr_1d\beta_1 \\ ds_0 &= R_0d\beta_0dL \quad . \end{aligned} \quad (A1.1\text{-}15)$$

These give

$$\frac{\cos\theta_{01}\cos\theta_{10}}{\ell_{01}^2} = \frac{L[R_0 - r_1\cos\gamma]}{[R_0^2 + r_1^2 + L^2 - 2R_0r_1\cos\gamma]^2} , \quad (A1.1\text{-}16)$$

and

$$G(2\pi R_0dL,S_1) = \frac{R_0LdL}{\pi}\int_{\beta_0}\int_{\beta_1}\int_{r_1}\frac{R_0 - r_1\cos\gamma}{[R_0^2 + r_1^2 + L^2 - 2R_0r_1\cos\gamma]^2}\, r_1dr_1d\beta_0d\beta_1 . \quad (A1.1\text{-}17)$$

The integrations over the angular variables are carried out in steps similar to those used in deriving $G(S_0S_1)$. These yield the result

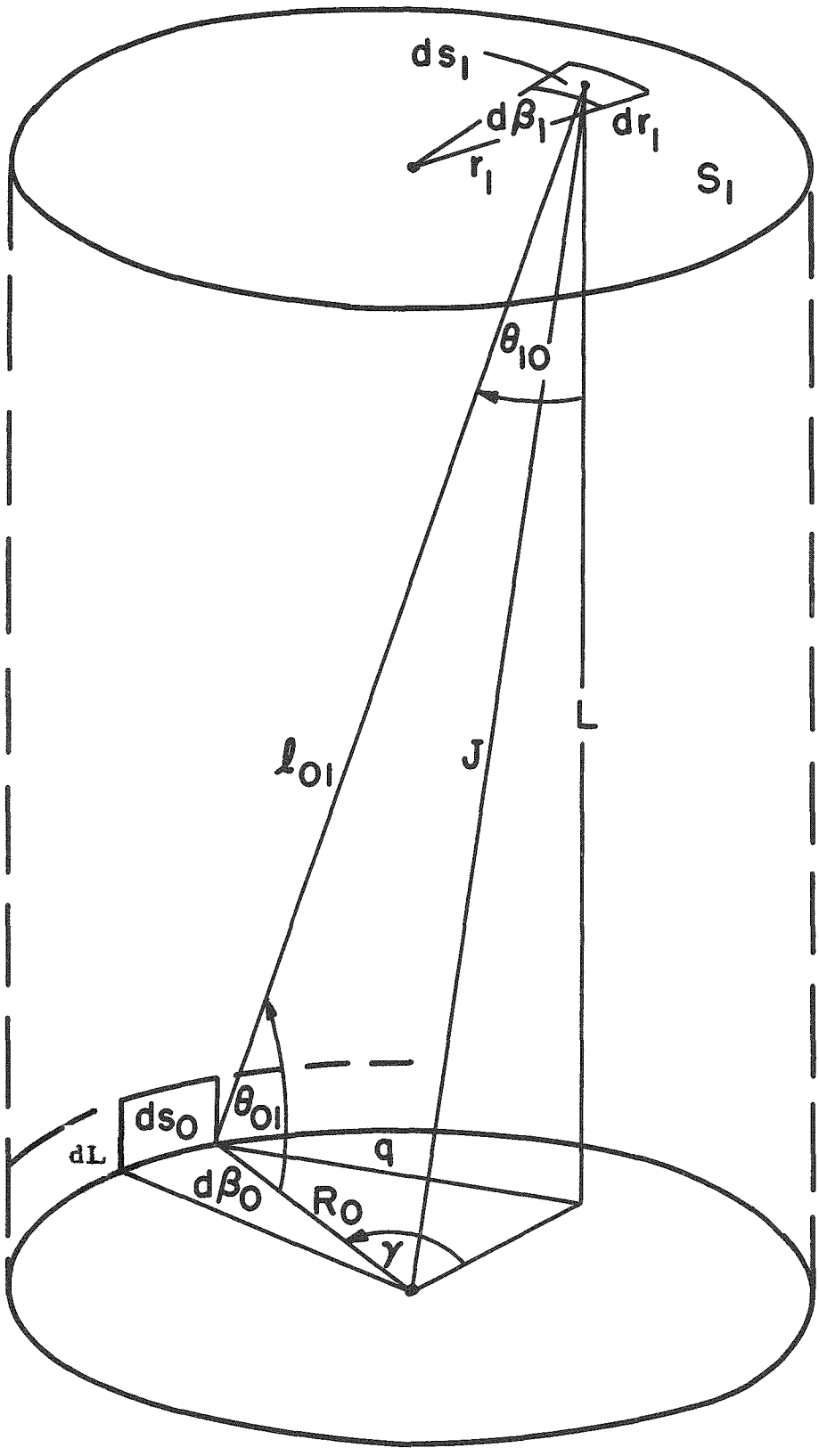

Fig. A1.1-2 Variables of the Geometry Factor for a Cylindrical Source and Circular Receiver

$$G(2\pi R_0 dL, S_1) = 4\pi R_0^2 L dL \int_{r_1} \frac{(R_0^2 + L^2 - r_1^2) r_1 dr_1}{[(R_0^2 + r_1^2 + L^2)^2 - 4R_0^2 r_1^2]^{3/2}} \quad . \tag{A1.1-18}$$

From this expression one may obtain directly the factor

$$G(2\pi R_0 dL, 2\pi r_1 dr_1) = 4\pi R_0^2 L dL r_1 dr_1 \left[\frac{R_0^2 + L^2 - r_1^2}{[(R_0^2 + r_1^2 + L^2)^2 - 4R_0^2 r_1^2]^{3/2}}\right] . \tag{A1.1-19}$$

Integration of expression (A1.1-19) over r_1 between 0 and $R_1 \neq R_0$ yields the factor

$$G(2\pi R_0 dL, S_1) = \pi L dL \left\{\frac{R_0^2 + R_1^2 + L^2}{[(R_0^2 + R_1^2 + L^2)^2 - 4R_0^2 R_1^2]^{1/2}} - 1\right\}. \tag{A1.1-20}$$

A1.2 The Probability Functions K

One may easily demonstrate the interrelationship of the previous geometry factors through differentiation of the principal factor $G(S_0 S_1)$. These relations lead to the following functions employed in the analysis of the extent of saturation in a Knudsen cell. From the definition,

$$K(h,a,b) = \tfrac{1}{4}\left[h^2 + a^2 + b^2 - \sqrt{(h^2 + a^2 + b^2) - 4a^2 b^2}\right] \quad ,$$

one may derive the following positive functions:

$$K(H,P,1) = \tfrac{1}{4}\left[H^2 + P^2 + 1 - \sqrt{(H^2 + P^2 + 1)^2 - 4P^2}\right]$$

$$\frac{\partial}{\partial \eta} K(H-\eta, P, 1) = \frac{H-\eta}{2}\left[\frac{(H-\eta)^2 + P^2 + 1}{\left\{[(H-\eta)^2 + P^2 + 1]^2 - 4P^2\right\}^{1/2}} - 1\right]$$

$$-\frac{\partial}{\partial \eta} K(\eta, 1, 1) = \tfrac{1}{4}\left[\sqrt{\eta^2 + 4} + \frac{\eta^2}{\sqrt{\eta^2 + 4}} - 2\eta\right]$$

$$+\frac{\partial^2}{\partial \eta \partial \eta'} K(|\eta - \eta'|, 1, 1) = \tfrac{1}{4}\left[2 - \frac{3|\eta - \eta'|}{\sqrt{(\eta - \eta')^2 + 4}} + \frac{|\eta - \eta'|^3}{[(\eta - \eta')^2 + 4]^{3/2}}\right]$$

$$\frac{\partial}{\partial \rho} K(L, \rho, 1) = \frac{\partial}{\partial \rho} K(L, 1, \rho)$$

$$= \frac{\rho}{2}\left\{1 - \frac{H^2 + \rho^2 - 1}{[(H^2 + \rho^2 + 1)^2 - 4\rho^2]^{1/2}}\right\}$$

$$\frac{\partial^2}{\partial \eta \partial \rho} K(H-\eta, \rho, 1) = 2(H-\eta)\rho\left[\frac{(H-\eta)^2 + 1 - \rho^2}{\{[(H-\eta)^2 + \rho^2 + 1]^2 - 4\rho^2\}^{3/2}}\right]$$

A1.3 An Iterate Property of the $\delta(\eta)$ Equation

For the integral equation

$$\delta(\eta) = \phi(\eta) + \int_0^H \delta(\eta')K(\eta,\eta')d\eta' \qquad \text{(A1.3-1)}$$

and the defined equation for the iterate

$$I\left\{f(\eta)\right\} = \phi(\eta) + \int_0^H f(\eta')K(\eta,\eta')d\eta' \quad , \qquad \text{(A1.3-2)}$$

whose kernels meet the conditions

$$\begin{aligned} &1.\ K(\eta,\eta') \geq 0, && \begin{cases} 0 \leq \eta \leq H \\ 0 \leq \eta' \leq H \end{cases} \\ &2.\ \int_0^H K(\eta,\eta')d\eta' < 1, && 0 \leq \eta \leq H \quad , \end{aligned} \qquad \text{(A1.3-3)}$$

Snyder[70] and DeMarcus[71] have proved a theorem:

if $\quad I\left\{f(\eta)\right\} \leq f(\eta)$ for $0 \leq \eta \leq H$,

then $\quad \delta(\eta) \leq I\left\{f(\eta)\right\} \leq f(\eta)$ for $0 \leq \eta \leq H$. $\qquad$ (A1.3-4)

The two equations (5.4-9) and (5.4-10) in Chapter 5 may be written in the form

$$\delta(\eta) = \frac{\partial}{\partial\eta} K(H-\eta,P,1) + \int_0^H K(\eta,\eta')\delta(\eta')d\eta' \quad , \qquad \text{(A1.3-5)}$$

where

$$K(\eta,\eta') = -\frac{\partial^2}{\partial\eta\partial\eta'} K(|\eta - \eta'|,1,1) + \int_P^1 \frac{1}{\rho'} \frac{\partial^2}{\partial\eta\partial\rho'} K(H - \eta',\rho',1) \frac{\partial^2}{\partial\eta\partial\rho'} K(H - \eta,\rho',1)d\rho' \quad . \qquad \text{(A1.3-6)}$$

This kernel, incidentally, is symmetrical with respect to η and η', a property which is useful in solving integral equations. Consequently, if we prove that $K(\eta,\eta')$ meets the conditions (A1.3-3), then the theorem as proved is applicable to the integral equations developed in Chapter 5.

The terms

$$+\frac{\partial^2}{\partial\eta\partial\eta'}\,K(|\eta-\eta'|,1,1) \quad ,$$

$$\frac{1}{\rho'}\,\frac{\partial^2}{\partial\eta'\partial\rho'}\,K(H-\eta',\rho',1) \quad ,$$

and

$$\frac{\partial^2}{\partial\eta\partial\rho'}\,K(H-\eta,\rho',1) \qquad (A1.3\text{-}7)$$

are positive, so that condition 1. of (A1.3-3) is satisfied. The integration of $K(\eta,\eta')$ is easily executed. Thus

$$\int_0^H K(\eta,\eta')d\eta' = 1 - \frac{\partial}{\partial\eta}K(H-\eta,1,1) + \frac{\partial}{\partial\eta}K(\eta,1,1)$$

$$+\int_P^1 \frac{1}{\rho'}\,\frac{\partial}{\partial\rho'}\left\{K(O,\rho',1) - K(H,\rho',1)\right\}\,\frac{\partial^2}{\partial\eta\partial\rho'}\,K(H-\eta,\rho',1)d\rho' \quad . \qquad (A1.3\text{-}8)$$

Since $K(O,\rho',1) = \rho'^2/2$, and the second term, $K(H,\rho',1)$, is positive and less than $K(O,\rho',1)$, then it is true that

$$\int_0^H K(\eta,\eta')d\eta' < 1 - \frac{\partial}{\partial\eta}K(H-\eta,1,1) + \frac{\partial}{\partial\eta}K(\eta,1,1) \quad . \qquad (A1.3\text{-}9)$$

Since $\frac{\partial}{\partial\eta}K(\eta,1,1)$ is negative and $\frac{\partial}{\partial\eta}K(H-\eta,P,1)$ is positive for $0 \leq \eta \leq H$, and if we keep $H \leq \infty$, then

$$\int_0^H K(\eta,\eta')d\eta' < 1 \text{ for } 0 \leq \eta \leq H \leq \infty \quad , \qquad (A1.3\text{-}10)$$

and condition 1. of (A1.3-3) is satisfied. Therefore, the theorem is applicable to the integral equations developed in Chapter 5. These conditions also apply to the theorem:

if $\quad I\left\{f(\eta)\right\} \geq f(\eta)$ for $0 \leq \eta \leq H \quad ,$

then $\quad \delta(\eta) \geq I\left\{f(\eta)\right\} \geq f(\eta)$ for $0 \leq \eta \leq H \quad . \qquad (A1.3\text{-}11)$

A1.4 The Clausing Factors

It has been pointed out repeatedly that the equations developed in the analysis in Chapter 5 are applicable to the Clausing problems for the case that P is unity. Consequently, the generalized equations for P = 1 represent the wall emission density of Clausing's problem, and the Clausing factor becomes

$$W(H,1,1) = 1 - 2\int_0^H \delta(\eta)\frac{\partial}{\partial\eta}K(H-\eta,1,1)d\eta \quad . \qquad (A1.4\text{-}1)$$

DeMarcus[42] recently has evaluated these factors for various values of H by employing an analysis based on the variational calculus. He was able to determine a variational value of W(H,1,1) which is known to be equal to or greater than the true value. Since his calculations yield in some cases values several per cent lower than those values calculated by Clausing by crude procedures, and since the value

$$W(H,1,1) = 8/3H = 8R/3L \qquad (A1.4\text{-}2)$$

for $L \gg R$, as deduced by Knudsen, is only an asymptotic solution,[42] we must accept the recent calculations by DeMarcus as being the most reliable values of the Clausing Factors.

The variational value of W(H,1,1) may be calculated from the analytical expression deduced by DeMarcus. In the notation of the symbols and functions used in this thesis, this factor may be written

$$W(H,1,1)^* = \tfrac{1}{2}[1 + 2K(H,1,1)] - \frac{\alpha^2(H)}{H\alpha^2(H) + 2\beta(H)} \quad , \qquad (A1.4\text{-}3)$$

where the functions $\alpha(H)$ and $\beta(H)$ have the following values:

$$K(H,1,1) = \tfrac{1}{4}\left[H^2 + 2 - H\sqrt{H^2+4}\right] \quad ,$$

$$\alpha(H) = -2\int_0^H \left(\frac{H}{2} - \eta\right)\frac{\partial}{\partial\eta}K(\eta,1,1)d\eta$$

$$= H\left\{\frac{1}{2} - K(H,1,1)\right\} + \left\{\frac{8}{3} + \frac{H^3}{3} + 2\sqrt{H^2+4}\right\}$$

NOTE: formula for $\alpha(H)$ is continued on p. 224.

$$- \left\{ 4 + \frac{1}{3}(H^2 + 4)^{3/2} \right\} \quad ,$$

$$\beta(H) = 2 \int_0^H \left(\frac{H}{2} - \eta \right) K(\eta, 1, 1) d\eta$$

$$= \left\{ \frac{2}{3} H + \frac{H(H^2 + 4)^{3/2}}{24} + \ell n 2 \right\}$$

$$- \left\{ \frac{H^4}{24} + \frac{H\sqrt{H^2 + 4}}{4} + \ell n \left(H + \sqrt{H^2 + 4} \right) \right\} \quad ,$$

where,

$$H = L/R \quad ,$$

and

$$W(H, 1, 1) \leq W(H, 1, 1)^* \quad .$$

APPENDIX 2
EQUILIBRIUM AND TRANSPORT PROPERTIES OF MERCURY VAPOR

A2.1 The Vapor Pressure of Mercury

A large number of investigators have reported sets of measurements of the vapor pressure of mercury, but of these only a few appear to be reliable. Douglas, Ball, and Ginnings[72] and Busey and Giauque[61] have analyzed selected vapor pressure data covering the temperature region near the normal boiling point (629.88°K) and, in conjunction with their enthalpy measurements for the liquid over an extended temperature range and the known properties of the monatomic vapor, have calculated the vapor pressure and associated equilibrium properties at small temperature intervals from the melting point (234.29°K) to 750°K. Thermodynamically consistent extrapolations of vapor pressures have a reliability which depends, aside from other considerations, on a knowledge of the extent of gas imperfection, and apparently little is known concerning this characteristic of mercury. The problem involved in such extrapolations consists of the determination of both the virial coefficient as a function of temperature and a heat of vaporization from the experimental data. The reported low-temperature vapor pressure measurements available to these workers is of such poor precision that they could not be used to obtain a reliable heat of vaporization. The high-temperature data utilized, however, experimentally indicate gas imperfections of less than two percent at pressures below two atmospheres.[72] Consequently, errors no larger than this are incurred in consistent extrapolations provided the auxiliary thermodynamic data are reliable.

The pressures calculated by Douglas, Ball and Ginnings are lower than those calculated by Busey and Giauque by about five percent at the melting temperature, three percent at 298.16°K, and decreasing differences up to the arbitrary agreement at the normal boiling

temperature. Both analyses have employed a nearly identical second virial coefficient, which alone is sufficient for the mercury vapor imperfections, so that the differences in the calculated pressures ostensibly are attributable to the differences in the free energy data for liquid mercury. The former investigators measured the enthalpy of liquid mercury between 273 and 723°K, and combined this information with previous low-temperature heat capacity data to derive the necessary thermal data employed in their extrapolations. Busey and Giauque subsequently carefully remeasured the heat capacity in the range from 15 to 330°K and combined their data with those of Douglas, Ball and Ginnings to construct the information necessary for their own analysis. Consequently, the pressures calculated by Busey and Giauque possibly are the more reliable of the two sets. It is difficult to make an estimate of the absolute reliability of these data, but it would appear that they are reliable certainly within ten percent and perhaps within two to three percent over the temperature region of interest to the present investigation.

More recent vapor pressure data of excellent precision and presumed reliability have been reported[73,74] but apparently not exploited. This writer has analyzed these data to calculate vapor pressures over the same temperature region as that cited above. These pressures are based on measurements of such outstanding precision that they should be reliable to within one or two percent, except that they lead to a perplexing conflict with either the thermal data for mercury, the dissociation energy of the mercury dimer, or the boiling point. The pressure data in question here are those reported by Spedding and Dye[73] for the region from 520 to 633°K and those reported by Ernsberger and Pitman[74] for low pressures in the region from 273 to 327°K. In contrast to the imprecise low-temperature data previously obtained by the molecular effusion method, the more recent measurements by a manometric technique have a precision of better than one percent and, in spite of the small temperature range, give a second law entropy of

vaporization at 300°K which agrees precisely with the third law entropy difference. The reported pressures are higher than those calculated by Douglas, Ball, and Ginnings and about two percent lower than those calculated by Busey and Giauque. The data of Spedding and Dye are more precise in the temperature range they cover than previous data and agree within five thousandths of a degree with the accepted normal boiling temperature.

For small gas imperfections the above-mentioned low-temperature data would allow one directly to derive a heat of vaporization for the liquid in its standard state to the ideal gas, both at zero degree Kelvin. This value may be used in conjunction with the free energy functions reported by Busey and Giauque[61] to derive the ideal gas pressure in the region of the data of Spedding and Dye, and from this by comparison with the experimental pressures to deduce experimental values of the second virial coefficient. The coefficients so obtained may be fitted to an equation giving the temperature dependence by appropriate means to effect a consistent and reliable extrapolation of the two sets of data. This procedure was used in the following analysis. A rough check demonstrated that the neglect of the virial coefficient for the low-temperature data would not influence significantly the analysis for the heat of vaporization. The heat reported below is in error by less than one calorie for this neglect, but no correction has been applied. The centigrade temperatures are corrected to the thermodynamic absolute scale,[72] and the same natural constants (NBS, 1947) used by Busey and Giauque and by Douglas, Ball and Ginnings have been employed.

For a gas having an equation of state

$$pV = RT + B(T)p \quad , \qquad \text{(A2.1-1)}$$

the free energy change for the transformation

$$\text{Hg(liq, 1 atm, T)} \longrightarrow \text{Hg(ideal gas, 1 atm, T)} \qquad \text{(A2.1-2)}$$

may be written as

$$\frac{\Delta F^\circ}{T} = -R \ell n\, p - \frac{B(T)p}{T} - \frac{V}{T}\frac{(1-p)}{41.2929}$$

$$= \left(\frac{F^\circ - H_0^\circ}{T}\right)_{gas} - \left(\frac{F^\circ - H_0^\circ}{T}\right)_{liq} + \frac{\Delta H_0^\circ}{T} \quad , \qquad \text{(A2.1-3)}$$

with the enthalpies H_0° and ΔH_0° and free energies F° and ΔF° expressed in units of calories, p in atmospheres, B in calories per atmosphere, V in cubic centimeters, and R in calories per degree, all for one gram-atom of mercury (200.61 grams). The free energy function of the gas is given by the Sackur-Tetrode equation,

$$\frac{F^\circ - H_0^\circ}{T} = 7.2821 - \frac{3}{2} R \ell n\, M - \frac{5}{2} R \ell n\, T \quad , \qquad \text{(A2.1-4)}$$

and the free energy function of the liquid is interpolated from the values reported by Busey and Giauque. The molar liquid volume V is required to correct the free energy of the liquid for the change in pressure from the saturation pressure to one atmosphere. The correction is small but is included for consistency with the previous analyses. The temperature dependence of V is given in an equation by Douglas, Ball, and Ginnings.

From the pressure data of Ernsberger and Pitman, the value of ΔH_0° for each experimental value was calculated by neglecting the virial coefficient B(T). These resulting values are reported below in Table A2.1-1, along with the second law value deduced from the reported least-squares vapor pressure equation. There appears to be an excellent consistency of these values, and the fluctuation at the low temperatures probably is attributable to the decreased precision of the apparatus at low pressures, as suggested by the investigators. The third law value for ΔH_0° was used in the free energy equation (A2.1-3), along with the experimental pressures reported by Spedding and Dye, to calculate at each experimental point a value of B(T). The calculated values were fitted to an empirical equation corresponding to the virial coefficient in Berthelot's equation of state. Admittedly, it is more

TABLE A2.1-1

Third Law Values of ΔH_0° from the Data of Ernsberger and Pitman

T (°K)	ΔH_0° (cal) Third law	T (°K)	ΔH_0° (cal) Third law
285.24	15418	306.19	15415
288.16	15410	309.25	15413
291.11	15408	312.13	15412
293.25	15411	315.17	15412
294.12	15416	318.19	15412
296.23	15413	321.17	15412
299.22	15415	324.14	15412
300.27	15411	326.65	15412
303.20	15412		

Third law av . . . . . 15,412.6 $\pm$ 0.5 cal
Second law . . . . . 15,414 cal

consistent with the theory of the virial coefficient to fit the data to a coefficient derivable from a potential function.[75] This was not done, however, for several reasons. First, the experimental virial coefficient, as will later be explained, leads to a conflict with the present knowledge of the dissociation energy of the dimer. Secondly, precision pressure data in excess of one atmosphere would be required to effect a meaningful potential function analysis. Thirdly, a simple, more amenable virial function equation is sufficient for the extrapolation in the present investigation, and Busey and Giauque chose an approximate Berthelot coefficient in their analysis.

The Berthelot equation of state has a two-term second virial coefficient:

$$B(T) = a - (b/T^2) \quad . \qquad \text{(A2.1-5)}$$

Busey and Giauque reasoned in effect that with many gases the constant a could be neglected at temperatures near and below the normal boiling point, and they derived for the virial coefficient of mercury vapor on this basis the expression

$$B(T) = - 1.35 \times 10^6/T^2 \quad , \qquad \text{(A2.1-6)}$$

which, combined with the equations (A2.1-3) and the pressure data they utilized, yielded a value for the heat of vaporization of

ΔH_0° = 15,402.5 calories per gram-atom. The present analysis, however, gives a virial coefficient having a temperature dependence which decidedly is not of the same form, but rather demands the inclusion of the constant a. Since this analysis is not in itself complete enough to decide on the reliability of the experimental boiling point, B(T) by equation (A2.1-5) was arbitrarily fixed at the accepted boiling point and the constants accordingly adjusted by least squares. This analysis yielded the equation,

$$B(T) = 67 \pm 16 - \frac{(32.255 \pm 6.3) \times 10^6}{T^2} \quad . \qquad \text{(A2.1-7)}$$

The correspondence of this equation with the experimental values admittedly is not as good as the data appear to demand, and it would be fallacious to use this for extrapolations much beyond the boiling point. It does appear to be sufficient for the present purposes, however. A few representative values of the experimental and empirical virial coefficient are given in Table A2.1-2.

TABLE A2.1-2

Representative Values of the Virial Coefficient of Mercury

T (°K)	-B(T)	-B(T), Eqn: A2.1-7	-B(T), Busey and Giauque
629.88 (BP)	14.3	14.3	3.4
573	31.3	31.0	
549	38.0	39.7	
534	47.1	46.2	

These coefficients are surprisingly large, especially compared with those deduced by Busey and Giauque. The ideal gas pressure at the accepted boiling point is found to be 751.4 mm Hg, and therefore the extent of gas imperfections amounts to 1.2 percent as compared with the value of 0.3 percent on the basis of the analysis by Busey and Giauque.

Although this is within the two percent maximum previously mentioned, it leads to the uncomfortable conclusion that the dissociation energy of the mercury dimer is much larger than suspected. The thermodynamic properties of the mercury dimer are practically unknown, although the evidence seems to indicate that the dissociation energy at zero degrees is less than two kilocalories per mole. There is insufficient information from which reliable entropy and free energy functions of the dimer may be calculated, so that little can be gained in an examination of the present data from the usual equilibrium considerations. One may turn, however, to an examination on the basis of a virial coefficient derived from a potential function.(75)

If a potential function for the interaction of two spherically symmetrical atoms is known as a function of the distance of separation, then B(T) may be derived from a statistical mechanical equation. Mercury is known to possess a singlet ground state, so that unless unusual and unsuspected circumstances occur for the essentially binary collisions of the atom of slightly imperfect mercury vapor, then the potential function may be taken as that applicable to the formation of the mercury dimer. Douglas, Ball, and Ginnings calculated a virial coefficient from a Morse potential function in which the dissociation energy was taken at 1.5 kcal, a choice based upon a serious examination of the spectroscopic evidence, an arbitrary equilibrium separation of 3.2×10^{-8} cm, and the first vibrational constant as 36 cm^{-1}. Epstein and Powers(66) more recently chose to evaluate the virial coefficient on the basis of a Lennard-Jones (6-9) potential with the dissociation energy taken as 1.54 kcal and an equilibrium separation as 3.25×10^{-8} cm, the latter value having been chosen from an analysis of the viscosity of mercury vapor. These various calculations of the B(T) dependence agree closely with that derived by Busey and Giauque. In contrast to these, a rough estimation of the dissociation energy necessary to give the present value of 14 calories per atmosphere for the virial coefficient at the boiling point yields an energy of nearly 4 kcal,

which is twice the highest value reported for the dissociation energy.[72] Although spectroscopic values for this energy are subject to large errors, the value of 4 kcal does seem unreasonable, even in view of the current ambiguousness of the value.

The conflict arising in the present analysis is traceable to several possible circumstances:

1. The data of Ernsberger and Pitman are in error such that $\Delta H_0^\circ < 15{,}413$ cal.
2. The peripheral entropy or free energy data of liquid mercury are in error.
3. The dissociation energy of mercury dimer is greater than 2 kcal.
4. The data of Spedding and Dye and the currently accepted normal boiling point of mercury are in error.

The low-temperature data of Ernsberger and Pitman are so consistent that one finds difficulty in attributing significant error to their data. Admittedly the temperature range covered in their work is not large, but the agreement of the second and third law heats leads one to conclude that the data are reliable. Indeed, it would be an unlikely set of circumstances which would give incorrect data of such excellent agreement, although the entropy agreement is a necessary but insufficient condition for reliability. Since the absolute entropies are in agreement, it is difficult to attribute significant error to the liquid thermodynamic data.

The dissociation energy of mercury dimer possibly may be larger than suspected, but a more detailed analysis would be required to evaluate this point fully. One can say, however, that it appears unlikely that the dissociation energy is as high as 4 kcal.

Despite the obvious precision of the measurements of the normal boiling point of mercury by at least two workers[73,77] and the fact that this temperature is accepted as a secondary fixed point on the 1948 International Temperature Scale,[78] it is not impossible that this

temperature may be in error. Boiling point determinations are subject to indeterminate temperature errors, a circumstance which, for example, appears to have occurred in measurements on the vapor pressures of potassium in the region of the boiling point.[79] One can estimate that a discrepancy of about 0.4 degree in the temperature of the pressures reported in the region of one atmosphere could account for the difference in the virial coefficients determined in the present analysis and those derivable from a potential function consistent with the spectroscopic evidence. Further analysis and certainly continued experimental study of the mercury vapor pressures are warranted.

The pressures reported by Busey and Giauque and those calculated on the basis of the present analysis have been fitted to four-parameter equations by a least-squares reduction. The agreement of both equations with the original pressures used in the reduction over the range of temperatures from the melting point (234.29°K) to the boiling point (629.88°K) are consistently within better than 0.2 percent for the equation applicable to the data of Busey and Giauque and within better than 0.8 percent for that applicable to the combined data of Spedding and Dye and of Ernsberger and Pitman. The general form of the vapor pressure equation used is

$$\log P\ (\text{mm Hg}) = A + \frac{B}{T} + C \log T + DT^2 \quad . \qquad \text{(A2.1-8)}$$

The constants applicable to both sets of information are tabulated in the following table:

EQUATION	A	B	C	$Dx10^6$	Source
A2.1-8A	+10.80644	-3322.183	-0.9576842	+0.0738591	Busey and Giauque
A2.1-8B	+10.44108	-3309.811	-0.8286779	+0.03352341	Present Analysis

The writer recognizes the inconsistencies in the data and believes a more detailed analysis is necessary to resolve these. Consequently, he chose the data of Busey and Giauque and therefore the pressure

equation A2.1-8A for the primary analysis of the data presented in this thesis. The present analysis indicates that these pressures may be too large by two percent in the low pressure region.

A2.2 The Viscosity of Mercury Vapor

The viscosity of mercury vapor as a function of temperature was measured by Koch[80] in 1883 and by Braune, Basch and Wentzel[60] in 1928. Apparently no more recent determinations have been made, although the discrepancies between these two determinations and the discrepancy of both with a theoretically calculated temperature dependence indicates that the data possibly are unreliable. Epstein and Powers[76] recently have analyzed the viscosity data to determine if possible the theoretical temperature dependence. They conclude that within the precision of the measurements and within the present available framework of the theory of transport phenomena, the theory and experimental results may be brought into reasonable agreement.

The data, in the opinion of the writer, do not appear to substantiate the conclusions drawn by Epstein and Powers, for clearly the two sets of data are in serious disagreement. Whereas an analysis of the combined data does indicate variations which are comparable to the extent of the agreement with theoretical values, and analysis separately of either set of data shows better internal consistency than can be provided by a theoretical prediction within the present framework.

Koch measured the viscosity by the so-called transpiration method over a temperature range of 100 degrees, and his 18 reported measurements defined approximately a temperature dependence of $T^{1.6}$. However, there is considerable variation in his data. The reliability of his method depends on a precise knowledge of the capillary dimensions and the vapor pressure of mercury, and for the latter Koch measured the pressures by a manometric procedure. Because of the difficulties associated with such measurements, the lack of pure mercury, and questions on the reliability of his temperature measurements, it appears that the more recent data of Braune, Basch, and Wentzel must

be accepted as more reliable, particularly because their method depends less rigidly on an absolute knowledge of parameters unique to the apparatus.

Braune, Basch, and Wentzel measured the viscosity by the oscillating disk method over a range of temperatures of 400 degrees. Their description of the procedure indicates that considerable attention was devoted to details for the temperature measurements and standardizations. Their apparatus was used prior to the mercury experiments for the measurement of the viscosity of air and bromine, and their data for air agree substantially with the more reliable of the reported data and within 2 percent or better with the recent NBS evaluation of the viscosity of air.[81] Since the method of measuring the mercury viscosity involved measurements relative to air, it would appear the the reliability of their mercury data is within two to five percent in the range of their measurements. The overall precision of their data, however, is within one-half percent.

A plot of the data reported both by Koch and the latter investigators is presented in Figure A2.2. A least-squares reduction of the data of Braune, Basch, and Wentzel was tried for equations of the general form

$$\mu\,(\text{poise}) = AT + BT^{b} \quad , \qquad \text{(A2.2-1)}$$

for values of b of 0, $\frac{1}{2}$, 1, and 2, and with T representing the absolute temperatures reported by these investigators. The best agreement with the data was obtained with the equation

$$\mu\,(10^{-7}\ \text{poise}) = -43.788\ T^{1/2} + 11.472\ T \quad . \qquad \text{(A2.2-2)}$$

It is of interest for the present investigation that the viscosity be extrapolated to temperatures lower than the experimental values obtained. Probably the most reliable way to effect this is to fit the data by suitable adjustment of parameters in the region of the measurements to a viscosity equation derivable from a potential function. The parameters so obtained may then be employed to calculate the viscosity at

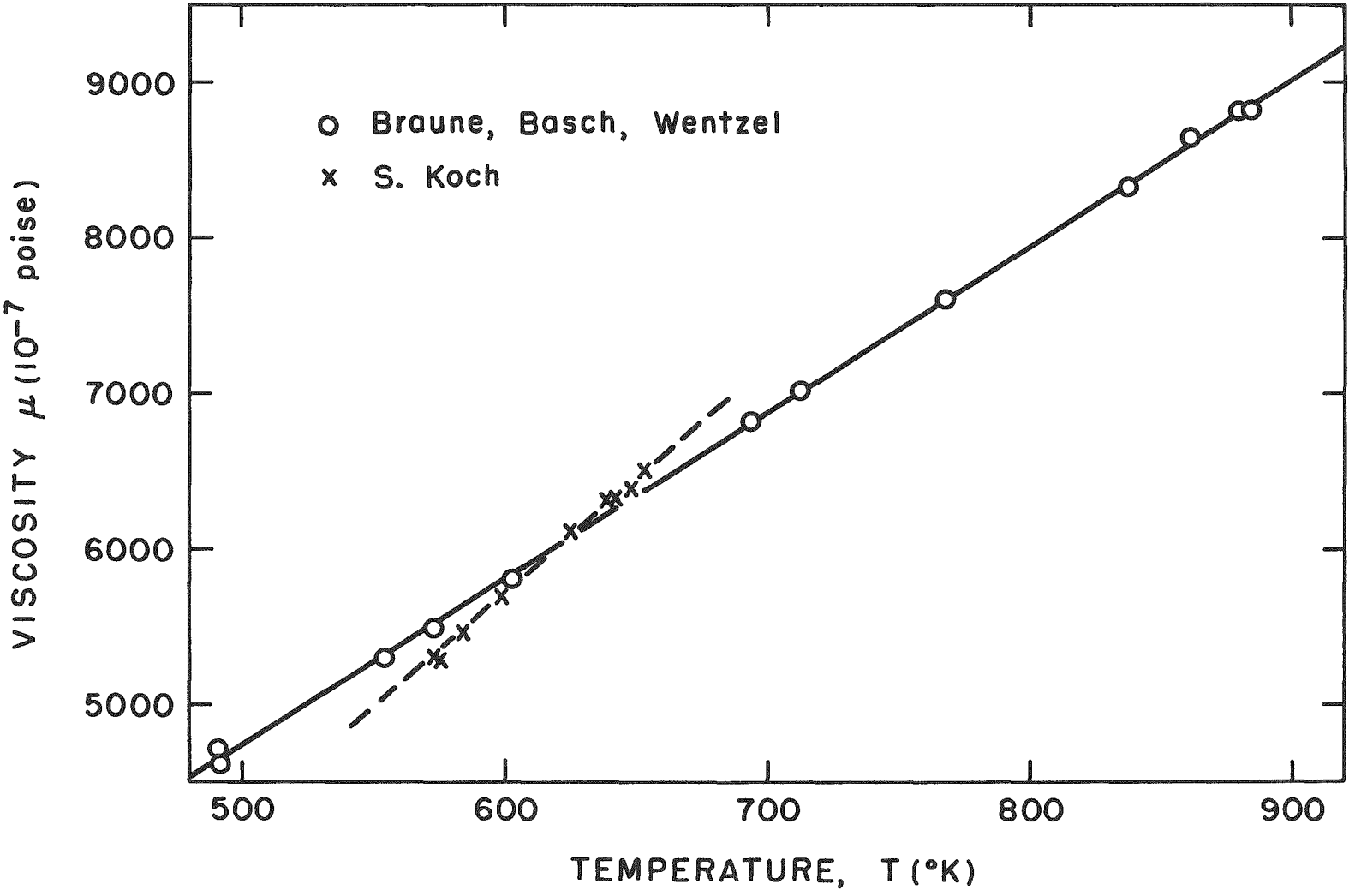

Fig. A2.2 A Graphical Representation of the Viscosity of Mercury Vapor as a Function of the Absolute Temperature

temperatures outside the range of the measurements. For sufficiently dilute gases in which only binary collisions occur, the viscosity of the vapor to a good approximation is given by the equation[82]

$$\mu(10^{-7} \text{ poise}) = 266.93 \frac{\sqrt{MT} f(T^*)}{\sigma^2 \Omega^{(22)}(T^*)} \quad . \qquad \text{(A2.2-3)}$$

In this expression σ is the collision diameter, related to the equilibrium separation of the two atoms. $\Omega^{(22)}(T^*)$ is a complicated integral function of the potential energy of the binary collision and the reduced temperature T^*, which is the absolute temperature divided by the depth of the potential well in units of ϵ/k (°K), and $f(T^*)$ is a small correction factor of nearly unit value. Numerical values of $\Omega(T^*)$ and $f(T^*)$ at small intervals of T^* have been tabulated[83] for various potential functions, but of these to date, only the Lennard-Jones (6-12) and modified (exponential -6)[83] functions represent realistic potentials.

Epstein and Powers[76] concluded from an analysis of the data of Braune, Basch, and Wentzel and the four of the values measured by Koch and reported in the International Critical Tables that the viscosity of mercury vapor, if it were to fit that derivable from a Lennard-Jones (6-12) potential, yielded unique parameters for the collision diameter σ, the equilibrium separation r_0, and the well depth ϵ/k as follows.

$$\begin{aligned} \sigma &= 2.89 \pm 0.04 \text{ Å} \\ r_0 &= 3.25 \pm 0.04 \text{ Å} \\ \epsilon/k &= 851 \pm 32 \text{ °K (1.7 kcal)} \quad . \end{aligned} \qquad \text{(A2.2-4)}$$

These conclusions, however, are drawn from an examination of the correspondence of the slope of the viscosity-temperature curve with that derivable from the Lennard-Jones potential within the limits of $818.6 < \epsilon/k < 883.2$, and their validity rests on the assumption that the slope has different properties outside the experimental range. Contrary to the opinion of these investigators, the theoretical fit of the data with the above parameters is quite unacceptable with respect to the apparent precision of the more recent data as the values cited in Table A2.2-1 illustrate.

TABLE A2.2-1

Comparison of Experimental and Derived Viscosities of Mercury Vapor

T(°K)	$\mu \times 10^7$ (exp., BBW)	$\mu \times 10^7$ (Eqn: A2.2-2)	%Dev.	$\mu \times 10^7$ (L-J, 6-12)	%Dev.	$\mu \times 10^7$ (exp-6)	%Dev.
491.0	4709	4662	+1.0	4739	-0.6	4720	-0.2
492.5	4672	4678	-0.1	4753	-1.7	4734	-1.3
496.5	4689	4720	-0.7	4793	-2.2	4774	-1.8
554.4	5310	5329	-0.4	5355	-0.8	5356	-0.9
573.5	5501	5530	-0.5	5546	-0.8	5550	-0.9
603.0	5831	5842	-0.2	5835	-0.1	5852	-0.4
694.0	6856	6808	+0.7	6730	+1.8	6790	-1.0
712.7	7029	7007	+0.3	6912	+1.7	6983	-0.6
769.0	7610	7607	+0.03	7471	+1.8	7567	+0.6
838.0	8343	8346	-0.03	8154	+2.3	8281	+0.7
861.5	8632	8598	+0.4	8387	+2.8	8523	+1.3
880.0	8766	8796	-0.3	8571	+2.2	8713	+0.6
883.0	8802	8828	-0.3	8601	+2.3	8744	+0.7

Epstein and Powers have suggested that the Lennard-Jones (6-9) potential function might fit the data better. This function has a weaker repulsive strength than the former potential, but apparently the necessary temperature-dependent function $\Omega^{22}(T^*)$ has not been evaluated for the (6-9) potential. The recent tabulations[83] for the (exp-6) function, however, allow one to test the effect of a weaker repulsive potential with the above parameters. For this potential function, the repulsive effect may be decreased by adjustment of a parameter α. In the present case, α was chosen as 12, which should yield a repulsive effect only very slightly larger than that for the (6-9) potential. The parameters

$$\begin{aligned} r_0 &= 3.25\ \text{Å} \\ \epsilon/k &= 850\ ^\circ\text{K} \\ \alpha &= 12 \end{aligned} \qquad \text{(A2.2-5)}$$

were used to derive the viscosity according to equation (A2.2-3) for the (exp-6) potential function. The values so obtained are tabulated in Table 2.2-1, and it is apparent that the agreement, as suggested by Epstein and Powers, is superior to those values derivable from the (6-12) function. However, these too show a systematic deviation.

The experimental data of Braune, Basch, and Wentzel are compared in Table A2.2-1 with the viscosities derived from the least-squares equation (A2.2-2) and the above-described theoretical treatments. The percent deviations listed are referred to the experimental values.

One now comes to the difficult task of deciding how the viscosity should be properly extrapolated to the lower temperatures. Certainly the best procedure would be that employing a potential function as described. However, this procedure does not appear to be valid enough since, with the potential parameters described, there are systematic differences between the experimental values and those derived theoretically. The writer finds that no consistent set of potential parameters

may be found to give the necessary agreement. Either the data are unreliable, or a different set of $\Omega^{22}(T^*)$ values for a potential function presently not examined is required, or possibly some aspect of the theory is incorrect in its application to mercury vapor.

There is an interesting point worth mentioning here in regard to this problem and that of the discrepancies in the vapor pressure of mercury. The distance of nearest neighbors, both in the solid and liquid phases of mercury, is 3.0 Å,[84] whereas a choice of $\epsilon/k = 850°K$ yields a value of 3.25 Å for the equilibrium separation in the gas. In contrast to this situation, the equilibrium separations of the sodium and potassium dimers[85] are several tenths of an angstrom less than nearest neighbor distances in the condensed phases.[86] An examination shows that for a (6-12) potential function a value of 3.11 Å for the equilibrium separation gives an ϵ/k value of 1006 °K and a dissociation energy of 2 kcal to give agreement with the experimental viscosities. This value of ϵ/k would have to be increased further to yield an equilibrium separation corresponding to nearest neighbor distances in the liquid phase.

In view of the difficulties involved in constructing an adequate theoretical correspondence for the viscosity of mercury vapor, one must accept the experimental data a priori to be more reliable than a theoretically deduced equation. One might wonder whether a Sutherland equation would extrapolate correctly to lower temperatures. Braune, Basch, and Wentzel fitted their data to such an equation, which at the time of their study was the most rigorous form for the temperature dependence. They obtained by least-squares the Sutherland equation

$$\mu(10^{-7} \text{ poise}) = \frac{612.3\ T^{3/2}}{T + 942.2} \quad . \qquad \text{(A2.2-6)}$$

This expression gives a good representation of their data, but, as can be demonstrated,[83] such an equation may lead to serious errors on extrapolation.

Since there is no other choice which appears more reasonable at present, the empirical equation (A2.2-2) will be used for

extrapolations of the viscosity of mercury vapor. A least-squares analysis indicates that an extrapolation to 300°K would not yield errors greater than five percent. In Table A2.2-2 a comparison is given of several extrapolated values for the Sutherland equation of Braune, Basch, and Wentzel, the empirical equation (A2.2-2), and values calculated for the (exp-6) potential with the parameters (A2.2-5).

TABLE A2.2-2

Comparison of Extrapolated and Interpolated Viscosities of Mercury Vapor

T°K	$\mu \times 10^7$ (Sutherland, BBW)	$\mu \times 10^7$ (Eqn. A2.2-2)	$\mu \times 10^7$ (exp-6)
300	2561	2683	2912
400	3650	3712	3833
500	4747	4757	4809
600	5835	5810	5821
700	6905	6872	6852
800	7952	7939	7888

The maximum percent difference between these values is 14 percent at 300°K. If the original data are reliable, then one may conclude that the extrapolated viscosity is reliable within 5 to 10 percent.

A2.3 The Mean Free Path of Saturated Mercury Vapor

The most commonly employed expression for the mean free path[87] is

$$\lambda = 1/\sqrt{2}\pi\nu\sigma^2 \quad , \qquad \text{(A2.3-1)}$$

where ν is the uniform molecular density and σ is the diameter of a hard, elastic spherical molecule. If the gas is ideal then $\nu = p/kT$, with the symbols representing the usual quantities, and therefore the mean free path may be written as

$$\lambda = kT/\sqrt{2}\pi p\sigma^2 \qquad \text{(A2.3-2)}$$

These prescriptions are derivable from considerations of an equilibrium gas, specifically, a Maxwellian hard-sphere gas. Their application to a description of a real gas in flow presumes a saturated gas contrary to the irreversible nature of the gas in flow. One must acknowledge then that a mean free path description provides only a qualitative picture of phenomena associated with a flowing gas.

Perhaps as serious as the above limitations is the fact that collision diameters vary with the temperature, a situation which explains in part why the viscosity is strictly not proportional to the square root of the temperature, as the classical derivation predicts. Apparently, there is no completely rigorous way in which this situation can be corrected, but one may resort to a subterfuge. In the simplified kinetic description of transport properties, the various properties (viscosity, diffusion, and conductivity) are considered as mean free path phenomena and are derivable on this basis. A rigorous theory of such properties of a gas of hard-sphere elastic molecules was used by Chapman and Enskog(88) to derive the viscosity and mean free path relationship for a dilute shearing gas:

$$\mu = 0.499\ M\nu\bar{c}\lambda \quad , \qquad \text{(A2.3-3)}$$

in which $\bar{c}$ is the average thermal speed and λ is the usual mean free path. Presumably, then, if the viscosity is known as a function of temperature, the mean free path is derivable. However, when the viscosity is that of a real gas, the mean free path so calculated must be considered as an equivalent hard-sphere free path, and in this devious way the change in the collision diameter with temperature is at least qualitatively included in the mean free path description of the gas. Since there is some question as to the uniqueness of the density ν, this description is subject also to the equilibrium limitations.

For the present purposes we may take the equation (A2.3-3) as defining the mean free path of mercury vapor. Thus, for pressure expressed in mm Hg, viscosity in poise, and temperature in degrees Kelvin,

$$\lambda\,(\mathrm{cm}) = 0.6064\,\frac{\mu\sqrt{T}}{p(\mathrm{mm})} \quad . \qquad \text{(A2.3-4)}$$

This equation gives the following mean free paths:

T°K	$\mu(10^7$ poise)	p(mm Hg)	λ(cm)
300	2683	2.33×10^{-3}	1.2
400	3713	1.048	7.1×10^{-3}
500	4757	39.42	2.7×10^{-4}

BIBLIOGRAPHY

1. M. Knudsen, The Kinetic Theory of Gases, Methuen and Company, Ltd., London (1950).
2. J. L. M. Poiseuille, Compt. Rend. 11, 961, 1041 (1840).
3. A. Kundt and E. Warburg, Ann. Physik (Pogg.) 155, 337 (1875).
4. T. Graham, Ann. Physik, 17, 341 (1829); Phil Mag. 2, 175 269, 351 (1833).
5. C. Christiansen, Wied. Ann. Physik 41, 565, (1890).
6. H. Hertz, Ann. Physik 17, 177 (1882).
7. T. Graham, Phil. Trans. 136, 573, (1846).
8. J. R. Partington, An Advanced Treatise on Physical Chemistry, Vol. 1, Longmans, Green and Company, London (1949), p. 754, footnote 6.
9. H. Lamb, Hydrodynamics, Sixth Ed. Dover Publications, New York (1932), p. 23.
10. Ibid, p. 27.
11. O. Reynolds, Papers ii, p. 311.
12. A. F. Benton, Phys. Rev. 14, 403 (1919).
13. M. Knudsen, Ann. Physik 28, 75, (1909).
14. W. C. Pollard and R. D. Present, Phys. Rev. 73, 762 (1948).
15. S. Dushman, Scientific Foundations of Vacuum Technique, John Wiley and Sons, Inc., New York (1949).
16. E. H. Kennard, Kinetic Theory of Gases, McGraw-Hill Book Company, Inc., New York (1938). p. 140.
17. M. Knudsen, Ann. Physik 28, 999 (1909).
18. W. Gaede, Ann. Physik. 41, 289 (1913).
19. H. J. Adzumi, Chem. Soc. Japan 12, 285 (1937).
20. W. Dong, "Vacuum Flow of Gases Through Channels with Circular, Annular, and Rectangular Cross Sections" University of California Radiation Laboratory, Report No. UCRL 3353; contains additional references.
21. W. H. Eberhardt, "Momentum Transfer and Molecular Transport," Report No. K-992.
22. J. W. Hilby and M. Pahl, Z. Naturforsch. a7, 533, 542 (1952).

23. W. C. DeMarcus, The Problem of Knudsen Flow, Report No. K-1302, Part 3, addendum, p. 4.

24. S. Visner, "Gaseous Self-Diffusion and Flow in Capillaries at Low Pressures," Report No. K-688.

25. E. H. Kennard, loc cit. p. 62.

26. Ibid, p. 55.

27. R. G. J. Frazer, Molecular Beams, Methuen and Co. Ltd., London (1937).

28. F. Knauer and O. Stern, Z. Physik 39, 764 (1926).

29. T. H. Johnson, Phys. Rev. 31, 103 (1928).

30. H. Mayer, Z. Physik 52, 235 (1928).

31. H. Mayer, Z. Physik 58, 373 (1929).

32. M. von Smoluchowski, Ann. Physik 33, 1559 (1910).

33. F. Knauer and O. Stern, Z. Physik 60, 414 (1930).

34. P. Clausing, Z. Physik 66, 471 (1930).

35. J. R. Partington, loc. cit., ref. (8), p. 931; also see L. B. Loeb, Kinetic Theory of Gases, McGraw-Hill Book Co., New York (1934) p. 323 et seq.

36. R. J. Ackermann, R. J. Thorn and G. H. Winslow, Some Fundamental Aspects of Vaporization (to be published).

37. W. Prüger, Setzber. Akad. Wiss. Wien Math. Naturw. Klasse Abt. III a 149, 31 (1940).

38. M. Knudsen, Ann. Physik 48, 1113 (1915).

39. J. B. Taylor, Phys. Rev. 35, 375 (1930).

40. W. C. DeMarcus, loc. cit., ref. 23, Part 1.

41. P. Clausing, Ann. Physik (5)12, 961 (1932); see this for additional references; also see ref. (34).

42. W. C. DeMarcus, loc. cit., ref. 23, Part 3.

43. R. J. Ackermann, P. W. Gilles and R. J. Thorn, J. Chem. Phys. 25, 1089 (1956).

44. J. W. J. Walsh, Photometry, Constable and Company, Ltd., London (1953), pp. 140-150.

45. R. J. Peavler and A. W. Searcy, J. Amer. Chem. Soc. 73, 2076 (1956).

46. C. I. Whitman, J. Chem. Phys. 20, 161 (1952).

47. Ibid. 21, 1407 (1953).

48. K. Motzfeldt, J. Phys. Chem. 59, 139 (1955).

49. M. G. Rossmann and J. Yarwood, British J. Appl. Phys. 5, 7 (1954).

50. Ibid, J. Chem. Phys. 21, 1406 (1953).

51. P. E. Blackburn, J. Phys. Chem. 62, 897 (1958).

52. R. J. Thorn, Saturation of Vapor in a Knudsen Effusion Oven, Argonne National Laboratory Report ANL-5417 (1957).

53. J. L. Lebowitz and H. L. Frisch, Phys. Rev. 107, 917 (1957).

54. R. Speiser and H. L. Johnston, Trans. Am. Soc. Metals 42, 283 (1950).

55. K. D. Carlson, P. W. Gilles, and R. J. Thorn, Vapor Saturation in a Knudsen Cell (to be published).

56. I. Langmuir, J. Am. Chem. Soc. 40, 1361 (1918).

57. R. J. Ackermann and R. J. Thorn, Vaporization of Oxides, Progress in Ceramic Sciences, Vol. I, Pergamon Press, Inc. New York.

58. J. A. W. Huggill, Proc. Roy. Soc. A212, 123 (1952).

59. A. S. Berman and L. M. Lund, Deviations from Classical Kinetic Theory in the Low-Pressure Transport of Gases through Porous Media, Second United Nations International Conference on Peaceful Uses of Atomic Energy, Geneva (1958) Vol. 4, p. 389, also see J. Chem. Phys. 28, 363 (1958).

60. H. Braune, R. Basch, and W. Wentzel, Z. Physik. Chem. 137A, 447 (1928).

61. R. H. Busey and W. F. Giauque, J. Amer. Chem. Soc. 75, 806 (1953).

62. H. Shenker, J. Lauritzen, Jr., and R. J. Corruccini, Reference Tables for Thermocouples, National Bureau of Standards Circular 508 (1951).

63. R. W. Schrage, A Theoretical Study of Interphase Mass Transfer, Columbia University Press, New York (1953).

64. R. T. Birge, Phys. Rev. 40, 207 (1932).

65. H. S. Taylor and S. Glasstone, A Treatise on Physical Chemistry, Vol. 2, D. Van Nostrand and Company, Inc. (1951), p. 108.

66. K. D. Carlson and E. Rauh, Measurements of the Vapor Pressure of Gold at High Source Pressures (unpublished).

67. T. E. Phipps, Private Communication, University of Illinois

68. R. Courant, Differential and Integral Calculus, Vol. II, Interscience Publishers, Inc., New York, 1948, p. 217 et seq.

69. H. B. Dwight, Tables of Integrals and Other Mathematical Data, 3rd Ed. The Macmillan Company, New York, 1947.

70. W. S. Snyder, Nucleonics 6 (2) 46 (1950).

71. W. C. DeMarcus, loc. cit., ref. 23, part 2.

72. T. B. Douglas, A. F. Ball, and D. C. Ginnings, J. Res. Nat. Bur. Stand. 46, 334 (1951).

73. F. H. Spedding and J. L. Dye, J. Phys. Chem. 59, 581 (1955).

74. F. M. Ernsberger and H. W. Pitman, Rev. Sci. Instr. 26, 584 (1955).

75. J. O. Hershfelder, C. F. Curtiss, and R. B. Bird, Molecular Theory of Gases and Liquids, John Wiley and Sons, Inc., New York, 1954, Chapter 3.

76. L. F. Epstein and M. D. Powers, J. Phys. Chem. 57, 336 (1953).

77. J. A. Beattie, B. E. Blaisdell, and J. Kaminski, Proc. Am. Acad. Arts Sci. 71, 361, 375 (1937).

78. H. F. Stimson, J. Res. Nat. Bur. Stand. 42, 209 (1949).

79. R. J. Thorn, Private Communication.

80. S. Koch, Wied. Ann. Phys. 19, 857 (1883).

81. N. B. S. Circular 564 (1955).

82. J. O. Hirshfelder, et al., loc. cit., ref. 75, p. 528.

83. J. O. Hirshfelder, et al., loc. cit., ref 75, see Tables and p. 543 et seq.

84. J. S. Lukesh, W. H. Howland, L. F. Epstein, M. D. Powers, J. Chem. Phys. 23, 1923 (1955).

85. G. Herzberg, Spectra of Diatomic Molecules, D. Van Nostrand and Co., Inc., New York, 1950.

86. N. S. Gingrich and R. E. Henderson, J. Chem. Phys. 20, 1117 (1952).

87. E. H. Kennard, loc. cit., ref 16, p. 113.

88. Ibid., p. 147.